EFFECT OF SCALE OF OPERATION ON HEAP LEACHING PERFORMANCE

Petrus Johannes van Staden

SOUTH AFRICA-CAPE TOWN, 03 May 2019

HYDRomet

EFFECT OF SCALE OF OPERATION ON HEAP LEACHING PERFORMANCE

Petrus Johannes van Staden

A thesis submitted at the University of Cape Town in fulfilment of the requirements for the degree of

Doctor of Philosophy

Department of Chemical Engineering

University of Cape Town

03 May 2019

ABSTRACT

The extent to which differences in bulk density and in irrigation geometry contribute towards the differences observed in leaching performance between laboratory-scale columns versus commercial-scale heaps was investigated. Furthermore, the contributions of segregation and stratification, which are absent from columns but unavoidable in heaps, were also investigated.

Four case studies provided data whereby the column and heap leaching of the respective sample materials could be directly compared. The first involved gold-bearing ore, the second gold-bearing sand, a third was conducted on oxide-copper ore and the fourth case study was performed on sulphidic copper ore. The first case study was published by others, while the other three were conducted by the author himself. Furthermore, custom-designed boxes were constructed whereby the segregation and stratification of ore could be simulated. Tests were performed to observe the leaching performance of segregated and stratified ore samples, compared to unsegregated and unstratified ore samples. The leaching characteristics of each case was quantified in terms of the parameters of a mathematical model, based on dual-porosity hydrology and diffusion with chemical reaction, which provided optimised fits to the experimental data. Furthermore, fundamental relations were derived for the impact that changes in bulk density and changes in drip-irrigation spacing are theoretically expected to have on the same model parameters. These relations were tested against the actual trends observed in the model parameters that best fitted the data of the four case studies and of the segregation/stratification experiments.

It was found that the diffusional distance, which places a mass-transfer limitation on the over-all rate of leaching, can be governed by either the ore bulk density, or by the irrigation dripper spacing. The relations derived under this study can be used to estimate the maximum dripper spacing that can be permitted to prevent dripper spacing from becoming the rate-limiting parameter. Estimates of the impact of dripper spacing on the ultimate extent of extraction are also provided. However, neither segregation nor stratification exhibited significant or reproducible effects on leaching kinetics. These findings can place the drafting of heap leaching design parameters on a more fundamental footing.

SUMMARY

The problem and objective

The heap leaching of crushed ore is a relatively low-cost extraction process that is of great significance for the exploitation of the smaller, high-risk and/or low-grade resources that it facilitates. It is also of relatively simple construction. However, two compromises to be made for these gains are a) slower and lower extent of extraction compared to the agitated leaching of milled ore and b) higher risk of misjudgement of the scale-up factors to be applied to the laboratory column testwork during specification of the pad footprint.

Heap leach design specialists apply empirical scale-up factors to the extent of extraction and leach duration observed during laboratory simulations in cylindrical columns. In this manner, no consideration is given to what the possible limiting factor could be, which is not necessarily common to all heap leaching operations. Furthermore, the same scale-up factors are apparently applied regardless of the irrigation means (sprinklers or drippers) to be applied. This study aims to correct the current lack of a fundamental basis for scale-up.

What is known

In the published literature, a relatively high bulk density and wide dripper spacing have been qualitatively correlated with poorer heap leaching performance. Furthermore, it has become almost customary in heap leaching publications to mention anecdotally that segregation (which usually includes stratification, as defined in this text), exhibits an important influence on heap leaching performance. Segregation and stratification result in finer and coarser particles being distributed non-homogenously and occur as a result of commercial-scale heap stacking practices. However, very little data has been published to support the supposed effect of segregation/stratification.

From residence time distribution observations, and more recently from direct experimental observation, it has been learnt that solution passing through beds of particulate solids flows through sparsely distributed flow channels, leaving most of the

solids immersed in immobile solution. This is termed ‘dual porosity’ hydrology. The implication is that heap leaching kinetics is largely governed by the rate of diffusion of reagents and leached species between the flow channels and mineral surfaces.

The hypotheses

It was hence hypothesised that the average distance between flow channels, and hence the diffusional distance (R) which in turn is an important determinant of kinetics, is governed either by heap densification which determines the number of available flow channels or, (in the case of drip-irrigation), by dripper spacing.

It was further hypothesised that, in cases of very wide dripper spacing, a proportion of the ore could be left without any contact with leach solution, reducing thereby what has been termed the ‘extractable fraction’.

It was further hypothesised that, in the presence of segregation and stratification, the flow channels would become even more widely spaced than when ore is homogenously packed. In the case of segregation this would be caused by the finer fraction overlaying the heap exhibiting higher densification and hence more sparse distribution of flow channels. In the case of stratification this would result from deflection of the flow channels by more conductive ore layers that border less conductive ore layers.

The approach

The published data was analysed of four case studies, for which the leach kinetics was available for both laboratory columns and large scale heaps. The data was fitted to a heap leaching model, in each case quantifying the kinetics of both the column and the heap in terms of the Transfer Time. For each case study, the Transfer Time prevailing in the heap, $\Theta = R^2.\tau^2/(D.\theta_{imm})$ could be compared to the Transfer Time on the same ore in a column. As the name suggests, Transfer Time is indicative of the time required for diffusion of a species with diffusivity D to occur across a tortuous path of toruosity τ^2 via a spherical zone of radius R. The resistance to diffusion is reduced (i.e. the Transfer Time is shortened) by a larger volumetric fraction θ_{imm} of solution held stagnant in the spherical zone, since diffusion can only occur via the solution phase; an increased value

for θ_{imm} increases the cross sectional area available for diffusional mass transfer (refer to Figure 26 on page 109 for a visualisation thereof).

Different conventions exist for the symbol whereby tortuosity is represented, the justification for the use of τ^2, as opposed to τ, is given in section 3.11.5. The relation between volumetric immobile moisture content θ_{imm} and other, more directly measurable indicators of moisture content, is shown in the Nomenclature.

It will be seen from section 5.2.2 how it follows that the Transfer Time is the fundamental parameter grouping that characterises the diffusional mass transfer, which has dimensions of time.

It was found that different ore types exhibit different Transfer Times even when leached under the same conditions in a column of the same dimensions. It was further found that the Transfer Time of a heap bears a relation to the Transfer Time observed on the same ore in a column. It is therefore not possible to predict the Transfer Time at heap-scale without having the Transfer Time of the same ore at column-scale as a reference. The Transfer Time observed on column-scale is therefore denoted Θ_{ref}, and the transfer at heap scale Θ. The ratio $(\Theta/\Theta_{ref})^{0.5}$ was denoted the Dimensionless Transfer Radius, DTR. It is so called since, as will be seen in section 5.5.3, it is directly proportional to the ratio of (a) the radius of the hypothetical spherical zone via which diffusion occurs in a heap R, and (b) the radius of the corresponding zone via which diffusion occurs in a column, R_{ref}.

Three types of DTR were defined, (a) Experimental-DTR, based on the ratio between Transfer Time fitted to model the column leaching kinetics and the Transfer Time fitted to model the heap leaching kinetics of the same ore (b) theoretical Densification-DTR based on the assumption that densification governs the scale-up behaviour and (c) theoretical Dripper-Spread-DTR based on the assumption that the increase in effective dripper spacing governs scale-up behaviour.

Based on theoretical principles, an expression was derived for the Densification-DTR as functions of immobile moisture content in the heap θ_{imm}, immobile moisture content in the column $\theta_{imm,ref}$, rock density ρ^*, bulk density of the heap, ρ, and bulk density of the

same ore in a column, ρ_{ref}. Similarly, a theoretical expression was developed for the Dripper-Spread-DTR, as a function of the same parameters plus the column diameter *Dia*, and the equivalent column diameter $Dia_{,ref}$ that has the same cross sectional area as the area contained between four neighbouring drippers on a drip-irrigated heap.

The findings

The column and heap leaching data of the case studies was fitted to determine the Experimental-DTR for each case study. It was then determined whether the Experimental-DTR could be correlated to either the theoretically-derived Densification-DTR or to the theoretically-derived Dripper-Spread-DTR. In cases where densification governed the manner in which the Transfer Time changed from column to heap, the Experimental-DTR was found to correlate with the Densification-DTR. If dripper spread governed it, the Experimental-DTR correlated with the Dripper-Spread-DTR.

From that analysis followed the trends shown in the graph below, which is based on a generalised hypothetical case. The horizontal line is the Densification-DTR, and the sloping line is the Dripper-Spread-DTR. For the example illustrated here, the diffusional distance of the heap is goverened by densification for any dripper spacing with equivalent diameter smaller than 350 mm. For any larger dripper spacing, the diffusional distance is governed by the dripper spacing. A dripper spacing of 350 mm is the largest that would not render the DTR governed by dripper spacing, and yields a DTR of 2.0. Any larger dripper spacing would yield a larger DTR and therefore heap leaching kinetics with a longer Transfer Time (i.e. slower kinetics). Hence with the value of the DTR known to be 2.0, the Transfer Time of the heap can be predicted as $\Theta = \Theta_{ref} (2.0)^2$. The value of Θ_{ref} will have been determined by fitting of the leaching model to the column leaching data. The kinetics of the heap can now be modelling by using the Transfer Time, Θ thus calculated, as model input parameter.

SUMMARY

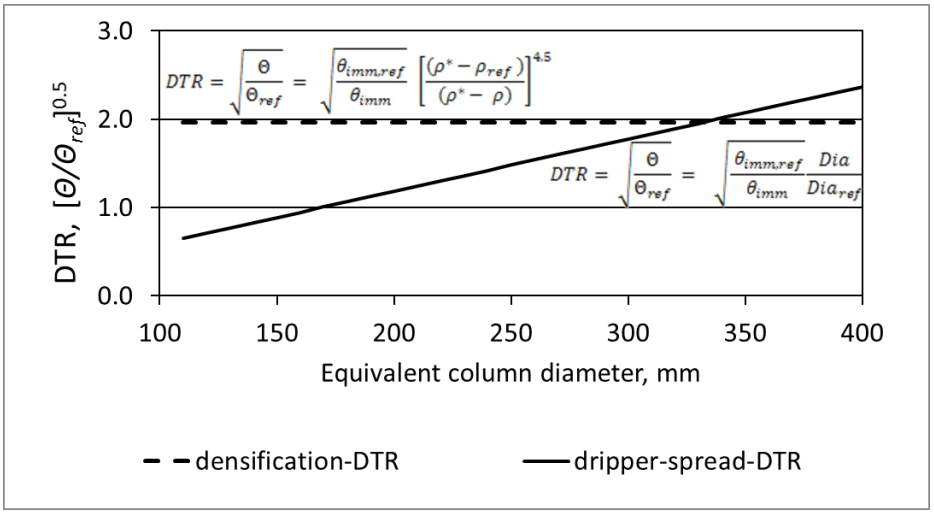

The magnitude of the power of the term bearing the bulk densities in the Densification-DTR followed from the fitting of the column and heap leaching kinetics of the various case studies to the model. From its magnitude of 4.5, it was concluded that the increase in Transfer Time with increasing bulk density is largely attributable to an increase in tortuosity of the flow channels, as opposed to a reduction in the porosity that is available for conducting flow. (From the analysis that appears in section 5.5.4 it will be seen that an increase in bulk density from the column to the heap contributes only 0.5 to the power of the term that bears the density terms, whereas the corresponding increase in tortuosity contributes the balance of 4 to that power).

The extractable fractions (i.e. proportion of ore that was effectively contacted by leach solution) were determined by extrapolation of the batch leaching curve of each case study to infinite time. It was found that a relatively narrow dripper spacing (between 111 and 225 mm) is required to ensure that no part of the ore remains effectively out of contact with leaching solution.

Neither segregation nor stratification was found to significantly affect heap leaching kinetics. However, it was learnt that for the laboratory determination of hydraulic conductivity on ore samples, the samples should be segregated and upper, middle and bottom fractions should be tested separately to obtain the most conservative

measurements. The most conservative values are found on column leach residues, with the conductivity test conducted in the column without disturbing the sample. (That is as opposed to excavating the residue for testing in a compression chamber).

Recommendations

Very few case studies have been published for which both column and heap leaching data is available on any given ore. A larger number of case studies similar to those presented in this text would serve to improve the level of confidence with which the scale-up concept provided here can be adopted.

Another topic for future research would be devising a more fundamentally-based means of predicting the gangue acid consumption rate constant, *k'*. Since gangue competes with the value-mineral for reagent in the case of acid heap leaching, this parameter can have as important an impact on heap leaching kinetics than the Transfer Time. However, thus far it has proven difficult to predict the value of *k'* from laboratory experiments.

DECLARATION

I declare that this thesis is my own unaided work in concept and in execution, apart from the assistance and support that has been explicitly acknowledged in the Acknowledgements section that follows, and literature references that have been cited.

It is being submitted for the degree of Doctor of Philosophy (PhD) in the University of Cape Town.

This thesis has not been submitted before for any degree or examination in any other university.

Signed by candidate

03 May 2019

Signature: Petrus Johannes van Staden Date

ACKNOWLEDGEMENTS

I gratefully acknowledge:

Mintek, who funded the research;

My supervisor, prof. Jochen Petersen, for his expert supervision;

The staff from the Mintek library, who would trace any literature article in record time;

Sibabalwe Mxinwa (Mintek) and his team, who faithfully executed the segregation and stratification testwork according to my experimental designs;

My wife Christina for her unwavering support and encouragement.

LIST OF PUBLICATIONS AND PRESENTATIONS

1. van Staden, P.J., Laxen, P.A., 1988. Process Options for the Retreatment of Gold-Bearing Sand Sumps. Journal of the Southern African Institute of Mining and Metallurgy No. 8., vol. 88, pp. 257-264.
2. van Staden, P.J., Petersen, J., 2016. A *PhreeqC* model of heap leaching, Hydrometallurgy Conference 2016, Sustainable Hydrometallurgical Extraction of Metals. SAIMM, Belmont Mount Nelson Hotel, Cape Town, 12 pp.
3. van Staden, P.J., Kolesnikov, A.V., Petersen, J., 2017. Comparative Assessment of Heap Leach Production Data – 1. A Procedure for Deriving the Batch Leach Curve. Minerals Engineering Volume 101C, pp. 47-57.
4. van Staden, P.J., Huynh, T.D., Kiel, M.K., Clark, R.I., Petersen, J., 2017. Comparative Assessment of Heap Leach Production Data – 2. Heap Leaching Kinetics of Kipoi HMS Floats Material , Laboratory vs. Commercial Scale. Minerals Engineering Volume 101C, Pages 58-70.
5. van Staden, P.J., Naseri, A., Petersen, J., 2017. *HeapSim* modelling of high temperature heap bioleaching data, ALTA 2017 Conference and Exhibition, Pan Pacific Hotel, Perth, Western Australia, pp. 210-246.
6. van Staden, P.J., Petersen, J., 2018. First Order Exchange and Spherical Diffusion Models of Heap Leaching in *PhreeqC*. Journal of the Southern African Institute of Mining and Metallurgy.
7. Van Staden, P.J., Petersen, J., 2018a. The Effects of Simulated Stacking Phenomena on the Percolation Leaching of Crushed Ore, Part 1: Segregation. Minerals Engineering vol. 128, pp. 202-214.
8. Van Staden, P.J., Petersen, J., 2019. The Effects of Simulated Stacking Phenomena on the Percolation Leaching of Crushed Ore, Part 2: Stratification. Minerals Engineering vol. 131, pp. 216-229.

TABLE OF CONTENTS

LIST OF APPENDICES

LIST OF TABLES

LIST OF FIGURES

NOMENCLATURE AND GLOSSERY

Roman symbols

A,	Area;
$A_{i,j}$	Contact area between **cells** *i* and *j* in the PhreeqC diffusional model, [m^2]
c	Proportionality constant in the expression for tortuosity as a function of bulk density.
C_i	Concentration with respect to species *i*;
$C_{i,j}$	Concentration of soluble species *i* in phase *j,* [gmol/L]; [gmol/kg_solution]
$C_{i,j}^0$	Initial (*t* = 0) concentration of soluble species *i* in phase *j*[gmol/L]; [gmol/kg_solution; mass fraction (as appropriate in each context).
Cor.	Pearson's correlation coefficient, dimensionless.
d	Diameter (of small particle) in Figure 11, [m]
D	Free diffusivity of dissolved species in solution, [m^2/s]. (Also used to represent diameter (of large particle) in Figure 11).
D_e	Effective diffusivity through the ore matrix, [m^2/s].
Dia	Diameter or Equivalent Diameter (being diameter yielding same cross sectional area as a unit cell), [m]
E	Activation energy, [kJ/mole]
f_{bc}	Correction factor for the mobile/immobile boundary in the equation for $MX_{i,j}$, dimensionless.
$f_{s,1}$	Shape factor of van Genuchten relating the first-order exchange coefficient to an equivalent diffusional path length, dimensionless.
F	Force, [N]
g	Gravitational acceleration constant, 9.8 m/s^2
h	Distance between mid-points of neighbouring **cells** in the diffusional PhreeqC model, [m]

H or h	Distance, height or hydraulic head, [m] *H* also for Henry's constant [Pa.m^3/mole] in equation [50]
J	Flux, [mole/(m^2.s)]
k, k(T), K	Leach reaction rate constants *k* [m^2] is also used for permeability, and *K* [m/s] is also used for hydraulic conductivity in section 3.11.6
K_i	Kinetic rate constant with respect to species *i,* [h^{-1}]
k'	GAC rate constant, [h^{-1}]
k_{La}	Oxygen mass transfer coefficient, [s^{-1}]
L	Length such as in-line dripper spacing or heap height, [m] or [mm].
M_i	Molar mass of species *i*, [g/g-mole].
$MX_{i,j}$	PhreeqC *MIX* factor from a neighbouring immobile **cell** number *i* into the central **cell** number *j*, dimensionless.
N_s	Number of radial (lateral) increments, number of immobile **cells** associated with each mobile **cell**, dimensionless.
N_z	Number of vertical increments, dimensionless.
p	Power term characterising the response of tortuosity to densification.
P_n	Geometric correction factor for immobile **cell** number *n* away from the mobile zone, dimensionless.
P	Pressure, [Pa]
q	Irrigation flux [L/(h.m^2)]; [kg/(h.m^2)].
r	Radius or position along the radius of the immobile zone, [m].
R	Radius or specifically the diffusional path length, being the radial dimension of the zone holding the immobile solution that surrounds a flow channel, [m]. Also the gas constant, [J/(mole.K)] in equation [52].

s	Source term, [mole/(m^3.s)]
S	Spacing between conductive channels, [m]
S_e	Relative saturation, dimensionless.
t	Time, [h] (also used in Figure 11. Approximate size of capillaries.Figure 11 to indicate length, [m])
Δt	Time increment, [s], [h] or [d]
T	Temperature, [^oC], [K]
U	Superficial solution flow velocity, [$m^3/(m^2.h)$]
u *or* v	Velocity, [m/h]
V	Volume,
V_j	Volume of **cell** j in the diffusional PhreeqC model, [m^3]
W	Spacing between dripper lines, [m] or [mm]
W_{imm}	Immobile moisture content, mass fraction of the moist solids. See also θ_{imm} and ϵ_{imm}.
W_i^0	Mass fraction of species i in the solid phase at t = 0, dimensionless.
W'	Mass, [tonne, dry basis]
$\dot{W}'$	Rate of stacking, [tonne per day, dry basis]
X_i	Extent of conversion of species i, dimensionless.
$\dot{X}_i$	Rate of conversion of species i, [h^{-1}]
$\Delta x; \Delta y; \Delta z$	Spatial increments, [m]

Greek Symbols

α_x	Mass fraction of mineral in ore that is liberated and reactive to the lixiviant, as applied to particle-cluster-scale (or micro-scale) kinetics, dimensionless.
α_w	Mass fraction of ore that is effectively contacted with leach solution, as applied to particle-cluster-scale (or micro-scale) kinetics, dimensionless.
α	As defined within each context, a constant in equation [46] and mass transfer coefficient in section 3.11.10, [m/s]
γ	Surface tension, [N/m]
Γ	Diffusion time, [days].
δ	Constrictivity, dimensionless.
ϵ_{ads}	Porosity available to adsorption, dimensionless.
ϵ_{imm}	Immobile moisture content, [kg_moisture/kg_dry_solids]. See also W_{imm} and θ_{imm}.
Θ	Transfer Time, [days].
κ_0	Rate constant in expression for heap-scale kinetics whereby extracted metal reports to drainage solution as the net result of all processes occurring over the height of the heap/column, [h^{-1}].
κ_1	Exponent in expression for heap-scale kinetics whereby extracted metal reports to drainage solution as the net result of all processes occurring over the height of the entire heap/column, [h^{-1}].
κ_x	Mass fraction of mineral in ore that is liberated and reactive to the lixiviant, as applied to heap-scale (or macro-scale) kinetics, dimensionless.
κ_w	Mass fraction of ore that is effectively contacted with leach solution, as applied to heap-scale (or macro-scale) kinetics, dimensionless.
μ	Viscosity, [Pa.s]

Θ Time duration for which an incremental quantity of ore has been irrigated and leached, [days].

Θ_{imm} The immobile moisture is most commonly determined experimentally in terms of a mass fraction W_{imm} [kg_moisture/kg_wet_solids], but for modelling purposes it is more conveniently utilised in terms of either a volume fraction θ_{imm} [m^3_moisture/m^3_bed], or as a fraction of the dry solids mass ε_{imm} [kg_moisture/kg_dry_solids]. These conversions can be performed as follows, on the basis of a liquid-phase density of 1,000 [kg/m^3], dry bulk density of ore of ρ [kg/m^3] and assuming that the bed volume (and hence dry bulk density) remains unaffected by moisture content:

$$W_{imm} = \frac{\theta_{imm}}{\frac{\rho}{1000} + \theta_{imm}} \quad \text{from which follows}$$

$$\theta_{imm} = \frac{\rho}{1000}\left(\frac{W_{imm}}{1 - W_{imm}}\right)$$

and:

$$\varepsilon_{imm} = \frac{1000\,\theta_{imm}}{\rho} = \left(\frac{W_{imm}}{1 - W_{imm}}\right)$$

θ_{void} Voidage as a volume-fraction. The voidage of a bed sets the upper limit for the volumetric immobile moisture content, Θ_{imm}

ξ Dimensionless distance along the radius of the immobile zone, dimensionless.

ρ Bulk density, [kg/m^3] on a dry basis.

ρ^* True density, [kg/m^3]

σ Contact angle

τ^2 Tortuosity, [m^2/m^2]

Φ Power of the unreacted fraction for mineral leaching kinetics, dimensionless.
Also as defined in each context, the angle of internal friction and as a constant in section 3.11.10.

Abbreviations

CAA Curing Acid Addition. Acid being added to ore prior to loading into a column or prior to stacking onto a heap.

CFD Computational fluid dynamics

COM Component Object Module

Cor. Pearson's correlation coefficient

CuO A generic chemical formula used to represent 'oxide' (i.e. acid-soluble) copper minerals

DTR Dimensionless Transfer Radius, being square root of the ratio between two Transfer Times, Θ and Θ_{ref}.

EW electrowinning

FAA Fresh Acid Addition. In this text it has the same meaning as NAC.

FBC Fitted batch curve. It is a description of the shape of a batch leaching curve in the form of equations [94] and [95][94].

GAC Gangue Acid Consumption. (Also see TAC).

GO Acid consuming gangue minerals

ILS Intermediate leach solution. It is drainage from near-exhausted heaps which is used for irrigation of more recently stacked heaps, used to raise the metal tenor in the PLS sent to downstream recovery.

IR Irrigation Ratio. The amount of solution irrigated onto a heap per amount of ore on the heap (dry basis), in such units as m^3/t. Can be calculated from $IR = \frac{q}{\rho\, H}\, t$

IX Ion exchange

LBC Laboratory batch curve. This is a plot of cumulative extent of metal extraction versus time or versus IR, based on the data collected during a column leaching experiment.

MBC Modelled batch curves. In the context of case study 3 (Kipoi heap leaching), it is the batch leach curve calculated by either the HeapSim or PhreeqC dual-porosity heap leaching model, fitted to observed heap leach data (which in turn could be in the form of a LBC or a FBC).

NAC Net Acid Consumption. A terms used here only in relation to the leaching of ores that include sulphides that are oxidised. It is the summation of acid consumed by all acid-consuming reactions but excluding leaching of the acid-soluble oxide-mineral bearing the value-metal, minus all acid yielded by acid-producing reactions such as pyrite oxidation.

PIB, PCS, PDS Naming of integrals for calculation of amount of metal extracted (a) from a batch, (b) during continuous stacking and (c) after discontinuation of stacking, respectively, [tonne].

PLS Pregnant leach solution. The metal-laden drainage from heaps being sent to downstream recovery of the value-element(s).

ROM Run-of-mine, referring to the size distribution of ore as it is hauled from the mine, before any further crushing or milling.

SSR Sum of Squared Residuals, used as an indication of goodness of fit between two sets of data. When optimising the fit of model calculations to experimental data it was sought to minimise the SSR, also known as the ‘least squares’ method.

SX Solvent extraction

TAC Total Acid Consumption. A term used here only in relation to the leaching of acid-soluble ores, where no sulphide oxidation occurs. It is the sum of the GAC and the acid consumed in leaching the oxide-mineral bearing the value-metal.

It can also be calculated as the sum of CAA plus all acid irrigated onto the ore minus all acid draining from the ore.

The total acid consumption (TAC) is determined from:

$$\begin{bmatrix}\text{TAC}\\ [kg_{acid}/t_{ore}]\end{bmatrix} = \begin{bmatrix}\text{Curing acid addition}\\ \text{[kg/t]}\end{bmatrix} + \begin{bmatrix}\text{cumulative acid}\\ \text{irrigated, [kg/t]}\end{bmatrix} - \begin{bmatrix}\text{cumulative acid}\\ \text{drained, [kg/t]}\end{bmatrix}$$

$$= \begin{bmatrix}\text{Curing acid addition}\\ \text{[kg/t]}\end{bmatrix} + \frac{q \quad \Delta[H_2SO_4] \quad \frac{1}{H} \quad \frac{1}{\rho} \quad \Delta t}{\left[\frac{L}{h.m^2}\right] \quad \left[\frac{g}{L}\right] \quad \left[\frac{1}{m}\right] \quad \left[\frac{m^3}{kg}\right] \quad [h]}$$

where q is the irrigation rate, $\Delta[H_2SO_4]$ is the difference in acid concentration between irrigated and drained solutions, H is the vertical distance between irrigation and drainage points and ρ is the ore bulk density (dry basis), with units as shown. (Note the equivalence between units of g/kg and kg/t).

The relation between TAC and GAC is calculated as follows:

$$\begin{bmatrix}\text{TAC}\\ [\text{kg}_{\text{acid}}/\text{t}_{\text{ore}}]\end{bmatrix} = \begin{bmatrix}\text{GAC}\\ \text{[kg/t]}\end{bmatrix} + \begin{bmatrix}\text{cumulative Cu}\\ \text{extraction, } [\text{t}_{\text{Cu}}/\text{t}_{\text{ore}}]\end{bmatrix} \times \left[\frac{\text{molar mass of acid}}{\text{molar mass of Cu}}, \left[\frac{\text{t}_{\text{acid}}}{\text{t}_{\text{Cu}}}\right]\right]$$

$$= \begin{bmatrix}\text{GAC}\\ \text{[kg/t]}\end{bmatrix} + 1000 \frac{C_{Cu}^0 \quad X_{CuO}(t) \quad \frac{M_{H2SO4}}{M_{Cu}}}{\left[\frac{\text{t}_{\text{Cu contained}}}{\text{t}_{\text{ore}}}\right] \quad \left[\frac{\text{t}_{\text{Cu extracted}}}{\text{t}_{\text{Cu contained}}}\right] \quad \left[\frac{\text{t}_{\text{H2SO4}}}{\text{t}_{\text{Cu extracted}}}\right]}$$

VBA Visual Basic for Applications

STANDARD TERMS

Aggregate	A mass of particles, bearing a size distribution, grouped together.
Angle of (internal) friction	The angle at which aggregate comes to rest when stacked onto a free-standing pile, (i.e. without side support). Also called the angle of repose.
Cells	PhreeqC terminology for the vertical and lateral spatial increments into which a mass of ore is divided for its finite difference modelling. Distinguished from the cells of a heap by being printed in bold, apart from the contextual distinction that there will be.
Cells	Heap leach plant operator terminology for a portion of a heap that gets equipped and leached as a batch. (Irrigation does not necessarily start simultaneously on all cells, but all cells of a heap contribute to a single common drainage solution).
Cribs	Boxes built to house ore being leached to simulate heap leaching. They are typically manufactured from wood (for acid media) or concrete (for alkaline media). The height equals that of the heap to be simulated, and the cross section is sufficiently large to house a number of irrigation drippers arranged according to the dripper spacing to be used on the heap.
Diffusional path length	Refer to the definition of “Transfer Time”.
Diffusional Model	PhreeqC terminology for the hydraulic model where the ore mass is divided into a number of vertical **cells** through which the mobile moisture passes, while each mobile **cell** is associated with any number more than one lateral **cells** holding Immobile Moisture. Fickian diffusion occurs as a result of the concentration profile developing amongst the immobile **cells**. This is termed the Profiled Side-Pore Diffusion (PSDP)’

	model by Bouffard and Dixon (2001) and is also akin to that described by the 'Turner Structure' underlying the HeapSim model.
Dripper grid	Spacing between drippers in a dripper line and between dripper lines on a drip-irrigated heap, expressed in terms of length x width.
First Order Exchange Model	PhreeqC terminology for the hydraulic model where the ore mass is divided into a number of vertical **cells** through which the mobile moisture passes, while each mobile **cell** is associated with a single lateral **cell** holding Immobile Moisture. A mass transfer coefficient determines the rate of flow between the mobile and immobile **cells** for a given concentration difference. This is termed the Mixed Side-Pore Diffusion (MSPD)' model by Bouffard and Dixon (2001).
Free-milling gold	Gold that is cyanide-soluble from its ore. That is as opposed to gold that is locked in sulphide mineral which needs to be oxidised to sulphate before the gold is released in cyanide-soluble form.
Gangue	A mineral devoid of any value-mineral content.
Immobile Moisture	PhreeqC terminology for the moisture held in ore after drainage under gravity. It is termed 'stagnant moisture' by Bouffard and Dixon (2001).
In-situ	Refers to ore in the ground. 'In-situ' processing therefore refers to conducting a process on the ore without hauling it from the ground to surface.
Lixiviant	An active ingredient that facilitates the reaction required for a value-element to be extracted from the solid-phase into solution.
Mobile Moisture	PhreeqC terminology for the moisture content regarded as flowing moisture during leaching, being that amount of moisture that drains from ore under gravity after irrigation is stopped, termed 'flowing moisture content' by Bouffard and Dixon (2001).

Narrow-diameter column	A column of diameter that is narrower than the dripper spacing of the heap being simulated. Hence the column diameter is smaller than a single unit cell of the heap being simulated.
Ore	Rock that contains a value-element.
Transfer time	Defined as: $\Theta = \frac{R^2}{D_e} = \frac{R^2 \tau_\delta^2}{D\theta_{imm}}$
Unit cell	Smallest sub-unit into which a heap can be divided which still retains the essential features of the whole heap. Illustrated in Figure 6 on page 32.
Shift	PhreeqC terminology for the advance of the solution inventory of a single **cell** to a neighbouring **cell** during a single finite difference time step.
Value-bearing mineral	A mineral bearing a value-element.
Value-element	An element contained in the ore which bears economic value. The leaching of this element is desired in order to recover it in saleable form.

1 INTRODUCTION

1.1 SIGNIFICANCE OF HEAP LEACHING

Heap leaching facilitates more than 10 percent of world gold production and about 20 percent of world copper production, (Dhawan et al., 2012; Kappes, 2002). A growing number of copper and uranium deposits in southern Africa have been evaluated for heap leaching in more recent years, of which some have been implemented, (van Staden, 2011).

Heap leaching is typically the techno-economically favoured process for projects involving ore of low grade that make the cost of milling unfeasible, or small reserves, or projects exposed to high risk, which cannot yield a safe return on a large capital investment, (Kappes, 2002; Petersen, 2016).

For heap leaching, the ore is merely prepared by secondary or tertiary crushing (as opposed to milling) at about one order of magnitude lower energy cost than milling. The trade-off in return for the lower processing cost is in the leaching kinetics which require a solid-liquid contact time of at least several weeks, up to a year or more.

Discounting anecdotal heap leaching practice from the sixteenth century, heap leaching can be considered as having started with the processing of uranium ores during the 1950's (Ghorbani et al., 2016). Since then, heap leaching has also been applied to copper ores, the first instance being the Bluebird mine in 1968 according to (Ghorbani et al., 2016; Kordosky, 2002), although Scheffel (2002) mentions the leaching of uncrushed copper ore at Bisbee, Arizona and a 'discussion' of heap leaching that had taken place during 1922. The first heap leaching application for gold is considered to be the Cortez operation in Nevada, USA, which commenced in 1969 .

1.2 THE 'MACROSCOPIC' CHARACTERISTICS OF HEAP LEACHING

A block flow diagram of a generic heap leaching process appears in Figure 1. Crushed ore is usually agglomerated in a horizontal rotating drum where it is wetted with an aqueous stream recycled from the downstream circuit. Wetting renders the ore sticky so that the fines lump together with coarser particles, which effectively narrows the size distribution. This avoids, or at least reduces, the possibility for deposition of separate

pockets of predominantly coarse particles and other pockets of predominantly fine particles, which would hinder the efficiency of solid-liquid contact during leaching. For leaching in acid media, concentrated acid is usually also added to the agglomeration drum (as 'curing' acid) to rapidly satisfy most of the gangue acid demand. If this is not done, the leaching time would be extended considerably if this acid demand is to be satisfied by irrigation.

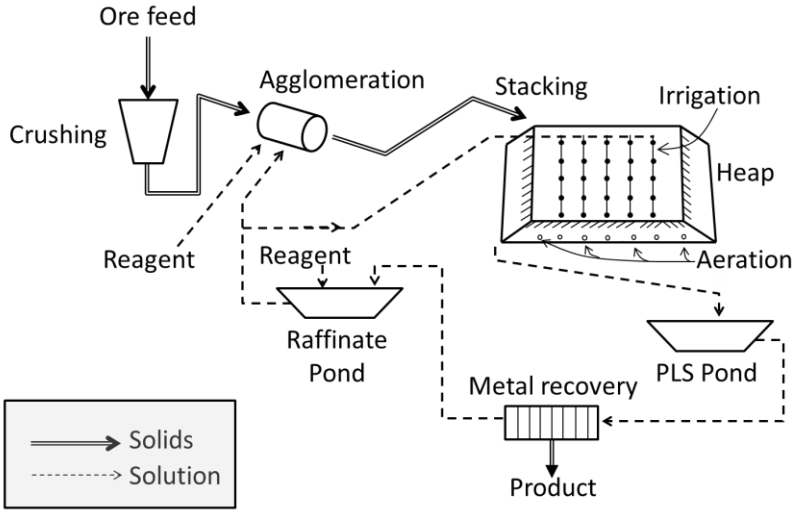

Figure 1. Block flow diagram of generic heap leaching process

Special pads are prepared upon which to stack the ore, more details of which are provided in section 3.6 below.

The agglomerates are transported to be stacked on the pads, typically using a conveyor travelling on the pad in front of the advancing face, as discussed in more detail in section 3.6 below. However this could also occur by trucks or conveyors travelling on top of the heap, throwing the agglomerates over the advancing edge.

An irrigation system is installed on top of the heap, consisting of either in-line drippers arranged on a square or rectangular grid, or sprinklers arranged on the heap to provide even coverage with solution. Once a sufficient area has been created on top of the heap, and/or an appropriate time period has elapsed for the curing of the ore with the acid added during agglomeration, irrigation might be initiated while the rest of the heap gets stacked. Alternatively irrigation might start only once an entire heap has been stacked.

The irrigation solution consists of the barren stream recycled after recovery of the value metal from the leach solution, and reagent replenishment. It percolates through the heap, leaching the valuable metal from the ore on its passage downward, until it exits the heap at the bottom and gravitates down the sloped, lined pad into the collection trough and into the pregnant leach solution (PLS) pond. From there it reports to the metals recovery section, the barren solution being re-directed to the raffinate pond. Irrigation solution, as well as solution for the agglomeration step, are usually obtained from the raffinate pond.

However, more complex arrangements are also used where an intermediate leach solution (ILS) pond is added (not shown in Figure 1 above). In such an arrangement, lower-tenor solution draining from older heaps is directed to the ILS pond. The ILS, which still contains a small amount of unreacted leach reagent, is used to irrigate newer heaps. The solutions draining from the new heaps are directed to the PLS pond. In such a circuit, the agglomeration solution and at least part of the irrigation solution can be drawn from the ILS pond. An ILS pond is used to effect an extent of counter-current leaching between multiple heaps of different ages, the raffinate (being more concentrated in lixiviant) and the ILS (being of moderate lixiviant concentration).

The heap leaching of sulphidic ores also involves the incorporation of microbial cultures into the ore during agglomeration, and aeration is provided from below the heap. This sustains the oxidation reactions, catalysed by the microbial cultures, which turn the sulphides into aqueous-soluble sulphates. This renders the heap leaching process highly heterogeneous, relying on effective transfer processes between solids, solution, gaseous/vapour phase as well as microbial cultures.

All processes upstream and downstream of the leaching heaps are conducted in continuous fashion. However, each individual heap leaches in batch mode, as a result of which conditions inside a heap vary spatially throughout the heap and over the course of time, Dixon and Petersen (2003).

1.3 SIMULATION AND DESIGN OF HEAP LEACHING

The metallurgical behaviour of minerals from different mines is too variable to be completely predictable from fundamental principles. Hence the achievable extent and rate of extraction that can be expected from the heap leaching of a mineral sample needs to be verified experimentally, (John, 2011; Scheffel, 2002). The most practical and economical way that has been devised to date for simulating the conditions in a heap has been 'column leaching', whereby a crushed sample of the ore is irrigated in a metal or polymer cylinder. During a testwork campaign, the effect of parameters such as the composition of the irrigation solution and the irrigation flux (in such units as $L/(h.m^2)$) on the extraction rate, extraction extent and reagent consumption are determined, (Scheffel, 2002).

Ideally, this should provide information from which the specifications for a heap leaching plant design can be drafted. However, it has been widely reported that column leaching yields optimistic results, (Afewu, 2009; Kappes, 2002; Lizama et al., 2004; Muller and Newton, 2008; Scheffel, 2002).

To compensate, heap leach design engineers commonly apply empirical experience-based factors to the extraction curve generated during column leaching, to predict the heap leaching performance. For example, the ultimate extent of extraction obtained in a column is multiplied by 0.8, and the time required to achieve that extraction is doubled to predict the performance of a heap, as illustrated in Figure 2 below, (Jansen and Taylor, 2002; John, 2011; Scheffel, 2002; Scheffel et al., 2016). A more complete example of the heap specification approach appears in Appendix A.

As an illustration of just how arbitrary the empirical scale-up rules are, no indication is found in the literature of whether the empirical factors ought to be adapted depending on the type of ore being leaching (gold or copper or uranium), the types of reactions occurring (non-oxidative or bacterial-oxidative), or the type of irrigation used (dripper or sprinklers).

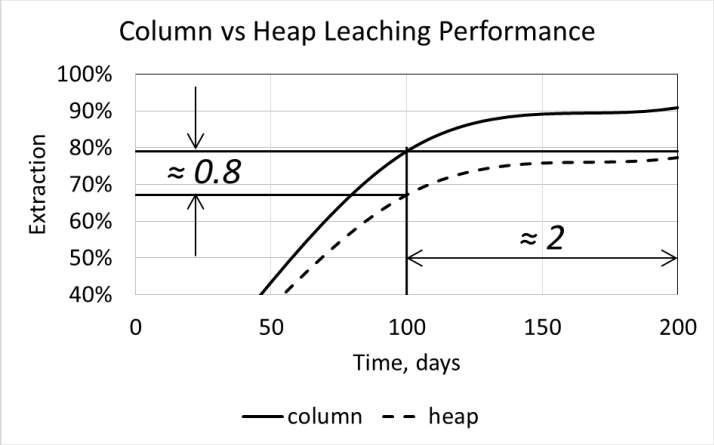

Figure 2. Illustration of application of empirical scale-up parameters

2 PROBLEM STATEMENT

The empirical experience-based scale-up factors used in current heap leach design practice are not related to the fundamental parameters affecting the process. That impacts negatively on the confidence with which commercial-scale heap leaching design specifications are drafted. It further makes it difficult to suggest measures for improving heap leaching performance, or to suggest how laboratory methods ought to be adapted to provide more realistic predictions of commercial-scale heap leaching performance.

3 CURRENT KNOWLEDGE AND UNDERSTANDING OF HEAP LEACHING

3.1 CLASSIFICATION OF HEAP LEACHING.

3.1.1 Heap leaching versus other leaching processes

It is useful to place heap leaching within the context of the larger field of hydrometallurgy: Hydrometallurgy relies on the contacting of the ore with an aqueous phase that carries a lixiviant. The lixiviant is the the active ingredient that facilitates the reactions required for the value-element to leach from the solid phase into the aqueous phase. Once an element is in solution, it is separated from other value-elements and from impurities for which a multitude of processing options are available. Ultimately, the value element is won from the solution phase into a saleable form such as metal or salts (Paynter, 1973).

The focus in this text is on the leaching step, in particular that of heap leaching. A classification of leaching processes is provided in Table 1, with additional literature references provided in the notes below the table. It illustrates the features that distinguish different processes from one another. It also shows the commonalities and differences between heap leaching and the other leaching options. The characteristics of heap leaching are underlined for clarity.

Heap leaching is one type of ‘percolation leaching’ processes, which are characterised by the ore remaining stationary while the leach solution is brought in contact with it, (van Staden, 2011). This is as opposed to ‘agitated leaching’, where the ore is milled sufficiently fine to be suspended in the leach solution in an agitated reactor.

Furthermore, the entire ore is heap leached, as opposed to some of the other processes listed in the table where a concentrate of the value-bearing mineral is produced from the ore first.

Since no containment is provided around the heap, the irrigated solution drains freely from the ore which means the ore seldom gets entirely saturated by the leach solution. This is as opposed to vat-leaching where the ore is contained in a chamber in which the ore gets flooded by leach solution, or the agitated leaching processes where the ore (or its concentrate) is mechanically suspended in the leach solution in an agitated reactor.

The processing features indicated in Table 1 are meant to represent the most common operational practices, although some exceptions from these can occur.

In-situ leaching is performed on ore in the ground. It relies on the ore being sufficiently permeable for solution to pass through it under hydraulic pressure applied from injection wells drilled into the ore. Leach solution pumped into the injection wells permeates through the porous ore, for the laden solution to be collected in collection wells.

For in-situ mining, a small proportion of the ore is mined to provide space for expansion for the principal part of the ore body when it gets blasted in-situ. Without hauling the ore to surface, leach solution is pumped onto the blasted ore in-situ and the laden solution is collected from the bottom end of the ore body.

Dump leaching is conducted on run-of-mine (ROM) waste, which is to say the ore remains in the form in which it is hauled from the mine after blasting, without further size reduction or agglomeration. This could therefore include pebbles of a metre in diameter.

Table 1. Classification of leaching processes

SIZE REDUCTION OF THE ORE								
none	blasted in-situ (not hauled)	none, blasted ROM ore 30-1,000 mm	crush 5-100 mm	mill 0.25-1.0 mm	crush 0.5-10 mm	milled <1mm		
SIZE- CLASSIFICATION OF THE CRUSHED/MILLED PRODUCT								
none						s. cyclone in closed circuit with mill		
UPGRADING OF THE ORE								
none				sometimes concentration		none	concentration	
CONDITIONING OF THE ORE (OR CONCENTRATE THEREOF)								
none			u. agglomeration, s. curing, s. inoculation	agglomeration	s. agglomeration	none	s. regrinding	roasting
CONTACT MEANS BETWEEN LEACH SOLUTION AND ORE (OR CONCENTRATE THEREOF)								
percolation						agitated in a leach reactor		
EXTENT OF LIQUID INGRESS INTO ORE (OR CONCENTRATE THEREOF)								
unsaturated					saturated	suspended		
PROCESS IDENTIFICATION								
in-situ leaching	in-situ mining	dump leaching	heap leaching	agglomerated fines heap leach	vat leaching	agitated leaching of whole ore	agitated leaching of concentrate	agitated leaching of calcine

Notes to Table 1:

Terminology: s: sometimes, u: usually
References for more detail:

In-situ leaching: (Corrans et al., 1972; Ghorbani et al., 2016; Gorbatenko, 2018; John, 2011; Maerten, 2013; Sarangi and Beri, 2000).
In-situ mining: (Bahamondez et al., 2016; Corrans et al., 1972)
Dump leaching: (Corrans et al., 1972; Ghorbani et al., 2016; John, 2011).
Heap leaching: (Ghorbani et al., 2016; John, 2011)
Agglomerated fines heap leaching: (John, 2011; Williams et al., 2018 (accessed))
Vat-leaching: (John, 2011; Nunez and Zarate, 2011)
Agitated leaching of whole ore, (Nisbett et al., 2009).
Agitated leaching of concentrate: (Gericke et al., 2009; Lundstrom et al., 2009)
Agitated leaching of roasted calcine: Wyethe et al. (2008).

In agglomerated-fines heap leaching, the ore is milled to less than 1mm or as small as 250µm. Sometimes the entire ore is then agglomerated to form pellets through which solution can be percolated when piled into a heap. Alternatively, a concentrate is produced from the milled ore, and the concentrate is then agglomerated. The agglomerates are stacked on a pile, and leaching proceeds as for heap leaching.

Vat leaching is conducted on ore that is crushed somewhat finer than for heap leaching, with 80 percent passing typically 0.5 to 10 mm. The ore is loaded into containers and leached by passing leach solution slowly upward through the ore so as not to fluidise it or carry fines into the overflow, (Nunez and Zarate, 2011). This means that the ore is flooded with leach solution, as opposed to heap leaching where the ore remains unsaturated with leach solution.

3.1.2 Leaching in heaps, columns and cribs

In this text, “heaps” will be reserved for piles of stacked ore without any side support, as illustrated in Figure 1 on page 2 for normal heap leaching practice. That would typically be a commercial scale heap, but could also include pilot scale heaps.

“Columns” or “narrow-diameter columns” is reserved for the laboratory apparatus in which heap leaching is usually simulated. These are usually cylindrical columns with a diameter smaller than the spacing that would typically be used for the drippers on drip-irrigated heaps. (Commercially-used dripper spacing is discussed in section 3.7.3 below). Irrigation in a column is applied with a single dripper. The irrigation might be applied at a single point on the axis of the column, or might be spread out over the cross sectional area by a layer on the surface or a mechanical device that disperses the irrigated solution over the cross sectional area.

“Cribs” is reserved for the boxes in which heap leaching is simulated at a larger scale, but still with side support. These boxes are typically built from wood with a square or rectangular cross section, sufficiently large to fit a number of drippers at the dripper spacing to be used on the heap being simulated, such as those used by Bouffard and West-Sells (2009) which had a 2.4m x 2.4m cross section and were 6.7 m tall. The drippers were laid on a 460 mm x 460 mm grid.

3.2 CHEMICAL STOICHIOMETRY

3.2.1 Displacement reactions

Displacement reactions involve merely the exchange of one or more elements without any change in oxidation state, and therefore without the requirement for an oxidant or reductant. An example is the leaching of malachite in sulphuric acid, (Bingol and Canbazoglu, 2004; Ghorbani et al., 2016):

$$Cu_2(CO_3)(OH)_{2(s)} + 2\ H_2SO_4 = 2\ CuSO_{4(aq)} + CO_{2(g)} + 3H_2O \quad [1]$$

Since oxygen plays no role in this reaction, there is no requirement for air supply to the heap, as opposed to some of the redox reactions discussed below. The only requirement is acid to be supplied during curing (discussed in section 3.4), and/or via the leach solution irrigated from the top.

Other examples of similar reactions are the acid dissolution of tenorite (CuO) and the silicate chrysocolla :

$$CuO_{(s)} + H_2SO_4 = CuSO_{4(aq)} + H_2O \quad [2]$$
$$Cu_2H_2Si_2O_5(OH)_4\ (s) + 2H_2SO_4 = 2CuSO_{4(aq)} + 2\ SiO_2 + 5H_2O \quad [3]$$

The above reactions are all acid dissolution reactions, yielding one mole of copper (Cu) in solution for each mole of sulphuric acid (H_2SO_4) consumed.

The water-dissolution of copper sulphate ($CuSO_4$), if it should ever occur in an ore, involves no acid, proceeding according to:

$$CuSO_{4(s)} = CuSO_{4(aq)} \quad [4]$$

It requires no other reagents, other than water to dissolve it to the aqueous form.

An example of a displacement reaction for uranium leaching would be that of the acid leaching of secondary uranium (which bears U in the 6-valent form), (Merritt, 1971):

$UO_3 + 3H_2SO_4 = H_4[UO_2(SO_4)_3] + H_2O$ [5]

3.2.2 Simplified redox reactions

Redox reactions can be broken down into half-reactions whereby electrons and protons are gained or yielded. One reagent serves as an electron donor and the other as electron acceptor, and therefore some of the elements involved undergo a change in oxidation state.

For the purpose of this section, in most cases only the overall reactions will be written, with species appearing in molecular (as opposed to ionic) form, with oxygen in each case being the electron acceptor, and all elements reverting to the highest oxidation state (i.e. sulphide-sulphur coverting to sulphate and iron reverting to the ferric form). A more detailed analysis of the reaction mechanisms involving other possible intermediaries than oxygen, sulphate and ferric is provided in section 3.3. Heat of formation and free energy of formation values for the species participating in these reactions were obtained from Weast and Astle (1980), except for that of $CuFeS_2$ which was obtained from Johnson and Steele (1981), and that of the gold and cyanide species which were obtained from Marsden and Jouse (2006).

In the case of free-milling gold, i.e. being cyanide-soluble from its ore, (Rademan and Groot, 2012), leaching occurs according to the following oxygen-consuming reaction (Stange, 1999):

$$Au + 2\,NaCN + {}^{1}/_{4}\,O_2 + \tfrac{1}{2}\,H_2O = NaAu(CN)_2 + NaOH \quad [6]$$

$$\Delta H = -95.2\ kJ/gmol\text{-}e^-$$

$$\Delta G = -67.5\ kJ/gmol\text{-}e^-$$

However gold occurs in the ore in concentrations measured in singular parts per million, hence the oxygen requirement is very small. Therefore, no specific design features are provided for introducing oxygen into the heaps of gold-bearing ore. The oxygen that is naturally present in the voidage and which is dissolved in the irrigation solution satisfies the oxygen requirement for this reactions, (Kappes, 2002).

The heap leaching of sulphide minerals (for example any of the copper sulphides or gold-bearing pyrite) requires more oxygen, (Dutrizac and MacDonald, 1974). It is common for ores bearing several percent of chalcocite (Cu_2S) to be heap leached. Watling (2006) listed 23 historical and operational (in 2006) heap leach operations treating copper sulphide ores. These ores contain around 1 percent copper, implying a chalcocite (which contains 80% Cu) content of 1.25 percent and a sulphide (S^{2-}) content of around 0.25 percent or 250 parts per million. At the end of this sub-section, comparative copper-to-mineral and sulphide-to-copper content figures will be provided for the leaching of chalcopyrite.

The stoichiometry of chalcocite leaching is shown to proceed according to two steps, the first (equation [7]) involving only the extraction of copper, followed by further extraction of copper and simultaneous sulphide oxidation (equation [8]), with the over-all stoichiometry shown in equation [9]:

$Cu_2S + {}^1/_2\, O_2 + H_2SO_4 = CuSO_4 + CuS + H_2O$	$\Delta H = -95.2$ kJ/gmol-e^- $\Delta G = -67.5$ kJ/gmol-e^-	[7]
$CuS + 2O_2 = CuSO_4$	$\Delta H = -99.2$ kJ/gmol-e^- $\Delta G = -78.4$kJ/gmol-e^-	[8]
$Cu_2S + {}^5/_2\, O_2 + H_2SO_4 = 2CuSO_4 + H_2O$	$\Delta H = -98.4$ kJ/gmol-e^- $\Delta G = -76.2$ kJ/gmol-e^-	[9]

The enthalpy of formation (ΔH) indicates the amount of heat generated or consumed by the reaction, with $\Delta H<0$ indicating an exothermic reaction. The free energy of reaction (ΔG) indicates how well the reaction is thermodynamically favoured, with $\Delta G<0$ indicating a thermodynamically spontaneous reaction. These values are presented per mole of electrons exchanged to render all reactions comparable on the basis of a common extent of oxidation/reduction. It can be seen that 4 electrons are accepted by every mole of oxygen (O_2) that reduces to water (H_2O), since two O-atoms with average oxidation state of zero revert to two water molecules in which the O-atoms possess an oxidation state of 2+.

To provide a qualitative, order-of-magnitude indication of the difference in intensity of oxygen supply required between gold and sulphide-copper leaching, two hypothetical

cases can be compared. Consider firstly the heap leaching of gold ore bearing 3 g/t Au (equal to that of the ore studied by Bouffard and Dixon (2007)), that leaches to completion in 105 days (the average of the 60-150 day range indicated specifically for gold heap leaching by Scheffel (2002)). Using the stoichiometry of reaction [6] and assuming no other oxygen-consuming reactions are occurring, the average rate of oxygen consumption is:

$$\frac{3\ \text{g Au}}{\text{t ore}}\ \text{x}\ \frac{16\ \text{g O}_2}{197\ \text{g Au}}\ \text{x}\ \frac{1}{105\ \text{d}} = 0.0023\ \frac{\text{g O}_2}{(\text{t ore})(\text{d})}$$

Compare that to an ore bearing 1.5% Cu as chalcocite (equal to that of the Girilambone ore studied by Scheffel (2002)), equalling 1.9% Cu_2S (being 19 kg/t), leaching to completion in 225 days (the average of the 150-300 days indicated specifically for chalcocite heap leaching by Scheffel (2002)). Using the stoichiometry of reaction [9] and assuming again that no other oxygen-consuming reactions are occurring, its average rate of oxygen consumption is:

$$\frac{19\ \text{kg Cu}_2\text{S}}{\text{t ore}}\ \text{x}\ \frac{80\ \text{kg O}_2}{159\ \text{kg Cu}_2\text{S}}\ \text{x}\ \frac{1}{225\ \text{d}} = 0.042\ \frac{\text{kg O}_2}{(\text{t ore})(\text{d})} = 42{,}5\ \frac{\text{g O}_2}{(\text{t ore})(\text{d})}$$

The average rate of oxygen consumption of the sulphide leach can be seen to be larger than that of the gold leach by a factor of more than 18,000.

A very common sulphide in the ores subjected to heap leaching is pyrite, leaching according to:

$$FeS_2 + {}^{7.5}/_{2}\ O_2 + \tfrac{1}{2}H_2O = \tfrac{1}{2}\ Fe_2(SO_4)_3 + \tfrac{1}{2}H_2SO_4 \qquad \Delta H = -103\ \text{kJ/gmol-e}^- \qquad [10]$$
$$\Delta G = -80.5\ \text{kJ/gmol-e}^-$$

And another common copper-bearing sulphide is chalcopyrite, reacting according to:

$$CuFeS_2 + {}^{17}/_{4}\ O_2 + \tfrac{1}{2}\ H_2SO_4 = CuSO_4 + \tfrac{1}{2}\ Fe_2(SO_4)_3 + \tfrac{1}{2}\ H_2O \qquad [11]$$
$$\Delta H = -104\ \text{kJ/gmol-e}^-$$
$$\Delta G = -81.0\ \text{kJ/gmol-e}^-$$

Chalcopyrite contains 34 percent Cu and 35 percent S^{2-}, hence 1.0 percent Cu in an ore bearing chalcopyrite as the only Cu-bearing mineral requires 2.9 percent chalcopyrite content, which will contribute 1.0 percent S^{2-}. This is much larger than the 0.25 percent S^{2-} shown above to be contained in a chalcocite ore of the same Cu content. From equations [9] and [11] the oxidation of chalcocite can be seen to require 1.25 moles O_2 per mole Cu leached, whereas the oxidation of chalcopyrite requires 4.25 moles moles O_2 per mole Cu leached.

An example of a redox reaction for uranium leaching would be that of the primary mineral (i.e. bearing U in the 4-valent form) uraninite (Roodt and Sandenbergh, 2003). The ultimate oxidant is MnO_2 as per reaction [14], with Fe^{3+} as intermediate, according to reactions [12] and [13]:

$$UO_2 + Fe_2(SO_4)_3 = UO_2SO4 + 2FeSO4 \quad [12]$$
$$\Delta H = 7.96 \text{ kJ/gmol-e}^-$$
$$\Delta G = -32.6 \text{ kJ/gmol-e}^-$$

$$2FeSO_4 + MnO_2 + 2H_2SO_4 = Fe_2(SO_4)_3 + MnSO_4 + 2H_2O \quad [13]$$
$$\Delta H = -94.7 \text{ kJ/gmol-e}^-$$
$$\Delta G = -41.5 \text{ kJ/gmol-e}^-$$

$$UO_2 + MnO_2 + 2H_2SO_4 = UO_2SO4 + MnSO_4 + 2H_2O \quad [14]$$
$$\Delta H = -86.7 \text{ kJ/gmol-e}^-$$
$$\Delta G = -74.1 \text{ kJ/gmol-e}^-$$

3.2.3 Gangue and precipitation reactions

Since heap leaching is mostly conducted on the entire ore, as opposed to a concentrate, a heap contains a much larger proportion of minerals with no economical value than the content of value-elements. Some of the non-value (i.e. gangue) minerals are unreactive, such as quartz, (Seyedbagheri et al., 2009). On the other extreme, a mineral such as calcite ($CaCO_3$) reacts very readily and rapidly with sulphuric acid, according to:

$$CaCO_{3(s)} + H_2SO_4 + H_2O = CaSO_{4(s)}.2H_2O_{(s)} + CO_{2(g)} \quad [15]$$

yielding gypsum, $CaSO_4.2H_2O$. The presence of any mineral that reacts with acid more readily than the minerals carrying the value-element mineral detracts from the economics of a heap leaching operation. Firstly, it consumes acid for no benefit and

secondly it competes with the value-bearing mineral for acid, resulting in retardation of the rate at which the value-element is leached. Specifically in the case of calcite, its reaction with sulphuric acid yields gypsum, the precipitation of which in the heap can reduce the permeability of the heap to leach solution, reducing the extent to which leach solution is spread throughout the heap. Precipitates can also block the perforations of aeration pipes, thereby hindering the supply of oxygen in the case of oxidising leaching applications, (Ghorbani et al., 2016).

Some gangue minerals fall between the two extremes, being moderately reactive to acid, such as chlorite, $(Mg,Fe)_5Al(Si_3Al)O_{10}(OH)_8$. The moderately reactive gangue minerals consume acid relatively slowly (as opposed to the virtually instantaneous reaction of calcite), and the rate of acid consumption is proportional to the acid concentration in solution. The reactivity is related to the strength of the bond between the metal cations (other than silicon) and oxygen of the mineral crystal lattice. Higher-valence cations (such as Ti^{4+} and Al^{3+}) form stronger bonds than for example Ca^{2+} and Li^{+}, and the stronger the bond the less reactive the mineral is to acid, (Chetty, 2018; Seyedbagheri et al., 2009).

Certain reactions of gangue constituents can also yield acid, such as the precipitation of ferric iron, which has a limited solubility in aqueous solution. Its solubility decreases with increasing pH, (Dutrizac and MacDonald, 1974) and upon becoming saturated, precipitates as some form of oxy-hydroxide, (Dreier, 1999; Dutrizac and MacDonald, 1974), which can be written in terms of the generic iron-oxy-hydroxide $Fe(OH)_3$, as:

$$\tfrac{1}{2}\ Fe_2(SO_4)_3 + 3\ H_2O = Fe(OH)_3 + \tfrac{3}{2}\ H_2SO_4 \qquad [16]$$

More commonly, it is expected that iron would precipitate in a heap as jarosite (as opposed to $Fe(OH)_3$), as indicated by Rivadenaira (2011) and by Watling (2006), which includes some sulphate as part of its formula. As an example, hydronium-jarosite forms according to:

$$\tfrac{3}{2}\ Fe_2(SO_4)_3 + 7\ H_2O = (H_3O)Fe_3(SO_4)_2(OH)_6 + \tfrac{5}{2}\ H_2SO_4 \qquad [17]$$

The hydronium group (H_3O^+) can also be replaced with other cations such as K^+, Na^+, Ag^+, $½Pb^{2+}$ or others, depending on which cations occur in solution, (Dutrizac, 1984). Any one of these iron precipitation reactions are acid-producing.

3.3 MICROBIOLOGY

Under the conditions of temperature and ambient pressure prevailing in heaps, the sulphide oxidation reactions discussed in section 3.2.2 do not proceed spontaneously directly with oxygen as electron-acceptor. As is the case with the leaching of many sulphide minerals, ferric iron serves as a much more effective oxidant than oxygen, (Dutrizac and MacDonald, 1974; Ghorbani et al., 2016). The net result of reactions [10] and [11] can therefore be achieved by using ferric iron as intermediate electron acceptor. According to Rawlings et al. (2003), Watling (2006) and Rivadenaira (2011), the sulphides of copper are first converted to elemental sulphur (via poly-sulphide intermediates), for example the leaching of chalcopyrite proceeds according to:

$$CuFeS_2 + 16\ Fe^{3+} = Cu^{2+} + 17\ Fe^{2+} + 2S \qquad [18]$$

However Watling (2006) also mentions a non-oxidative leaching mechanism for chalcopyrite under acidic conditions:

$$CuFeS_2 + 4H^+ = Cu^{2+} + Fe^{2+} + 2H_2S \qquad [19]$$

Chalcopyrite leaches very slowly at near-ambient temperature, which has been attributed to passivation, although there does not seem to be final consensus on the mechanism of passivation. Based on electron- and X-ray-spectroscopy, Hackl et al. (1995) attributed the passivation that occurs to a layer of copper-enriched (i.e. iron depleted) copper polysulphide CuS_n. This study was performed at temperatures of 110°C and above, but they argued that the same should apply during oxidative leaching at lower temperatures. However, Klauber (2008) rejected the polysulphide mechanism and concluded that layers of sulphur and/or jarosite were causing the passivation. Whichever the passivation mechanism, it is generally accepted that the rate can be accelerated to economically viable levels if the temperature is raised to about 60°C or

higher (Gericke, 2012; Petersen, 2011). Pyrite and most of the other copper-sulphide minerals react more readily with ferric iron even at near-ambient temperatures, (Gericke, 2012).

Fortunately, ores universally contain iron that leaches from the ore together with the value-element, so that leaching can be achieved and sustained as long as the ferrous iron can continuously be regenerated to ferric iron, for which oxygen can be used. Furthermore, even a low concentration of iron in solution can effect oxidative leaching, (Dutrizac and MacDonald, 1974). The reaction is shown in terms of its half-reactions and standard oxidation-reduction potentials, (Weast and Astle, 1980), which add up to the over-all reaction [22]:

$17\ Fe^{2+} = 17\ Fe^{3+} + 17\ e^-$	$Eh^0 = 679$ mV $\Delta H = 40.1$ kJ/gmol-e^- $\Delta G = 74.3$ kJ/gmol-e^-	[20]
$^{17}/_4\ O_2 + 17H^+ + 17e^- = {}^{17}/_2\ H_2O$	$Eh^0 = 1{,}229$ mV $\Delta H = -143$ kJ/gmol-e^- $\Delta G = -118$ kJ/gmol-e^-	[21]
$17\ Fe^{2+} + {}^{17}/_4\ O_2 + 17H^+ = 17\ Fe^{3+} + {}^{17}/_2\ H_2O$	$\Delta H = -103$ kJ/gmol-e^- $\Delta G = -44.1$ kJ/gmol-e^-	[22]

However this reaction does not proceed at a practically useful rate under heap leaching conditions, despite it being thermodynamically favourable as indicated by the (net negative) -44.1 kJ/gmol-e^- free energy of the over-all reaction. (Granted that heap leaching conditions do not constitute the 'Standard' conditions of 1 molar activities of dissolved constituents at which Eh^0 applies). Under the moderate temperatures typically encountered in heap leaching, this reaction needs to be catalysed by minerals-metabolising micro-organisms. The mechanism whereby this occurs is summarised by Rivadenaira (2011), using the pathway of the iron and sulphur oxidiser *Acidithiobacillus ferrooxidans* as example, which is discussed in simplified terms here, with the aid of Figure 3 below.

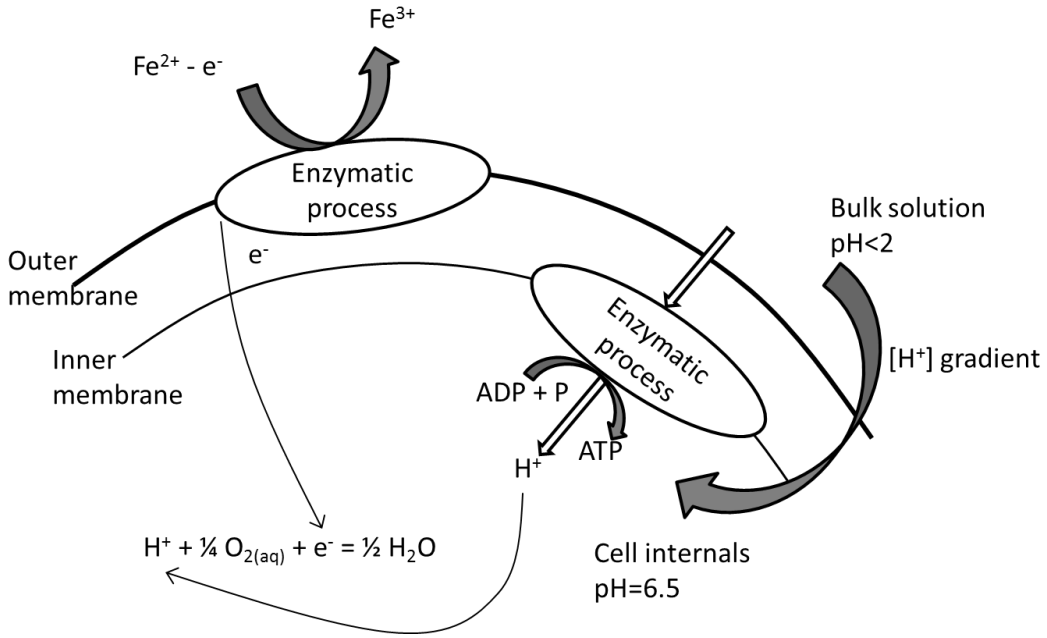

Figure 3. Microbiological mechanism for the oxidation of ferrous to ferric iron. Adapted from Rivadenaira (2011).

These micro-organisms possess an outer membrane (in contact with the bulk solution) and an inner membrane (enveloping the cell contents). Enzymes are present in each of these membranes that regulate the cell processes. (Enzymes act as catalysts to facilitate reactions that are thermodynamically favoured but kinetically slow, (Hohls, 2009)). Enzymes in the outer membrane can facilitate the oxidation of ferrous iron to ferric iron. The iron ions are therefore not absorbed into the cell. Only the electron that is released from the oxidation of a ferrous atom to ferric is absorbed by the cell. A charge balance is maintained by, at the same time, absorbing a proton. These organisms rely on an acidic environment with bioleaching processes typically operating at a pH of 1.4 to 1.6 according to Rawlings et al. (2003) and Rivadenaira (2011), and in the range 1-2 according to Watling (2006). This provides a proton concentration gradient between the bulk solution and the cell interior which is close to neutral pH of 6.5, (Rivadenaira, 2011). The proton passes into the cell via enzymes which utilise the energy harboured in the proton concentration gradient. This energy is utilised to add a phosphate group to adenocine di-phosphate (ADP) to form adenosine tri-phosphate (ATP), which serves as an energy store. The energy stored in the ATP is utilised for, amongst other functions, the fixing of carbon dioxide (CO_2) as organic carbon to grow the cell and ultimate divide

to add to the number of cells. (CO_2 is considered inorganic despite the carbon being SP3 hybridised, since the carbon in it is not bound to hydrogen or any atoms other than oxygen). From the more elaborate explanation of it given by Rivadenaira (2011), an extremely simplified and unbalanced equation for cell growth can be written as:

$$n\text{Cells} + x\text{CO}_2 + 3x\text{ATP} + \text{other1} \rightarrow (n+1)\text{Cells} + 3\text{ADP} + 3\text{P} + \text{other2} \qquad [23]$$

The energy from ATP is required for cell building since the conversion of CO_2 into organic carbon is not thermodynamically spontaneous, (Rivadenaira, 2011). Dissolved oxygen in the cell interior is combined with the proton to form water, which avoids acidification by accumulation of protons in the cell. The need for dissolved oxygen implies that the organisms are also dependent on an aerated environment. In the manner described above, the half-cell reaction [21] occurs in the cell interior, while the half-cell reaction [20] occurs outside the cell. It can be seen that [21] is a very exothermic reaction, but the micro-organism utilises reportedly only about 10 percent of that energy, the balance by implication being dissipated into the bulk solution.

This establishes a link between the microbial oxidation reaction, cell growth and CO_2 absorption. Petersen and Dixon (2007b) fitted column leaching data obtained on zinc sulphide ore to a model, and pointed out the possibility that the process could become limited by CO_2 supply. That is to say that without CO_2, no cell growth can take place, the ATP cannot be utilised and hence the oxidation process becomes governed by the rate of CO_2 supply. On the other hand, Bryan et al. (2012) found that there is not a fixed ratio between the amount of CO_2 being utilised and the amount of ferrous iron being oxidised by *A. ferrooxidans*. When the CO_2 concentration was raised above that of atmospheric air, the microbes utilised more CO_2, but did not multiply faster and did not support a faster rate of ferrous iron oxidation. And the species could withstand an extent of CO_2 starvation, requiring a minimum of 8-25 ppm CO_2 below which no growth occurred. However even at very low CO_2 levels where no cell growth occurred, it was still oxidising ferrous iron, although they did not report the quantitative data.

By a similar mechanism, the elemental sulphur formed is microbially converted to sulphate. According to Rawlings et al. (2003), most of the sulphur-oxidising bacteria can

utilise either oxygen (according to reaction [24]) or ferric iron (according to reaction [25]) as electron acceptor for this reaction:

$$S + {}^{3}/_{2}O_2 + H_2O = 2H^+ + SO_4^{2-} \quad \Delta H = -104 \text{ kJ/gmol-e}^- \quad \Delta G = -84.0 \text{ kJ/gmol-e}^- \quad [24]$$

$$S + 6Fe^{3+} + 4H_2O = SO_4^{2-} + 6Fe^{2+} + 8H^+ \quad \Delta H = -0.85 \text{ kJ/gmol-e}^- \quad \Delta G = -39.8 \text{ kJ/gmol-e}^- \quad [25]$$

In the ferric leaching of pyrite, the sulphide-sulphur converts to sulphate via thiosulphate but without elemental sulphur as intermediate, according to Sand et al. (2001), Rawlings et al. (2003) and Rivadenaira (2011), as follows:

$$FeS_2 + 14Fe^{3+} + 8H_2O = 15Fe^{2+} + 16H^+ + 2SO_4^{2-} \quad \Delta H = -0.036 \text{ kJ/gmol-e}^- \quad \Delta G = -39.0 \text{ kJ/gmol-e}^- \quad [26]$$

This also applies to other disulphides namely MoS_2 and WS_2, (Sand et al., 2001).

Watling (2006) lists more than 30 species of micro-organisms that can mediate the oxidation of ferrous iron, or the oxidation of elemental sulphur, or both. Different organisms are adapted to different temperature ranges, and mesophiles (functioning at 20-40^{o}C), moderate thermophiles (functioning at 40-60^{o}C) and extreme thermophiles (functioning at 60-80^{o}C) are distinguished.

It used to be speculated that the micro-organisms metabolise the minerals directly by releasing enzymes that assist in the leaching process. Other authors have argued that only an indirect mechanism is at work, with the micro-organisms only oxidising ferrous iron to ferric and sulphur to sulphate, and that the ferric and acid perform the leaching chemically. Giaveno et al. (2011) regard that debate as now being closed, with the indirect mechanism now being accepted universally. The hypothesis of direct enzymatic attack of the mineral surface has been discredited by the supposed enzymes never being observed or identified. Sand et al. (2001) has also demonstrated that no hypothesis for direct microbial attack is required, the observed leach kinetics and reaction products can be explained by purely chemical leaching with acid and ferric iron. Furthermore, in the complete absence of iron in solution, micro-organisms could not oxidise pyrite. Crundwell (2014) showed that the enhancement of the leaching of pyrite by micro-

organisms can be ascribed to the localised raising of the pH on the mineral surface where micro-organisms are attached. It can be seen that the leaching of pyrite according to reaction [25] produces acid, while the microbial oxidation of ferrous iron to ferric iron according to reaction [22] consumes acid. Hence the microbial ferrous iron oxidation on the pyrite surface lowers the acid concentration, which enhances the tendency of the pyrite oxidation reaction to occur by Le Chatelier's principle.

Sand et al. (2001) has pointed out that the micro-organisms occur in two states, namely either free-floating in the aqueous phase (i.e. planktonic), or attached to mineral surfaces with *extra-cellular poly-saccharide* or more generically *extra-cellular polymeric substances* (both abbreviated as EPS), which is an adhesive substance excreted by the cells. In both states they perform the same bio-chemistry. Sand et al. (2001) are of the opinion that the conditions of pH and redox potential can be more severe in the contact area between a mineral grain and an attached colony of micro-organisms than conditions in the bulk solution. In this manner, a large proportion of attached cells could accelerate the kinetics compared to the kinetics if all cells are planktonic.

Furthermore, a passivating layer of elemental sulphur forming on the mineral surfaces during its ferric leaching (in the absence of micro-organisms) could retard the leach kinetics. This is for example the case during the oxidative leaching of sphalerite (ZnS), with the elemental sulphur becoming a diffusional barrier in the absence of microbial action, (Crundwell et al., 2000). However, in the presence of sulphur-oxidising micro-organisms, this passivating layer gets removed. The presence of micro-organisms therefore enhance the reaction kinetics by these mechanisms, but they perform nevertheless only the functions of oxidation of ferrous iron and of sulphur.

In summary therefore, it is currently believed that microbes do not leach minerals ‘directly’ (i.e. enzymatically). Their only function is to oxidise ferrous iron to ferric iron, and reduced sulphur species to sulphate. However their presence can enhance reaction kinetics by creating more favourable localised conditions for leaching on surfaces to which they are attached and by removing potentially passivating layers of sulphur. Furthermore, the possibility of CO_2 starvation is not a very important parameter to consider in biological heap leaching

It is pointed out by Brierley (2001) that the conditions (notably temperature) in a heap of sulphidic ore are not well controlled and subject to spatial and temporal variability. Therefore, the consortium of micro-organisms actively participating in the oxidation reactions in a leaching heap are likely to be different from one location to another and to vary with time. However, closely controlled studies to provide quantitative data on this supposed variation is still lacking. Practical aspects such as the effect of organics (from the solvent extraction step downstream of heap leaching) on bacterial activity and over-all heap leaching performance had also not been studied in detail by the time of publication of her article. Neither has any subsequent literature been sourced which address these aspects.

Brierley (2001) advocates that the microbes can derive sufficient quantities of essential nutrients such as phosphates from the ores being leached, obviating the need for nutrient additions during bio-heap leaching.

3.4 ORE PREPARATION PRACTICE

In preparation for heap leaching, the ore is crushed to a top-size that can range from 5 mm (for the finest crush size) to 100 mm (for the coarsest crush size), as reported by John (2011). Bouffard (2005) reported crushing to less than 12-16 mm specifically for copper ores. The crushed ore is usually not classified (for example by a screen or cyclone that separates particles by size), therefore the crushed product consists of an aggregate exhibiting a particle size distribution from the top-size down to microns.

Exceptions to this have occurred, for example the separation of the coarser and finer fractions of a uranium ore, for agitated leaching of the fine fraction and heap leaching of the coarse fraction, was proposed by Mantra Resources Ltd (2010). However that was only a concept being considered at the feasibility stage of a project. Another is the experimental concept of separating the finest fraction from gold sand dump material by hydrocyclone, for agitated leaching of the finer fraction and heap leaching of the coarser fraction, (van Staden and Laxen, 1988). However that was a concept that was only tested at a small scale.

The ore is commonly agglomerated by wetting it while tumbling it in a cylinder, the rotating axis of which is tilted at typically 5-7^{o} below the horizontal, (Bouffard, 2005). The angle causes material fed into the inlet to proceed towards the outlet. Agglomeration causes the finest particles to adhere to the coarser particles, and some of the fine particles to aggregate to one another to form pellets. The agglomerator provides an excellent environment for obtaining good mixing between ore and reagents. Agglomeration renders the ore more permeable to the leach solution and air (if the latter is required), thereby improving contact between the ore and leach solution and hence the rate and extent of extraction. The leaching of gold is performed in alkaline media, and cement is often used as a binder to strengthen the agglomerates. However copper is leached in acidic media which will dissolve any cement binder. Copper ores are therefore agglomerated using only acidified water or raffinate from the metal recovery step, which can be supplemented by the addition of concentrated sulphuric acid. The aggomerates thus formed are stacked on impermeable pads without any side support of the heap. Some agglomeration can also occur during the subsequent conveyance and stacking of the ore, (Bouffard, 2005).

Curing can also be done in the case of acid leaching, whereby a significant portion of the acid required for leaching is added to the ore in the agglomerator, as opposed to adding it mostly by irrigation (Dreier, 1999). A few days are typically allowed before irrigation is commenced, to allow the reactions between the ore and curing acid to proceed close to completion before diluting the curing acid with leach solution. Curing provides a rapid means for acidifying the ore and initiating the leaching reactions. Note that up to 40 kg curing acid per tonne ore could be required according to Bouffard (2005). Administering such a quantity of acid to a heap by means of irrigation alone would require a relatively long time, thereby negatively affecting metal production. For example, to achieve even a modest acid addition of 10 kg/t by irrigation to a 6m high heap with bulk density of 1.5 t/m^3, using a relatively high irrigation rate of 12 L/(h.m^2) (which equals 0.012 m^3/(h.m^2)) and acid concentration in the leach solution of 6 g/L (i.e. 6 kg/m^3) as indicated by Scheffel et al. (2016), the time (t) required to administer 10 kg/t acid by irrigation can be calculated from:

$$10\ \frac{\text{kg acid}}{\text{m}^3\text{solution}}\ \text{x}\ 0.012\ \frac{\text{m}^3}{\text{h.m}^2}\ \text{x}\ \frac{\text{m}^3}{1.5\ \text{t}}\ \text{x}\ \frac{1}{6}\frac{1}{\text{m}}\ \text{x}\ t\frac{\text{h}}{1} = 10\ \frac{\text{kg acid}}{\text{t}}$$

from which it follows that t = 750 h = 31 days.

If the ore is destined to be bio-leached in the heap, a microbial inoculum can also be added to the agglomerator.

Agglomeration does not produce an entirely uniform product. A representation of the composition of a typical agglomeration product is shown in Figure 4 below, based on illustrations provided by McClelland and Van Zyl (1988), by Bouffard (2003b) and by Bouffard (2005).

.

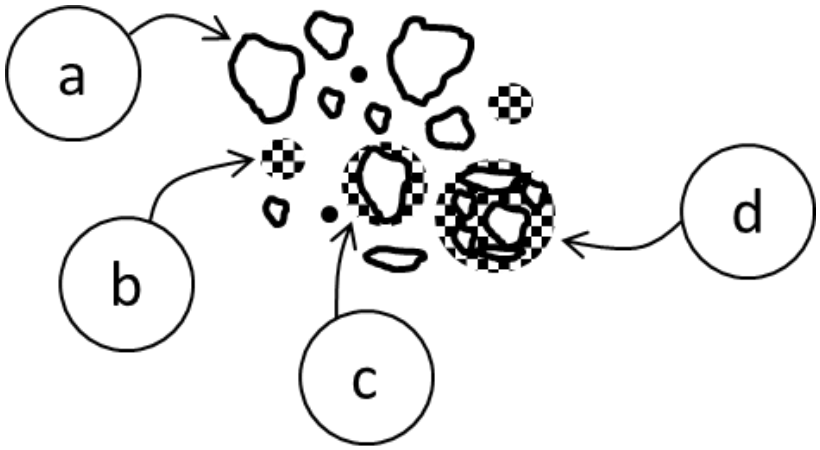

Figure 4. A typical composition of an agglomeration product.
Shown here are (a) individual particles (termed 'truffles' by Bouffard (2003b)), (b) particles bound together in a pellet, (c) fines bound to the outside of a coarser particle, (d) finer and coarser particles bound together.

3.5 PAD PREPARATION PRACTICE

For heap leaching, pads are usually prepared on relatively flat ground with a 1-2 percent slope, (Ulrich et al., 2003), in the direction in which the leach solution is required to drain. However, in areas where the topography is undulating, the contours of the landscape can be filled with ore in a so-called 'valley-fill' approach, (Scheffel, 2002). The pad surface is rendered 'impermeable' by constructing it of compacted clay, covered by a geomembrane, (Scheffel, 2002), being typically a polymer such as high density poly-ethylene (HDPE), (Ghorbani et al., 2016). While no material can truly be made totally impermeable, the pad design specifications are aimed at meeting and exceeding the regulatory requirements from which the maximum permissible rate of seepage through the pad would be determined. A summary of the applicable legislation is provided by Geldenhuys (1988), which aims to ensure such aspects as environmental protection, rehabilitation, safety of working conditions, erosion control and protection of water resources.

A drainage layer, consisting of coarsely crushed rock that is resistant to the leach medium, is placed over the geomembrane. Drainage pipes are embedded in this layer during its construction, and if the heap is to be aerated, the aeration pipes are also embedded in this layer. The pads are then ready to receive the ore, to be placed on top of the drainage layer.

3.6 HEAP STACKING PRACTICE

Heaps can be stacked in so-called ‘dynamic’ or ‘on-off’ manner, with the ore being removed from the pad after leaching for disposal elsewhere, for fresh ore to be stacked on the same pad. The alternative is to use ‘permanent’ pads, where the leached residue is left on the pad indefinitely, with the possibility of fresh ore being stacked on top of it.

It used to be common practice to stack ore on the heaps by trucks that drive over the heap surface and tip their loads at the advancing face. Due to the compaction that vehicle traffic causes on heaps, it has become much more popular to convey the ore to the heaps using conveyors which travel either on the heap, advancing with the stacking front, or the conveyor system travels across the leach pad, retracting away from the advancing face being stacked.

In their review, Ghorbani et al. (2016) indicate the typical stacking height for heaps ranging from 2 to 10m. However, the stacking of heaps up to 100m (similar to the typical heights used for dump leaching), also used to be practised. But that has become less common due to the efficiency of extraction being found to decrease with increasing heap height, (Ghorbani et al., 2016; Johnson, 1975). In his patent, Johnson (1975) advocates the stacking of ‘thin layers’ of only 0.5 to 1m thick. Something between these extremes have been adopted by industry with heights of 2-10 m high now being regarded as ‘thin layers’, to set it apart from the up to 100m high heaps used previously. However, successive layers (or ‘lifts’) are often stacked, with freshly mined ore being stacked on top of layers that have been leached to completion. A multitude of such lifts stacked on top of one another can still lead to an over-all height of several tens of meters, (Scheffel, 2002).

Figure 5 below examines the stacking process in more detail, illustrating the example where stacking occurs from a conveyor belt travelling on the pad in front of the advancing face of the heap. The heap is not stacked in layers from the bottom up, instead the top of the conveyor is maintained constantly at the intended stacking height, or a little higher. Ore is projected from the conveyor against the upper part of the advancing slope, the ore then rolls down the slope and spreads itself in a layer over the

advancing slope. Once the new layer has grown by some centimeters, the conveyor is retracted by a small distance and the process is repeated.

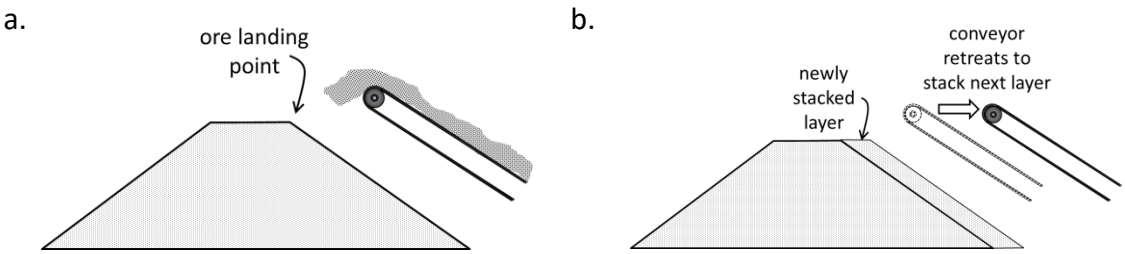

Figure 5. Simplified illustration of conveyor stacking.
(a) upon initiation of a new layer, (b) upon completion of a new layer
Reproduced from Van Staden and Petersen (2018a)

The manner in which ore gets arranged on the heap during this mode of stacking is not homogenous. Even after agglomeration, the ore still exhibits a size distribution, leading to segregation and stratification during stacking. Segregation refers to the predominance of coarser particles along the lower parts of the pile and of finer particles in the upper parts. Stratification refers to the formation of successive layers of coarser and finer materials along the advancing face, sloping at the internal angle of friction of the ore. These phenomena will be discussed in greater detail in section 3.16.3 below.

According to Ghorbani et al. (2016), heaps possess bulk densities ranging typically from 1,400-1,900 kg/m^3 on a dry basis. Bouffard and West-Sells (2009) determined the bulk density of a heap immediately after stacking as 1,450 kg/m^3 and 2,010 kg/m^3 upon completion of leaching. Most rocks exhibit a true density of 2,600-3,000 kg/m^3, (Taggart, 1954), hence the average can be taken as 2,800 kg/m^3. The volume-fraction of voidage θ_{void} in a heap can hence be calculated from:

$$\theta_{void} = 1 - \frac{\rho}{\rho^*} \qquad [27]$$

with ρ being the bulk density (dry basis) and ρ^* the true (rock) density. Taking ρ^* as 2,800 kg/m^3, it follows that a heap with bulk density of 1,400 kg/m^3 possesses 50 percent voidage and a heap with bulk density of 2,000 kg/m^3 possesses 29 percent voidage.

3.7 HEAP IRRIGATION PRACTICE

3.7.1 Flooding

An outdated means of getting the leach solution to percolate through heaps used to be to create shallow ponds on the heap surface. These would be periodically filled with leach solution, and given time to drain before getting re-filled. However, because it saturates the upper surface, it prevents air convection through the heap, which is a reason mentioned by Scheffel (2002) for it being discontinued.

3.7.2 Sprinklers

One common irrigation method in use is sprinklers (or so-called 'wobblers' that create larger droplets than regular garden-type sprinklers to minimise evaporation), first adoped at Bagdad in 1970, (Kordosky, 2002). Sprinklers provide even distribution of the solution over the heap surface, and can be used in rainy climates to deliberately enhance evaporation in order to retain a water balance, (Kappes, 2002). However, the impact of the droplets from sprinkler irrigation has been found to compact the uppermost layer of the ore, reducing its permeability, (Walsh et al., 1997). Furthermore, operational staff working on the heap surface irrigated by sprinklers need to wear safety gear to protect them against the sprays of leach solution, (Scheffel, 2002).

3.7.3 Drip irrigation

Drip irrigation was reportedly first used at the Johnson Camp copper mine in Tucson, Arizona, USA in 1976, (Bikerman et al., 2007; Kordosky, 2002).

It gained popularity since it reduces evaporation in dryer climates and can reportedly lead to increased heap temperature, thereby accellerating the leach kinetics, (Kordosky, 2002). Furthermore, drippers can be covered with sheets to further reduce evaporation and preserve heat and are more flexible in allowing variations in the application rate. However, drip irrigation is recognised as presenting an uneven distribution of the leach solution, which reduces the efficiency of solid-liquid contact, and Kappes (2002) estimated that the first 1m of ore below the surface may not be uniformly contacted by leach solution. The use of drippers also requires clarification of the leach solution to prevent blockages in the drippers, (Scheffel, 2002). Nevetheless, the perceived benefits of drip irrigation (or rather the sprinkler irrigation problems that it avoids) must weigh

more than the disadvantages of drip irrigation, since from the references cited here it seems drip irrigation has become very common if not the norm.

3.7.4 Dripper spacing and unit cell defined

Bouffard and West-Sells (2009) reported drippers being placed on a 0.46m x 0.46m grid to apply an irrigation rate of 6 L/(h.m^2) to both a crib with 2.4m x 2.4m cross section and to a pilot heap of gold-bearing ore. van Staden et al. (2017a) reported the use of 0.5m x 0.5m dripper spacing on commercial oxide-copper heaps to irrigate at a rate of 7.4-13.4 L/(h.m^2), although double that spacing was used at times when logistical problems caused a shortage of irrigation materials. Ilankoon and Neethling (2016) mention industrial dripper spacings being typically 0.5m x 0.5m to 0.5m x 1.0m while van Staden et al. (2017c) reported the use of a 0.4m x 1.0m dripper spacing for the heap bioleaching of copper-sulphide ore at an irrigation rate that was varied between 1 and 5 L/(h.m^2).

For the purposes of design, simulation and modelling of drip-irrigated heap leaching, it is convenient to define a dripper unit cell. A unit cell is the smallest sub-unit into which a physical body can be divided, so that the unit cell still exhibits all the features of the whole. It therefore follows that if the behaviour of a unit cell is understood, or can be predicted then, (in principle), the behaviour of the whole can be understood or predicted from a mere summation over the number of unit cells comprising the whole. For example, the philosophy of simulating heap leaching at laboratory scale by irrigating ore contained in a tall column is based on the principle that a column should represent a unit cell of a heap.

Figure 6 below shows the upper surface of a heap with drippers arranged on it in a rectangular pattern. A unit cell of this heap has a cross section equal to the dripper spacing, centred around a dripper, with its borders halving the distance between the central dripper and neighbouring drippers. Since physical and chemical conditions vary with height in a heap, the vertical dimension of the unit cell cannot be divided into any smaller portions that would exhibit all features of the whole. Therefore, vertically, the unit cell extends over the entire height of the heap that is being simulated.

However, it is common to perform laboratory column leaching in cylindrical columns. In that case, to provide the same cross sectional area per dripper as the case would be with a rectangular column of dimensions *L* x *W*, the equivalent cylindrical column would have a radius (R_{eq}), or diameter (Dia_{eq}), to be calculated from:

$$R_{eq} = \sqrt{\frac{L.W}{\pi}} \quad ; \quad \text{OR} \quad Dia_{eq} = \sqrt{\frac{4.L.W}{\pi}} \qquad [28]$$

The reasons why this is often not so, and its effect, is discussed in section 3.16.2.

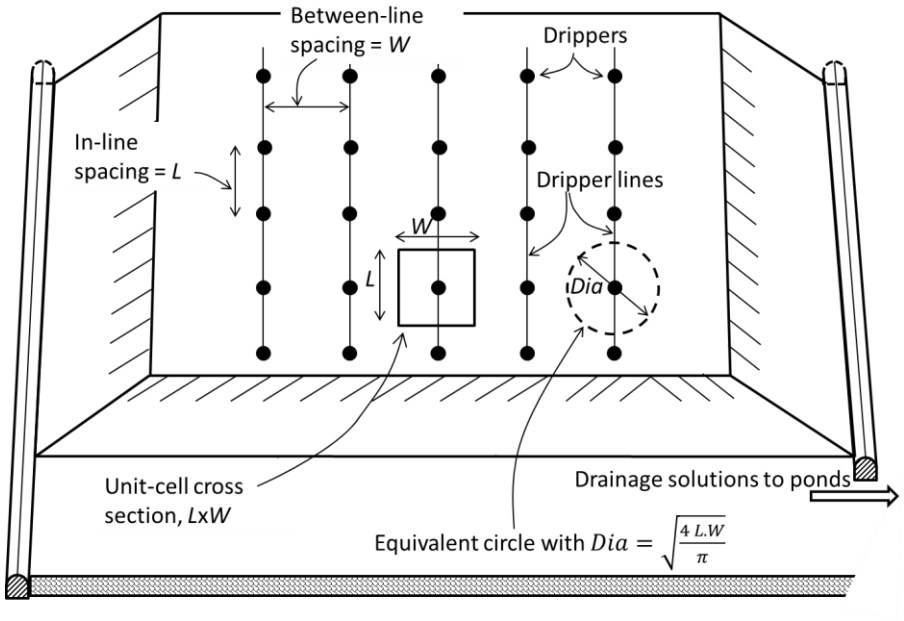

Figure 6. Illustration of heap unit-cell and dripper grid diagonal.

3.7.5 Extent of saturation

Bouffard and West-Sells (2009) reported that an operating heap of gold-bearing ore possessed 14 mass percent moisture throughout, except near the bottom where it reached 20 percent. Kappes (2002) provided a rough indication of 20 percent moisture in a heap.

The voidage (θ_{void}) represents the maximum volume-fraction that solution can occupy in a heap. In order to calculate that limit as a mass percentage, assume a liquid-phase density of 1,000 kg/m^3. One cubic meter of ore contains ρ kg ore (dry basis) and voidage

of 1000. θ_{void} litres. If the total voidage is filled with solution, the mass fraction of solution in the (saturated) heap, W_{sat}, is:

$$W_{sat} = \frac{\theta_{void}}{\frac{\rho}{1000} + \theta_{void}} \quad [29]$$

In Table 2, the saturated moisture content is calculated for a few cases that consider the extremes of bulk density observations provided above, assuming ρ^* = 2800 kg/m^3.

Table 2. Saturated moisture contents for hypothetical cases

Case	Bulk density, ρ [kg/m^3]	Voidage, θ_{void}, vol-fraction	Saturated moisture content, W_{sat}, mass%
1	1,400	0.50	26
2	1,600	0.43	21
3	1,800	0.36	17
4	2,000	0.29	13

From Table 2, it can be seen that a heap possessing a moisture content of 14 percent is likely to be unsaturated, unless its bulk density increases to about 2,000 kg/m^3. A heap holding 20 percent moisture will be saturated with moisture if its bulk density exceeds about 1,600 kg/m^3.

3.8 HEAP AERATION PRACTICE

Since the heap leaching of copper sulphide ores require a relatively large flow of oxygen, heap leaching operators have found it beneficial to use blowers to mechanically force air into heaps of sulphidic copper ore. The requirement for blowing air into heaps where sulphide oxidation is required was also theoretically confirmed by Bartlett and Prisbrey (1995). They used as an example the oxidation of pyrite to liberate refractory gold, considering cases of 0.5 up to 2.0 weight percent pyrite in the solid phase prior to oxidation. They showed for example that for ore bearing only 0.5 percent pyrite, in the absence of any mechanical blowing of air into the heap, oxidation can occur only about 3.3 m into the heap over 2 years, with the rate being completely limited by the rate of oxygen diffusion into the heap.

The air supply is therefore distributed through aeration pipes installed typically 1m off the bottom of the heap, (Walsh et al., 1997). Typically low-pressure air (7-21 kPa) is supplied by fans or low-pressure blowers into the aeration pipes made of high-density poly-ethylene (HDPE) that are perforated for distributing the air along the length of the pipes, (Ghorbani et al., 2016).

3.9 METAL RECOVERY PRACTICE

3.9.1 Copper recovery

Copper used to be cemented from heap leaching solutions by cementation with iron, according to, (Agrawal and Kapoor, 1982):

$$Cu^{2+} + Fe_{(s)} = Cu_{(s)} + Fe^{2+} \quad [30]$$

However, cementation produced a very impure product, bearing typically only 65-85 percent copper, requiring further pyro-refining, (Ghorbani et al., 2016).

The advent of large-scale copper solvent extraction (SX) in combination with electrowinning (EW) is regarded as a revolutionary advance in copper hydrometallurgy, enabling the on-site production of copper cathode of high quality, (Ghorbani et al., 2016). An illustration of the SXEW process is provided in Figure 7 below. In the extraction step, the copper-bearing PLS is mixed counter-currently with an organic extractant (suspended in an aliphatic diluent) that is highly selective for copper, exchanging two protons for each copper molecule, according to the following equation where “R-“ designates an organic compound, (Readett and Townson, 1997):

$$2R\text{-}H + Cu^{2+} = R_2\text{-}Cu + 2H^{+} \quad [31]$$

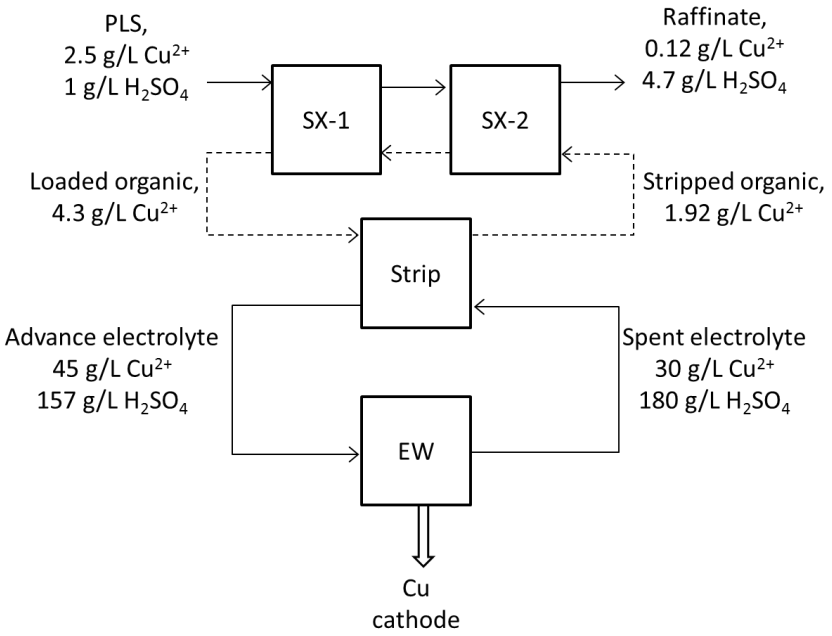

Figure 7. Illustration of the SXEW process
Based on an example provided by Readett and Townson (1997).

The organic-aqueous mixture is then allowed to separate, utilising the natural immiscibility of the organic and aqueous phases. With the lower-density organic phase floating on top of the aqueous phase, the two are separated with relative ease.

Copper can be stripped from the organic phase with relatively strong acid solution (spent electrolyte) (for which Readett and Townson (1997) indicated an acid concentration of 180 g/L), by the reversal of reaction [31]. This makes the combination of the extraction and stripping steps acid-neutral. The advance electrolyte thus obtained contains essentially only copper, with the other elements having remained behind in the PLS.

The copper is electrowon from the advance electrolyte by electrolysis, according to:

Anodic reaction:

$H_2O = ½ O_2 + 2H^+ + 2e^-$ $\Delta H = 143$ kJ/mole-e^- [32]

$\Delta G = 119$ kJ/mole-e^-

Cathodic reaction: [33]

$Cu^{2+} + 2e^- = Cu^0$ $\Delta H = -32.2$ kJ/mole-e^-

$\Delta G = -32.5$ kJ/mole-e^-

Over-all reaction: [34]

$Cu^{2+} + H_2O = Cu_{(s)} + ½O_2 + 2H^+$ $\Delta H = 110$ kJ/mole-e^-

$\Delta G = 86.2$ kJ/mole-e^-

This can be seen to be an acid-producing reaction, yielding 2 protons (or one mole of H_2SO_4) per mole of Cu extracted. For this reason, acid consumed in the process of leaching of acid-soluble copper minerals such as malachite is not regarded as a true consumption. While one mole of H_2SO_4 is consumed per mole of copper leached (see reactions [1] to [3]) another mole of H_2SO_4 is regained during its recovery as metal during SX-EW.

Therefore, where copper is recovered by acid leaching and SXEW, a distinction is made between total acid consumption (TAC) over the leaching step and gangue acid consumption (GAC), according to:

$$\left[\begin{matrix}\text{GAC}\\ [\text{kg/t}]\end{matrix}\right] = \left[\begin{matrix}\text{TAC}\\ [\text{kg}_{\text{acid}}/\text{t}_{\text{ore}}]\end{matrix}\right] - \left[\begin{matrix}\text{cumulative Cu}\\ \text{extraction, } [\text{t}_{\text{Cu}}/\text{t}_{\text{ore}}]\end{matrix}\right] \times \left[\frac{\text{molar mass of acid}}{\text{molar mass of Cu}}, \left[\frac{\text{t}_{\text{acid}}}{\text{t}_{\text{Cu}}}\right]\right] \quad [35]$$

In the case of the oxidative bioleaching of sulphidic copper minerals, acid is produced by sulphide oxidation while it is consumed by some of the gangue reactions during the leaching step. It might be hard to distinguish between the contributions of these two reactions to the over-all acid balance of the leaching step. The combination of those two is therefore termed the net acid consumption (NAC), which replaces the GAC term in [35] for the case of sulphide leaching applications.

3.9.2 Gold recovery

Historically gold-cyanide was recovered from solutions by zinc cementation, according to Muhtadi (1988):

$$2Au(CN)^{2-} + Zn = 2Au + Zn(CN)_4^{2-} \quad [36]$$

This process is still recommended for cases where a high Ag/Au ratio (more than 5:1) exists in the PLS. However, where that is not the case, granular activated carbon is used to adsorb the gold-cyanide from solution. The solution emanating from carbon adsorption is recycled to the heap leach. The gold is eluted from the activated carbon, the carbon is regenerated and recycled to the adsorption circuit. In gold recovery there is no regeneration of lixiviant as is the case in copper leaching, where each mole of copper yields a mole of acid from SXEW, (Muhtadi, 1988).

3.9.3 Uranium recovery

In the case of uranium heap leaching, the dissolved uranium is typically recovered from the PLS by SX, using an extractant that is selective for uranium. This can be preceded by ion exchange (IX), which operates on the same chemical principles as SX but the functional groups responsible for the exchanges are held in solid polymer beads. IX is more suited to recovering low concentrations of the valuable species from solution. The resin is stripped into a smaller volume of solution which hence bears a higher concentration of it. This higher-concentration eluate proceeds to SX where its concentration is upgraded further. A saleable uranium product is ultimately recovered from the solution by precipitation, as a uranium salt such as ammonium di-uranate [$(NH_4)_2U_2O_7$] or uranium peroxide (UO_4), (Van Tonder and Edwards, 2012). As in the case of gold, no leach reagent is regenerated from the recovery.

3.10 PROCESSES OCCURRING DURING HEAP LEACHING

3.10.1 Introduction to processes

Based mostly on sketches and information provided by Dixon and Petersen (2003), by Bouffard (2003b), by Giaveno et al. (2011) and by Ghorbani et al. (2016), the visualisation of the processes occurring in a heap are shown in Figure 8 below. It explores increasing levels of detail from the macroscopic heap scale to the microscopic scale of mineral grains and microbial cells.

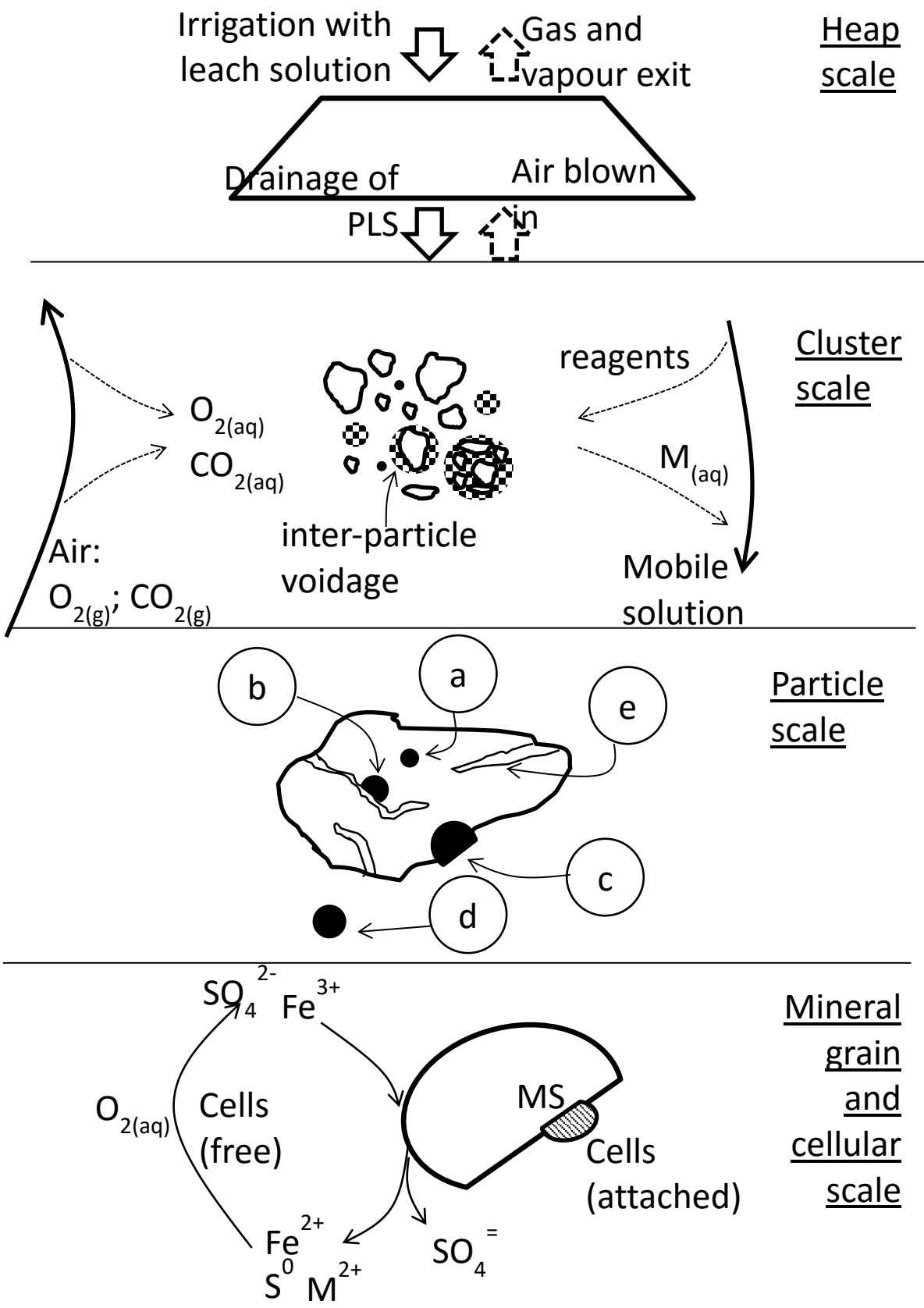

Figure 8. Illustration of in-heap processes

3.10.2 Heap scale

At the macroscopic scale, two flows occur, namely leach solution that is applied at the top and drains to the bottom, and air supplied from the bottom with a mixture of air and water vapour exiting from the top. The supply of leach solution from the top is a universal feature of all heap leaching operations. It serves to supply leaching reagent into the heap, and to carry dissolved constituents from the heap out via the drainage. Air is supplied only in cases where sulphide minerals are being bioleached.

Heat also gets exchanged between the heap and the fluids entering and leaving it. If sulphide oxidation occurs in the heap, a significant amount of heat will be generated. The reactions that generate most of the heat are those involving the reduction of oxygen (according to reaction [21]), as can be seen from the ΔH values of reactions [6] to [11] which all range around 100 kJ being evolved per mole electrons. This energy could potentially be harnessed for raising the temperature in the heap (which in turn could enhance the leaching kinetics), as shown by Dixon (2000). However, it requires the balancing between irrigation and aeration rates to minimise the energy being lost from the heap in the heated solution, the heated gas phase and water vapour.

3.10.3 Cluster scale

A cluster consists of a collection of particles and agglomerates as illustrated in Figure 4 on page 27. The leach solution does not envelop each individual particle in the heap. In section 3.11, evidence will be provided that the majority of the solid phase is bathed in immobile solution. Therefore, reagents carried in a flow channel need to diffuse from the flow channel through the immobile solution, passing via the inter-particle voids in order to arrive at the individual ore particles.

Constituents dissolved from the solid phase need to diffuse in the opposite direction to reach the mobile solution channel, to be carried towards the drainage at the bottom of the heap.

Oxidative reactions make use of bioleaching which utilises the principles discussed in section 3.3. Oxygen being carried in the air stream that is passing via the voids in the

heap needs to dissolve into the aqueous phase in order to be available for absorption into the cells of the micro-organisms.

3.10.4 Particle scale

The various reagents required for leaching need to pass via an increasingly tortuous pathway from the mobile solution first through the inter-particle voids amongst particles and agglomerates. It then needs to penetrate the bound agglomerates to reach individual particles within the agglomerates. Some of the mineral grains may be fully liberated amongst the ore particles. However the leaching reagents need to penetrate pores in individual particles to reach those minerals that are held inside particles. For example, Ghorbani et al. (2013) showed that a combination of diffusion and leaching of sphalerite (ZnS) grains occurs along the cracks and pores of >5 mm particles submerged in ferric iron solution.

3.10.5 Mineral grain and cellular scale

For leaching to occur, the leach reagents need to reach the surfaces of the mineral grains. In Figure 8 on page 38, the example is shown of ferric iron leaching a sulphide mineral oxidatively, according to the stoichiometry and microbiology discussed earlier. The same would apply to sulphuric acid that is required for the leaching of acid-soluble minerals. As discussed in section 3.3, the micro-organisms responsible for oxidation of ferrous iron and sulphur could occur suspended in solution, with the ferric iron and sulphuric acid they produce diffusing to the mineral surfaces. Alternatively the micro-organisms could be attached to some of the mineral grains, producing their products directly on the mineral surface.

3.11 HEAP FLUID DYNAMICS, HYDROLOGY AND MECHANICS

3.11.1 Definition and relevance of fluid dynamics and hydrology

Szekely and Themelis (1971) point out that the kinetics of heterogenous reactions (such as leaching reactions) rely on both the intrinsic reaction kinetics between the reactants and the hydrology of the system (i.e. the manner in which contact is established between the different phases). Therefore in what follows, it will be seen that heap leaching models firstly adopt a type of hydrology, and then superimpose the reaction

kinetics upon it by means of source terms that describe the appearance and disappearance of species into and out of solution.

For the purposes of this study, fluid dynamics is concerned with the velocity (which is a vector with magnitude and direction) at which fluids flow as a result of forces acting upon them. Hydrology is related, but refers specifically to the manner in which solution infiltrates the porous bed of ore on a heap, moves through it and establishes contact between the solids and fluids.

The solution irrigated onto a heap and (if oxygen is required) the air blown into a heap, carry the necessary reagents into the heap and reaction products from the heap. The leaching reactions can only occur as rapidly as the necessary reagents arrive at the reaction sites. Furthermore, the leached products can only be collected as rapidly as they report to the drainage solution. Therefore, the manner in which contact is being established between the ore, the liquidous and gaseous fluids and the reagents carried in them determines the over-all heap leaching performance.

Based on field observations and experimental evidence, the hydrology of heap leaching has been characterised in various ways. In order to facilitate calculations and predictions of heap leaching performance, various means have been proposed for the visualisation of the ore matrix and the flow through it. The various observations, the visualisations following therefrom and the related theoretical concepts are elaborated on in sections that follow.

However the basic principles of surface tension, capillary forces and diffusion are first introduced.

3.11.2 Surface tension and contact angle

Molecules within the bulk of a solution experience on average equal attractive and repulsive forces from the other molecules surrounding them, as illustrated in Figure 9 below. However, molecules at the surface have these forces exerted upon them only by the neighbouring molecules in the bulk of the solution, but not from the side of the surface that is open to the outside environment, causing tension at the surface. This surface tension, γ, has units of [Force per Length], such as N/m, and gives rise to the

meniscus. The surface tension can be reduced if the liquid surface were to curve, or spread out over a longer distance by covering (i.e. 'wetting') a solid surface, (Atkins, 1978; Norgaard and Nygaard, 2014).

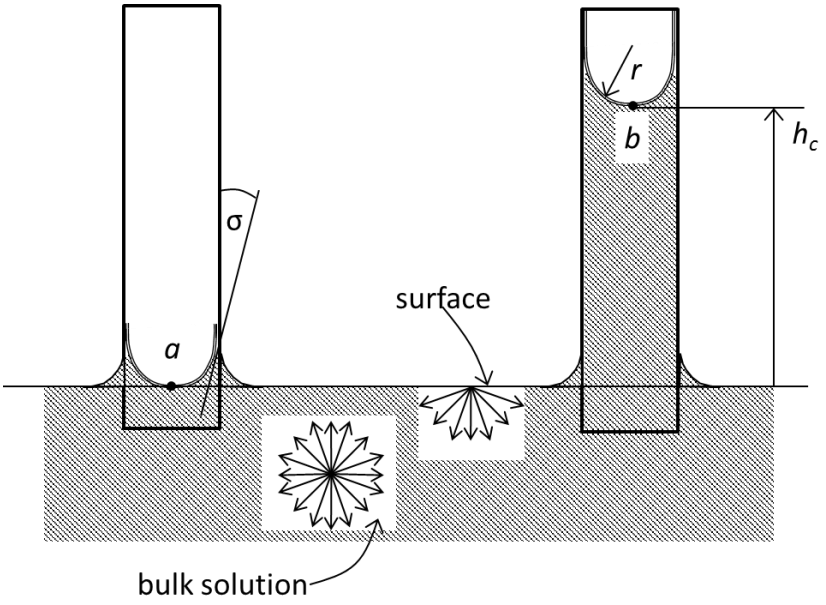

Figure 9. Liquid being lifted into a capillary

When a solution gets in contact with a solid surface that is initially dry, the forces acting between the solution and solid phase results in the solution adopting a certain 'contact angle' between the solution and solid. This angle cannot be predicted, but can be experimentally measured, as discussed by Ethington (1990). Distinction is made between the sessile contact angle (σ_s), advancing contact angle (σ_a) and receding contact angle, (σ_r). As shown in Figure 10 below, σ_s is measured for a stagnant droplet while σ_a and σ_r are measured at respectively the advancing and receding ends of a droplet in motion over the solid surface. The contact angle is measured between the solid surface and the tangent to the edge of the droplet, on the liquid-side. Examples of contact angles measured by Ethington (1990) between water and surfaces of the minerals silica and biotite appear in Table 3. It can be seen that the contact angle with silica was variable, while that on biotite was consistent between repeated measurements. However, the

authors did not venture to offer an explanation for the variability of the contact angle with silica.

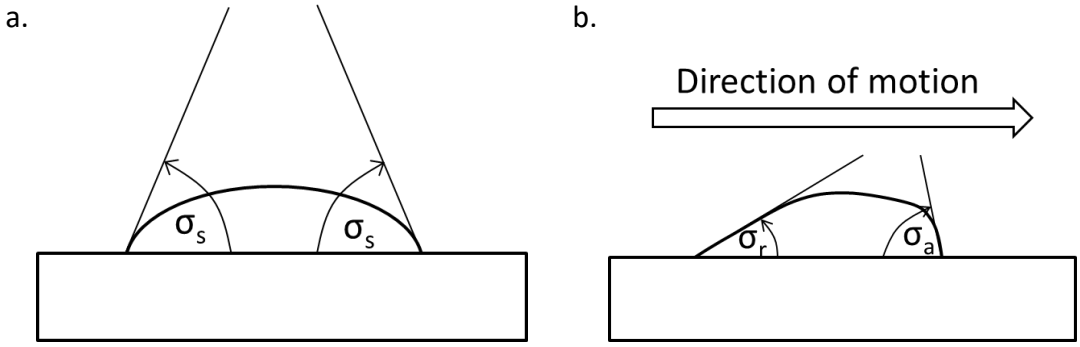

Figure 10. Illustration of contact angle.
(a) sessile (σ_s) and (b) advancing (σ_a) and receding (σ_r)

Table 3. Examples of contact angles between water and mineral surfaces

	Silica (SiO_2)	Biotite (K,Mg,Fe,Al-silicate)
Sessile (σ_s)	29-42°	9°
Advancing (σ_a)	39-41°	11°
Receding (σ_r)	8-10°	0°

Note: The measurements were repeated on two crystals of each mineral type, hence the ranges for silica (the angles measured on 2 biotite crystals were consistent).

3.11.3 Capillary action

The combination of liquid surface tension and contact angle between liquid, solid and air leads to the phenomenon of capillary action. As will become clear in the sections that follow, capillary action plays an important role in the manner in which solution becomes distributed in a bed of particulate solid material. It is therefore an important determinant for establishment of contact of the ore in a heap with the leach solution irrigated over it.

Figure 9 on page 42 shows the tip of a tube being immersed into a liquid. With the liquid meniscus initially at point (a), the meniscus is at the same elevation as the level of the

liquid outside the tube, hence there is no hydraulic pressure head acting at point (a). However, the surface tension in the liquid tends to spread the liquid over the surface of the tube, moving the solution column up into the tube. This continues until the downward gravitational force on the liquid in the column equals the upward force caused by the surface tension. The ultimate height to which the column moves up in the tube, h_c, is the capillary head. The contact angle is σ, hence the vertical component of the force caused by surface tension (γ) is $\gamma.\cos(\sigma)$. The length of the contact between solution and solid is the inner circumference of the tube with radius r, the solution density is ρ and the gravitational acceleration is g. The liquid column pushes up into the tube until the sum of forces acting on it are zero, i.e.

(vertical surface tension component)		(length of solid-liquid contact)	+ (gravity) = 0
[N/m]	x	[m]	+ [N]
$-\gamma.\cos(\sigma)$	x	$2\,\pi\,r$	+ $(\rho.\pi r^2 h_c)g$

$$= 0$$

which, upon re-arangement, results in (Batchelor, 2000; Norgaard and Nygaard, 2014):

$$h_c = \frac{2.\gamma.\cos(\sigma)}{\rho g r} \quad \text{or} \quad \rho g h_c = p_c = \frac{2.\gamma.\cos(\sigma)}{r} \qquad [37]$$

Therefore the liquid at position (a) in Figure 9 on page 42, before starting to move up the tube, can be said to be subjected to a capillary pressure p_c, (acting opposite to the direction of gravity), of magnitude $\rho g h_c$, which in turn depends on γ, σ and r according to equation [37].

The order of magnitude of crushed ore particle sizes that will exhibit significant capillary action in the pores formed between them can be calculated. Consider firstly an agglomerate or particle cluster formed from particles of similar size as might occur in Figure 11(a) below. Assume the particles to be spherical of diameter D. If packed together so that they are touching, they form a void between them, the diameter of which is of the order of a small sphere fitting between them of diameter d. The equilateral triangle with side length D connecting the three centre points has internal

angles of 60° between them. The lines connecting the centre points of the larger spheres with the centre point of the small sphere halve those angles, which therefore equals 30°.

a. b.

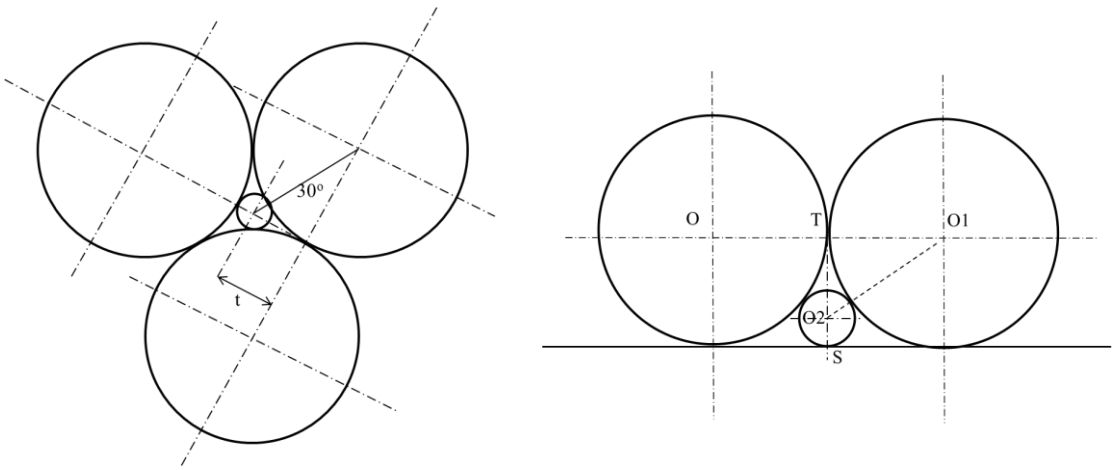

Figure 11. Approximate size of capillaries.
(a) between three touching spheres of equal diameter, (b) between two touching spheres and a large surface

From trigonometry follows:

$\text{Sin}(30) = ½ = t/(d/2+D/2) = 2t/(d + D)$ hence $t = (d+D)/4$ [38]

Further, from Pythagoras:

$t^2 + D^2/4 = (D/2+d/2)^2 = (D + d)^2 / 4$

and upon substitution of *t* from [38] and re-arrangement follows:

$d = \frac{2-\sqrt{3}}{\sqrt{3}} D = 0.155\, D$ (rounded to 3 decimals).

Consider secondly the voids formed between small particles attached to a much larger particle, as might occur in agglomerates of type (c) and (d) in Figure 4 on page 27. This can be represented by particles of diameter *D* arranged side by side on a flat surface as shown in Figure 11(b) above. The magnitude of the void formed between the small particles and the flat surface is of the order of *d* (i.e. the smaller sphere in Figure 11(b) above). The length of line *T*-*O*2 euals (*D* – *d*)/2 and the length of line *O*1-*O*2 equals (*D* + *d*)/2. Applying Pythagoras over the triangle *O*1-*T*-*O*2 yields:

$$\left(\frac{D}{2}\right)^2 + \left(\frac{D-d}{2}\right)^2 = \left(\frac{D+d}{2}\right)^2$$

From which follows:

$D^2 = 4\,d.D$ with non-zero solution of

$d = D/4$.

To calculate the capillary heads that can form between particles of different sizes, use a water surface tension of γ = 72.8 mN/m at 20°C as per Batchelor (2000), and an average sessile contact angle between silica and water listed above of 36°. The results of the calculations appear in Table 4.

Table 4. Calculated capillary heads formed between dry particles

Particle diameter, mm	Void radius, mm	Capillary head formed in void, mm
Between spherical particles of equal diameter		
0.0260	0.0020	6,000
0.125	0.010	1,241
1.25	0.10	124
6.32	0.49	25
12.5	**0.97**	**12.5**
28	2.17	6.0
Between small particles attached to a much larger particle		
0.0160	0.0020	6,000
0.125	0.0156	769
1.25	0.156	77
6.33	0.790	15
9.80	**1.23**	**9.8**
14.7	1.84	6.5
25.0	3.13	3.8

Surface tension is a function of temperature and of electrolyte concentration in solution, which would cause these values to deviate from those shown in Table 4. It decreases with increases temperature and, in most cases, increases with increasing concentration although it can also decrease, (Chen et al., 2017; Weissenborn and Pugh, 1996).

However, it changes by less than 10 percent over a one molar increase in concentration or 20 degrees change in temperature. Leelamanie and Karube (2013) found the contact angle to vary only slightly with concentration of electrolyte in solution.

Is is observed that three particles of 26µm diameter attached together, or particles of 16µm attached to a much larger particle, give rise to capillary head of the order of the entire height of an average heap (according to the information in section 3.6).

For particles of equal diameter smaller than 12.5 mm, the capillary head is larger than a single particle diameter. The same applies to 9.8 mm particles attached to a much larger particle (according to the information in section 3.1, the top-size for heap leaching can be up to 100 mm). Particles smaller than that size will form capillaries that exert a capillary head larger than a particle diameter, hence a cluster of particles of that size and smaller can be expected to be bathing in immobile moisture, since the capillary force caused by the voids between then would be greater than the weight of the water under gravity.

3.11.4 Diffusion

Fick's first law of diffusion states that the flux (*J*) is proportional to the free diffusivity (*D*), and to the gradient of concentration (*C*) along the spatial dimension (*r*), from the position of higher concentration to the lower concentration, namely:

$$J = -D\frac{\partial C}{\partial r} \qquad [39]$$

3.11.5 Tortuosity and effective diffusivity

The free-diffusivity *D* of chemical species that can be found in text books relates to its diffusion in the stated medium, under the stated conditions and in the absence of any obstruction or boundaries to the solution space. To describe diffusion through solution contained in a porous bed requires consideration of the fact that connectivity between spatially separated parts of the solution is restricted to passage via the pores, that the shortest path connecting two points in the solution phase is not a straight line, and that the more tortuous the pores, the greater the constriction that it effectively poses to diffusional transport.

The common approach towards diffusion through porous media has been to ascribe to the entire porous bed (i.e. solid, void and solution-filled portions together) an effective diffusivity D_e, so that in [39], D would be replaced by D_e and ∂C is the concentration difference between two points in the porous bed separated by a (straight-line) distance ∂r apart, (Gommes et al., 2009b; van Genuchten, 1985; Zalc et al., 2004). No distinction is made between the porosity of individual particles and the porosity between particles, the entire mass is treated as homogenous, exhibiting a single average porosity. Whether the concentration C is expressed in terms of moles per volume of porous bed or per volume of solution or per volume of pores needs to be stated clearly, but does not affect calculations, provided consistency with the convention adopted is maintained. An example of how effective diffusivity is measured can be seen from Mezedur et al. (2002), and an example of how it is applied can be seen from Bouffard (2003a).

The effective diffusivity D_e in a porous medium is expected to be lower than the free diffusivity D, as a result of the tortuous path connecting two points along the radius being longer than the straight-line distance, accounted for by a tortuosity factor τ or $\tau^2 \geq 1$. Clennell (1997) distinguishes between (a) geometric tortuosity (based on the measurable spaces between particles), 'retardation' tortuosity (based on the most flow-efficient paths provided in the porous mass), network-model tortuosity (which is relevant where a porous space is modelled as a connected network) and mere lumped-correction-factor tortuosity (mentioned again below).

Following the sketches and insights provided by Saripalli et al. (2002) and by Clennell (1997), the concepts of tortuosity and constrictivity are illustrated in Figure 12 below for (a) the idealised case providing no restrictions to diffusion and (b) a case with tortuous and constrictive porosity.

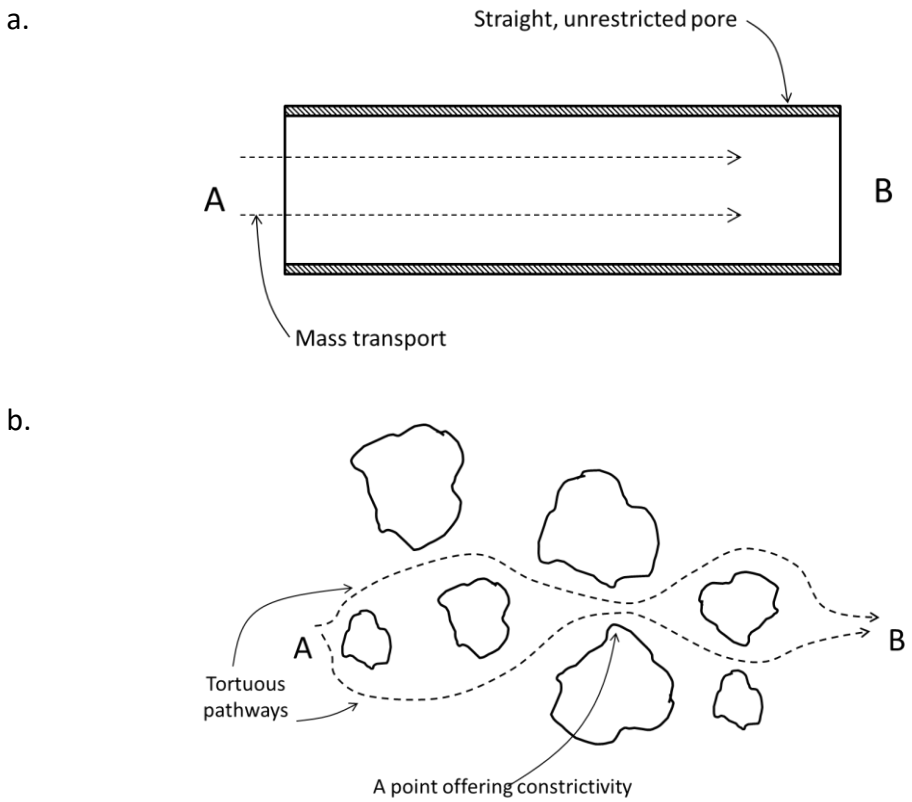

Figure 12. Illustration of diffusional transport between points A and B
(a) via an idealised straight, unrestricted pore, (b) via tortuous and constrictive porosity

The most common definition of tortuosity is the ratio of the average distance along connected pores (which is a tortuous path) through a porous maze through which diffusion occurs, to the straight-line distance, between two points in a porous medium, (Clennell, 1997). Some authors represent tortuosity by τ and others by τ^2, as another example of different conventions. There is also a definition of tortuosity which uses the reciprocal, ($^1/\tau$, in such cases the convention is that τ<1), (Clennell, 1997).

The reason for the multitude of conventions adopted regarding tortuosity and constrictivity, as pointed out by Saripalli et al. (2002), is that they are empirically defined to suit different applications for relating effective diffusivity to free diffusivity. And as a result they do not lend themselves to unambiguous measurement.

In this text, τ^2 is used throughout since it possess units of [length^2)/[length^2], as shown in the details provided in APPENDIX DAPPENDIX C. Bouffard (2003a) and Dixon (2003) have followed the same convention. Clennell (1997) discusses different models for the calculation of tortuosity, some of which use τ and others τ^2 as the symbol for tortuosity. Gommes et al. (2009a) provide more formal arguments for the power of tortuosity being strictly 2 and not 1. This convention is of no consequence in this text since the value of τ^2 or τ is not to be determined or used explicitly or compared to any published values for τ anywhere, it is always contained within a grouping of other constants or as a ratio between tortuosities at different conditions. Hence in the work here, τ^2 is merely a symbol that would have served as well as τ.

There are also other factors contributing to resistance to diffusion through porous media. The average area perpendicular to the direction of diffusion that is available for diffusion equals that of the solution-filled porosity $\theta_{imm} \leq 1$, hence the lower the moisture content in the pores, the slower diffusion can occur. Furthermore, the porous pathways can be constricted at certain points forming 'bottle-necks', for which a constrictivity factor ($\delta \leq 1$) can be introduced.

Considering all of those factors, Saripalli et al. (2002) relates D_e to D by (substituting τ^2 for the τ used by these authors, to remain consistent with the current text):

$$D_e = D \frac{\delta \, \theta_{imm}}{\tau^2} \qquad [40]$$

Other factors can also be considered that cause D_e to deviate from D, for example Lee et al. (1981) proposed the introduction of terms to account for adsorption of solubilised species to the solid phase during its passage through the pores. This would serve a similar purpose to the 'retardation factor' used by authors such as van Genuchten (1985), to account for the chromatographic effect that adsorptive minerals have on the effective rate of diffusion of dissolved species through the pores amongst particulate solids.

Despite all that refinement in the formulation of the relationship between D_e to D, ascribing values to each of the individual parameters that contribute to the retardation of diffusion is often impractical and unnecessary.

The immobile moisture content θ_{imm}, is a parameter that can be experimentally measured relatively easily. Furthermore, for lack of data from direct measurements, reasonable estimates for it can be made as per Table 2 on page 33 and the accompanying discussion. But since it is unlikely that information will be available whereby the contribution of tortuosity τ^2 and constrictivity δ can be distinguished, these two parameters can be lumped together into a new 'constrivtivity-tortuosity' τ_δ^2 to yield

$$D_e = D\frac{\theta_{imm}}{\tau_\delta^2} \quad [41]$$

It is much more common to find, in texts such as those by Bouffard (2003a) and by Dixon (2003), that all effects that retard diffusion are lumped into a single 'correction-factor-tortuosity' $\tau_{\delta\theta}^2$ to yield

$$D_e = \frac{D}{\tau_{\delta,\theta}^2} \quad [42]$$

In fact, Saripalli et al. (2002) proposed a parameter τ_s which lumps the effects of tortuosity with that of constrictivity and moisture content on fundamental grounds, with τ_s being the ratio of (a) the measured solid-water interfacial surface area in the solid under study and (b) the solid-water interfacial area of idealised (straight and unconstructed) pores of the same volume as the real pores. Their tortuosity τ_s would therefore appear in the expression for effective diffusivity D_e in exactly the same manner as $\tau^2_{\delta,\theta}$ in Equation [42].

3.11.6 Solution flow calculation using Darcy's law

According to Darcy's law, the velocity of fluid flow passing through a porous medium is proportional to the pressure gradient and permeability (k) of the ore bed, and inversely proportional to the fluid viscosity (μ). The constant k represents a combination of all characteristics of the porous solid phase that determine the ratio between flow rate and

pressure gradient, averaged over at least the spatial element *ΔxΔyΔz*, if not over the entire heap.

The equation has been found to agree with experimental observations of flow through porous media such as sand, (Batchelor, 2000). It can commonly be assumed that solution density remains constant at 1 kg/L so that the transport of solution on a volumetric basis equals mass transport since, as argued by Dixon and Afewu (2011), its possible range of variation in heap leaching applications is only about 2 percent. Then, for fluid with constant viscosity μ and density ρ passing through a porous element of dimensions *ΔxΔyΔz* in Cartesian coordinates were *z* is depth (i.e. vertical position downward), subjected to capillary pressure gradient $\nabla \boldsymbol{P_c}$, the velocity vector $\boldsymbol{v}$ can, in catezian coordinates, be calculated as:

$$\boldsymbol{u} = \begin{bmatrix} v_x \\ v_y \\ v_z \end{bmatrix} = \frac{k}{\mu} \begin{bmatrix} -\frac{\partial P_{c,x}}{\partial x} \\ -\frac{\partial P_{c,y}}{\partial y} \\ -\frac{\partial P_{c,z}}{\partial z} + \rho g z \end{bmatrix} \quad [43]$$

Subscripts *x, y* and *z* are used to indicate direction. The negative of pressure gradients are used since flow occurs from regions of high to low pressure. The permeability *k* is defined by Batchelor (2000), and the ratio $k/\mu = K$ is termed the hydraulic conductivity, as applied by Dixon and Afewu (2011).

A challenge with the solution of models based on Darcy's law is finding constitutive relationships for describing both *k* (or *K*) and p_c as functions of moisture content (θ). Correlations for providing that are discussed under Richard's equation below.

3.11.7 Computational fluid dynamics (CFD)

Computational fluid dynamics (CFD) has been used to study the manner in which fluids (leach solution from above and air from below) move through ore stacked in a heap or column. It requires the set-up of a digital map of where particles and voids are located in a bed. The digital map can be created by dividing the volume of the heap into small increments, with each increment being assigned a permeability and other relevant physical properties, as done for the 'virtual heap' simulated by Bennett et al. (2012). The

modeller then has the option of keeping all properties constant for all increments, or to programme in local variations thereof, as done by McBride et al. (2017). An alternative followed by Lin et al. (2005) was to use a computed tomography (CT) scanner to map the locations of particles in a column. Whichever way it is created, the particle map defines the pathways available to fluids for passage through the bed, as well as the resistance to flow at each location. Relations such as Darcy's law, Richard's equation and the Navier-Stokes equations, discussed further below, can then be used to calculate the flow patterns of fluids passing through the bed of solids.

3.11.8 Solution flow calculation using Richard's equation

When the accumulation of mass in a differential spacial element of a porous bed of particulate material over time is calculated, using Darcy's law to describe the fluid motion, the result is Richard's equation, (Richards, 1931). The conservation of liquid volume (being equated to liquid mass as mentioned before), in terms of moisture content (θ) in a spatial element is:

$$\frac{\partial \theta}{\partial t} = -\nabla \boldsymbol{v} \qquad [44]$$

(This states that if the downstream (outbound) flow is slower than the upstream (inbound) flow, solution will be accumulating in the spatial element).

By substituting [43] (Darcy's law) into [44], the moisture content as a function of time and position is calculated from the prevailing capillary and gravitational pressures. The result is:

$$\frac{\partial \theta}{\partial t} = \frac{\partial}{\partial z}\left[K\left(\frac{\partial h_c}{\partial t}+1\right)\right] + \sum_i S_i \qquad [45]$$

where S_i represent any source terms that might be present.

Both h_c and K are related to moisture content θ and a few different correlations have been proposed to represent the experimentally observed relationships between h_c, K and θ, including that by Brooks and Corey (1964), which provides two different functions for calculating h_c for two regions of the solution. However the correlation proposed by

Van Genuchten (1980) is more popular for modelling purposes since it provides a single closed-form relationship. Firstly, the relative saturation S_e relates moisture content to hydraulic head:

$$\frac{\theta - \theta_r}{\theta_s - \theta_r} = S_e = \left[\frac{1}{1 + (\alpha h_c)^n}\right]^m \quad [46]$$

where θ_r is the residual moisture content (i.e. the minimum moisture content to which the bed will drain under gravity) and θ_s is the saturated moisture content and α, m and n are constants to be fitted to the experimental data for each material.

Secondly, the relative hydraulic conductivity K_r (being the ratio of hydraulic conductivity K as a fraction of the maximum hydraulic conductivity which is measured under saturated conditions), is:

$$K_r = S_e^{\frac{1}{2}} \left[1 - \left(1 - S_e^{\frac{1}{m}}\right)^m\right]^2 \quad [47]$$

It has been found that many materials tested yielded the same trends. The graphs shown in Figure 13 below were constructed using specifically the parameters fitted to experimental data obtained on acid-soluble copper ore from the Mantoverde copper mine in Chile (with D_{50} of about 5 mm and D_{90} of about 10 mm, (Afewu, 2009)), namely m = 0.421; n = 7.14, $1/\alpha$ = 0.050, θ_r=0.146 and θ_s=0.380.

a. b.

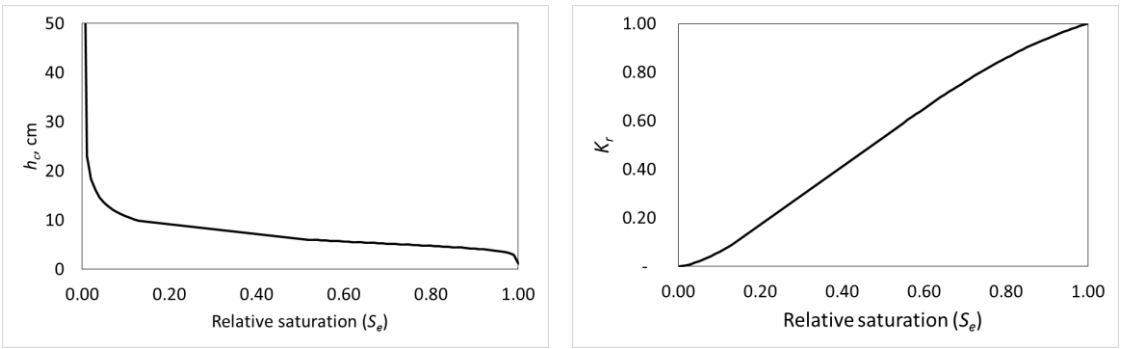

Figure 13. Relations between (a) h_c and S_e, (b) K_r and S_e.

The very low hydraulic head at high relative saturation (approaching unity) is due to the small hydraulic head exerted by the coarsest particle fractions. If the voids between the largest particles are drained, the aggregate hydraulic head increases to reflect the aggregate hydraulic head caused by the smaller particles. Finally, only the moisture adsorbed on the particle surfaces remain, yielding the exponentially growing capillary head, and this remaining moisture can only be removed by evaporation (Afewu, 2009). Therefore, while solution will be rapidly distributed throughout crushed ore particles that are initially dry, this movement will slow down and eventually cease as the saturated moisture content is being approached, (Dixon, 2003).

The hydraulic conductivity increases with increasing moisture content (represented by S_e), since only the wetted volume is available for conducting solution movement.

Examples of the use of the Richards equation includes that by Dixon and Afewu (2011) (in radial coordinates), Bennett et al. (2012) and Robertson (2017), with the latter two authors using the vertical dimension as the only spacial independent variable. McBride et al. (2017) also considered only the vertical special dimension, but utilised a source term to channel a proportion of the solution into preferential flow paths that by-pass the solid phase.

3.11.9 Solution flow calculation using Navier-Stokes and Lattice Botzman equations

The Navier-Stokes equations apply Newton's second law, namely that the acceleration of a body equals the sum of forces acting on it, divided by its mass (Dobek, 2012). In the context of heap leaching, these forces include gravity, capillary forces and frictional forces (which are particularly relevant to laminar flow, of which flow in narrow capillaries is an example). This is applied to each finite element into which the simulated heap is divided, over small time increments, in all directions of the selected coordinate system, as applied for example by Wu et al. (2010).

For example, if F_i is the sum of forces in direction i (excluding gravitational force), F_g is the gravitational force, v_i is velocity in direction i, the fluid density is ρ, and the fluid occupies a volume fraction θ in a finite element $\Delta x \Delta y \Delta z$ in cartezian coordinates where z is depth into the heap (i.e. the vertical direction downward):

$$\begin{bmatrix} F_x \\ F_y \\ F_z + F_g \end{bmatrix} = \rho\theta \begin{bmatrix} \dot{v}_x \\ \dot{v}_y \\ \dot{v}_z \end{bmatrix} \Delta x \Delta y \Delta z \quad [48]$$

These equations would typically be utilised for devising a computational fluid dynamic (CFD) model, to trace the movement over time of differential elements of matter. However, if conditions are selected such that the acceleration terms are small, equation [48] simplifies to the balance of forces that maintains a constant velocity ***v***. If the only forces present are those appearing in Darcy's lay, then [48] simplifies to [43] (Darcy's law).

The Lattice Botzmann (LB) method applies the laws of conservation to collisions between hypothetical 'particles' that the fluid is assumed to be composed of, and the walls of the porous solid phase that the fluid is passing through. Wagner (2008) can be consulted for more details of the method.

3.11.10 Field observations and experimental evidence

A heap is not uniformly wetted by the solution being irrigated onto it, and the solution is not following evenly distributed plug flow. In contrast, the solution is following preferential paths. This has been known at least from the time that Johnson (1975) filed his patent, citing preferential flow as motivation for the adoption of 'thin layer' leaching.

Until the time of the publication by Van Genuchten and Wierenga (1976), hydrologists analysed the flow of nutrients, pollutants and other solutes through soils in terms of 'convective-dispersive' flow, (alternative terminology for this is 'advective-diffusive' flow, as used for example by Leahy et al. (2004)). This assumes a combination of convection and diffusion in only one dimension, as illustrated in Figure 14(a) below on page 58. Soil hydrology deals mostly with aquifers, porous rock, sand and clay as it occurs undisturbed in the earth. In contrast, the flow of solution through heaps involves the wetting of rock that has been excavated, relatively coarsely crushed and stacked in a deliberately engineered fashion. Nevertheless, some commonalities exist so that at least some of the knowledge gained in soil hydrology could be transferred to heap leaching hydrology. The crushed ore product includes, similarly to naturally occurring aggregates, particles possessing a size distribution, it includes fines down to

micrometers in the size distribution and the solid phase remains stationary while solution moves through it, (van Genuchten, 1985).

The convective-dispersive model predicted that the concentration of a pulse of solute passing a fixed point would describe a curve that is symmetrical, i.e. having the same shape before and after the peak. However, experimental observations during pulse tests on irrigated aggregates yielded non-symmetrical drainage concentration curves. The part of the concentration curve that follows the peak exhibits a longer tailing down in concentration than the ramp-up in concentration before the peak. Van Genuchten and Wierenga (1976) then offered a theoretical analysis of how the concentration of the tracer element in the drainage would vary over time, if part of the moisture content in the bed of aggregate is immobilised.

They modelled such a bed as consisting of two compartments side-by-side, as shown in Figure 14(b). Mobile solution was passing through the one compartment, while the solution content of the other was immobile. No solution passed between the compartments, but the tracer could diffuse between the two. No concentration gradient was assumed in the immobile solution, as if it was perfectly mixed. A ‘mass transfer coefficient’ α (which can actually be termed a diffusivity), was defined whereby the ease of diffusion between the two compartments was specified. Selecting $\alpha=0$ eliminates the participation of the immobile solution while $\alpha \rightarrow \infty$ causes the mobile and immobile solutions to assume the same tracer concentration. Any other value for α represents something between those two extremes.

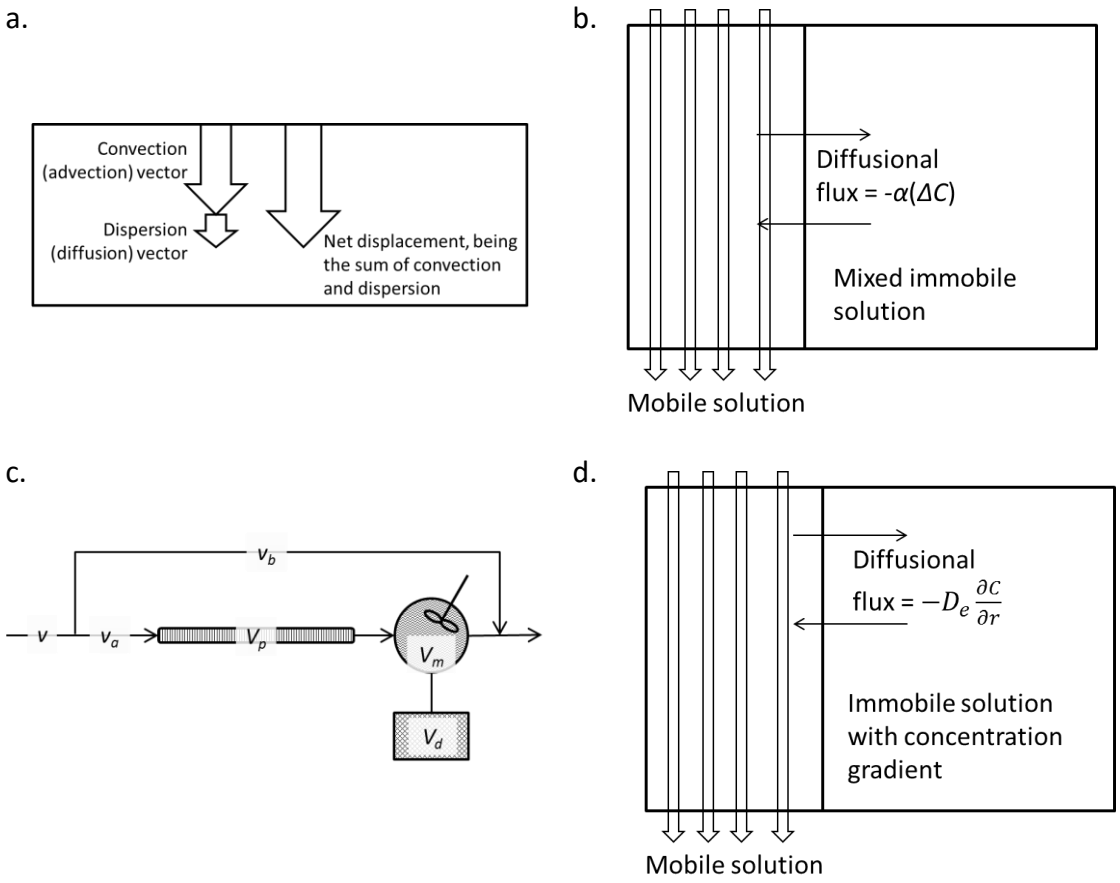

Figure 14. Four representations of hydrology.
(a) convective-dispersive model previously used in soil science, (b) mobile and mixed immobile regions proposed by Van Genuchten and Wierenga (1976), (c) Levenspiel multiple parameter model, (d) mobile and immobile region with concentration gradient adopted by Bouffard and Dixon (2001)

The analysis by Van Genuchten and Wierenga (1976) showed that the presence of immobile solution in the bed (with any non-zero value of α) leads to a non-symmetrical curve of drainage concentration, with a long tail after the peak, corresponding qualitatively with the experimental observations. One of the curves they produced is shown in Figure 15 (labelled V. Genucht., α=0.5), which was generated with α=0.5. The curve shows dimensionless concentration (i.e. as a fraction of concentration at the inlet during the pulse) versus the number of solution inventories irrigated. This can be compared to their curve for which α=0.0, which eliminates the participation of the immobile zone, (labelled V. Genucht., α=0). The concentration response reflects in this case only the plug flow behaviour of the mobile zone in the bed, which yields a much

more symmetrical curve. It must be added that their model also included an adsorptive term. However that causes essentially only a delay in the time at which the tracer appears in the drainage solution and affected the two curves equally. The difference in the shapes of the two curves can be ascribed entirely to the presence or absence of immobile solution.

Miller (2003b) developed a shrinking core model of heap leaching, the formulation of which is discussed in section 3.12.4. It approximates a heap as consisting of spherical particles (which he termed 'meta-particles' to distinguish it from indivual ore particles) of uniform (effective) radius R_{eff}. As solution percolates through the heap it envelops each meta-particle. Each meta-particle leaches by shrinking core kinetics which involves leach reagent entering each particle by diffusion, and solubilised metal diffuses out.

Miller (2003b) used R_{eff} as a fitting factor to calibrate the model to the column leaching results of two different ores, the pilot-scale results of another single ore, and commercial heap-scale results of five other ores. He observed that R_{eff} was consistently larger than the radius of the biggest particle in the ore size distribution, in one case (with a crush size of <8mm), by a factor of 40 (Miller, 2003a). (Some of his raw data appears in Appendix B). He concluded that R_{eff} represents the average spacing between mobile solution flow channels, with a meta-particle representing a particle cluster, as opposed to an average individual particle.

Evidence of non-uniform flow through percolated ore was also observed during column, crib and heap leaching tests performed by Bouffard and West-Sells (2009) on gold-bearing ore mined by Barrick. This experiment is discussed later in the text as Case Study 2 in section 8, but for ease of reference the essentials are repeated here. They monitored the rate at which the (unspecified) lixiviant was being rinsed from the ore by irrigation with clean water after gold leaching had been completed. The lixiviant concentration was therefore used as the tracer of a 'step-down' test. The curves of dimensionless concentration (in this case being fractions of the concentration immediately before rinsing started) versus number of solution inventories irrigated are also shown in Figure 15 below on page 61, together with the curves of Van Genuchten and Wierenga (1976). The column can be seen to yield a drainage concentration that

drops to virtually zero quite quickly and does not form a prevailing tail – as would be expected of plug flow. However the heap and particularly the crib yielded quite a long tail, compared to the result obtained with the column.

They fitted these responses to a multi-parameter model as proposed by Levenspiel (1972). This entails the representation of the total volume of a reactor as a combination of mixed, plug-flow and dead-volume compartments, as shown in Figure 14(c) on page 58. Furthermore, the flow through it is divided between a proportion that passes through the plug flow and mixed compartments, with the balance of the flow by-passing directly to the outlet.

A summary of the model parameters resulting from the studies of both Van Genuchten and Wierenga (1976) and of Bouffard and West-Sells (2009) is given in Table 5. The two models are different representations of reality and different numerical values were assigned to those parameters that could be regarded as being related (such as the mobile solution fraction, ϕ, of Van Genuchten and Wierenga (1976) and the plug flow volume fraction V_p of Bouffard and West-Sells (2009)). However, the similarity in trends suffice in this case to suggest that the elongated tails in drainage concentrations modelled by Van Genuchten and Wierenga (1976) and observed by Bouffard and West-Sells (2009) are both due to the the same phenomenon of namely the existence of immobile solution with diffusion between the mobile and immobile solution fractions.

According to the multi-parameter values fitted by Bouffard and West-Sells (2009), the crib and heap contained respectively 57 and 88 percent immobile solution. However the column contained only mobile solution, behaving as if being partly mixed and partly advancing by plug flow. Only the crib exhibited solution by-passing, which caused it to exhibit the longest tail in drainage concentration.

Table 5. Multi-compartment characteristics

Characteristic	**(Van Genuchten and Wierenga, 1976)**		**Barrick, (Bouffard and West-Sells, 2009)**		
	No exchange	**First-order exchange**	**Column**	**Crib#1**	**Heap**
Partitioning of reactor volume, volume fraction[1]					
Plug flow	ϕ=0.65		V_p=0.59-0.71	V_p=0	V_p=0
Mixed	0(NA)		V_m=0.21-0.41	V_m=0.43	V_m=0.12
Immobile	(1 - ϕ)=0.35		V_d=0	V_d=0.57	V_d=0.88
Partitioning of flow, fraction[1]					
Active[2]	1.0	1.0	v_a=1.0	v_a=0.77	v_a=1.0
By-passing	0(NA)	0(NA)	v_b=0	v_b=0.23	v_b=0
Exchange between flowing and stagnant volumes[1]					
Diffusion coefficient	α=0.0	α=0.5	0(NA)	0(NA)	0(NA)

[1]For ease of cross-referencing the symbols used by the respective authors are included.
[2]'Active' being flow that passes through the 'Plug flow' and 'Mixed' reactor volumes.
NA: not applicable since the parameter does not appear in the respective model.

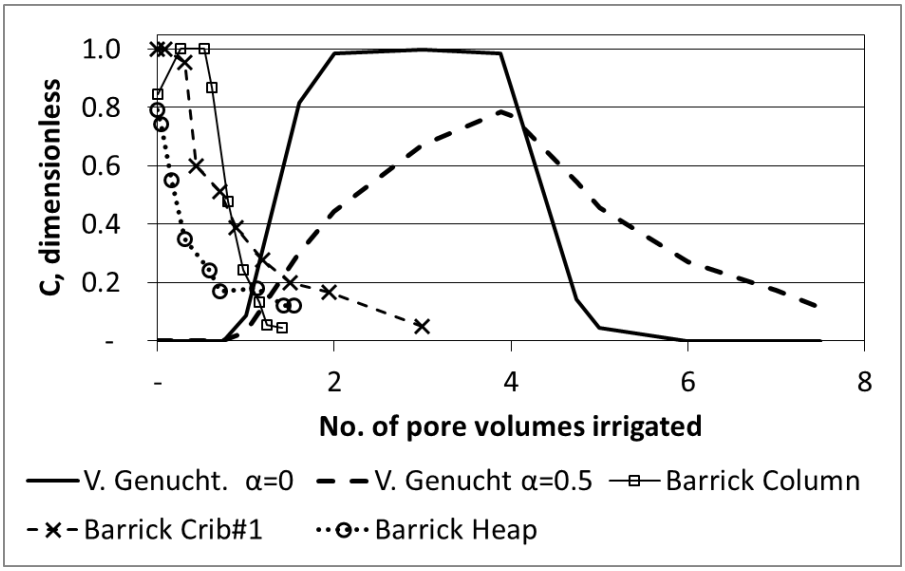

Figure 15. Drainage concentration responses via multi-compartment regimes

In their analysis of the hydrodynamics in heaps, Bouffard and Dixon (2001) fitted the responses of tracer tests in columns with two-compartment models. The one model assumed a mixed immobile zone as that of Van Genuchten and Wierenga (1976), while

the other assumed a concentration profile in the immobile zone, as illustrated in Figure 14(d) on page 58. The latter was found to provide a better fit to the experimental data.

Lin et al. (2005) used a medical scanner to observe the voids between the ore particles in a column before and after leaching. Using Lattice Boltzmann simulation, they calculated where flow would have occurred. They concluded that, even during saturated flow of solution through a column, the majority of active flow occurred via a very limited proportion of the available porosity in the bed.

In a more recent investigation by Fagan-Endres et al. (2015), magnetic resonance imaging was used to show that the solution content in the ore below a dripper increased with increasing irrigation rate. However, the effect was limited to the immediate vicinity of the dripper, and did not improve the over-all solid-liquid contact within the ore. Locations 30-40 mm laterally away from the dripping point possessed about half the moisture content of locations immediately below the dripper.

Petersen (2016) performed positron emission tomography (PET) on a column, 100 mm in diameter and 40 mm high, filled with copper porphyry ore. The column was irrigated on the axis (i.e. as opposed to having the solution spread over the cross section), with solution bearing a tracer, so that the solution flow path appeared brighter on the image than regions not receiving any flow. The solution could be clearly observed to flow mostly along two flow paths, as opposed to being spread evenly over the column cross section. A manual trace over the PET scan image is represented in Figure 16(a) below on page 64.

Ilankoon and Neethling (2016) studied the distribution of solution being irrigated into a 600 mm high box with cross section of 800 mm x 100 mm. The boxes were made from tansparent material so that wet and dry particles could be distinguished visually and quantified by image analysis. It was referred to as a “2D” box since it restricted the opportunity for lateral solution distribution mostly along the 800 mm long dimension of the box. It allowed the assumption that profiles of flow would exist over the 600 mm height from top to bottom, and sideways across the 800 mm, but that there would not be much variation over the relatively small 100 mm dimension. The box was fitted with

25 outlets evenly distributed every 30 mm along the bottom to separately collect solution draining from different positions along its 800 mm length. An ore sample with narrow size distribution (20-26.5 mm) and another with a wide size distribution (2-26.5 mm) were irrigated in the box. Initially, irrigation was supplied via a single dripper placed at the centre of the cross sectional area at the relatively high rate of $4.2L/h/[(0.8)(0.1)m^2] = 52.5\ L/(h.m^2)$. Solution broke through to the bottom within 1.7 minutes for the narrow size distribution and and 11.4 minutes for the wide size distribution. Within an hour the rate of drainage from both boxes had steadied to equal the irrigation rate. The boxes were irrigated for 15 days. From the box containing the ore with narrow size distribution, by far the majority of the solution reported to the drainage point vertically below the irrigation point, consistently throughout the duration of the test. Solution drained from up to 5 drainage points away from the irrigation axis (i.e. 5 x 30 mm = 150 mm), but no further.

From the box containing the ore with wide size distribution, the distribution of drainage became more evenly distributed over those drainage points that did collect solution. There were instances where the drainage rates observed 4 positions (120 mm) and 6 positions (180 mm) removed from the irrigation axis were higher than that emanating from the drainage point on the irrigation axis. Solution drained from up to 7 drainage points away from the irrigation axis (i.e. 210mm). But several drainage points remained dry between other points from where solution was reporting, for example drainage might be collected from the point at the irrigation axis and from 6 drainage points further, but nothing from the 5 drainage points in-between.

Hence the rate of drainage did not decrease consistently with increasing distance from the irrigation axis. Some of the observations made by Ilankoon and Neethling (2016) are illustrated in Figure 16(b) below. Instances were also observed where flow was reporting to a drainage point for a limited period and then stopped. This illustrated the existence of preferential flow channels, and that the route of those flow channels can occasionally change.

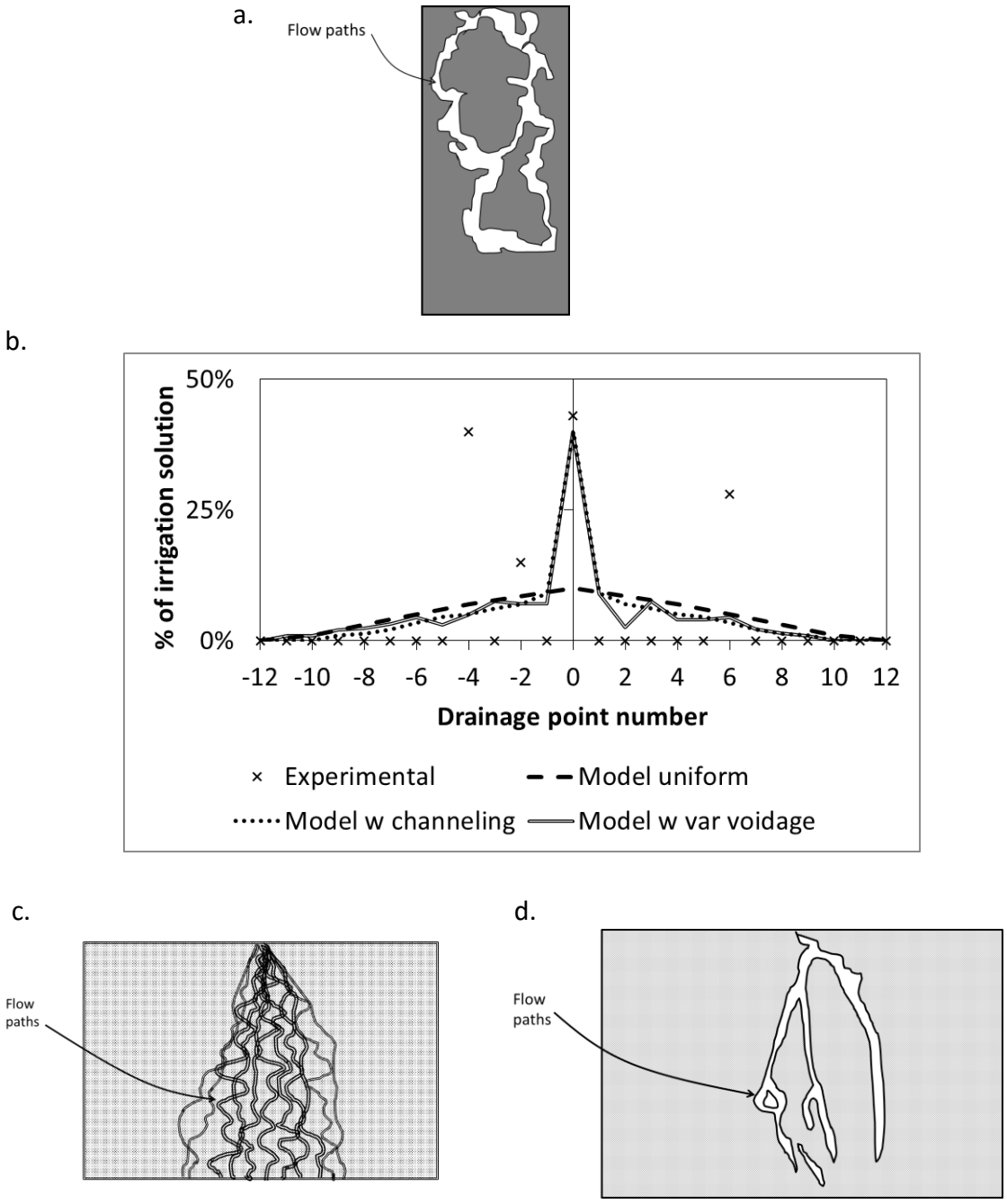

Figure 16. Flow distribution patterns

(a) PET scan of flow paths reported by Petersen (2016), (b) Drainage patterns observed by Ilankoon and Neethling (2016), (c) flow patterns modelled by McBride et al. (2017) based on drainage patterns observed by Ilankoon and Neethling (2016), (d) ulta-violet image of flow path presented by McBride et al. (2017).

For both the narrow and wide size distributions, the extent of wetting of the ore extended further than the extent to which drainage solution reported to the drainage

points. The ore with the narrow size distribution became wetted over a width of about 600 mm towards the bottom (61% of the entire mass became wetted), after 14 days of irrigation, but drainage was occurring from drainage points spread over only 180 mm. The ore with the wide size distribution became wetted over the full 800 mm of the width of the box towards the bottom (96% of the entire mass became wetted), but was draining from dripper points spread over only 300 mm. This illustrated that the observation that ore is getting wetted does not imply that flow is passing through it. The authors also point out that all wetted ore is not holding the same solution content, although no data was presented on moisture content versus time or position.

A conclusion was that the rate of leaching at any given position might be more dependent on the distance away from a channel of mobile solution than on the extent of wetting of the ore. However, no leaching was performed during this experiment, this was merely an inference based on the solution flow patterns observed. Another conclusion was that the formation of preferential flow channels is practically unavoidable, since channeling was observed during these experiments where every care practically possible had been taken to ensure as even packing as possible of the particles.

The observation that solution was being spread more widely through the ore with wide size distribution was attributed firstly to the smaller pore spaces existing between the particles due to the presence of smaller particles (as opposed to the ore with narrow size distribution from which the 2-20mm particles were absent), giving rise to stronger capillary forces. Secondly, the ore with wider size distribution provides more particle-particle contact points where capillary forces can operate to assist in wider distribution of solution throughout the ore.

The ore with the wide size distribution was then left to drain for 3 months, when irrigation resumed the drainage pattern was very similar to that observed before irrigation had been stopped. Therefore, it was concluded that the prefential flow channels established during the first period of irrigation had remained in place over the prolonged period of drainage. The bed was then flooded with the intention of destroying the flow channels. It was then drained and irrigated was re-started. Even then the drainage pattern was similar to that observed before flooding, but drainage also started

occurring from drainage points further removed from the irrigation axis than before, spread over 19 drainage points (570 mm). The single centrally-placed dripper was then replaced by three evenly distributed drippers for delivering the same total irrigation rate. That made the spread of drainage somewhat more even over the drainage points. However, channeling was not totally eliminated, with drainage still occurring from some drainage points while other drainage points between them remained dry.

This same experimental data was analysed further by McBride et al. (2017) by means of a CFD model based on Richard's equation. They created three different textures for the solid phase via which the solution percolated, namely (a) possessing spatially homogenous voidage and permeability, (b) possessing flow channels via which solution could partially by-pass the ore, which possessed homogenous voidage and permeability between the flow channels, and (c) exhibiting non-homogenous distribution of permeability and voidage, albeit with the same over-all average properties as in (a) and (b). Case (a) predicted the very uniform drainage rate distribution labelled "model uniform" in Figure 16(b) on page 64, which did not emulate the experimentally observed high peak in the proportion of solution reporting to the central drainage point. Case (b) labelled "Model with channeling" did exhibit the experimentally observed peak at the central drainage point. However it predicted that the amount of solution would decrease monotonically with increasing distance away from the central drainage point, which was inconsistent with the experimental observations. Case (c) (labelled "Model w var voidage") provided the best emulation of the experimental observations by predicting the amount of drainage to vary randomly with distance away from the central drainage point as observed, although the variations predicted by the model were still not as pronounced as the variations observed experimentally. An approximate reproduction of the distribution of mobile solution flow calculated for case (c) and of their 'ultra-violet' image of the solution flow paths are shown in Figure 16 (c) and (d) on page 64. (However, the authors did not explain how the ultra-violet observations were made. It is assumed that a substance was added to the water which fluoresced under ultra-violet light, which facilitated observation and photography of the flow channels).

3.11.11 Definition of densification, compaction and consolidation

Densification is the more generic term used in soil mechanics to describe the process whereby a given mass of soil is compressed into a smaller space, thereby increasing its bulk density, (McCarthy, 2014; West, 2018). Compaction refers to densification whereby air is forced from the spaces between particles. Consolidation refers to densification whereby liquid is forced from the spaces between particles. In this text, the generic term 'densification' is used throughout to account for scenarios where either or both of compaction and/or consolidation might be at work.

3.11.12 Measurement of mechanical and hydraulic properties

In the heap leaching industry, geomechanics concerns the physical response of individual ore particles and of the collective aggregate of crushed particles and agglomerates to compressive stress. Of primary concern is to what extent the ore will densify under its own weight, and under the weight of some unavoidable human and/or equipment traffic over the heap during installation of the irrigation system. An increase in bulk density reduces the hydraulic conductivity, and it would be undesirable if the ore were to densify to such an extent that it becomes impossible to pass the required irrigation flux (Guzman, 2011). Standard laboratory apparatus are available for testing the compressibility of solid materials. For example, Messerklinger et al. (2004) provides details of a press that is used for placing solid samples under pressure in 3 dimensions and measuring the resulting displacement. In principle, such measurements can be used to predict the bulk density to which an ore will densify under its own weight, as illustrated by Guzman (2011).

A number of authors such as Nimmo et al. (1992) and Stibinger (2014) describe laboratory methods for determining the hydraulic conductivity. In principle, they all rely on the measurement of a solution flux under a given pressure head so that the hydraulic conductivity can be calculated from Darcy's law described in section 3.11.6.

A procedure that has been used for determining the immobile moisture content is simply to measure the residual moisture content after complete drainage under gravity, as described for example by Bouffard and Dixon (2001).

3.11.13 Summary of fluid dynamics, hydrology and mechanics

Particles of about 10 mm in size and smaller that are clustered together can be expected to be immersed in solution that is immobilised by the capillary forces existing in the voids amongst the particles that are stronger than gravity.

If follows from Richard's equation that ore that is initially dry will attract moisture into the voids amongst the particles. That ensures that solution is spread laterally throughout an ore mass. However, as the voids approach saturation with solution, this attractive force becomes smaller and flow into the voids will eventually stop. Hence, while capillary forces will ensure that solution is spread throughout the ore mass to wet it, those forces do not sustain solution flow through the ore mass over the long term.

There exists ample evidence from direct observation and inferences based on modelling of observed phenomena to accept that solution passing through a bed of ore does not exhibit plug flow. Rather, it passes through discrete flow channels that are spaced apart.

When the flow of solution under capillary action has stopped, the transport of reagents and dissolved species between the mineral surfaces and the solution flowing via the sparsely distributed flow paths can only occur by diffusion across the immobile solution held in the particle voids. It cannot categorically be stated that capillary flow ever stops completely in a heap, since heaps typically operate under unsaturated conditions, hence some capillary force should always remain. But it can be stated that a large part of the solution content held in a bed of ore is essentially immobilised, if not completely immobilised.

This should serve as caution to the validation of heap leaching models by fitting it to narrow-diameter column leaching results. Provision for the existence of immobile solution is essential for representing the hydraulics of heaps and cribs. A model that lacks that feature would appear to be valid due to the success with which it can fit column leaching data. Yet the result would be misleading because the good fit could be due only to the fact that immobile solution is essentially absent from columns, and the model would not be useful for any predictions of crib or heap leaching performance.

Laboratory methods are available for determining the bulk density, hydraulic conductivity and immobile moisture content of ore samples.

3.11.14 Definition of "dual porosity hydrology"

The concept that a proportion of the moisture content in a heap is flowing (mobile) while another portion remains stagnant (immobile), with transport occurring between the two portions occurring by diffusion, is henceforth referred to as "dual porosity hydrology", after Gerke and Van Genuchten (1993).

3.12 KINETICS OF HEAP LEACHING PROCESSES

3.12.1 The need for considering kinetics

The processes involved in heap leaching, which have been discussed above, include the exchange of reagents and reaction products between gaseous, liquid, solid and bacterial phases, making heap leaching a thoroughly heterogenous process. As discussed, once reagents are irrigated onto the heap, advective flow, diffusional transport, chemical reaction and bacterial metabolism need to occur before the leached elements report to the drainage solution. The rate-limiting process could be variable. For example, leaching could be reagent-limited soon after start-up while an abundance of fine-grained liberated mineral particles are present wherever the leach solution is delivered. The rate could eventually become diffusion limited when the only remaining mineral grains are located at the end of cracks and pores in rock particles, or at the end of a diffusional pathway well removed from a mobile solution flow channel, (Dixon, 2003). With slow-leaching minerals such as covelite or chalcopyrite, leaching could also be chemical reaction limited, (Dixon, 2000). In the case of oxidation reactions, the availability of oxygen, the number of microbes present and the suitability of the chemical environment to the microbes are additional factors that could be limiting the kinetics of processes occurring in a heap.

As part of this study, the kinetics of column leaching will be compared to that of heap leaching. Such a comparison can only be done meaningfully if the observed differences can be ascribed to one or more of the processes occurring during leaching. That in turn dictates that the kinetics of the various processes occurring within the heaps (and columns) should be considered individually, as opposed to merely comparing the

effective rates of extraction at macro scale as evidenced by the rate at which leached species report to the drainage solution.

3.12.2 Kinetics of microbially mediated processes

As discussed earlier, the oxidation of ferrous iron to ferric iron, and of reduced sulphur species to sulphate, rely on the mediation of microbes. In return, the microbes utilise some of the energy released by the oxidation reactions for their growth. In this way, the growth rate of microbes and the oxidation rates of ferrous iron and of the reduced sulphur species are mutually dependent on one another, and are therefore discussed together.

Monod kinetics is the most common form of kinetic expression used to describe microbial oxidation of ferrous iron, (Dixon, 2003; Leahy et al., 2007; Wu et al., 2010). It contains a term for the substrate concentration (for example ferrous iron or elemental sulphur) both in the numerator and denominator, which is a feature it shares with Michaelis-Menten kinetics, (Mahanta et al., 2014). A simple example using ferrous iron as the substrate is shown in equation [49]:

$$rate = \frac{K_1[Fe^{2+}]}{K_2 + [Fe^{2+}]} \quad [49]$$

where K_1 and K_2 are constants. This describes a rate that slows down towards zero if the ferrous iron concentration becomes very low. However, as the ferrous iron concentration increases, the rate initially increases relatively rapidly, but eventually asymptotes towards a finite value. The example illustrated in Figure 17 below with K_1 = 1 mole/(L.h) and K_2 = 0.05 mole/L asymptotes towards a rate of $1h^{-1}$ as $[Fe^{2+}]$ approaches infinity. Various authors have included other terms to account for other effects such as ferric iron and dissolved oxygen concentration, temperature and pH, as reviewed by Ojumu et al. (2006).

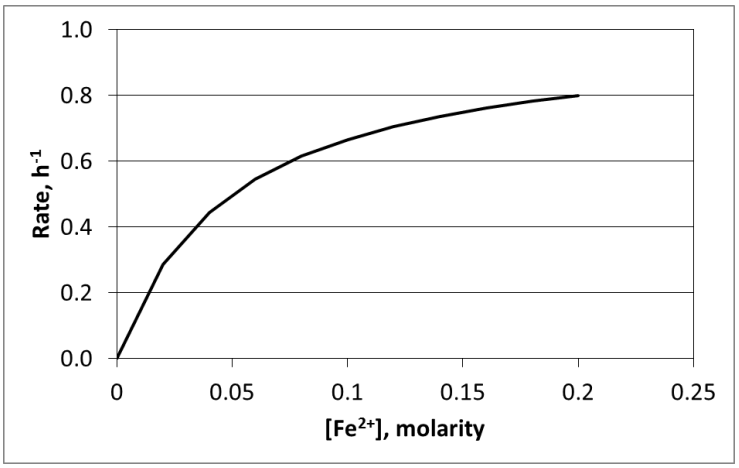

Figure 17. Illustration of Monod-kinetic trend

The published rate equations have been developed for agitated tank bioleaching where operating conditions are maintained close to that required for optimal microbial performance. That condition does not apply to heap bioleaching. However no kinetic expressions have been published specifically for heap leaching, and the monod-type expressions are the best available to date.

3.12.3 Kinetics of oxygen mass transfer

The rate of oxygen transfer from the gaseous phase into solution can be described by a standard mass transfer equation (Petersen, 2010a):

$$O_2 \text{ transfer rate} = k_{La}(H.p_{O2} - C_{O2}) \quad [50]$$

where k_{La} is the mass transfer coefficient, H is Henry's (temperature dependent) constant and C_{O2} is the oxygen concentration in the bulk solution. The term $H.p_{o2}$ is the equilibrium oxygen concentration that would be reached in the bulk solution if there is no oxygen-consuming reaction taking place. (Bennett et al., 2012) reasoned that an assumption of equilibrium conditions could be made under typical heap leaching conditions.

3.12.4 Kinetics of mineral leaching

The chemical reaction kinetics of the leaching of solid substrates (i.e. when the rate of supply of reagent to the reaction surface is not limiting), are firstly proportional to the

surface area exposed to the leaching medium. As the solid phase leaches, the remaining surface area diminishes and the leach kinetics slow down. Therefore, in order to relate the rate of reaction to the extent of leaching, the geometry of the leaching particle must be known or assumed.

Secondly, the rate of leaching usually exhibits some dependence on the concentration of the leach reagent(s) in solution. Thirdly, chemical reaction kinetics accelerates exponentially with increasing temperature according to the Arrhenius equation, (BioMinE, 2018).

Mineral dissolution kinetics has been described by a number of expressions that differ in details, but the expressions used by Ferrier et al. (2016), by Dixon and Petersen (2003) and by Petersen and Dixon (2003b) are all of the form:

$$\dot{X(t)} = k(T)f(C)w(1-X) \quad [51]$$

where $k(T)$ is the rate constant with Arrhenius-type temperature dependency:

$$k(T) = k(T_0)exp\left[-\frac{E}{R}\left(\frac{1}{T}-\frac{1}{T_o}\right)\right] \quad [52]$$

with T_0 being a reference temperature for which k is known, E is the activation energy and R the gas constant. The expression $f(C)$ is a function of reagent concentrations in solution and $w(1\text{-}X)$ is a function of the fraction of mineral that is left unreacted, representing the exposed surface area, termed the "topological function", (Dixon and Petersen, 2003).

Discussion of the topological function (i.e. the term $w(1\text{-}X)$).

Spherical particles consisting of pure mineral follow the shrinking sphere relationship. The volume and therefore mass of a single spherical particle with radius R is proportional to R^3. If the particle possesses an initial radius R_0 at time zero, before reaction started, then after it has undergone an extent of conversion X, the remaining mass fraction (1-X) thereof at any given time, t is:

$$(1 - X) = \left(\frac{R}{R_0}\right)^3$$

Re-arrangement yields

$$R^2 = R_0^2(1 - X)^{2/3}$$

Since the reaction rate is proportional to the remaining surface area, it follows that:

$$w(1 - X) \propto \text{remaining surface area} \propto R^2$$

hence:

$$w(1 - X) = K(1 - X)^{2/3} \quad [53]$$

with *K* being a rate constant. Similarly, expressions have been derived for various particle shapes and modes of occurance, which can be found in texts on heterogeneous non-catalytic kinetics, such as Perry and Chilton (1973).

The shrinking-core model is commonly known, representing the case of mineral being evenly distributed throughout spherical particles of inert material. As leaching continues, the inert material remains intact, leaving an inert 'ash layer' via which the leach solution needs to diffuse in order to reach remaining unreacted mineral deeper inside the inert host material. The particle is assumed to retain its original size, R_0, however the distance that the leach reagent needs to diffuse in order to reach the mineral surface increases over time from time *t*=0.

The most convenient way in which to write the resulting rate expression is in terms of the reaction time *t* as independent variable and extent of conversion *X* as dependent variable, as follows (Perry and Chilton, 1973):

$$t = \left[\frac{s\, C_b \rho\, R_0^2}{6\, D\, C_{a,r=R0}}\right]\left[1 - 3(1 - X)^{\frac{2}{3}} + 2(1 - X)\right] \quad [54]$$

where *s* is the stoichiometric ratio of moles reactant in solution reacting with a mole of mineral in the solid phase, C_b is the initial mass fraction of reacting mineral in the solid phase before leaching, ρ is the bulk density of the solid phase and $C_{a,r=R0}$ is the concentration of reactant in the bulk solution surrounding the particle. If it is assumed the diffusional path from the outer surface of the sphere to the reacting surface is a straight line, then the diffusional distance will asymptote towards R_0 as $t \rightarrow \infty$. However,

if it is a tortuous and constrictive path being only partially filled with solution, it will be a distance that is effectively larger than R_0 by a factor of $\tau_{\delta\theta'}$, which can be corrected for by replacing the free diffusivity D in equation [54] by an effective diffusivity, $D/\tau_{\delta\theta}$.

Note that equation [54] includes the term $C_{a,r=R0}$, which therefore represents the function $f(C)$ already included as part of the topological function. In that form, it can therefore represent the entire solution to $\dot{X}(t)$ of equation [51]to model leaching under isothermal conditions that does not require the introduction of the Arrhenius relationship contained in $k(T)$ (as in the case of acid heap leaching of acid-soluble copper minerals). Alternatively, to model heap leaching that is entirely diffusion rate controlled, the temperature-dependency of the diffusivity, D, can be included in equation [54] to represent the entire solution to $\dot{X}(t)$ of equation [51]. Such a model has been used by Miller (2003b), in which he uses an 'effective particle' size R_{eff} as characteristic. He explains that R_{eff} represents the radius of a cluster of ore particles, hence R_{eff} can be larger than the largest individual particle in the crushed ore. In his shrinking core kinetic expression, R_{eff}^2 replaces R_0^2 in equation [54]. His model could therefore rather be called a 'shrinking-cluster' model.

This is as opposed to texts such as Bartlett (1995) and Roman et al. (1974) in which each individual particle is assumed to be surrounded by leach solution, and the rate of leaching is calculated by integration of shrinking core kinetics per particle over the entire particle size distribution.

However, Ghorbani et al. (2013) showed that, for individual mineral-bearing ore particles of 5 mm and larger, the leach kinetics do not follow either shrinking sphere or shrinking core kinetics. This can be ascribed to the fact that ore particles are of various shapes, as illustrated for example by Bouffard (2003b). Furthermore, the mineral grains are not evenly distributed throughout the ore particles, nor are ore particles homogenously porous (as shown by Ghorbani et al. (2013)), which violates the assumption upon which the shrinking-core model has been derived. Ferrier et al. (2016) also found that a shrinking core model calibrated to the experimental results of one column leaching experiment yielded poor prediction of the leaching results achieved during a second experiment conducted under different conditions. Ferrier et al. (2016)

found that the model of Dixon and Hendrix (1993), which describes mineral leaching as the product of a rate constant, reagent concentration and topological term could be more successfully calibrated to the experimental data.

Dixon and Hendrix (1993) conducted a theoretical study of the leaching of a hypothetical aggregate of spherical particles possessing a particle size distribution, (as opposed to being uniformly sized). Each particle was assumed to leach according to shrinking sphere kinetics, defined by equation [54] above. By integration of the extent of leaching per particle over the entire size distribution, they calculated the rigorous extraction curve for the size distribution. They repeated this for six different size distributions from a uniformly sized collection of particles to a very wide size distribution of particles. They also calculated an effective reaction order for the aggregate of all particles in a given size distribution and found that for any non-uniform size distribution, the kinetics of the aggregate exhibited an effective reaction order larger than $^2/_3$. Furthermore, the apparent reaction order varied over time (i.e. with extent of conversion). And, the wider the size distribution, the larger was the apparent reaction order, and the more it varied with time (i.e. with extent of conversion). They then determined an average reaction order for each size distribution as the single reaction order that provides the best fit to the leaching kinetics over the course of leaching from zero up to 99 percent of conversion. This single reaction order Φ was then substituted back into the following equation of generic reaction order with respect to unreacted fraction:

$$w(1-X) = (1-X)^{\emptyset} \qquad [55]$$

They found that it provided an estimate of the extent of extraction over time that correlated very well with the rigorous extraction curve calculated as an integration over the particle size distribution.

Bouffard (2003b) went a step further and fitted this equation to the kinetics of the oxidation of the pyrite content of five different ore samples, each crushed to -12.5 mm. She managed to obtain good fits between this equation and the experimentally determined extraction curves of all five samples, yielding optimally fitted values for Φ ranging from 1.0 to 3.2.

The use of equation [55] has has also been applied in the HeapSim model described by Dixon and Petersen (2003) and in the model of Robertson (2017).

The form of the topolocial term represented by equation [48] dictates that leaching would continue until complete extraction is reached. This follows from the fact that the rate of extraction $\dot{X}(t)$ tends towards zero only as the extent of extraction (X) tends towards unity.

Ghorbani et al. (2013) found this property problematic. In their study of the oxidative bio-leaching of sphalerite (ZnS) from coarse (5-25 mm) particles, they attempted to fit the extraction data to the model formulated as:

$$\dot{X(t)} = k(1-X)^{\emptyset} \qquad [56]$$

They used isothermal conditions and constant solution composition and hence did not require an Arrhenius term of concentration function $f(C)$. The model can hence be seen to consist of the topological term defined by equation [55], preceded by a rate constant.

In coarse particles, some of the mineral grains are obstructed from contact with leach solution which prevents them from leaching. Or they could be considered as unleachable at least over the order of magnitude of time frame employed for heap leaching. Leaching would then, for practical purposes, seize before the total mineral content has been leached and the rate expression of the form [56] would over-predict the extent of extraction towards the later stages of leaching of coarse particles.

They solved this problem by distinguising the "extractable mineral content" (αC_0 with $0 \leq \alpha \leq 1$) from the "total mineral content" (C_0). The extent of extraction based on the total mineral content is $X = (C_0-C)/C_0$, while the extent of extraction based on the extractable mineral content is $(C_0-C)/(\alpha C_0) = X/\alpha$. Hence the unreaced fraction of the extractable mineral content is $(1-X/\alpha)$. This led them to modify [56] to the following:

$$\dot{X}(t) = k\left(1-\frac{X_{Cu}(t)}{\alpha}\right)^{\emptyset} \qquad [57]$$

where α is the mass fraction of copper that is extractable from the particle scale under the leaching conditions. This modified form yielded much improved the fitting of the experimental data.

Equation [57] has the following solution for $X_i(t)$:

$$\frac{X_i(t)}{\propto} = 1 - \left(1 + (\emptyset - 1)\frac{kt}{\alpha}\right)^{\frac{1}{(1-\emptyset)}} \qquad \forall\ t \text{ if } \emptyset > 1; \qquad [58]$$

$$\forall\ t \leq \frac{\alpha}{(1-\emptyset)k}\ if\ \emptyset < 1$$

The time boundary in the second line of the above expression is required to limit the function to an extent of conversion ≤ 1 in the case where κ_1<1.

They also proposed a further term βt to be added to equation [58] to represent a final period of very slow leaching of mineral grains within microscopic crevices, over a time scale that is orders of magnitude longer than the time required to leach to completion the fraction α. This last slow part of leaching is ignored for this study as its time scale extends beyond the production period of a heap leach operation.

Hence they were not proposing that leaching absolutely terminates when the faction α has been extracted. However they identified two time scales according to which leaching occurs, a relatively shorter time scale to leach the first fraction of α and an orders of magnitude longer time scale to leach beyond that. And the two time scales are so different as to prohibit its correlation within a single expression of the form of either equation [56] or [57]. They speculated that the kinetics might become governed by solid-state diffusion, i.e. diffusion through the ore matrix, as opposed to diffusion through the solution held in the pores that harbour the mineral grains. They did not provide evidence for specifically solid-state diffusion and did not offer any further discussion on it. Supposedly they might equally have speculated that the kinetics were becoming governed by surface diffusion (where molecules move along the walls of pores), or Knudsen diffusion (where molecules bounce between the opposing walls of a pore) in the progressively narrower crevices in which the remaining mineral grains resided, (Yang et al., 2016).

Of significance is that the change in time-scale is attributed to a change in diffusion mechanism, which occurs in the cracks and crevices of the particle, not on the mineral grain surface. Hence the difference is not attributed to a change in reaction mechanism or to the topological function discussed above. This change in time scale could therefore equally be observed where non-oxidative chemical leaching is performed, as opposed to the oxidative bioleaching that applied in their case. The use of equation [56] could therefore be universally applicable wherever coarse ore particles are being leached.

Discussion of the effect of reagent concentration *f*(*C*)

Afewu (2009) experimentally found an oxide-Cu leaching reaction order of 0.363 with respect to acid concentration, (refer to their page 130). Both Afewu (2009) and Dreier (1999) point out that oxide and carbonate-copper minerals dissolve orders of magnitude faster in acid than gangue minerals. Afewu (2009) experimentally found rate constants k=1.5x10^{12} and k'=1.2x10^{-8}, he pointed out that the effective rate of oxide copper leaching is more sensitive to the rate of GAC, which is competing for acid as reagent, than to Cu extraction rate constant. Relative to the amount of copper being present, gangue is present in infinite quantity so that its rate of acid consumption does not diminish over the course of leaching since.

Bingol and Canbazoglu (2004) found that the acid leaching of malachite (a common acid-soluble copper-bearing mineral), yielded more than 90 percent extraction within less than one hour, even at ambient temperature. Relative to the time scale according to which heap leaching occurs, this can be taken as instantaneous.

In summary, for the purposes of the modelling of heap leaching, it can be assumed that acid-soluble copper minerals leach instantaneously with acid, the rate being limited only by the rate of acid supply to the mineral surface, which can be limited by the rates of mass transfer and the rate of GAC.

As discussed in section 3.3, sulphide mineral dissolution occurs by mediation of ferric ions, rendering their dissolution kinetics a function of redox potential, (i.e. the ratio of the concentrations of Fe^{3+} and Fe^{2+}). The dissolution of pyrite is also a function of acid

concentration. Holmes and Crundwell (2000) proposed the following expression for the concentration dependence of pyrite oxidation kinetics:

$$f(C) = k[H^+]^{-0.5}\left(\frac{k_{Fe3+}[Fe^{3+}]}{k_{FeS2}[H^+]^{-0.5} + k_{Fe2+}[Fe^{2+}]}\right)^{0.5} \quad [59]$$

while Petersen and Dixon (2003b) and Dixon and Petersen (2003) used the following "universal electrochemical rate law" for the oxidation of sulphide minerals:

$$f(C) = \frac{[Fe^{3+}]}{(K_A + [Fe^{3+}])^{1-m}(K_B + [Fe^{2+}])^m} \quad [60]$$

where K_A, K_B and m are parameters to be calibrated to experimental data.

Other forms have also been used, and Holmes and Crundwell (2000) provided a summary of rate expressions for the oxidative leach kinetics of sulphide minerals.

3.12.5 Kinetics of gangue acid consumption (GAC)

Since heap leaching involves the treatment of whole ores (as opposed to concentrates), the value-bearing mineral is typically present in the solid phase at much lower concentration than the gangue. It would be ideal if the gangue minerals were unreactive to the leaching reagent. Unfortunately, the gangue minerals typically exhibit at least moderate reactivity to the leach reagent, particularly to acid (Chetty, 2018). Since acid-consuming gangue competes with the value-mineral for the same leaching reagent, gangue acid consumption (GAC) suppresses the rate at which the value mineral leaches and increases the reagent consumption (Afewu, 2009).

A large number of minerals can be found in gangue, exhibiting a range of reactivity to acid from virtually inert to highly reactive (Jansen and Taylor, 2003). An ore bearing a large quantity of gangue that is more reactive to acid than the value-bearing mineral would be uneconomic to process by heap leaching, and is therefore irrelevant to this study, (Chetty, 2018).

The rate of GAC increases with increasing acid concentration and decreases with increasing ionic strength of the leach solution, (Jansen and Taylor, 2003).

From rolling bottle dissolution tests, Afewu (2009) (refer to his page 130) concluded that the rate of GAC was first-order with respect to (sulphuric) acid concentration, [C_{acid}]. This can be expressed in terms of the rate of acid 'supply' as a result of gangue reactions (s_{GAC}), (while GAC represents acid consumption being a negative rate of supply), as follows:

$$s_{GAC} = -k'[C_{acid}] \quad \text{with} \quad k \geq 0 \qquad [61]$$

It is to be expected that the GAC kinetics would vary with acid concentration only, and not be related to the remaining portion of unreacted gangue. That is because the gangue is present in such a large proportion relative to the value minerals that the supply of gangue is effectively infinite. Therefore, it exhibits a very small extent of conversion in the time within which the value minerals are leached. (It has already been indicated above that, if the gangue is so reactive that this statement is untrue, its acid heap leaching would not be an economic prospect).

While the rate equation [61] fitted the bottle rolling results, Afewu (2009) also found that the GAC rate constant *k'* that best fitted the experimental results varied between experiments conducted at different scales of column leaching.

Care is required where the kinetics of GAC is expressed as an *n*-th order reaction with respect to acid concentration such as equation [61], since that renders the rate of GAC in a heap a function of the moisture content in the heap. (The consumption of, say, 1 g/L acid per hour from 2 L of solution represents a larger number of moles of acid consumed per hour than the consumption of 1 g/L acid per hour from 1 L of solution). It is intended that the rate of gangue acid consumption (measured in such units as kg_acid per tonne_solids per hour], which is a property derived from the mineralogy of the solid phase, should be a function of acid concentration only and not a function of moisture content. This requires the following adjustment for a comparison between tests conducted at different moisture contents with units of [L-solution/kg-solids] (of ε_{test} and ε_{imm} respectively):

$$k'_{test} \cdot \quad C_{acid} \cdot \quad \varepsilon_{test} \quad = \quad k' \cdot C_{acid} \cdot \varepsilon_{imm}$$

$$\left[\frac{1}{s}\right]\left[\frac{mole\_acid}{L\_soln}\right]\left[\frac{L\_soln}{kg\_solids}\right]_{test} \equiv \left[\frac{1}{s}\right]\left[\frac{mole_{acid}}{L_{soln}}\right]\left[\frac{L_{soln}}{kg_{solids}}\right]_{model} \equiv \left[\frac{mole\_acid}{kg\_solids \cdot s}\right]$$

so that

$$k' \quad = \quad k'_{test}\,\frac{\varepsilon_{test}}{\varepsilon_{imm}} \qquad [62]$$

$$\left[\frac{1}{s}\right] \quad \equiv \quad \left[\frac{1}{s}\right]\left[\frac{L_{test}/kg\_solids}{L_{model}/kg\_solids}\right]$$

Therefore, whenever GAC rate constants are compared, it should be on the basis of a common immobile moisture content ε_{imm}. Direct comparability can also be achieved by comparing the term $k'\varepsilon$ between different cases, instead of directly comparing values of k' independently of ε.

3.13 GASESOUS FLOW THROUGH A HEAP

The number of published studies on the flow paths of the gaseous phase through heaps does not equal the number of studies on solution flow. This may be due to the fact that non-oxidative heap leaching applications do not require air injection, while solution irrigation is a universal requirement of all heap leaching applications. Secondly, experimentally verifying the flow path followed by air and water vapour through a packed bed might prove technically more challenging. For example the air passing through a bed of particulate solids would be visually indistinguishable from void spaces that are isolated from the flowing gaseous phase.

Petersen (2010a) determined the rate of oxygen mass transfer from air into column bioleaching experiments. Two experiments were conducted of the 'agglomerated fines' type (referring to section 3.1 above), using concentrates of respectively chalcopyrite (Petersen and Dixon, 2002) and of copper-gold-bearing sulphide (Petersen and Dixon, 2006). The concentrates were agglomerated onto 5-10 mm granite pebbles to render the bed permeable to solution and gaseous flow. The mixes of concentrate and granite pebbles contained 2.9 percent sulphide (as S^2) in the case of the (2002) chalcopyrite concentrate, and 1.7 percent sulphide in the case of the (2006) copper-gold concentrate.

The reaction kinetics were found to remain relatively insensitive to temperature from 22 to 68^{o}C in both cases. At least under these conditions, the reactions were therefore clearly limited by the rate of oxygen mass transfer. The oxygen mass transfer rates remained quite constant, with the reduction in oxygen solubility being countered by a commensurate increase in mass transfer coefficient, as the diffusivity of oxygen increases with temperature.

Leahy et al. (2005) and Leahy et al. (2007) offered a computational fluid dynamics (CFD) model of air passing from aeration pipes at the bottom of a heap, with consumption of the oxygen by the oxidation of pyrite and chalcocite. They used Darcy's law for calculation of solution flow since solution was assumed to be spread evenly across the cross section of the bed. They used Navier-Stokes equations to calculate the gaseous flow in order to model the dissipation of air from spargers placed at the bottom of the column. Their model assumes incompressible flow, although the change in air density with temperature is accounted for, which causes warmer gas to be more buoyant and the resulting air ingress from the outside environment is also calculated. Heat exchange between the two phases is considered, being assumed to be in termal equilibrium. The model also considers microbial oxidation kinetics and the temperature-dependent solubility of oxygen in the aqueous phase. It was assumed that oxygen was being transported by both gaseous advection flow and diffusion of oxygen in the gas phase, but oxygen diffusion in the solution phase was not considered, hence assuming the gasous phase gets in contact with all solid surfaces. One generally applicable finding from their investigation was that the mechanical blowing of air into heaps is essential for typical microbial sulphide oxidation applications to prevent reaction rate limitation by oxygen starvation. In most cases there were not signicant profiles of oxygen concentration, bacterial population or metal extraction predicted, with these profiles advancing in a more or less straight front, except for the most extreme case where aeration lines were spaced too far apart (>4m).

Their results suggest that assuming the gaseous phase to be distributed evenly throughout the bed cross section does not represent a gross assumption.

Bennett et al. (2012) also offered a CFD model of heap leaching, simulating gaseous flow as an incompressible fluid passing through the voids amongst the ore partices according to Richard's equation. The model was validated against column leaching results, but they did not offer any additional insights.

3.14 HEAT BALANCE IN A HEAP

Dixon (2000) and Wu et al. (2010) visualised heat transfer in a heap as shown in Figure 18 below.

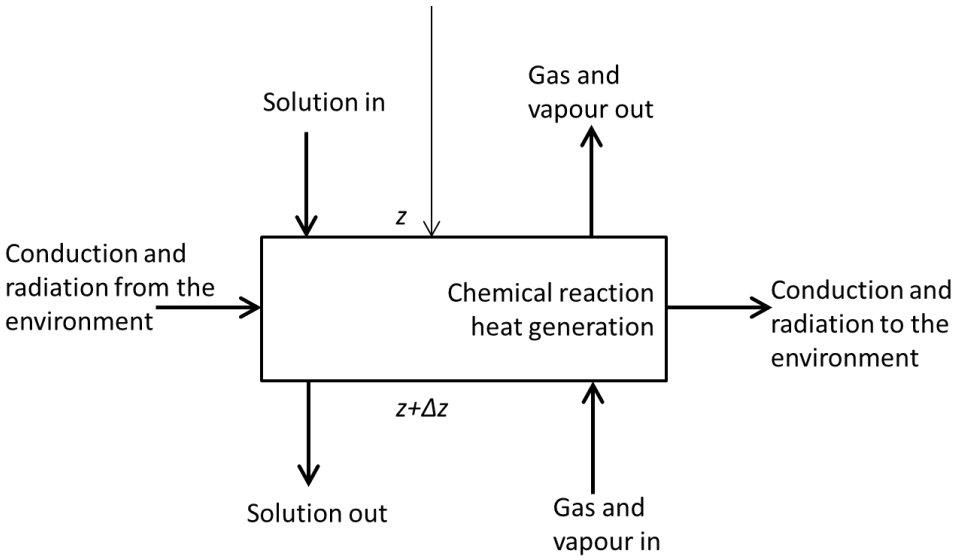

Figure 18. Visualisation of energy balance around a heap spatial element.

The energy balance contains the following terms (Dixon, 2000) which are added (for reaction heat and for arrows pointing into the element of Figure 18) and substracted (for arrows pointing out of the element) as shown:

Enthalpy of solid, solution & gas at time $t+\Delta t$ =

Enthalpy of solid, solution & gas at time t +

reaction heat over duration Δt +

enthalpy added by inflow of solution from the top and gas and vapour from the bottom over duration Δt −

enthalpy removed by outflow of solution downwards and gas and vapour upwards over duration Δt +

enthalpy added by radiation from the sum over duration Δt −

enthalpy removed by natural convection cooling on the outer heap surface over duration Δt.

3.15 VARIABILITY IN COMMERCIAL HEAP LEACHING PERFORMANCE

The data published by Miller (2003b), which he fitted to his shrinking cluster model discussed earlier in section 3.11.10 as well as the data of "Operation F", appear in APPENDIX B. It serves as a good example of the limited precision with which heap leaching performance can be reproduced, since it involved the monitoring of the leaching performance of 24 heaps of the same ore under a single set of operating conditions. The maximum and minimum diffusional distance, R_{eff}, fitted to the performances of those heaps varied by +44-39% around the mean of 56 mm. That represents a standard deviation of 12 mm, or a 95 percent confidence interval (i.e. plus and minus 2 standard deviations) of 31.4 to 79.6 mm, being the range 56 mm±42%.

In summary, based on this set of data it is concluded that a variation in diffusional distance of more than ±42% would be statistically significant. Since diffusional distance (R_{eff}) appears to the power of 2 in a diffusion time equation such as [54], it is more convenient to state that a variation in the square of diffusional radius (R_0^2 in equation [54]) by a factor of more than 2 would be statistically significant.

Direct evidence does not exist to attribute this variability to specific contributing factors, but can be speculated to be due to a combination of statistical variability of mineralogy (for the 'same' ore), and limitations to which the crushing, agglomeration, stacking, heap surface traffic during irrigation installation, process and equipment interruptions and failures and weather conditions can be reproduced from one heap to another.

During laboratory experiments, much more control can be exercised over homogenuity of sample preparation and sample loading into the leaching container. Therefore, an increase in the square of diffusional distance by a factor of 2 amongst laboratory results would be even more significant.

3.16 CONSIDERATION OF POSSIBLE REASONS FOR DIFFERENCES BETWEEN COLUMN AND HEAP LEACHING KINETICS

3.16.1 Effect of wall support on bulk density

Authors such as Scheffel et al. (2016) have commented on bulk density being a determinant of heap leaching performance, with a higher bulk density leading to a slower rate of leaching and/or lower ultimate extent of achievable extraction.

Miller (2003b) fitted his model (assuming shrinking core leaching kinetics at the particle-cluster scale as discussed above), to the kinetic data of heaps from 5 different commercial operations, and columns from 2 operations.

The raw data, which is presented in APPENDIX B, does not comprise the full data set. Miller (2003b) also included data for cases where run-of-mine ore was used that was excluded from this analysis to restrict the analysis to a single particle size per operation.

He used the effective radius of particle clusters, R_{eff}, as fitting factor. A larger value for R_{eff} implies a longer average diffusional distance between stagnant solution and flow channels, which leads to a slower effective rate of leaching. In Figure 19 below, the values for R_{eff} are plotted against the bulk densities measured, firstly for all individual data points in Figure 19(a), and for the averages per operation in Figure 19(b). Despite the considerable scatter existing in Figure 19(a), a clear trend is observed of increasing R_{eff} (i.e. decreasing rate of leaching) with increasing bulk density.

a.

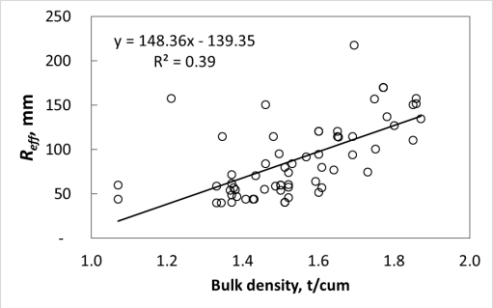

b.

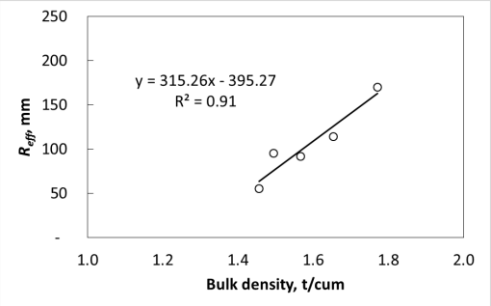

Figure 19. Diffusional distance vs. bulk density from the data of Miller (2003) (a) Individual heaps, (b) Averages per operation

In their review of a few literature sources, Ilankoon and Neethling (2016) comment that lower bulk density is associated with higher permeability (or lower resistance) to solution flow. A high permeability eases solution ingress into the heap, although a localised area of high permeability neighbouring an area of lower permeability will of course lead to preferential channeling of solution via the high-permeability area.

Similarly, Ghorbani et al. (2016) indicated the existence of an inverse relationship between heap height and rate of extraction, with taller heaps compacting more, thereby reducing the permeability to leach solution.

If the bulk density of a given ore tends to be lower in laboratory columns than on free-standing heaps, it would account for one mechanism that causes column leaching kinetics to be faster than heap leaching kinetics. Because of the frictional support provided by column walls (which is absent from commercial heaps), such a trend would indeed theoretically be expected.

According to Tournier and Judd (1954), the weight of ore contained in a column is not dissipated completely vertically, but partly laterally towards the column walls. Hence effectively a proportion of the weight of the ore is carried by the walls. Therefore, the densification of ore under its own weight while contained in a column can be expected to be less that the densification of ore in a free-standing heap without wall support. These authors provide expressions that reportedly agree well with experimental

observations, from which the ratio between lateral pressure (P_L) and vertical pressure (P_v) exerted by ore in a column can be calculated as:

$$\frac{P_L}{P_V} = \frac{(1 - \sin(\beta))}{(1 + \sin(\beta))} \quad [63]$$

where β is the internal angle of friction of the ore. For ore with a typical internal angle of friction of 35^o, this ratio is 0.27. Hence according to this, ore in a column exerts 27 percent less vertical pressure under which to compact than ore in a free-standing heap without wall support. Note that this ratio is independent of the column diameter, hence according to this relationship, ore in an arbitrarily large crib is not expected to compact more than ore contained in a narrow-diameter column.

However, what this relationship does not account for is that the column walls permit less random packing of particles in the vicinity of the column walls. This effect is a function of column diameter, such that a larger-diameter column does permit higher over-all density of packing inside the column, according to German (2009). Hence, considering the effects of both lateral pressure distribution and local packing order simultaneously, ore can be expected to compact more in cribs than in columns due to the smaller effect of orderly packing at the walls in cribs. However, the densification will not occur in cribs to the same extent as in free-standing heaps since the weight of the ore is partly disseminated laterally in any container. This is in agreement with the findings of Bouffard and West-Sells (2009). They compared the leaching performance of one narrow-diameter column, two cribs and one commercial heap on a common crushed ore. During leaching, the ore compaced to final densities of 1.37 kg/m^3, 1.73-1.88 kg/m^3 and 2.01 kg/m^3 in the columns, cribs and heap respectively. They also found that, with increasing bulk density, the proportion of immobile solution increased while the rate of extraction decreased.

Therefore, both theoretical grounds and experimental evidence exist to conclude that ore is subjected to less densification in a crib than on a heap, and to even less densification in a small-diameter column. A higher extent of densification leads to slower effective leaching kinetics, thereby providing one reason for column leaching kinetics being faster than heap leaching kinetics. What remains is to determine the form

of the relationship between bulk density and leach kinetics (as quantified in terms of diffusional distance), and whether a consistent correlation can be observed between the extent of densification occurring on a heap relative to that occurring in a column.

3.16.2 Effect of column diameter on simulated dripper spacing

As discussed before, drip irrigation has become very common, therefore its effect on leaching performance deserves specific attention. A laboratory column of ore that is intended to be drip irrigated should ideally represent at least one unit cell of a heap. As discussed in section 3.7.4, drippers are typically placed on a 0.5m x 0.5m grid, requiring a column of at least those dimensions for a rectangular cross section, or a cylindrical column with diameter of 560 mm. Such a column would represent the correct dripper spacing and therefore, as much as practically possible, the efficiency of contact between the leach solution and the ore. (Although it does not eliminate the differences in densification occurring between columns and heaps as discussed above).

However, this requirement is usually not met and in the author's own experience one reason for it is the expense involved in collecting a sufficient quantity of sample. The ore sample requirement is proportional to the square of the column diameter. Even a single 6m high column of 200mm diameter, filled with crushed ore with typical bulk density of 1,500 kg/m^3, requires 280 kg of ore sample. Preparing the <15 mm to <30 mm crushed sample typically required necessitates feed material with a minimum top-size of about 60 mm. For a greenfields project, that can often only be provided from drill cores which is quite expensive to obtain (as opposed to reversed-circulation drillings which are cheaper to obtain but too fine for column leaching purposes). Minimising the sample size upon which to conduct the column leaching testwork is an important economic consideration, particularly for greenfields exploration projects operating on very constrained budgets. Therefore, laboratory columns of around 150 mm (Scheffel et al., 2016) to 250 mm (Bouffard and West-Sells, 2009) in diameter are commonly prescribed.

The main concern mentioned in publications with the diameter of the columns being used has been the avoidance of 'undue' wall effects, whereby solution might by-pass the ore by running between the ore and column wall. The prescribed requirement for the column diameter to avoid wall effects is that the diameter should be at least three

to four times larger than the largest ore particle, according to Potter (1981) and Scheffel et al. (2016)).

It has already been mentioned above that drip irrigation is known to reduce the efficiency of contact between ore and leach solution compared to that achieved by sprinklers, as discussed by (Kappes, 2002). The experimental results of Ilankoon and Neethling (2016) discussed above showed that a narrower dripper spacing served to provide a somewhat more even distribution of solution flow through a bed of ore. It is only logical that improved contact between solution and ore should enhance the leaching performance.

In summary, column leaching is typically conducted with an effective dripper spacing that is smaller than that to be used on the commercial heap that it attempts to simulate. Therefore, the efficiency of contact between leach solution and ore is, by experimental design, better in the columns than it is ultimately going to be in the commercial heap. What remains is to be established is the nature of the relationship between dripper spacing and leaching performance.

3.16.3 Segregation and stratification

Academic authors such as Benito et al. (2014) and Shimokawa and Ohta (2007) recognise two phenomena that can occur on piles of aggregate, namely segregation and stratification. Where authors on applied heap leaching refer to segregation, it can be read as the two related but different phenomena of both segregation and stratification.

A combination of segregation and stratification on a heap with angle of internal friction Φ is illustrated in Figure 20 below on page 91, as adopted from simulation outputs by Benito et al. (2014). Segregation refers to the predominance of coarser particles along the lower parts of the pile and of finer particles in the upper parts. Stratification refers to the formation of successive layers of coarser and finer materials along the advancing face, sloping at the internal angle of friction of the ore.

Segregation and stratification are absent from laboratory column leaching since great care is usually taken to ensure the ore is homogenously distributed in the columns. However, several authors on applied heap leaching such as Gross and Gomer (1992),

Bartlett (1995), Kerr (1997) Miller (1998), O'Kane et al. (1999), Kappes (2002), Smith (2002) and Guzman et al. (2006) have referred to 'segregation' (thereby implying segregation and stratification) as being an inevitable consequence of current stacking practice. They have all speculated that it must be affecting heap leaching performance. Dixon (2003) identifies segregation as one of the '*non-linear effects'* (quoting his terminology) which had up to the date of his publication not been studied systematically for the purpose of describing its effect on heap leaching performance. And neither have the effects of segregation/stratification been characterised in terms of any design calculations or safety factors.

Segregation is the more commonly observed phenomenon and is virtually certain to occur when a mixture of particles of different sizes are stacked, unless special precautions are taken such as moving the stacker back and forth laterally. However stratification has been observed to occur only over a limited range of combinations of particle size ratios, differences in internal angle of friction and stacking rates, (Benito et al., 2014). Implicit in these definitions is therefore that stratification can always be assumed to be accompanied by segregation as well, although the inverse does not necessarily apply.

O'Kane et al. (1999) is one of very few authors who have made any attempt at a systematic study of the effect of (what they termed) segregation, studying the passage of irrigated solution via a column loaded with coarser particles stacked side-by-side with finer particles, as illustrated in Figure 21 below. Wu et al. (2007) performed a very similar experiment. They both concluded that solution travels preferentially via the finer ore fractions as long as the hydraulic conductivity of the fine fraction is not exceeded, attributed to the strong capillary action ("*negative pore water pressure*" according to their terminology), exhibited by the small voids amongst fine particles. At higher irrigation rates, solution flows preferentially via the coarser fraction, while Miller (1998) refers to similar observations having been made during chloride tracer tests.

However, none of them offered data on direct observations of its effect on the kinetics or efficiency of leaching.

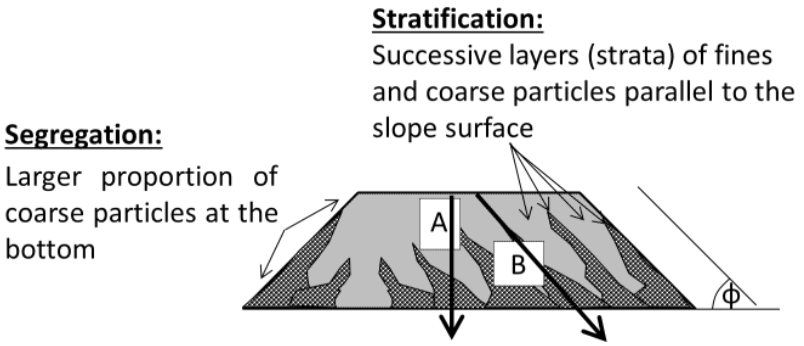

Figure 20. Concepts of segregation and stratification.

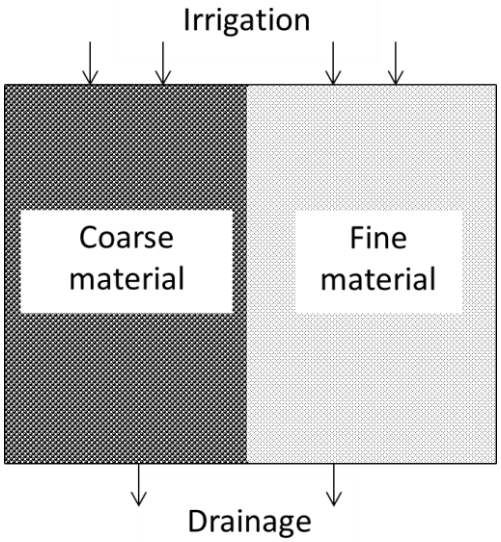

Figure 21. Experiment conducted by O'Kane et al. (1999)

What therefore remains to be done is to conduct comparisons between the leaching performance in the presence and in the absence of segregation and stratification. If these phenomena are indeed found to exert a strong influence over leaching performance, the nature of the relationships should be formulated so that its effect on leaching performance can be separted from the effects exerted by bulk density and dripper spacing, discussed above.

3.17 SUMMARY OF CURRENT KNOWLEDGE AND UNDERSTANDING

Laboratory-scale column leaching performance has been reported to be superior to large-scale heap leaching performance. This has led design engineers to adopt empirical scale-up factors for the deriving heap leach design specifications from column leaching results. These scale-up factors do not account fundamentally for the phenomena

underlying the differences between column and heap leaching performance. Furthermore, they are being applied in the same manner to all cases, without systematically accounting for such factors as the reactions that are due to take place or the type of irrigation to be used.

A review has been provided of the stoichiometry and kinetics of the various chemical reactions that can be expected to occur during heap leaching. The historic development of insights into the hydrology of heaps has been reviewed, up to the most recent evidence for the existence of discrete and relatively sparsely distributed flow channels throughout the ore mass. The solid mass between flow channels relies to an extent on capillary action, but mostly on diffusion for the transport of reagents and leached constituents to and from the mineral surfaces. This has been defined as ‘dual porosity’ hydrology.

It has been established that a difference in the square of the diffusional distance by a factor of 2 or more between two sets of heap leaching results that are compared would be statistically significant. Smaller variations might be attributable to the practical limitations in the extent to which ore composition and heap preparation can be reproduced amongst different heaps. Applying the same criterion to the comparison of column leaching results should be conservative since column leaching results are expected to be more reproducible than heap leaching results.

Possible factors that could account for the differences between column and heap leaching performance include (a) lesser densification of the ore in columns than in heaps, (b) an effectively narrower irrigation spacing in columns than on heaps and (c) segregation and stratification which occur in heaps but which are absent from columns.

4 STUDY SCOPE AND OUTLINE

4.1 OBJECTIVES

It is aimed to:

1. Verify independently whether the leaching performance obtained on commercial heap scale is indeed statistically significantly inferior to that obtained on laboratory column scale, or whether it could be ascribed to merely the random variability inherent in commercial heap leaching results.

   This objective was pursued by analysing the data from four case studies for which both the laboratory column and commercial heap leaching performance data is available for the same ore, as discussed in sections 7, 8, 9 and 10.

2. Verify the effect of segregation and stratification on column leaching performance, while ore type, leaching conditions and leach vessel dimensions are maintained constant.

   Towards this objective, experiments were conducted in custom-built boxes to emulate segregation and stratification, to obtain comparative data on the leaching performance achieved on segregated versus unsegregated, and stratified versus unstratified ore samples. This is presented in sections 11, 12 and 13.

3. Verify which fundamental leaching kinetic parameters are affected by scale-up from columns to heaps if any, and formulate their relation to measurable characteristics.

   Towards this end the formulation of a heap leaching model that accounts for reaction kinetics, diffusional mass transfer and all other phenomena known to occur in a heap, is analysed in sections 5.1 to 5.4. Furthermore, theoretical predictions were formulated of how dripper spacing and densification would affect diffusional mass transfer kinetics in section 5.5. These theoretical predictions were compared to the actual changes observed in the model

parameters that optimised the fitting of the model to the data of the four case studies discussed in sections 7 to 10, and to the segregation and stratification data discussed in sections 11, 12 and 13.

Meeting all of the above objectives would:

1. Provide a fundamental basis for rationalising the differences claimed to have been observed between column and heap leaching performance, by establishing which model parameters need to be manipulated to fit column and heap leaching data respectively, and to what extent.
2. Identify the contributions that each of segregation and stratification make to the differences observed in leaching performance between laboratory columns and commercial heaps.
3. Advance heap leach design towards fundamentally-based prediction of heap leaching performance by extrapolation from column leaching performance. With the knowledge of the adjustments to be made to the relevant model parameters to account for each contributing factor, the effect of scale-up can then be modelled, and novel means for improving heap leaching performance might be identified.
4. Determine whether commercial heap leaching performance could be emulated more realistically in laboratory columns by segregating and/or stratifying the samples prior to column leaching.

4.2 HYPOTHESES

4.2.1 Hypothesis 1

It is hypothesised that the kinetics of laboratory column leaching is fundamentally faster than that of commercial heap leaching due to inferior liquid-solid contact in heaps compared to that accomplished in columns. This is based on the observations discussed in the literature review, which have shown that the ore is not uniformly permeable to solution flow. Rather, solution can find only a limited number of relatively sparsely distributed flow paths through a heap, leaving much of the ore reliant on diffusion for the supply of reagents and removal of leached species.

4.2.2 Hypothesis 2

The first factor contributing to the difference in kinetics between heap leaching and column leaching kinetics is that heaps are subject to greater densification which reduces the voidage and therefore reduces the number of permeable flow channels (i.e. causing these channels to become spaced further apart, as shown in Figure 22(c) below on page 97). This happens because heaps lack the wall support that is provided in columns, so that the ore on heaps experiences more of it own weight. Furthermore, column walls restrict the randomness with which particles can pack in a column, thereby reducing the ultimate extent of densification occurring in columns. It is conceivable that the flow channels might even become spaced further apart than the dripper spacing.

4.2.3 Hypothesis 3

Another factor proposed to be contributing to the inferior kinetics of heap leaching compared to column leaching is that the effective dripper spacing used in narrow-diameter columns is smaller than the dripper spacing on the ultimate commercial heap being simulated. In the ideal case, the dripper spacing should match the spacing of permeable flow channels, as illustrated in Figure 22(a) below. However, with wider dripper spacing being used on heaps, there exists a greater probability that solution will be irrigated at points that are spaced further apart than the spacing between permeable flow channels, as shown in Figure 22(b) below.

4.2.4 Hypothesis 4

It is further hypothesised that segregation and/or stratification, which are absent from columns but inevitable in heaps, further detract from the solid-liquid contact in heaps. Segregation results in a greater proportion of the finer fractions appearing at the upper surface of the heap. The finer fraction is less permeable to solution flow due to the smaller voids amongst smaller particles, and the greater capillary force whereby finer particles retain solution. This futher reduces the number of permeable flow channels in the upper regions of the heap. This causes relatively widely spaced flow channels to develop in the upper surface as illustrated in Figure 23(b) below on page 98, which prevail despite the possibility that more potential flow channels might exist lower down in the heap, amongst the coarser particles.

Stratification might have the effect of diverting flow away from a vertical flow path, as illustrated in Figure 24(b) below on page 99. It is hypothesised that leach solution on its way down through a heap will become displaced in the direction of downward slope of the stratification layers. This follows from the reasoning that as solution migrates downward from the point of irrigation, it should soon encounter a stratification layer that is more conductive to flow than the vertically downward flow channel, while all stratification layers are sloped at the internal angle of friction.

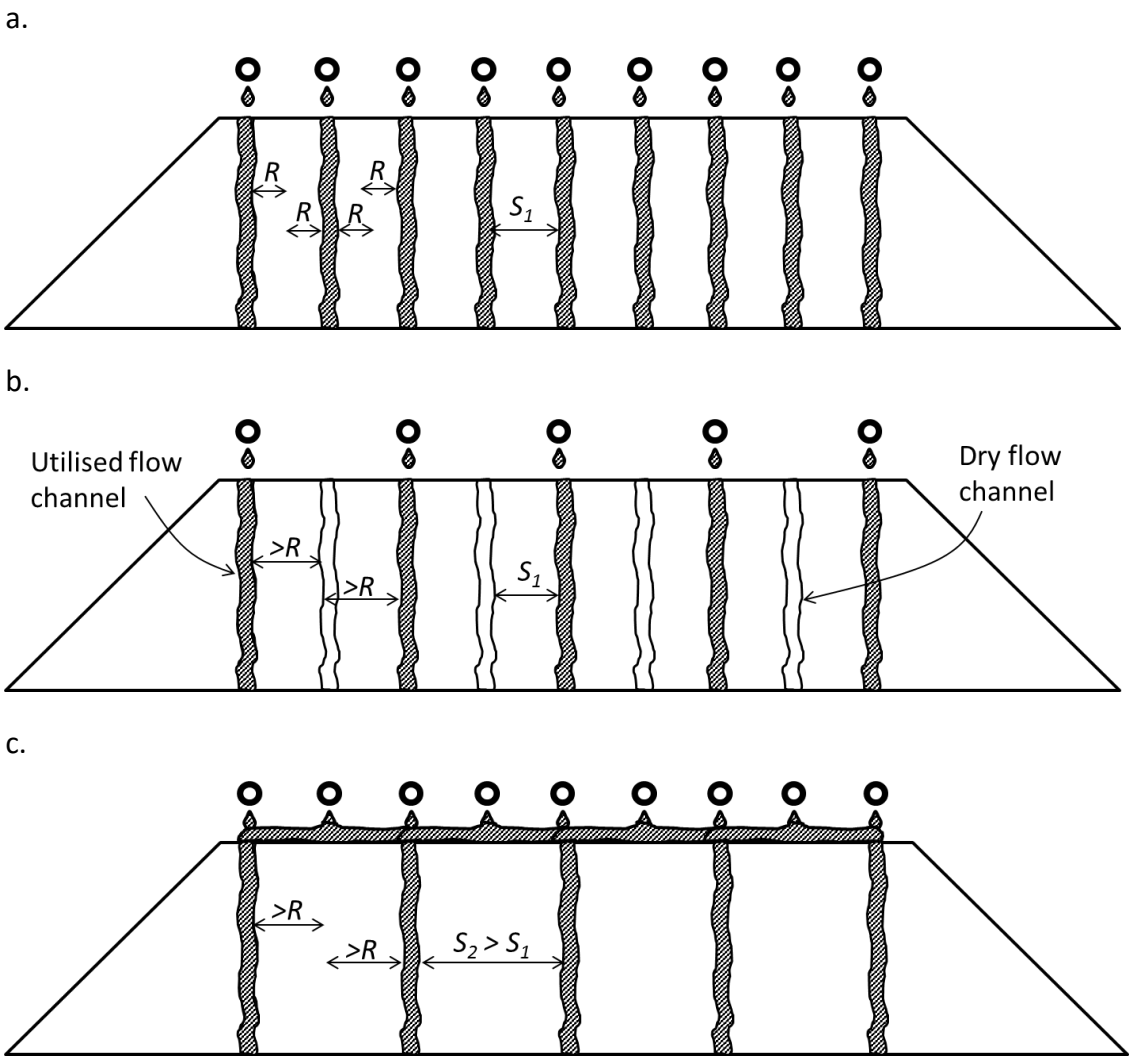

Figure 22. Effect of dripper spacing and densification on diffusional distance. being (a) R when ideal, (b) >R with dripper spacing wider than flow channel spacing, (c) >R with flow channel spacing wider than dripper spacing due to heap densification. The spacing between flow channels is shown here to double in length in each case, but of course the increase can be by any factor larger than unity.

The larger spacing between flow channels can lead to a longer diffusion path via which solution needs to migrate from active solution flow channels to the surrounding ore, with this mass transfer restriction slowing down the effective leach kinetics.

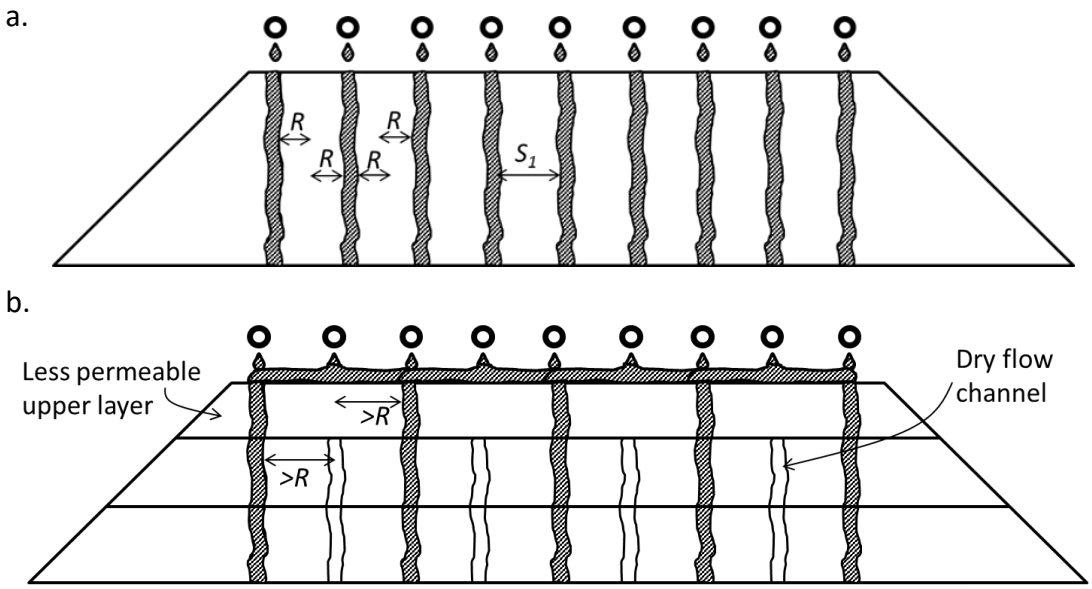

Figure 23. Effect of segregation on diffusional distance.
Being (a) *R* when ideal, (b)>*R* due to less permeable upper-layer after segregation

4.2.5 Hypothesis 5

In more severe cases it might be found that the ultimate extent of extraction achievable by heap leaching is lower than that achievable by column leaching, even if an 'infinite' time period is provided (relative to the typical practical time scale of heap leaching). This would be attributable to parts of the ore remaining completely out of contact with leach solution. This would in turn be the result either of segregation layers diverting flow away from certain parts of the ore in a heap, or due to the dripper spacing or densification extending the diffusional distance to such an extent that virtually no leaching occurs within the practical time scale of heap leaching.

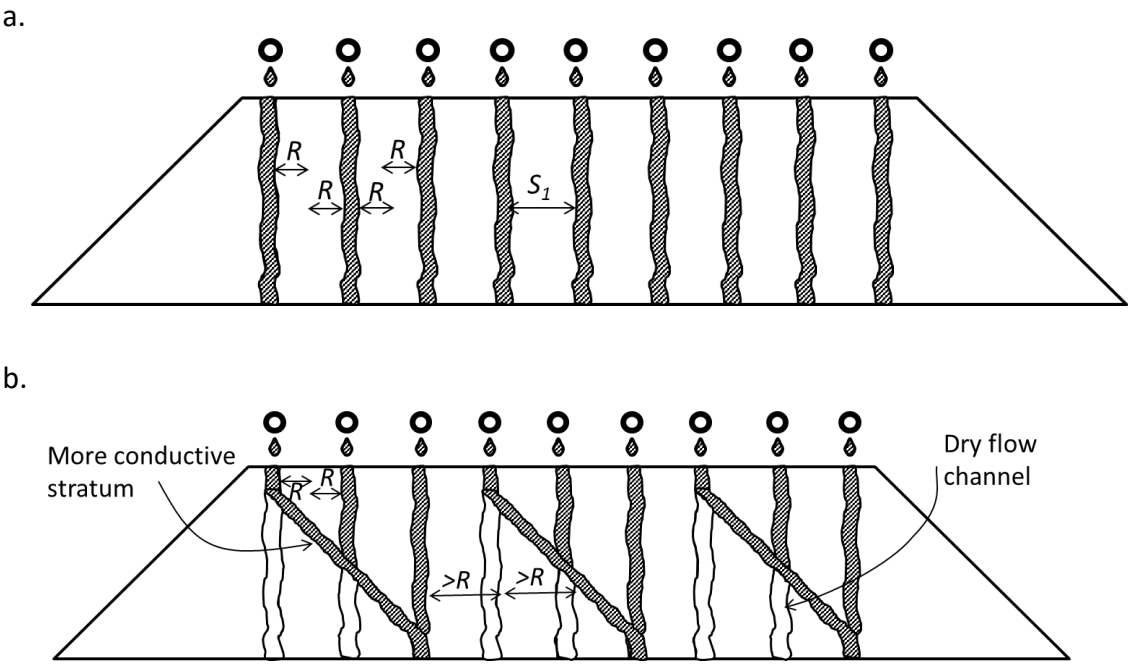

Figure 24. Effect of stratification on diffusional distance.
Being (a) *R* when ideal, (b)>*R* on average due to channeling via more conductive stratification layers

4.3 RESEARCH QUESTIONS

The questions to be addressed towards testing of the hypothesis are:

a. Is heap leaching performance statistically significantly inferior to that of column leaching for a given ore sample?
b. Can the difference in leaching performance between laboratory columns and commercial heaps on the same ore samples be quantified by suitable model parameters?
c. What is the effect of segregation on those geophysical and hydraulic ore properties that are relevant to column and heap leaching performance?
d. What is the effect of segregation on the macro-scale rate and extent of metal extraction and reagent consumption?
e. Since segregation is a phenomenon associated with commercial-scale stacking and is typically absent from laboratory-scale column leaching, to what extent

could the differences observed between laboratory column leaching kinetics and large-scale kinetics be attributed to segregation?

f. Could the results from laboratory column leaching be made more directly applicable for drafting large-scale heap leaching specifications if the ore is artificially segregated in preparation for laboratory column leaching experiments?

g. Does a measurable difference exist in the extent and direction of displacement of the solution flow path as solution passes through stratified ore, compared to when it passes through unstratified ore?

h. What is the effect of stratification on the hydrology (and therefore the efficiency of liquid-solid contact), as measured by the asymptotic extent of dissolution?

i. What is the effect of stratification on heap leaching performance, as quantified in terms of fitted parameters?

j. Since stratification is a phenomenon associated with large-scale stacking and is typically absent from laboratory-scale column leaching, to what extent can the differences between the leaching performance observed in laboratory columns versus commercial heaps be attributed to the effects of stratification?

k. Can laboratory-scale leaching experiments provide data that compares more realistically with large-scale heap leaching performance by stratifying the ore samples in preparation for laboratory column leaching experiments?

l. Should alternative stacking means be devised to avoid segregation and stratification on commercial heaps?

4.4 METHODOLOGY OUTLINE

In order to answer the research questions, it is required that heap leaching performance be quantified. The two aspects of performance to be quantified are namely (a) the leach kinetics and (b) the maximum achievable extent of extraction.

Towards this end, a mathematical model is identified which is based on the most modern understanding of heap hydrology, which has been applied not only at column-scale but also at crib and heap scale, and which contains suitable parameters for the quantification of kinetics of all relevant reactions and the maximum ultimate extent of extraction.

Data was obtained from four case studies that provided comparative heap and column leaching data. The case studies were, in sequence of publication of the results, (a) cyanide leaching of free-milling gold from the Rand Leases sand dump material from the Witwatersrand, published by the author in 1988, (van Staden and Laxen, 1988), (b) leaching with an unidentified reagent of gold from Nevada ore exploited by the Barrick company, published by Bouffard and West-Sells (2009), (c) acid heap leaching of copper from the Kipoi oxide-copper ore, published by the author in 2017, (van Staden et al., 2017a) and (d) heap bioleaching of sulphidic ore from a copper mine belonging to NICICO, located in the Kerman province of Iran, the data of which was published by the author in 2017, (van Staden et al., 2017c). A separate section is dedicated to the analysis of each case study. The data of these case studies were fitted to the model. The model parameters which optimised the fit to the case study data served as quantifiers of the leaching performance of each case.

The Transfer Time served to quantify the kinetics. The Transfer Time is related to the distance over which diffusion needs to occur via immobile solution, with a shorter distance leading to faster kinetics.

To gauge the maximum extent of extraction, the parameter grouping $\kappa_x\kappa_w$ was introduced into the topological term, where $0 \leq \kappa_x \leq 1$ represents that proportion of the mineral content that is not occluded by inert gangue and is not refractory to leaching under the applied leaching conditions. Parameter $0 \leq \kappa_w \leq 1$ is that proportion of the ore

that is effectively in contact with leaching solution. The ultimately achievable extent of extraction is therefore limited to $0 \leq \kappa_x\kappa_w \leq 1$. Its value was determined by fitting the batch extraction curve to a power-law function bearing $\kappa_x\kappa_w$ in such a way that the extraction asymptotes to $\kappa_x\kappa_w$ as $t \rightarrow \infty$. The term $\kappa_x\kappa_w$ is also introduced into the mineral leaching rate expression of the model so that the ultimate extent of extraction is limited to $\kappa_x\kappa_w$.

In order to render the Kipoi heap leaching data (case study c above) suitable for analysis, it was necessary to develop a diagnostic technique for converting the data from this continuous operation into the form of a batch curve. Section 1 is dedicated to the development of that technique.

Two versions of the heap leaching model were required. The pre-existing HeapSim model was particularly useful for its speed and ability to incorporate the aeration and microbially-assisted oxidative leaching of sulphide minerals. However, a second version, coded in PhreeqC, had to be developed to simulate the spatial variations in physical and chemical kinetic parameters that were encounted during segregation. However, the PhreeqC model accommodates only chemical leaching that does not require aeration or microbial reactions.

The Transfer Times of each heap leaching case study, Θ, was expressed as a multiple of the Transfer Time observed during the column leaching of the same sample, Θ_{ref}. The square root of this ratio was termed the Dimensionless Transfer Radius (DTR). Theoretical correlations were derived for the expected relationships between DTR and densification, and between DTR and dripper spacing. It was then verified how well the observed (i.e. model-fitted) DTR's correlated with the theoretically derived DTR-vs-densification and DTR-vs-dripper-spacing correlations.

Conclusions could then be drawn regarding the effects of dripper spacing, densification, segregation and stratification on the DTR, representing an expansion in diffusional distance with scale-up. Similarly, conclusions were drawn regarding the effect of dripper spacing, densification, segregation and stratification on the ultimate extractable fraction, $\kappa_x\kappa_w$.

5 MODEL DEVELOPMENT

5.1 HEAP LEACH MODEL SELECTION

5.1.1 Criteria

A multitude of models of heap leaching have been published. Criteria that are relevant to this study whereby they can be compared to one another are (a) the type of hydrology assumed, (b) the type of mineral leaching kinetics assumed, which is related to the geometry of the particle or particle clusters within which the leaching mineral is assumed to occur, (c) whether it provides for only a single fluid flow, or for counter-current flow of both solution and gaseous phases and (d) the scale at which it has been proven to be capable of fitting operating data.

5.1.2 Hydrology

The hydrology, i.e. the manner in which the solution passes through the ore to establish liquid-solid contact, is regarded as a critical factor in determining heap leaching performance as mentioned by McBride et al. (2017) and also concluded in section 3.11.13. The basis upon which all models are formulated is the type of hydrology selected. The appearance into solution and disappearance out of solution of dissolved species, as a result of chemical reactions, is provided for by means of source terms. The source terms are merely added to the equations that describe the movement of solution through the heap, regardless of whether solution movement is described as being plug flow, or formulated according to Darcy's law, as diffusion with reaction or described by any of the CFD models.

The simplified visualisations of the different types of hydrology upon which models have been based are illustrated in Figure 25 below on page 105. It shows a) Solution plug flow via uniformly distributed particles as per Jansen and Taylor (2002), (b) solution in plug flow which envelops individual particles leaching by shrinking core kinetics as per Leahy et al. (2004), and (c) the dual-porosity concept according to which solution passes amongst particle clusters via sparsely distributed flows paths, as per the 'meta-particle' (or cluster) shrinking core model of Miller (2003b) and the HeapSim model of Petersen and Dixon (2003a).

Despite the evidence for dual-porosity hydrology prevailing in heaps as discussed in section 3.11.13, a number of mathematical models of heap leaching have been published in which solution is envisaged as passing through a heap by plug flow. For example, Jansen and Taylor (2002) proposed such a model, but they did not validate it against experimental observations. It requires the user to make experience-based adjustments to column leaching kinetics to allow the model to reflect heap leaching kinetics. This model was more intended for planning the stacking-sequence and anticipated rate of production related to multiple heaps. For its application the user needs to either have prior knowledge of the heap leaching kinetics, or needs to be able to predict the heap-scale performance from column-scale data from experience. A plug-flow assumption was also used for the purpose of the heat and oxygen balance derived by Dixon (2000), where the effective heap leaching kinetics was not the primary concern.

Heap leaching models based on plug-flow have been successfully fitted to narrow-diameter column leaching data, such as that by Leahy et al. (2004) which was fitted to the column bioleaching results of Dixon and Petersen (2003). This suggests that leaching in narrow-diameter columns data may closely approximate plug flow. However, no examples exist of fitting such a model to larger-scale leaching performance.

Although the 'meta-particle' (or cluster) model of Miller (2003b) and the HeapSim model of Petersen and Dixon (2003a) are based on the same visualisation of the hydrology, the formulations of the mineral leaching kinetics differ from one another. The model of Miller (2003b) assumes that each particle cluster exhibits shrinking core kinetics (i.e. according to equation [54]). However, the HeapSim model describes mineral leaching by equation [56] with the additional parameter Φ (i.e. the power of the unreacted fraction). This permits greater flexibility in fitting the effective leaching behaviour of different size distributions of particles, as discussed in section 3.12.4. The model of Miller (2003b) has been used to model to the extraction curves of a large number of commercial heaps, and the HeapSim model has been used by Bouffard (2008) to model the performance of cribs of 9 m^2 cross sectional area. That provides confidence that this visualisation of hydrology can be applied to the modelling of heap leaching and not only of column leaching.

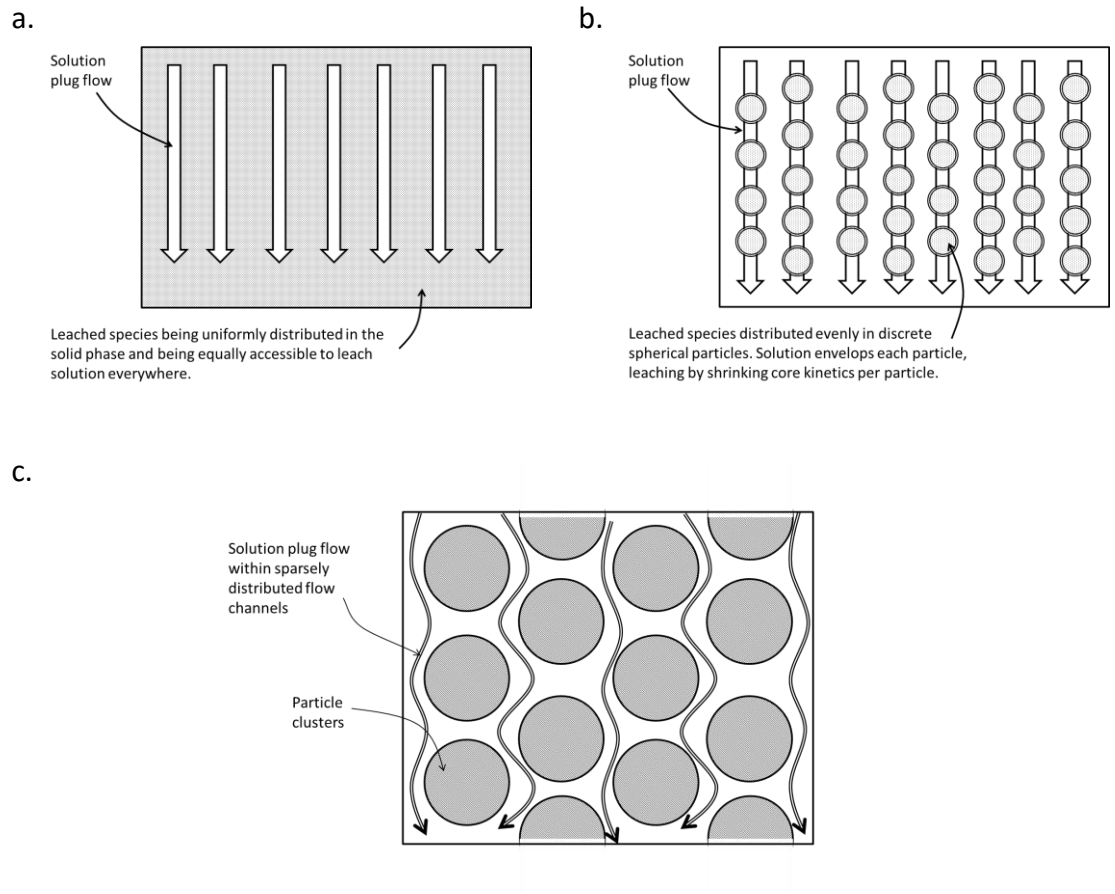

Figure 25. Various visualisations of heap hydrology for modelling.
(a) Solution plug flow via uniformly distributed leached species, (b) solution plug flow enveloping individual particles which leach by shrinking core kinetics, (c) dual porosity flow via sparsely distributed paths amongst particle clusters.

5.1.3 Leach kinetics

The manner in which the kinetics of leaching of various minerals can be represented have been discussed in section 3.12. A heap leaching model should ideally provide for all the chemical and oxidative leaching reactions discussed in section 3.12. By implication it should therefore also provide for multiple leaching reactions that compete for a common leach reagent.

5.1.4 Counter-current advection

A model that provides for the movement of only a single fluid through the heap from a single entry point (for example only solution entering from the top, or only air entering from the bottom), is relatively simple. It provides a single set of boundary conditions to describe the state and composition of the fluid at the entry point. From there, the state and composition in each subsequent vertical increment can be calculated directly. In

contrast, if two fluids are flowing counter-currently (i.e. solution from the top and air from the bottom) which are assumed to be in thermal and/or gas-liquid equilibrium, an iterative solution is required. For example, an assumption needs to be made about the states and compositions of the two fluids at the top. From there, the states and compositions are calculated per vertical increment down to the bottom. The states and compositions thus calculated at the bottom need to be compared to the known or required states and compositions at the bottom. The assumed states and compositions at the top need to be adjusted and the calculation repeated, until the states and compositions calculated at the bottom conform to what is known or required. Therefore, a model that provides for the flow of only a single fluid would require significant re-coding to facilitate the flow of two fluids in equilibrium.

5.1.5 Validation versus larger-scale results

In order to analyse heap leaching data by fitting a model to its performance data, confidence is required that the model provides a reasonable representation of the processes underlying its performance.

The shrinking-cluster model of Miller (2003b) has been fitted to numerous commercial-scale heaps by Miller (2003b) himself.

Dixon and Petersen (2003) calibrated the HeapSim model to the column bioleaching data obtained on a chalcocite ore. Referring to their Figure 2, the copper concentration in the drainage was fitted virtually perfectly. With the same set of model parameters the extent of copper extraction, bacterial cell counts as well as ferrous and ferric iron concentrations extraction were all fitted well. The timing of peaks and flattening of curves were correctly predicted. Petersen and Dixon (2007b) calibrated the kinetic parameters of the HeapSim model against the oxidative leaching results of zinc-sulphide-bearing ore leached in a 6m tall column with 150 mm diameter. Using the set of kinetic parameters thus calibrated, they managed to predict quite successfully the performance of a 6m high, drip-irrigated pilot heap with a 5m x 20m footprint. To fit the model to the heap data, it was necessary to only adjust the diffusional distance, despite the fact that the mineralogy of the ore on the heap did not exactly match that of the ore in the column. With the same model, Bouffard (2008) successfully modelled the

bioleaching of ore bearing precious-metals in pyrite. The drainage iron concentration, extent of iron extraction and extent of sulphide conversion observed in four cribs of 9 m^2 cross sectional area were modelled using a single set of model parameters.

Both the model of Miller (2003b) and HeapSim use the dual porosity visualisation of hydrology combined with a form of 'diffusion with chemical reaction' kinetics, providing confidence in the rigour with which such models represent the reality of heap leaching performance, even at a scale larger than a narrow-diameter column.

5.2 THE HEAPSIM MODEL

As already mentioned, the HeapSim model is based on dual porosity hydrology combined with diffusion with chemical reaction in the region occupied by immobile solution. At the time of publication of the paper by Dixon (2003), the HeapSim model possessed the most comprehensive features in comparison to other modelling approaches at the time, including kinetic expressions for the various dissolution, oxidation, precipitation and microbial reactions occurring in the heap. As a result of the previous model-fitting undertakings, the ranges within which the kinetic and equilibrium constants can vary have been determined, providing reliable default values for use where the opportunity does not exist to determine them independently, as discussed by Petersen (2010b).

Despite its sophistication, HeapSim solves very rapidly, within 30 seconds to calculate 1,000 time increments on a 1.8 GHz PC.

The HeapSim model provides for the counter-current flow of both irrigation solution and air, and an energy balance between the two phases, as per Dixon (2000). As part of the energy balance and in providing for the mass transfer of oxygen, plug flow of the gaseous phase from the bottom to the top of the heap is assumed. As mentioned in section 3.13, this seems a reasonable assumption.

However, there is some contradiction inherent in the formulation of the transport of the gaseous phase. For the purpose of the energy balance, is it assumed the gaseous phase shares the space occupied by flowing solution. However, for the purpose of oxygen

distribution, it is assumed the gaseous phase occupies the region filled with stagnant solution.

Furthermore, the transport of dissolved oxygen via the solution phase is effectively assumed to occur instantaneously, relative to the rate of oxygen transfer from the gaseous to the aqueous phase. This should not pose a serious limitation if it is considered that dissolved oxygen (O_2(aq)) is not necessarily required at the mineral surface, it is only required in the aqueous phase for the oxidation of ferrous to ferric iron (with the latter performing the oxidative leaching), and for the oxidation of sulphur/sulphide to sulphate.

On the basis of it being based on dual-porosity hydrology, being comprehensive and that it has been fitted to larger scale data, the HeapSim model was selected for most of the heap leach modelling work presented in this study.

HeapSim permits an unlimited number of step-changes in the temperature, flow rate and composition of the leach solution, and inlet flow rate of the air. However, for the purpose of investigating the effect of segregation, it was also required to specify different values of composition, density, moisture content and rate constants of the ore contained at different elevations in a column of ore. This is not provided for in HeapSim.

A model based on the same hydrology and kinetics was therefore coded in PhreeqC, and calibrated against the HeapSim model. However, the PhreeqC model was not coded to provide for bacterial or oxidative reactions, and also does not provide for counter-current flow of two fluids. Therefore, the application of the PhreeqC model has been limited to the modelling of the isothermal acid heap leaching of acid-soluble mineral.

5.2.1 Formulation of hydrology and kinetics

A more detailed visualisation of the dual porosity hydrology used in HeapSim is shown in Figure 26 below. It shows a spherical porous region of ore with radius *R*, constituted of ore particles over the entire size distribution which might be present individually or contained in agglomerates. The porosity of the region is partially filled with immobilised solution, the balance is filled with air. The spherical region under consideration is situated in the flow path of an advective flow channel, and mobile solution is enveloping

it. Dissolved species pass between the immobilised solution within the spherical region and the mobile solution enveloping it, by diffusion along tortuous diffusion paths, indicated by the wavey arrows. As reagents pass through the immobile region, it reacts chemically with the metal-bearing minerals as well as the reagent-consuming gangue minerals contained in the solid phase. Leached metal diffuses from the immobile region into the mobile solution which carries it vertically downward, to eventually exit the heap by draining from the bottom.

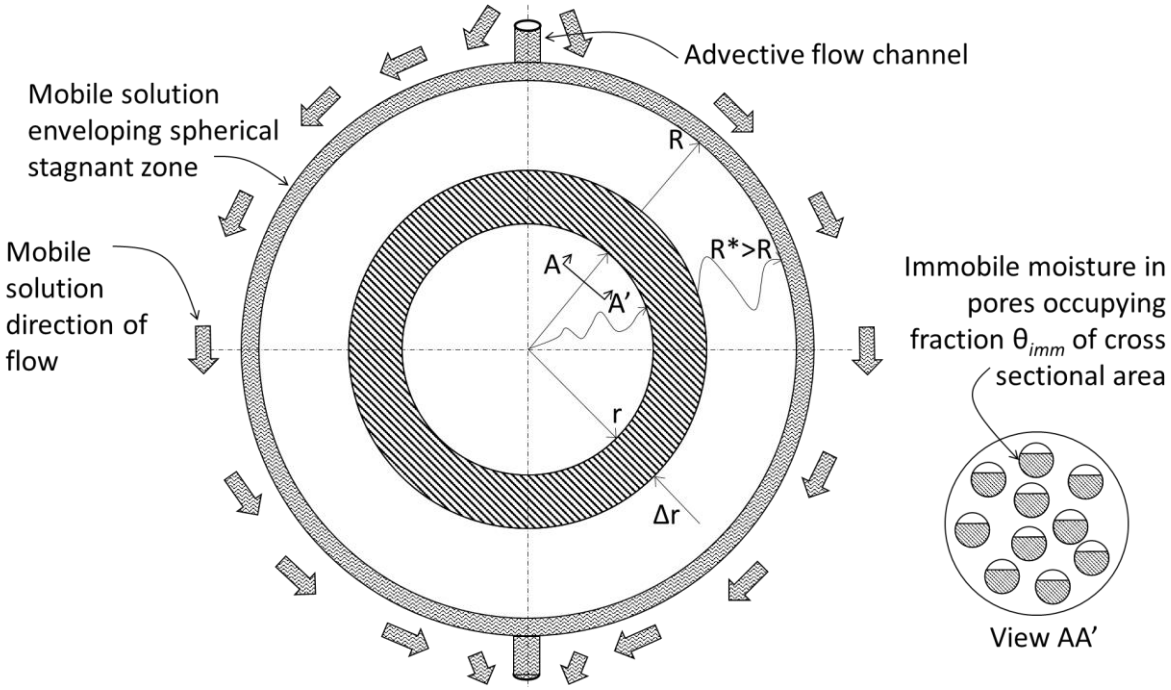

Figure 26. Visualisation of dual porosity hydrology

In one sense the dual porosity model considers flow in two dimensions, namely advective flow of mobile solution vertically from top to bottom, and diffusion of ions 'laterally' (to be understood in the case of a spherical immobile region as illustrated here, to actually mean 'radially'), from the mobile solution into a spherical mass of stagnant solution. Yet it is devised such that the two flows can be analysed separately, each as a one-dimensional phenomenon, with vertical flow of mobile solution being entirely advective, and the exchange of ions between the mobile and immobile solutions and within the immobile solutions being entirely diffusional.

The derivation of the equation to describe the diffusion of ions through the solution that is immobilised within the porosity of the spherical mass relies on Fick's first law of diffusion. Fick's law in a single dimension suffices for the purpose. Furthermore, the model addresses a transient process, yet in the derivation of the continuity equation for the immobile solution phase a pseudo-steady state assumption is made over a short time interval (Δt), which allows the use of Fick's first law, as opposed to the second law for transient diffusion.

Different forms of the continuity equation for the dual porosity model are encountered in literature. Although they might superficially seem different, they can all yield the same result provided their model parameters are calibrated against one another. To avoid confusion and to illustrate how the apparently different formulations can come about from analyses of the same system, two examples of different (yet equally valid) derivations are offered in Appendix C. It leads to:

$$\frac{\partial C}{\partial t} = D_e \left[\frac{\partial^2 C}{\partial r^2} + \frac{2}{r} \frac{\partial C}{\partial r} \right] + \sum s_i \qquad [64]$$

with effectively units of $\left[\frac{\text{mole}}{\text{m}^3_{\text{imm}}\ s}\right]$ where D_e is the effective diffusivity, C is the concentration of any species in the immobile solution at radial position r at time t and Σs_i is one or more source terms describing the rate at which species i enters the immobile solution by leaching from the solid phase. One example is the source term for GAC that appears in equation [61], another is the mineral leaching term that is generalised in equation [56]. The final form of the topological term for mineral leaching that is used for this study is discussed in section 5.5.1.

Note that there also exists a HeapSim-2D formulation which is not to be confused with the HeapSim model selected for this study. In the HeapSim-2D model, the hydrology is based on Richard's equation (discussed in section 3.11.8) and the formulation is detailed by Dixon and Afewu (2011).

5.2.2 Introduction of Transfer Time

Estimating the value of R as about half of dripper spacing on a heap, or half of the diameter of a laboratory column, has been suggested by (Dixon and Petersen, 2003).

However that assumption would be invalid if multiple flow channels were to split away from a dripping point, as opposed to a single flow channel emanating from each dripping point. That flow channels split into multiple flow channels has been observed by McBride et al. (2017). The magnitude of *R* would be very sensitive to such phenomena. Furthermore, in the model of Dixon and Afewu (2011) for the spread of an advective plume of solution below a dripper, (which they reported is incorporated into the HeapSim-2D software, to which the author has not had access), it is evident from their equation [2a,b,c] that a non-zero component of the solution flux vector $\mathbf{v} = v_z + v_r$ prevails in any direction in which a gradient in level of liquid saturation prevails. For the case that yielded the saturation profile depicted in their Figure 3(a), non-zero radial saturation profiles (implying radial advection) were shown to exist at steady state across about $^2/_3$ of the cross sectional area in the upper parts of the column, so that solution is spread evenly across the entire cross sectional area by about ¼ to $^1/_3$ into the depth of the column. From that point downwards the radial saturation profiles are about zero indicating zero radial advection. However, it also means that the solution hence spread over the cross sectional area gravitates downward to contact the entire ore mass below it by vertical advection. This is in total contrast with the Turner structure assumed for the HeapSim model where the entire ore mass is assumed to bathe in stagnant solution, which communicates with the sparely distributed flow channels of zero dimension by diffusion only. This also seems to be hinted at in the section addressing Hydrology and Solute Transport by Dixon (2003) where he states that ideally the modelling of the hydrology of a heap should include provision for lateral flow due to capillary action (although he also argued there that it will only prevail for a relatively short time until the porous space is saturated with stagnant solution).

Both are conceptual models and probably contain some elements of the truth, with reality probably being some combination of the two models plus some factors not yet considered. The implication thereof for the HeapSim model is that it is hard to attribute clear physical meaning to the effective diffusivity appearing in [64] since it can be affected by radial advection in at least part of the ore mass. It is also hard to attribute half of the dripper spacing to the diffusion path length *R*, since the mobile solution flow path is not a singularity on the cross sectional area, but describes a plume radiating

outward from the drip application point, which means the diffusion path length should be smaller than half of the dripper spacing.

The use of Transfer Time (Θ) as a single characteristic parameter is therefore proposed to overcome this difficulty. If the dimensionless diffusional path length is defined as:

$$\xi = \frac{r}{R} \quad \text{so that } 0 \leq \xi \leq 1 \qquad [65]$$

then [64] can be re-written as:

$$\frac{\partial C}{\partial t} = \frac{D_e}{R^2}\left[\frac{\partial^2 C}{\partial \xi^2} + \frac{2}{\xi}\frac{\partial C}{\partial \xi}\right] + \sum s_i \qquad [66]$$

The Transfer Time Θ, is given by the inverse of the term before the square brackets, namely R^2/D_e, and by further substitution of the definition of D_e according to equation [41] follows:

$$\Theta = \frac{R^2}{D_e} = \frac{R^2 \tau_\delta^2}{D\theta_{imm}} \text{ with units of time} \qquad [67]$$

Transfer Time can be seen to indicate the time required for diffusion of a species with diffusivity D to occur across a tortuous path via a spherical zone of radius R. The resistance to diffusion is reduced (i.e. the Transfer Time is shortened) by a larger volumetric fraction θ_{imm} of solution held stagnant in the spherical zone, since diffusion can only occur via the solution phase; an increased value for θ_{imm} increases the cross sectional area available for diffusional mass transfer, as illustrated in Figure 26 on page 109.

A long Transfer Time implies that solutes travel more slowly by diffusion between the flowing solution around a spherical immobile zone than the rate at which they are being carried in the flowing solution, (refer back to Figure 26 on page 109). One effect of that phenomenon is that, under conditions of a long Transfer Time, un-utilised leaching reagent would break through to the drainage solution sooner, yielding hence poorer utilisation of the reagent resulting in a slower rate of leaching. An example of that phenomenon is observed in the comparison of the leaching performance in narrow

column versus that in wide boxes that is discussed later in section 13, specifically in Figure 59 (c) and (d) on page 224.

A mathematical model would typically not provide for Transfer Time as a model input, but would rather require specification of (a) diffusional radius, (b) diffusivity and (c) moisture content. To give effect to the concept of Transfer Time, the user could consider the input to (a) as representing $R^2\tau^2$, the input to (b) as representing D and the input to (c) as representing θ_{imm}. The Transfer Time represented by these inputs can then be calculated either as part of, or outside of the programme code from equation [67].

The Transfer Time is similar to the diffusion time (Γ) used in texts such as Van Staden and Petersen (2018a). However, D_e has there been assumed to be invariant and it was hence implicitly assumed that variations in τ_δ^2 and θ_{imm} would cancel one another. In this text D_e is treated also as a function of τ_δ^2 and θ_{imm} so that, for the purposes of comparisons between the different texts, $\Theta = \Gamma/\theta_{imm}$. To avoid confusion, the concept has been provided the new name and symbol of "Transfer Time", Θ.

5.2.3 Equivalent parameter sets

The characterisation of leaching performance in terms of Transfer Time as opposed to all of R, τ_δ^2 and θ_{imm} reflects the fact that these parameters do not affect leaching performance independently. Rather, it is the ratio between these parameters that determine leaching performance, and any number of different values for R, τ_δ^2 and θ_{imm} that yield the same value for Θ will result in the same leaching performance. (In so doing it also needs to be borne in mind that a change in θ_{imm} changes the effective rate of gangue acid consumption (GAC) as a result of the formulation of rate of GAC, as discussed in section 3.12.5. The adjustment that is required to retain the same rate of GAC is explained there.

To illustrate the principle, the copper and GAC kinetics are compared in Figure 27 below for two sets of inputs that both yield a Transfer Time of 55.5 days and a rate of GAC of 0.01 kg acid per tonne per hour (by mainaining a constant product of $k'\varepsilon_{imm} = 0.0014$ h^{-1} as discussed in section 3.12.5, but using the two very different input data sets of respectively (R; D; θ_{imm}; k') = (0.143; $1.56\text{x}10^{-8}$; 0.27; 0.0068) and

(0.161; $3x10^{-8}$; 0.18; 0.10). The bulk density ρ was maintained at 1,327 kg/m^3 in both cases so that the two moisture contents values ε_{imm}, in terms of t moisture per t dry ore, correspond to respectively 0.20 and 0.14 t/t. These are variations of the modelling of the un-stratified wide box leaching data of the Oxide 1 sample, being presented as one of the case studies that follow in section 11. The two sets of model outputs can be seen to be indistinguishable.

a.

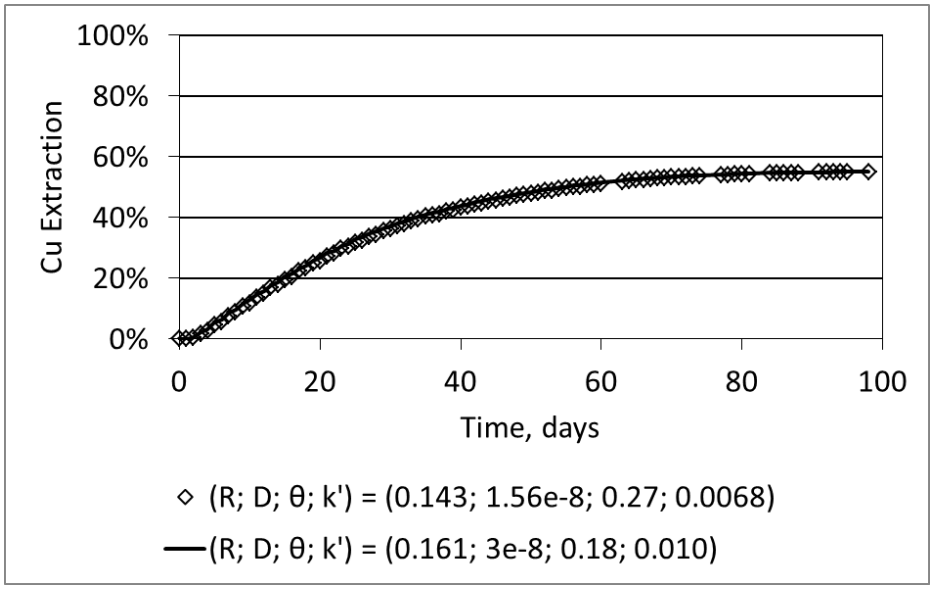

b.

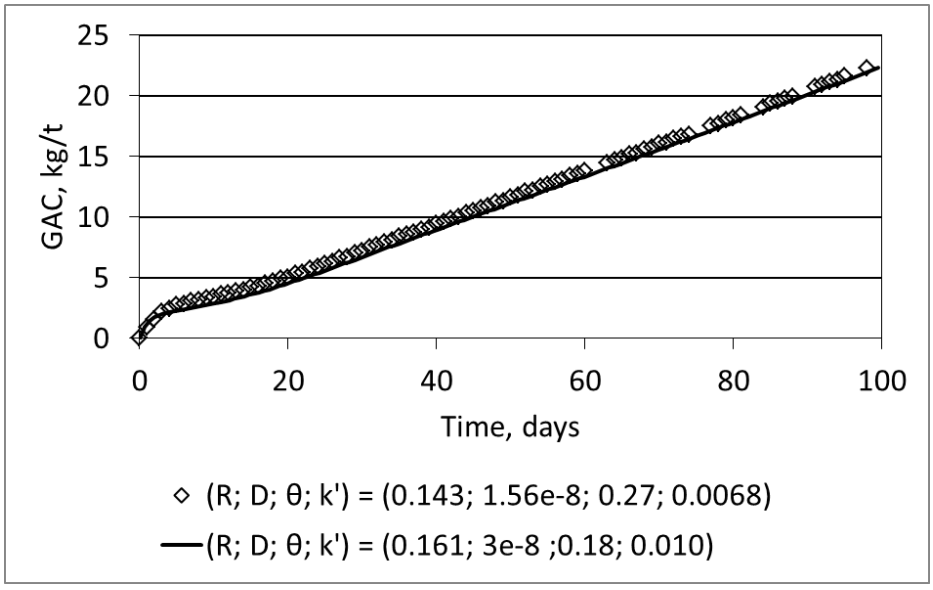

Figure 27. Comparison of leaching results using equivalent sets of parameters
(a) Rates of copper extraction; (b) Rates of GAC

5.2.4 Sensitivity to Transfer Time

Simulations were performed in HeapSim for two sets of heap height (*L*) and feed acid concentration, while varying the Transfer Time over a large range as indicated in Figure 28 below. It shows that Transfer Time starts exerting a strong effect on the extraction curve for Transfer Times greater than the order of 15 days for the case where *L* = 0.7 m while it had a strong effect for the case where *L* = 6 m only for a Transfer Time greater than 150 days. However it has a weak effect for shorter Transfer Times, in the case of the 6 m column with 25g/L acid the results for 1.5 and 15 days are indistinguishable. Therefore if the model needs to be fitted to experimental data with a Transfer Time of 15 days or shorter it would be virtually impossible to determine whether the fit needs to be improved by variation of the Transfer Time or another parameter such as the leach kinetic constant. It is therefore not essential to prepare a PhreeqC model that can model Transfer Times shorter than the order of 15 days.

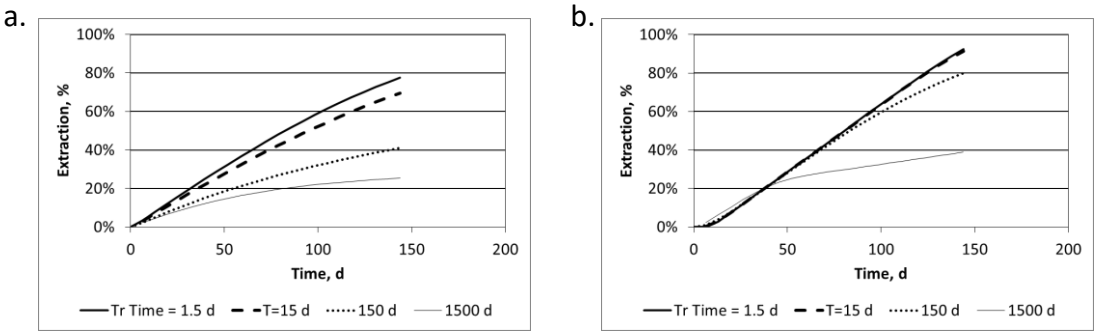

Figure 28. Effect of a Range of Transfer Times on the Extraction Curve
(a) *L* = 0.7m; [acid] = 3 g/L, (b) *L* = 6m; [acid] = 25 g/L

5.2.5 Microbial kinetics

The Monod kinetic expression used in HeapSim for describing the kinetics of microbial processes as a function of ferrous and ferric iron concentrations appears in equation [49].

5.2.6 Concentration function

The universal electrochemical rate law for calculating the kinetics of oxidation reactions is provided in reaction [60].

5.3 THE PHREEQC MODEL

5.3.1 The need for the PhreeqC model

For the purpose of the modelling of the columns of segregated ores, it was necessary to specify different bulk densities, moisture contents and rate constants for the Upper, Middle and Bottom segregation layers. Furthermore, for the modelling of the data of scale-up case study 4 (Kipoi, in section 9), it was found necessary to specify two different GAC rate constants, one prevailing for a short time after commencement of irrigation, and another for the rest of the duration of the leach.

While the "Events Manager" feature of the HeapSim model provides for changes in operating parameters (such as irrigation rate and irrigation solution composition), it does not provide for changes in physical or chemical constants, either during the time course of leaching, or spatially throughout the heap. The PhreeqC model construction does offer the flexibility for these required spatial and temporal variations, and was therefore selected for the task.

For these purposes, the same mathematical description of dual porosity modelling was programmed into PhreeqC and it was calibrated against the HeapSim model to ensure that the model parameters of the two can be directly compared.

5.3.2 About PhreeqC

The PhreeqC geochemical open-source software was developed and is being maintained by the United States Geological Survey. Like the HeapSim model, it is based on dual porosity hydrology and any number of chemical reactions, sorption equilibria and any type of reaction kinetics and can be programmed by the user.

It facilitates the modelling of various different combinations of mobile and immobile **cells** and any extent of exchange of leach solutions between them if the full versatility of the software is being utilised. However it also facilitates simpler versions of dual-porosity flow.

The relatively simple 'first-order' version, illustrated in Figure 29 below, permits lateral mass transfer from each mobile **cell** to a single immobile **cell**, with the rate of transfer being directly proportional to the concentration gradient, from whence its naming is

derived. It allows exchange of species only between a mobile **cell** and its single associated immobile **cell**. It is the easiest to programme since it only requires number entries into the graphic user interface (GUI) and it is the most rapid to execute. However, in van Staden and Petersen (2018b) it was shown that, although the first-order version reproduced short-term pulse test data convincingly, it yielded unrealistic results for longer-term leach tests conducted over the typical time frame of column/heap leaching tests.

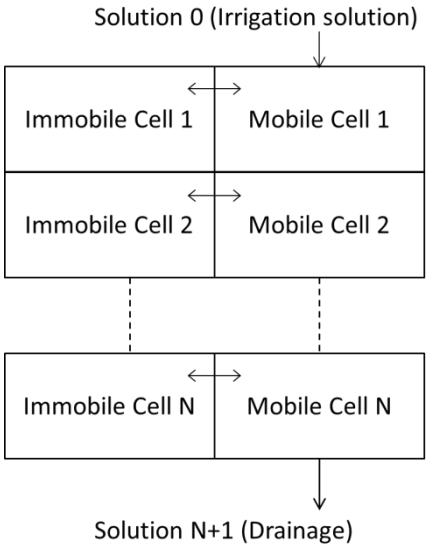

Figure 29. First-order dual porosity hydraulics

The most powerful and flexible specification becomes possible if multiple immobile **cells** are specified per mobile **cell** and the user enters explicit MIX factors. The MIX factors determine the rate at which solution is exchanged between any two **cells**. A generic example is shown in Figure 30 below, with multiple immobile **cells** per mobile **cell**, and with exchanges occurring between all neighbouring **cells**. Note that even exchanges between immobile **cells** of neighbouring mobile **cells** are possible in the general case.

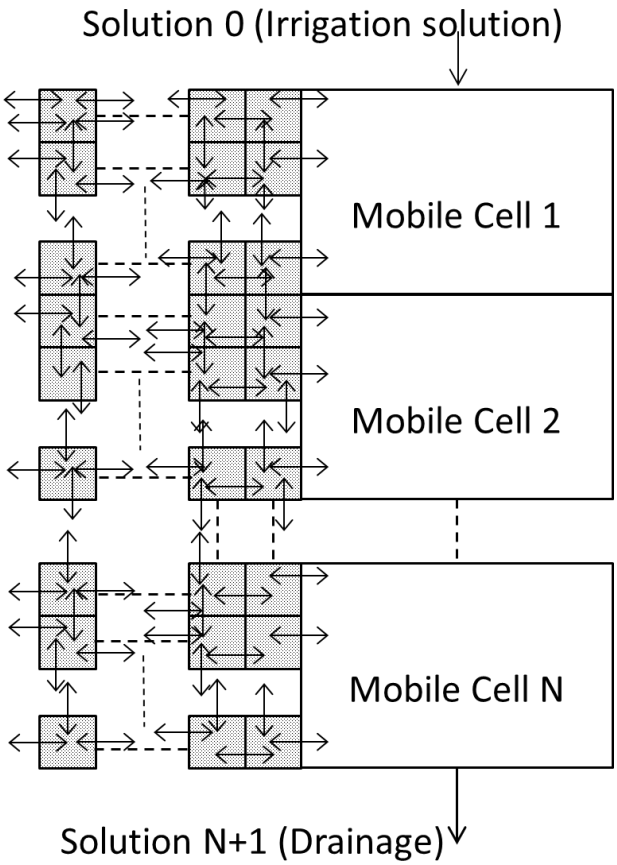

Figure 30. The most general dual porosity hydrology facilitated by PhreeqC (The shaded blocks represent immobile **cells**).

5.3.3 PhreeqC formulation of diffusion with chemical reaction

Parkhurst and Appelo (1999) illustrated the equivalence between diffusion mass transfer in the immobile zone and the operation of the *MIX* data blocks of PhreeqC. The manner in which the mixing factor is derived, such that it would apply to any geometry, is briefly repeated here. A somewhat more detailed derivation is provided by van Staden and Petersen (2018b).

A single mobile **cell** with its associated spherical immobile zone with radius *R*, divided into 5 immobile **cells**, is shown in Figure 31 below on page 120. Consider the accumulation of a solute in **cell** *j* between time *t1* and *t2* (with $t2 = t1 + \Delta t$, the latter term being the time increment) with **cell** *j* being positioned between **cells** *i* and *k* (with *i*

being the stagnant **cell** to the outside of *j*, closer to the mobile **cell**, and **cell** number *k* is the **cell** on the inside towards the centre of **cell** *j*). That is to consider only diffusion laterally between **cells** associated with a single mobile **cell**, without any exchange vertically between immobile **cells**, although PhreeqC can accommodate vertical exchange as well. By writing [64] (or refer to [111] in APPENDIX C) in terms of finite differences for any geometry it follows that:

$$\theta_{imm}\, V_j\, C_j^{t2} = \theta_{imm}\, V_j\, C_j^{t1} + \frac{\theta_{imm} D\, A_{k,j}}{\tau^2} \frac{\left(C_k - C_j\right)}{h_{j,k}}\, \Delta t + \frac{\theta_{imm} D\, A_{i,j}}{\tau^2} \frac{\left(C_i - C_j\right)}{h_{i,j}}\, \Delta t + 1000 \dot{X}\, C_i^0 \theta_{imm} V_j \Delta t$$

which can be re-arranged after elimination of θ_{imm} to yield:

$$C_j^{t2} = \left(1 - \sum_{n \neq j} MX_{n,j}\right) C_j^{t1} + \sum_{n \neq j} MX_{n,j}\; C_n^{t1} + 1000 \dot{X}\, C_i^0 \Delta t$$

where

$$MX_{n,j} = \frac{D\, A_{n,j}\, \Delta t}{\tau^2 V_j\, h_{n,j}}\, f_{bc} = \frac{D_e\, A_{n,j}\, \Delta t}{V_j\, h_{n,j}}\, f_{bc} \;\; \forall\, n \neq j \qquad [68]$$

represents the proportion of the content of **cell** *n* that is mixed into **cell** *j*, where *n* can be on either side of *j*, V_j is the volume of **cell** *j*, $A_{n,j}$ is the contact area between **cells** *n* and *j* and $h_{n,j}$ is the distance between the mid-points of **cells** *n* and *j*. The mixing factor of the central **cell** *j* to itself (i.e. the proportion of **cell** contents of **cell** *j* that remains behind after mixing to neighbouring **cells**) namely MX_{jj} is the difference between unity and the sum of the mixing factors to neighbouring **cells**. Example 13c of the PhreeqC software provides a working model of this type.

The term f_{bc} is unity for the mixing between all **cells** inside the spherical immobile zone. For mixing at the boundary between mobile and immobile solution, the diffusional distance h_{bc} extends from the centre of the outer spherical **cell** to the boundary wall (as opposed to centre-to-centre for diffusion between elements inside the sphere), i.e. $h_{n,j}/2$ so that:

f_{bc} = 2

for calculating the mixing factor between the outer **cell** of the sphere and the mobile **cell**.

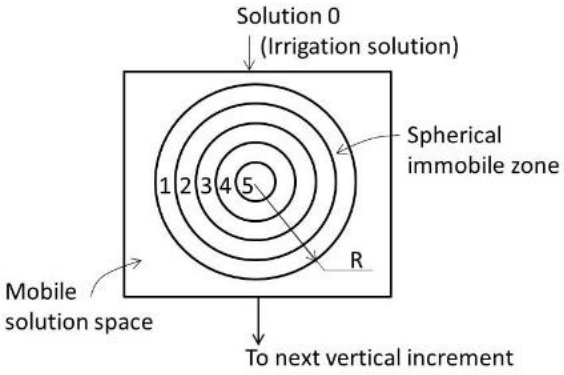

Figure 31. "Spherical Diffusion" hydrology adopted for this study
Reproduced from van Staden and Petersen (2018b).

It is not simple to eliminate $A_{i,j}$ and V_j from [68] to express it in terms of Transfer Time, since the expression needs to provide for the contact area $A_{i,j}$ on both the inside and outside of spherical element *j* to provide for mixing into **cell** *j* from neighbouring **cells** on either side of it. The manner in which to effectively provide a desired Transfer Time input has been discussed in section 5.2.2.

5.3.4 PhreeqC Mass balancing

In van Staden and Petersen (2018b) it was shown how to derive a mass balance for calculation of the extent of value metal *i*, reporting to the drainage solution, from the outputs generated by PhreeqC. The extent of extraction of species *i* to drainage is:

$$X_{i,drain} = \sum_{shifts} \frac{\theta_{mob} C_{i,drain}}{\theta_{imm} C^0_{i,imm} N_z} \qquad [69]$$

$$= \sum_{shifts} \frac{C_{i,drain}\, u\ \Delta t}{\theta_{imm}\ C^0_{i,imm}\ N_z\ \Delta z} = \sum_{shift} \frac{M_i\ C_{i,drain} u\ \Delta t}{W_i\ \rho\ N_z\ \Delta z}$$

where N_Z is the number of vertical increments.

The extent of extraction based on the solid-phase composition is at any given time slightly more than the extraction to drainage, by the amount of species *i* extracted from the solid phase but still residing in one of the solution phases inside the ore column. It is calculated from:

$$X_i = 1 - \sum_{n=1}^{N_z} \frac{P_n C_{i,n}}{N_z C_{i,imm}^0} \quad [70]$$

where:

$$P_n = \frac{r_{n,out}^3 - r_{n,in}^3}{R^3} \quad [71]$$

with $r_{n,out} = R - n.h + h$ and $r_{n,in} = R - n.h$, $0 \leq n \leq N_s$ and N_s the number of immobile **cells** associated with each mobile **cell**.

5.3.5 Determination of TAC and GAC in PhreeqC

The relationship used for calculation of Total Acid Consumption (TAC) during laboratory experimentation and commercial plant operation appears in the Nomenclature, (ref. TAC). It requires acid concentrations (in g/L or molarity of H_2SO_4) in irrigated and drainage solutions as inputs, which are obtained by titration. For the acid leaching of oxide-copper ores, the calculation of GAC follows by deduction of the Cu^{2+} reporting to drainage. However, since PhreeqC fully speciates the solution compositions, the concentration of H_2SO_4 does not appear in the PhreeqC output, acidity is represented by pH instead. That requires conversion between pH and H_2SO_4 concentration towards calculation of TAC and GAC from PhreeqC outputs. This was the approach followed for the modelling results presented in this text, since the experimental GAC calculations also relied on inlet and outlet acid concentrations. The following correlation provided the best fit between experimentally measured pH values and molarity of H_2SO_4 determined by titration:

$$\mathrm{pH} = 0.162 - 0.853 \log[\mathrm{H_2SO_4}] \quad [72]$$

An alternative approach whereby the modelled GAC curve can be calculated is to include $CaCO_3$ as the sole gangue acid consuming species in the solid phase, being also the only species in the solid phase giving rise to Ca^{2+} ions in solution. The kinetic constant for its reaction with acid is set equal to the GAC rate constant, *k'*. The GAC calculation (in moles) in PhreeqC then relies simply on the summation of the moles of Ca^{2+} ions that report to drainage.

In the vicinity of *t*=0, the shapes of the GAC curves calculated from pH/[H_2SO_4] and from [Ca^{2+}] are respectively convex and concave. This is because the reduction in acid concentration in drainage (due to the GAC reaction) precedes the appearance of Ca^{2+} ions by the time lag required for the solubilised Ca^{2+} to report to drainage. The effect is illustrated in Figure 32 below, which is a reproduction of Figure 79(d) on page 296, but with the calculation based on solubilised Ca^{2+} added. But over longer time periods the slopes of the GAC curves calculated by the two methods become equal, and would therefore provide equally valid indications of the long-term rate of GAC.

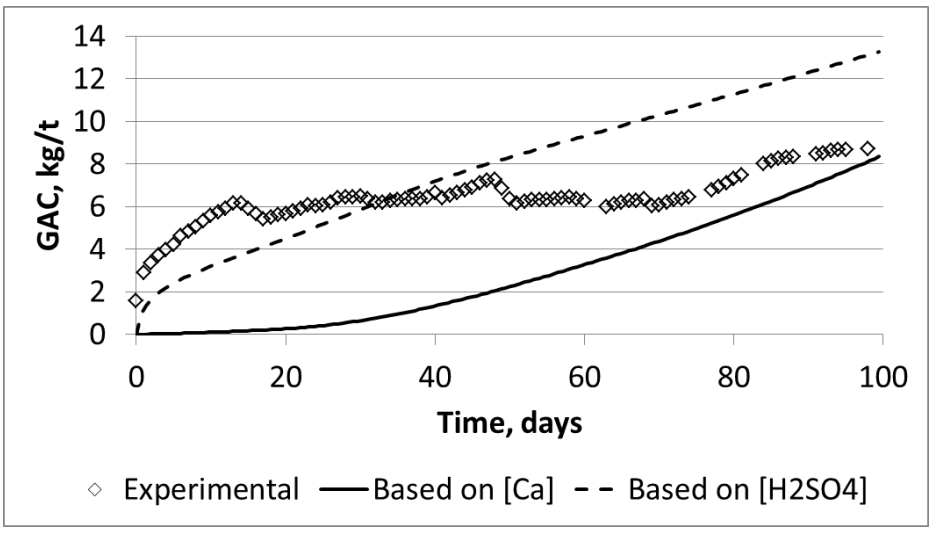

Figure 32. Different calculations of GAC

5.3.6 Spatial and Time Grid for PhreeqC

A feature of the ADVECTION and TRANSPORT data blocks of PhreeqC for simulating percolation through permeable columns is that they are based on the displacement of one mobile **cell** volume per shift. Accuracy and stability of advection flow calculations in PhreeqC therefore require that the following relationship should always be maintained, according to Parkhurst and Appelo (1999):

$$\Delta t = \Delta z / v = (\Delta z\ \theta_{mob}) / U \qquad [73]$$

where Δz is the vertical increments, Δt is the time increment, v is the velocity of flow through the mobile zone and U is the superficial velocity calculated as the flux per unit area of empty column. This means that Δz and Δt cannot be selected independently by the user; selecting one determines the other.

As mentioned above, *MX* factors are used in PhreeqC to emulate diffusion in the immobile zone. In doing so, a further stability requirement prescribed by to Parkhurst and Appelo (1999) is that the amount of solution mixed from any **cell** to any of its neighbours should always be less than 1/3 (conversely after mixing each **cell** should retain at least 1/3 of its content from the previous time step, i.e. all the mix factors of **cells** to themselves, MX_{jj} should be greater than 1/3).

A requirement prescribed by the same authors for stability of diffusion calculations is that the time step Δt should be chosen such that:

$$\Delta t < \frac{(\Delta z)^2}{3\,D} \quad \text{or} \quad \Delta t < \frac{h^2}{3\,D} = \frac{R^2}{3(N_r)^2 D} = \frac{\Gamma}{3(N_r)^2} \qquad [74]$$

where D is the diffusivity and Δz is, by normal convention, the vertical special increment. The model considered here does not incorporate diffusion in the vertical direction, but this requirement is nevertheless observed for the radial direction by substituting Δz with the radial spatial increment h as shown. It can be seen that the limiting value for Δt (and therefore of Δz through [73]) decreases by the square of the increase in radial increments.

The parameter θ_{mob} does not feature explicitly in either the continuity equation, its source term or in the mix factors ($MX_{i,j}$). But from [73] it can be seen that θ_{mob} can be used as an indirect means of manipulating the size of the time step to retain the stability requirement of [74] above, provided Δt is always calculated from [73]. Hence θ_{mob} can be manipulated to meet the stability requirements for both the *MX* factors and diffusion calculations.

Since it was the intention to consider spatial variation of physical, hydrodynamic and kinetic parameters by three vertical sections in a heap (Upper, Middle and Bottom), it was a requirement that the number of vertical elements should be a multiple of 3. No fewer than 6 vertical increments are desired in order to allocate at least two vertical increments per vertical partitioning.

In PhreeqC grids of $N_z x N_r$ = 6x5; 12x5; 12x6 and 21x5 yielded to three decimal places the same correlation (0.999) to the HeapSim benchmark. This illustrates that any increase beyond 6 vertical and 5 radial increments has no effect on accuracy. The 12x4 grid yielded a slightly poorer correlation (0.998) suggesting 5 radial increments as the minimum spatial resolution, although the deviation is hardly noticeable. In these variations the heap height was not varied, in the general case for any heap height it is the height increment (Δz) that will affect numerical precision, not the number of increments N_z. In contrast, laterally it is indeed the number of increments N_r that determines accuracy since it affects the extent to which plug flow is approximated by the number of mixed reactors in series whereby diffusion in the immobile zone is described.

Even in the case where the suggested limit of stability for the mix-factors (MX_{jj}) was not met (where the smallest factor was 0.287) it can be seen from Figure 33 below that the result had not grossly deteriorated, still exhibiting a correlation of 0.998 to the HeapSim reference.

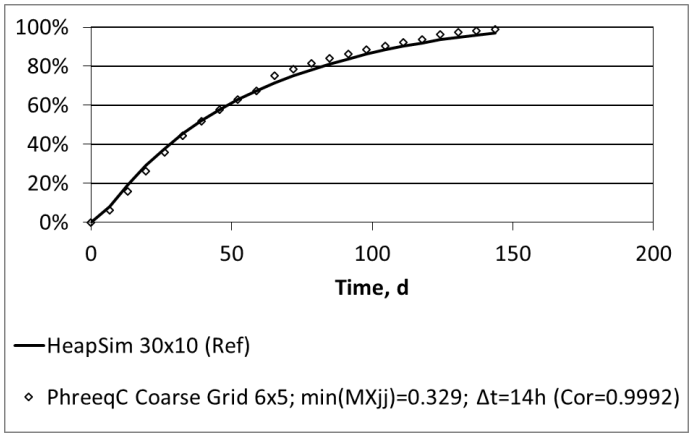

Figure 33. PhreeqC extraction curve with coarser grid

5.4 COMPARISON BETWEEN HEAPSIM AND PHREEQC

In van Staden and Petersen (2018b), calibration between PhreeqC and HeapSim was performed based on comparisons of extraction and GAC curves at different Transfer Times with the two model.

Excellent agreement has been shown between the two models. However, small differences do exist. The two models differ in the manner in which acid is allocated between the competing oxide-copper dissolution and GAC reactions. HeapSim apportions the acid allocations at the start of each time-step in accordance with the rate constants. PhreeqC divides each time step into smaller time steps and conducts all reactions iteratively in turn for each smaller time-step, with recalculation of residual amounts and reaction kinetics for each smaller time-step. Another difference is that HeapSim performs stoichiometric calculations in terms of molecular species (such as H_2SO_4 and $CuSO_4$), while PhreeqC performs ionic solution speciation before and after each temporal and spatial increment, and acid concentrations are dealt with in terms of pH. As a result, for a typical GAC rate-constant of 0.037 h^{-1}, a 20 percent difference in copper extraction was found for a GAC rate constant of 0.1 h^{-1}.

However the GAC rate constants required during the case studies were mostly smaller than 0.03 h^{-1}, so that these differences would usually not impact on the simulation results presented here. The exceptions being GAC rate constants of 0.5-0.6 h^{-1} required to describe the curing acid consumption during the first 20 days out of a total of 150 days of the Kipoi oxide copper case studies, and 0.09 h^{-1} required for the unsegregated

column leach. In cases of such fast GAC kinetics, direct comparisons between results generated with HeapSim and PhreeqC would therefore be questionable.

To mitigate for these differences in GAC calculations, each case study was always modelled by only one of the two models. All of the Kipoi, segregation and stratification data was modelled using PhreeqC because of the requirement for modification of the kinetics temporally and spatially as discussed above. All of the NICICO and both gold-application case studies were modelled by HeapSim. Hence while the potential effects of the GAC rate constants could have on the cases pointed out above when comparisons are made between different case studies, at least those effects will not exist for comparisons of the different tests within a case study.

A summary of the varied input parameters used by van Staden and Petersen (2018b) during the calibration of PhreeqC with HeapSim appears in Table 6 below. A 30x10 grid in HeapSim is used as a conservative reference here against which to compare the PhreeqC results, although it has been found that in HeapSim any grid finer than 8x4 yields results indistinguishable from an even finer grid. The correlations between the HeapSim and PhreeqC models for the varied parameters, using k'=0, are illustrated graphically in Figure 34 below.

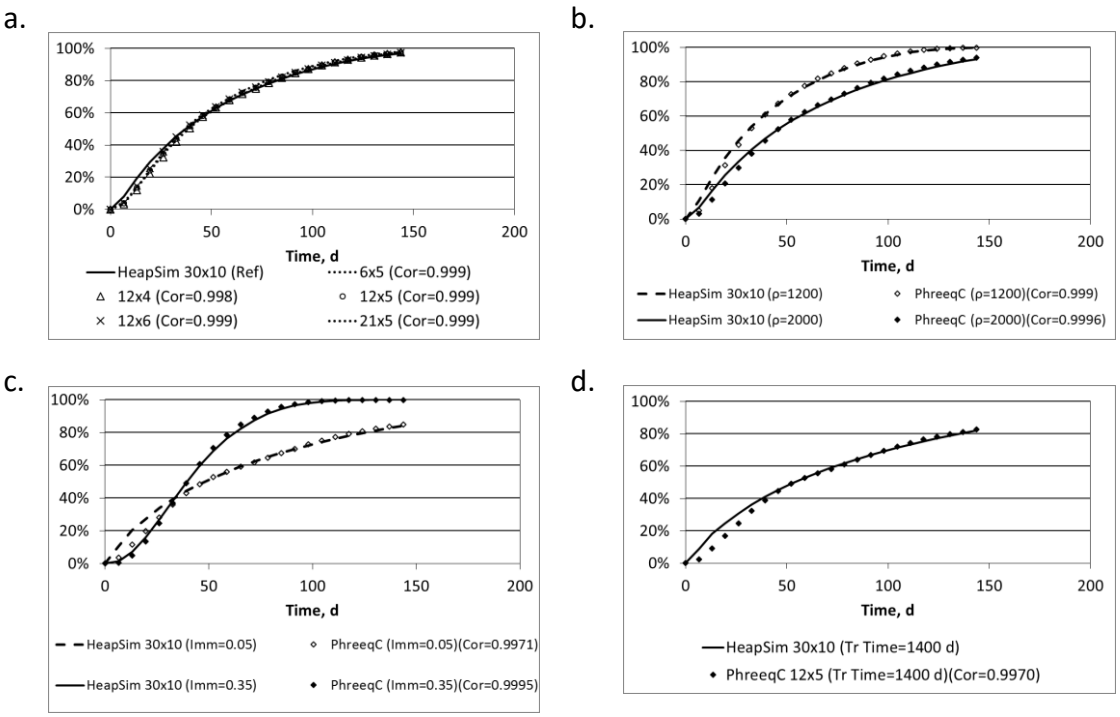

Figure 34. HeapSim and PhreeqC model responses to major variables.
(a) Grid resolution, (b) Density, (c) Immobile moisture content, (d) Transfer time.

Correlations better than 0.99 were achieved in all cases. Hence where *k'*=0, the results produced by HeapSim and PhreeqC can be seen to be virtually indistinguishable and respond identically to changes in bulk density, immobile moisture content and Transfer Time. The deviations to be expected with values for *k'*>0 have been quantified above.

Table 6. Parameters Used for PhreeqC Model Calibration

Parameter	HeapSim		PhreeqC				
	HeapSim Stability Guidance	HeapSim Reference	PhreeqC Spatial grid	Limiting Δt, (adjust MX_{jj} via θ_{mob})	*Varied Transfer Time*	*Varied bulk density*	Varied moisture content
t_{total},days		150	150	150	150	150	150
CuO content, as %Cu		0.44	0.44	0.44	0.44	0.44	0.44
Nz x Nr	No coarser than 8 x 4	30x10	6x5 12x4 12x5 12x6 21x5	12x5	12x5	12x5	12x5
θ_{mob}			0.03	0.17	0.03	0.03	0.03
Δt, s	(<86,400)		19,111 9,556 9,556 9,556 5,460	54,148	9,556	9,556	9,556
H, m			5.71	5.71	5.71	5.71	5.71
Δz, m		0.476	0.951 0.476 0.476 0.476 0.272	0.476	0.476	0.476	0.476
Smallest MX_{jj}			0.690 0.876 0.845 0.814 0.911	0.287	0.845	0.845	0.874 0.457
ρ, kg/m^3			1,650	1,650	1,650	1,200 2,000	1,650
θ_{imm}, vol-frac			0.1	0.1	0.1	0.1	0.05 0.35
q, L/(h.m^2)			5.38	5.38	5.38	5.38	5.38
[H_2SO_4], mole/L		0.11	0.11	0.11	0.11	0.11	0.11
k, h^{-1}	8.33x10^{-5} 0.3	8.33x10^{-5} 0.3	8.33x10^{-5} 0.3	8.33x10^{-5} 0.3	8.33x10^{-5} 0.3	8.33x10^{-5} 0.3	8.33x10^{-5} 0.3
GAC rate constant k', h^{-1}			0.0	0.0	0.0	0.0	0.0
Curing acid addition			0.0	0.0	0.0	0.0	0.0
Θ, days		710	710	710	710 1400	710	710
Correlation to HeapSim Reference			0.9989 0.9984 0.9991 0.9993 0.9991	0.9975	0.9970	0.9990 0.9996	0.9971 0.9995

5.5 MODEL APPLICATION

5.5.1 The topological term

The topological term as it is coded into HeapSim appears in equation [56], bearing the extent of extraction in the form $(1\text{-}X)^{\Phi}$. That implies that extraction would always continue to 100 percent, since $(1\text{-}X)$ (and therefore the rate of extraction), approach zero only once X approaches unity.

However, as discussed in section 3.12.4, Ghorbani et al. (2013) found that the extent of mineral leaching from 5-25mm particles does not asymptote towards unity. That is, at least not within the time scale that would be practicle for heap leaching.

That the topological term as it appears in HeapSim permits 100 percent conversion implies the assumption that all mineral grains are accessible within the time scale of heap leaching, some are less accessible due to greater mass transfer barriers, but they are all accessible nevertheless. How Ghorbani et al. (2013) dealt with the deviation from a 100 percent extraction asymptote has been discussed in section 3.12.4.

In this study the topological term is to be modified to include a term for limiting the ultimate extent of extraction, as was done by Ghorbani et al. (2013) in their model of the leach kinetics of coarse particles. To avoid confusion between their rate expression and the topological term to be used here, the symbols used are modified so that κ_1 is used instead of their Φ. Futher, the term α they used to represent the extractable fraction is replaced here with a grouping $\kappa_x\kappa_w$ to account for two mechanisms that could reduce the extractable fraction below unity. Namely, κ_x represents the fraction of the mineral that is not completely occluded by host rock and that is not refractory under the leaching conditions employed, while κ_w represents the fraction of mineral that is in contact with leach solution (i.e. 'wetted'). The parameter κ_x can be determined experimentally as the ultimate extent of extraction achievable in an agitated laboratory leaching test (i.e. eliminating the inefficiencies of wetting occurring in a heap or column), at the appropriate conditions of concentration and temperature. The parameter κ_w could deviate from unity as a result of solution by-passing part of the ore, or as a result of a fraction of the mineral content being contained at the end of diffusion paths, or at

the end of intra-particle fissures, that cannot be accessed within the time scale typically utilised for heap leaching.

The topological term then becomes:

$$f(1-X) = \left(1 - \frac{X_{Cu}(t)}{\kappa_x \kappa_w}\right)^{\kappa_1} \quad [75]$$

where $0 \leq \kappa_x ; \kappa_w \leq 1$.

It is possible to achieve the effect of such a topological term in HeapSim without having to modify the HeapSim code. Consider that for the extraction of species *i,* [X_i(t)], is calculated as a fraction of the total head value C^0_i and the concentration of unreacted mineral $C_i(t)$ at any given time *t* as:

$$X_i(t) = \frac{C_i^0 - C_i(t)}{C_i^0} \quad [76]$$

Now define the extractable head value C^E_i as:

$$C_i^E = \kappa_x \kappa_w C_i^0 \quad [77]$$

The extent of extraction calculated as a fraction of the extractable head value, is

$$X_i^E(t) = \frac{C_i^0 - C_i(t)}{C_i^E} = \frac{C_i^0 - C_i(t)}{\kappa_x \kappa_w C_i^0} = \frac{X_i(t)}{\kappa_x \kappa_w} \quad [78]$$

By using C_i^E as the model input to represent the head value and by then considering the extraction curve calculated by the model to represent $X_i^E(t)$, the topological term coded into HeapSim assumes the meaning:

$$f(1-X_i^E) = (1-X_i^E)^{\kappa_1} = \left(1 - \frac{X_i(t)}{\kappa_x \kappa_w}\right)^{\kappa_1} \quad [79]$$

as per equation [75].

Transformations between total head value and extractable head value can be made using [77] and transformations between extraction as a fraction of C^0_i and extraction as a fraction of C_i^E can be made using [78].

It can be seen that the term (1-X_i^E) approaches zero as X_i^E approaches unity, in accordance with the topological term coded into HeapSim. As X_i^E asymptotes towards unity, the extraction based on the head value C^0_i asymptotes towards the extractable fraction, i.e. $X(t) \rightarrow \kappa_x.\kappa_w$. The amount of species *i* extracted, calculated as head value multiplied by extent of extraction, remains consistent in the two different transforms, since:

$$C_i^E . X_i^E(t) = (\kappa_x \kappa_w C_i^0) \left(\frac{X_i(t)}{\kappa_x \kappa_w}\right) = C_i^0 . X_i(t) \quad [80]$$

5.5.2 Determination of the constants in the topological term

In fitting a model to experimental data by adjustment of the model parameters, it is obviously desirable to limit the parameters to be adjusted to a minimum. The parameters of the topological term were determined by subjecting a sample of the ore to agitated leaching in a rolling bottle, under constant conditions of temperature and solution composition. The extraction results were then fitted to the rate expression [58] (being the integral of [57]) developed by Ghorbani et al. (2013) to yield the optimised values for α (which was equated to κ_x in [75]) and for Φ (which was equated to κ_1 in [75]). During an agitated leach test, κ_w is known to equal unity. This leaves κ_w as the only parameter in the topological term to be manipulated in order to fit the model to experimental data.

5.5.3 Correlating scale-up with Transfer Time

If the Transfer Time (defined by equation [67]) of a heap can be predicted, its leaching performance can be modelled from the solution of equation [66]. However, assigning absolute values of R and τ_δ^2 to a heap for calculation of the Transfer Time is not possible based on current knowledge. That is because the manner in which flow channels might split and merge is not known, as discussed in 5.2.2. Furthermore, tortuosity is a poorly defined concept, as discussed in 3.11.5.

However, the approach proposed here is to use the results of a column leaching experiment as a reference from which to extrapolate the kinetics of a heap. The Transfer Time observed under column leaching conditions reflects the combination of the four parameters that appear in equation [67], namely the diffusional distance (R), tortuosity (τ_δ^2), diffusivity (D) and moisture content (θ_{imm}), of which D is a constant and θ_{imm} can be measured or estimated reasonably well. The supposition is that, for a given ore sample, it should be feasible to correlate the deviation of R and τ_δ^2 (and hence of $R^2\tau_\delta^2$ in equation [67]) from the values they assume under column leaching conditions, as a function of the parameters identified in section 3.16 that change during scale-up, such as densification and dripper spacing. That is as opposed to attempting to calculate absolute value of $R^2\tau_\delta^2$ under any given combination of densification and dripper spacing.

To that end, the ratio between (a) Transfer Time observed under heap leaching conditions Θ and (b) the Transfer Time observed under column leaching conditions Θ_{ref}, (being the 'reference'-set of conditions), is defined as the experimental Dimensionless Transfer Radius, DTR, namely:

$$\text{Experimental} - DTR = \sqrt{\frac{\Theta}{\Theta_{ref}}} = \sqrt{\frac{\tau_\delta^2\ \theta_{imm,ref}}{\tau_{\delta,ref}^2\ \theta_{imm}}}\ \ \frac{R}{R_{ref}} \qquad [81]$$

The Experimental-DTR can be determined by finding (a) the Transfer Time Θ_{ref} that yields the best model fit to the column leaching data and (b) the Transfer Time Θ that yields the best model fit to the heap leaching data, and substituting Θ and Θ_{ref} thus determined into equation [81].

To be able to attribute the ratio between Θ and Θ_{ref} to one of the factors listed in section 3.16 (densification, dripper spacing and segregation/stratification), it is necessary to develop theoretical correlations for the ratio Θ/Θ_{ref} as a function of each of those factors. In accordance with the illustrations of Figure 23 on page 98 and Figure 24 on page 99, segregation/stratification is hypothesised to effectively modify the dripper spacing, hence the ratio Θ/Θ_{ref} needs to be correlated only with densification and dripper spacing. If segregation/stratification is experimentally found to affect heap leaching kinetics, the effect would need to be quantified in terms of the effective increase in dripper spacing.

5.5.4 Deriving the "Densification-DTR"

Consider the instance where the change in Transfer Time during scale-up from a column to a heap is governed by the difference in densification prevailing in the column and heap respectively.

The following relationship exists between bulk density and void fraction of ore:

$$\rho = \rho^*(1 - \theta_{void}) \text{ or } \theta_{void} = \frac{(\rho^* - \rho)}{\rho^*} ; \text{ where } 0 \leq \theta_{void} \leq 1 \quad [82]$$

where ρ is the bulk density of a heap and ρ^* is the true density of the solid phase, (both on a dry basis), while θ_{void} is the void fraction. A similar expression can be written for the bulk density (the 'reference' bulk density) ρ_{ref} of the same ore in a column with void fraction (the 'reference' void fraction) $\theta_{void,ref.}$

For the purposes of solution flow, the ore particles are assumed to be solid, not permitting flow to pass through them. Therefore solution can pass only through the void spaces between particles.

A lower over-all void fraction in the heap (due to increased densification) implies that the voids in the heap are on average smaller. Furthermore, fewer of the voids can be expected to be connected to allow passage of solution, with Figure 35 below illustrating how densification in a heap can increase the toruosity, and reduce the number of flow channels. For ease of reference, Figure 35(a) and (b) are copies of Figure 12(a) and (b) on page 49, with Figure 35(c) being added here to show the effect of densification.

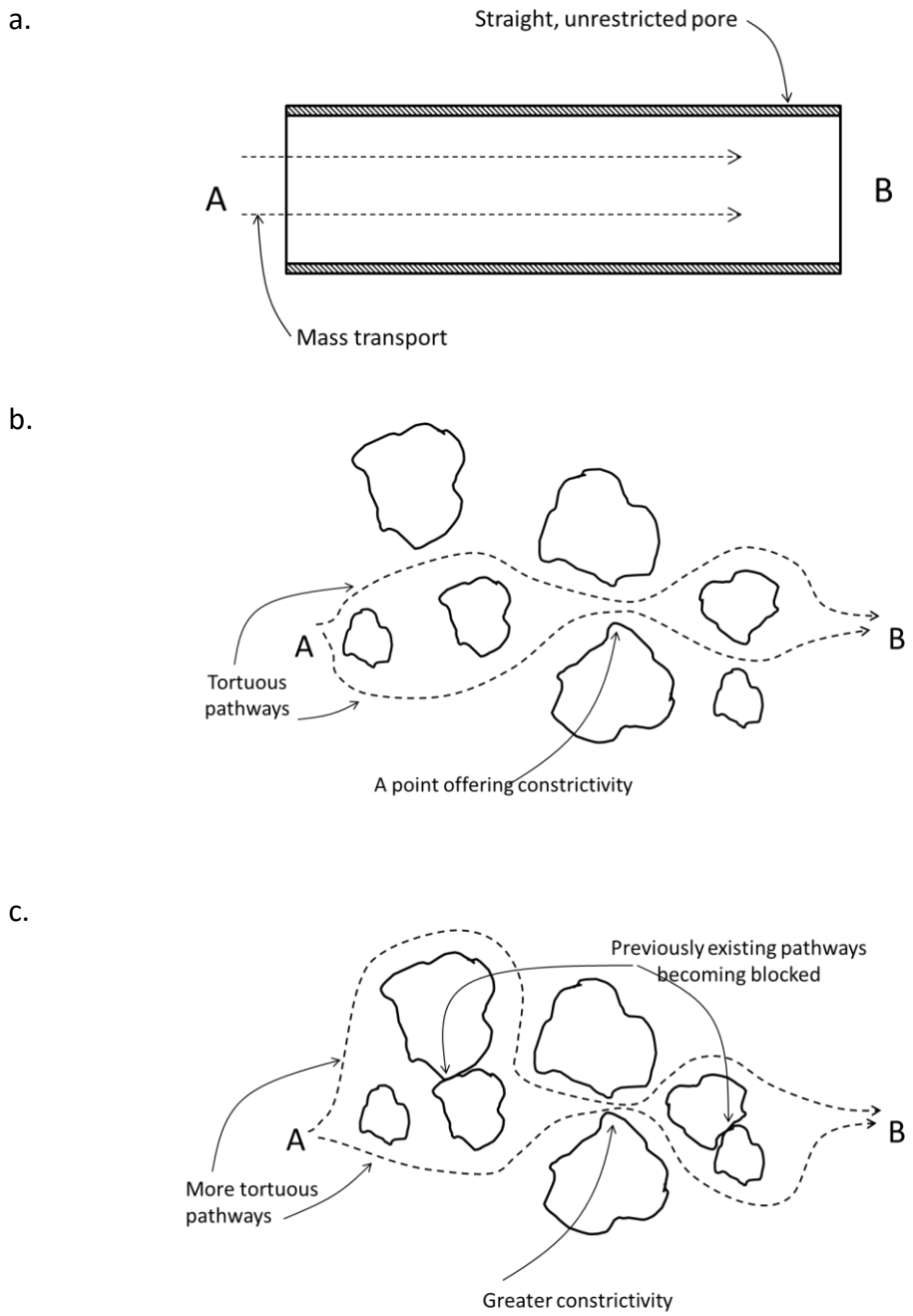

Figure 35. Effect of tortuosity on diffusional transport between points A and B. via (a) an idealised straight, unrestricted pore, (b) moderately tortuous and constrictive porosity, (c) more tortuous and constrictive porosity due to densification

It is envisaged that the number of connected open passages of sufficient size to permit mobile solution flow from the top to the bottom of a heap is proportional to the over-all void fraction. Therefore, on a given cross sectional area, more hydraulically

conductive passages will be found through a less compacted mass of ore than through a more compacted mass of ore. To express the relationship in terms of bulk densities, let the spacing between conductive solution flow passages in a relatively low-bulk-density mass of ore be S_{ref} (i.e. the 'reference' spacing), as shown in Figure 36(a) below. In a mass of more compacted ore there will be fewer conductive passages, with a wider spacing between them of S, as shown in Figure 36(b) below. It therefore follows that, on the less compacted ore, there is 1 conductive passage per S_{ref}^2 square meters of cross sectional area (i.e. one quarter passage per corner of the rectangle connecting the centres of four adjacent passages), that is to say a passage density of $1/S_{ref}^2$ in units such as [m^{-2}]. Similarly, the more compacted ore will possess a conductive passage density of $1/S^2$ [m^{-2}]. It is envisaged that the ratio between passage densities equals the ratio of void fractions, to yield:

$$\frac{\theta_{void}}{\theta_{void,ref}} = \frac{S_{ref}^2}{S^2} = \frac{(\rho^* - \rho)}{(\rho^* - \rho_{ref})}$$

which can be re-written as:

$$\frac{S}{S_{ref}} = \sqrt{\frac{(\rho^* - \rho_{ref})}{(\rho^* - \rho)}} \quad [83]$$

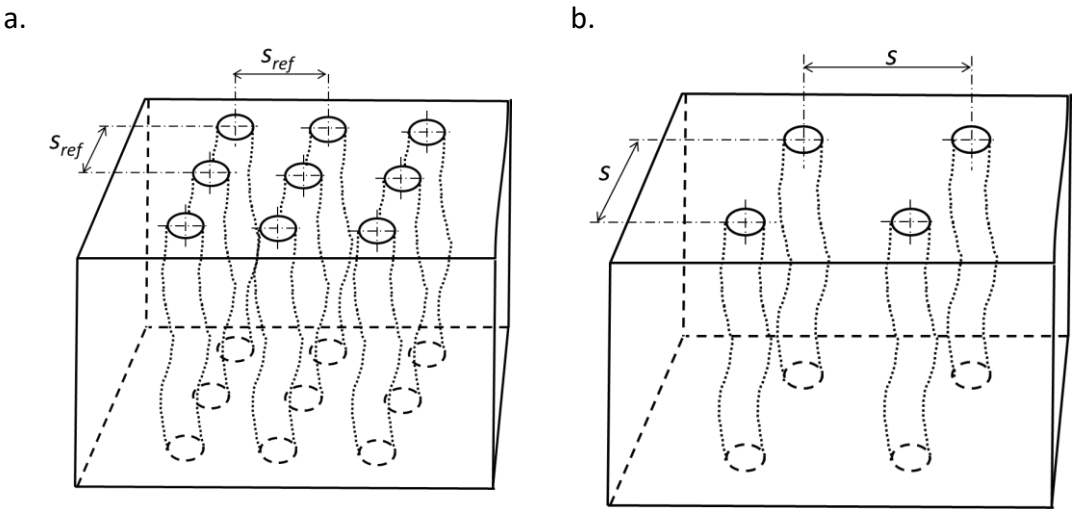

Figure 36. Distribution density of hydraulically conductive passages.
(a) via less compacted ore and (b) via more compacted ore.

A reduction in voidage (i.e. increased densification) therefore decreases the probability that solution would encounter void space via which to flow. The diffusion path length should be half of flow channel spacing in order for solution and reagents to reach the entire heap volume, so that:

$$\frac{S}{S_{ref}} = \frac{R}{R_{ref}} = \sqrt{\frac{(\rho^* - \rho_{ref})}{(\rho^* - \rho)}} \quad [84]$$

By substituting it into the definition of DTR in [58], it follows that:

$$\sqrt{\frac{\Theta}{\Theta_{ref}}} = \sqrt{\frac{\tau_\delta^2}{\tau_{\delta,ref}^2}} \sqrt{\frac{\theta_{imm,ref}}{\theta_{imm}}} \sqrt{\frac{(\rho^* - \rho_{ref})}{(\rho^* - \rho)}} \quad [85]$$

Increasing bulk density is further expected to lead to larger tortuosity, so that the terms on the right-hand side of equation [85] bearing τ_δ^2 and ρ will both be larger than unity if $\rho > \rho_{ref.}$ Reference can be made again to Figure 35(c) on page 134, which illustrates how constrictive points become more constrictive by particles being forces closer together.

There is no theoretical ground upon which to expect any specific functional form to describe the response of tortuosity to densification. However, a power function can be

fitted to most trends, describing a linear function for a power of unity, a logarithmically-shaped curve for a power smaller than unity and an exponentially rising function for a power larger than unity. The following power-relationship is therefore proposed, with the power chosen such that the resulting power for the last term in equation [87] conveniently becomes "*p*".

$$\sqrt{\frac{\tau_{\delta}^{2}}{\tau_{\delta,ref}^{2}}} = \left[\frac{(\rho^{*} - \rho_{ref})}{(\rho^{*} - \rho)}\right]^{p-\frac{1}{2}} \quad [86]$$

Substituting this into eqation [85] yields what will be termed the "densification"-DTR:

$$\text{Densification} - DTR = \sqrt{\frac{\Theta}{\Theta_{ref}}} = \sqrt{\frac{\theta_{imm,ref}}{\theta_{imm}}} \left[\frac{(\rho^{*} - \rho_{ref})}{(\rho^{*} - \rho)}\right]^{p} \quad [87]$$

With ρ larger than ρ_{ref}, the Transfer Time of a compacted heap will be larger than that of a column (Θ_{ref}). For ease of reference, the term bearing the densities will be referred to as the Densification, i.e.

$$\text{Densification} = \left[\frac{(\rho^{*} - \rho_{ref})}{(\rho^{*} - \rho)}\right] \quad [88]$$

5.5.5 Deriving the "Dripper-spread-DTR"

Now consider the instance where the change in Transfer Time during scale-up from a column to a heap is governed by the difference in dripper spacing used in the column and on the heap respectively.

Consider the case where the dripper spacing becomes larger than the flow channel spacing, as per Figure 22(b) on page 97. The diffusional distance is then no longer determined by the spacing of flow channels, but by the dripper spacing. In order to distribute reagents throughout the entire heap volume, diffusion needs to occur up to half the diagonal length of the dripper grid from the dripping point, shown in the unit cell illustration of Figure 6 on page 32. Using once again the ratio between two Transfer Times in Equation [81] and substituting half of column diameter *Dia*, (or equivalent

diameter bearing the cross sectional area of the unit cell defined by the dripper grid) for the diffusional distances *R* and R_{ref}:

$$\sqrt{\frac{\Theta}{\Theta_{ref}}} = \sqrt{\frac{\tau_\delta^2\ \theta_{imm,ref}}{\tau_{\delta,ref}^2\ \theta_{imm}}}\ \ \frac{R}{R_{ref}} = \sqrt{\frac{\tau_\delta^2\ \theta_{imm,ref}}{\tau_{\delta,ref}^2\ \theta_{imm}}}\ \ \frac{Dia}{Dia_{ref}} \qquad [89]$$

An increase in dripper spacing, in the absence of any densification, should not lead to any change in tortuosity, so that the coefficient $\tau_\delta^2/\tau_{\delta,ref}^2$ should in that case remain unity. However, it cannot be stated in advance whether the case study data that is to be analysed in the sections that follow might not exhibit the effects of both dripper spacing and density (and therefore tortuosity). Therefore, in order to preserve all possible variables in the expression for Dripper-Spread-DTR, the correlation between tortuosity and densification of equation [86] is substituted into equation [89] to yield what will be termed the "dripper-spread"-DTR:

$$\text{Dripper-Spread} - DTR = \sqrt{\frac{\Theta}{\Theta_{ref}}} \qquad [90]$$

$$= \left[\frac{(\rho^* - \rho_{ref}\ )}{(\rho^* - \ \rho)}\right]^{p-\frac{1}{2}} \sqrt{\frac{\theta_{imm,ref}}{\theta_{imm}}}\frac{Dia}{Dia_{ref}}$$

where Dia_{ref} is the diameter of the narrow-diameter column serving as the reference case.

For ease of reference, the ratio between equivalent diameter of the dripper grid diagonal, *Dia*, and the diameter of the small-diameter column serving as references, will be termed the "Dripper spread". i.e.

$$\text{Dripper spread} = \frac{Dia}{Dia_{ref}} \qquad [91]$$

5.5.6 The effect of dripper spacing on extractable fraction, $\kappa_x\kappa_w$.

When the dripper spacing (or column diameter) becomes so wide that all areas of the heap are no longer reachable by diffusion (within the time scale used for heap leaching), the parameter κ_w will become smaller than unity. The magnitude of $\kappa_x\kappa_w$ will then reduce

correspondingly. For dripper spacings that are sufficiently narrow to permit wetting of the entire heap, κ_w will remain at unity, and the term $\kappa_x\kappa_w$ will remain constant and equal to κ_x.

6 DIAGNOSTICS: DERIVING BATCH CURVES

6.1 INTRODUCTION

On some commercial heap leaching operations it is practice to stack a heap in its entirety before irrigation is initiated, so that it will leach as a batch, as in the case reported by van Staden and Laxen (1988).

However, this is often not the case in current commercial practice. The heap leaching data from the two commercial heap leaching operations treated in van Staden and Petersen (2018b) and in van Staden et al. (2017a) was generated with irrigation commencing whenever a sufficient upper surface area had been created to house a number of irrigation lines, referred to as a 'cell' of ore, being a sub-division of a heap.

This is done to speed up production from very large heaps, where several months can be required to complete the stacking of a single heap. As ore is added to the heap, the surface area being irrigated is expanding and the irrigation solution pumped onto the heap (and draining from the heap) is increasing. Therefore at any given time, the ore that was stacked first has been irrigated for longer than the most recently stacked ore. All drainage collects on the leach pad and runs into a common drainage pond, no effort is made to separate drainage solutions from older or newer cells. The solution thus collected therefore consists of a mixture of solutions emanating from cells ranging in age from the most recently stacked to that stacked first.

To compare the leaching performance obtained on an ore during a column leaching experiment with that obtained on a heap of the same ore, or to calibrate a model to the leaching performance of a heap, it is necessary to derive the batch leach curve according to which the ore on the heap is leaching. However, no direct comparison can be drawn between the (batch) data of a column leaching experiment, (or of the batch output of a heap leaching model), and the (continuous) production data of a heap where irrigation and stacking continue simultaneously.

The concept of continuous stacking and irrigation as done commercially can be explained with reference to van Staden et al. (2017a). Consider a heap being stacked on a prepared pad which is sloped towards a drainage collection point, as shown in Figure

37(a) below. After having stacked an initial quanity of ore, labelled “Cell 1”, that amount of ore is fitted with an irrigation system, irrigation onto it is initiated and the drainage solution emanating from it starts draining towards the drainage collection trough.

(For ease of illustration, the heap is shown here as sloping towards the drainage collection point in the same direction as the progression of stacking. However it would be more practical for the heap to be sloped ‘out of the page’, at 90 degrees with respect to the direction in which stacking progresses. That would prevent the stacker from standing in a stream of drainage solution. However, as shown is serves to clearly illustrate the principle).

The ore on cell 1 leaches according to the batch curve labelled “Cell 1” in Figure 37(b), showing extent of extraction $X_i(t)$ of species i as a function of time t.

For the purpose of the illustration, time zero is taken as the time when irrigation to cell 1 commences. Drainage is further assumed to appear from cell 1 at time zero (although in practice the appearance of drainage might lag initiation of irrigation by a day or two). Hence the cell 1 batch curves represents the rate of copper production contributed by cell 1.

a.

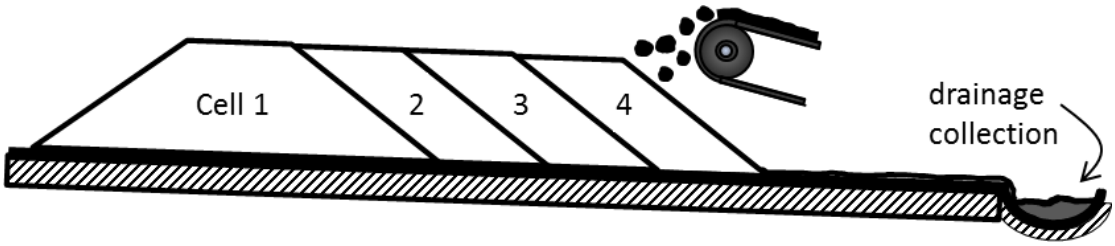

b.

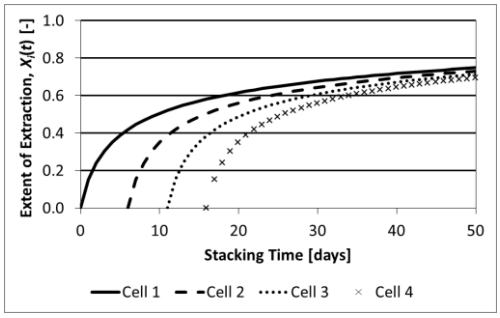

c.

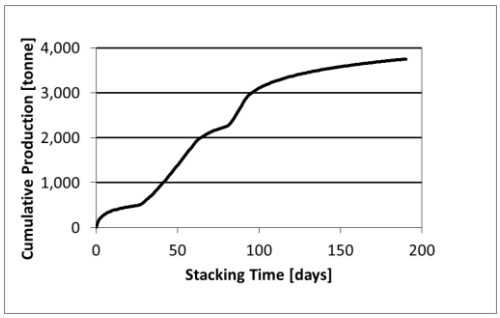

Figure 37. The practice of adding irrigation during continuous stacking
(a) Stacking multiple cells on a pad with common drainage collection, (b) Batch leach curve per cell, (c) Resulting production graph recorded by the plant operator.

Stacking continues without interruption and the procedure is repeated to initiate sequentially the irrigation of cells 2, 3 etc. until the entire pad is covered in leaching cells. For the purpose of illustration, it is assumed here that 6 days were required to stack Cell 1 (requiring a somewhat greater tonnage to be stacked to create a given upper surface area since it contains the slope towards the left-hand side which the other cells do not), and then 5 days to stack each of the subsequent cells. The batch curves according to which each of the cells are leaching are shown in Figure 37(b), with the batch curves of all cells exhibiting exactly the same shape, but lagging one another in time.

As cells are being added to the heap, the total rate of irrigation, and hence the total rate of drainage solution reporting to the drainage collection trough, is increasing over time. The plant operators record the cumulative amount of species *i* reporting to drainage as their production graph from:

$$\text{Cum. production by time t [days]} = \sum_{t} V_{daily} \Delta C_i \qquad [92]$$

with V_{daily} being the daily amount of solution collected, which is typically taken as being equal to the daily volume of solution irrigated, which can be adjusted to account for evaporation and rainfall if the necessary weather data for its estimation have been recorded. The term ΔC_i is the difference between the concentration of species *i* in the drainage solution and in the irrigated solution. An example of daily cumulative production as a function of time thus calculated is shown in Figure 37(c). Note that the volume V_{daily} of drainage solution being collected consists of a mixture of drainage solutions emanating from all cells that are operational on the pad at any given time, with each cell having progressed to a different extent of extration.

The production graph can also be taken as representing the following integration over time, being somewhat simplified here but developed in greater detail in Section 6.4:

$$\text{Cum. production by time } t = \int_0^t C_i^0 \, \dot{W} \, X_i(t) \mathrm{d}t \qquad [93]$$

where $\dot{W}$ is the rate at which ore is being stacked onto the pad, and C_i^0 is the concentration of species *i* in the unleached ore. In this expression, the batch leach curve being sought, $X_i(t)$, can be seen to appear implicitly in the cumulative production data which was determined by the heap operator from equation [93].

A numerical technique was therefore developed for deriving the function $X_i(t)$ for the batch leach curve according to which ore in a heap is leaching, being given the cumulative production graph data collected by a heap leach operator. In principle, it involves a numerical search for the function $X_i(t)$ that sets the result of equation [93] equal to the result of equation [92].

6.2 Approach

It was assumed that the extraction of species *i* occurs from all cells on a heap according to the same "fitted batch curve" (FBC) which can be represented by a function $X_i(t)$. The method is intended to derive the FBC for metal extraction as well as for lixiviant consumption, therefore *i* can be any number of metals, as well as lixiviant (lixiviant consumption would result in a negative rate of extraction thereof).

The integrals of $X_i(t)$ were then derived which yield the Calculated Production Graph, according to which metal reports to the commonly collected drainage solution. The variable parameters of $X_i(t)$ were then adjusted to minimise the sum of squared residuals (SSR) between the Calculated Production Graph and the Observed Production Graph.

6.3 The form selected for $X_i(t)$

Various functional forms that could be considered for $X_i(t)$ are discussed in van Staden et al. (2017b). The minimum requirement for this procedure was that a functional form could be identified that would provide a good fit to most, if not all batch leach curves. Obviously it would be ideal if it were fundamentally-based, which would further ensure a good fit to all but the most exceptional batch leaching data sets.

A literature search revealed that various authors have successfully described their batch leaching data by expressions that could all be expressed as the rate of leaching being first-order with respect to the unreacted fraction, as per equation [56] with Φ=1. However, the fact that Ghorbani and co-authors (2013) identified two time scales of leaching from coarse particles, as discussed in section 3.12.4, was also considered. As discussed, the change in time scales is attributed to a change in diffusional regime, not to a change in chemical reaction mechanism and not to a change in the topological function at work at the mineral grain. It was therefore concluded that this change in time scales could potentially be observed during any type of leaching, not only during the oxidative bioleaching that applied in their case. In order to make the functional form $X_i(t)$ maximally general, it therefore needs to include provision for the phenomenon that the extraction curve could asymptote to a finite extent of extraction $\alpha<1$ over the time scale relevant to heap leaching, although it might continue over a much longer time scale.

Ghorbani et al. (2013) identified that, for coarse particles, the leaching kinetics can be represented by equation [57]. While Ghorbani et al. (2013) submerged their coarse particles in leach solution, their expression is made even more general here by replacing their "extractable fraction" α by a combination of $\kappa_x\kappa_w$. Here, κ_x represents the faction that is extractable within the shorter time scale by not being occluded by host rock deep within particles and by not being refractory to the leaching conditions. During heap leaching, the possibility is foreseen that a proportion of the ore might remain out of contact with the leach solution, as observed by Petersen and Dixon (2007a) and by Guzman et al. (2006). Therefore κ_w represents the fraction that is in contact with leach solution. That yields:

$$\dot{X}_i(\mathrm{t}) = \kappa_0 \left(1 - \frac{X_i(t)}{\kappa_x \kappa_\mathrm{w}}\right)^{\kappa_1} \qquad [94]$$

with the following solution for $X_i(t)$:

$$\frac{X_i(t)}{\kappa_x \kappa_w} = 1 - \left(1 + (\kappa_1 - 1)\frac{\kappa_0 t}{\kappa_x \kappa_w}\right)^{\frac{1}{(1-\kappa_1)}} \qquad \forall\ t \text{ if } \kappa_1 > 1; \qquad [95]$$

$$\forall\ t \leq \frac{\kappa_x \kappa_w}{(1-\kappa_1)\kappa_0} \text{ if } \kappa_1 < 1$$

The time boundary in the second line is required to limit the function to an extent of conversion ≤ 1 in the case where κ_1<1. The function is undefined for κ_1=1, but that does not constrain its use since the value of κ_1 can be selected arbitrarily close to unity if necessary.

The calculation of the shape of the batch curve now proceeds as illustrated in Figure *38* below. The integral calculations were coded in Excel®, and the Solver function was used for minimisation of the SSR.

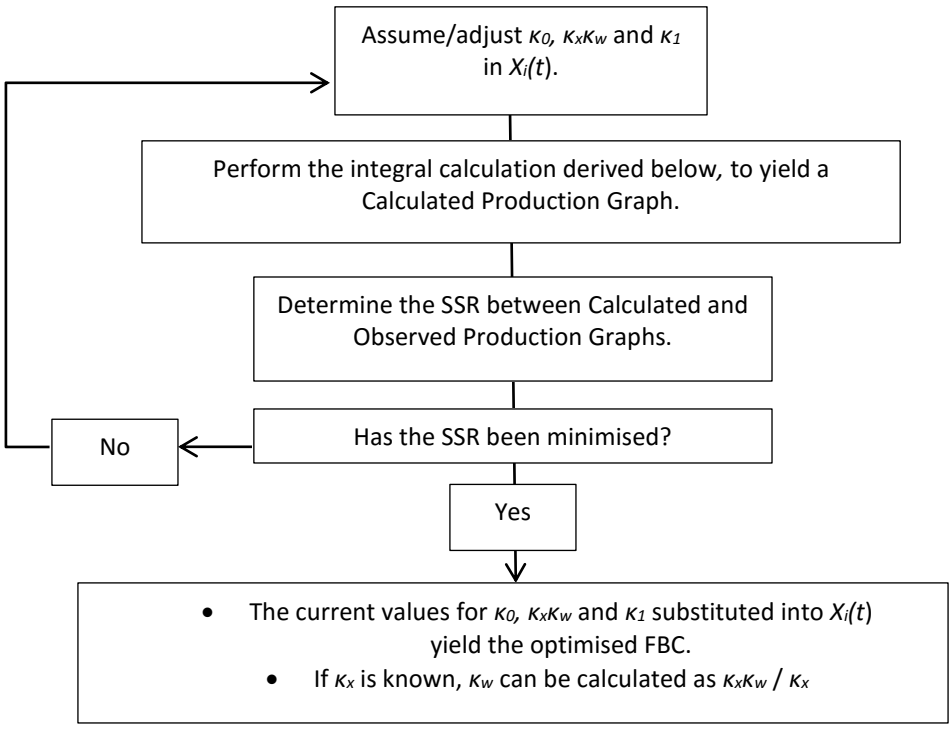

Figure 38. Procedure for Deriving the FBC from the Observed Production Graph

6.4 DERIVATION OF THE INTEGRALS

The stacking and leaching sequence of a commercial heap is illustrated in Figure *39* below. Provision was made for one temporary interruption in the stacking schedule (t_2 to t_3) and completion of stacking after time t_4; of course, in the general case any number of interruptions can be treated in the same manner.

The stopping and re-starting of stacking leads to discontinuities over which integration cannot be performed. The integral therefore needs to be performed as a summation over the continuous parts of the stacking schedule. The method therefore provides for three terms that contribute to the Calculated Production Graph.

The first is Production in Batch, (PIB), being the rate of metal production from the first cell or number of cells of ore to be stacked before any irrigation starts, so that when irrigation starts, this first quantity of ore will leach as a batch for as long as it gets irrigated (which can be for the full leach cycle of the entire heap).

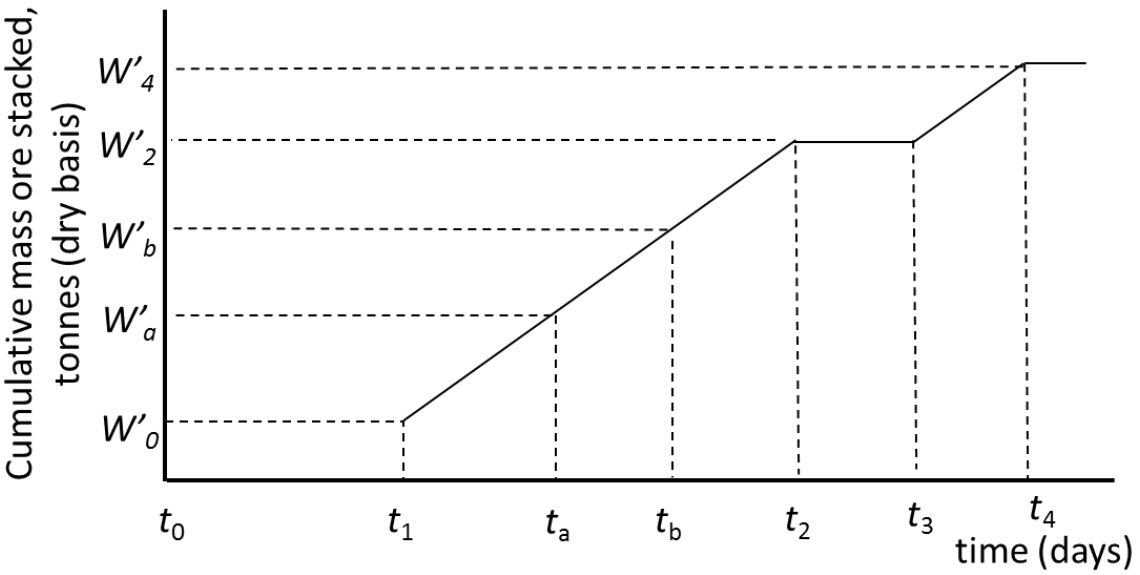

Figure 39. Representation of stacking schedule of a commercial heap leach plant
Reproduced from van Staden et al. (2017b)

In Figure 39, this is the mass of ore W'_0 (dry basis), that had been stacked before and up to time t_0. Irrigation of this entire mass starts at time t_0. The cumulative amount of metal species *i* extracted from the batch of ore mass W'_0 up to any time *t* is:

$$\begin{cases} PIB_{0,i}(t) = C_i^0 \, W'_0 \, X_i(t) \quad \forall \;\; 0 \leq t \leq \infty \quad if \;\; \kappa_1 > 1 \\ \\ \forall \;\; 0 \leq t \leq \dfrac{\kappa_x \kappa_w}{K_0(1-\kappa_1)} \quad if \;\; \kappa_1 < 1 \end{cases} \qquad [96]$$

The case is different when an amount of ore ($W'_2 - W'_0$) is stacked between time t_1 and t_2, while the irrigation of each incremental mass of ore ΔW commences immediately upon its stacking.

Consider an incremental amount of ore $\Delta W'_a = \dot{W}' \Delta t$ which is stacked at rate $\dot{W}'$ between time t_a and $t_a + \Delta t_a$. By time t_b the period of time for which incremental mass $\Delta W'_a$ has been leaching is $t_b - t_a$.

The cumulative amount of Production during Continuous Stacking (PCS) of species *i* that has been extracted from incremental ore mass $\Delta W'_a$ between time t_a and t_b is

$$\Delta PCS_{i,a}(t_b) = C_i^0\ \dot{W}'\ X_i(t_b - t_a)\ \Delta t$$

The cumulative amount of species *i* extracted from all incremental ore masses stacked between time t_1 (when $W'_a = W'_0$) and time t_b (when $W'_a = W'_b$) with the irrigation network being expanded as ore gets added to the heap, is:

$$PCS_{1,i}(t_b) = \sum_{t=t_1}^{t=t_b} C_i^0\ \dot{W}'\ X_i(t_b - t)\Delta t$$

In integral form:

$$\begin{cases} PCS_{1,i}(t_b) = \int_{t_1}^{t_b} C_i^0\ \dot{W}'\ X_i(t_b - t)\, dt & \forall\ \ t_1 \le t_b \le t_2 \quad if\ \ \kappa_1 > 1 \\ & \forall\ \ 0 \le (t_b - t) \le \dfrac{\kappa_x \kappa_w}{\kappa_0(1-\kappa_1)} \quad if\ \ \kappa_1 < 1 \end{cases}$$

Its physical meaning is more conveniently visualised when expressing it in terms of the 'leaching-age', being the time elapsed since irrigation from a given incremental mass of ore has started, denoted by

$\theta_1 = (t_b - t)$ so that $\mathrm{d}t = -\mathrm{d}\theta_1 \quad \forall\ \ t_1 \le t \le t_b$

which yields upon substitution:

$$\begin{cases} PCS_{1,i}(t_b) = \int_0^{t_b - t_1} C_i^0\ \dot{W}'\ X_i(\theta_1)\, d\theta_1 & \forall\ \ t_1 \le t_b \le t_2 \qquad if\ \ \kappa_1 > \\ & \forall\ \ 0 \le \theta_1 \le \dfrac{\kappa_x \kappa_w}{\kappa_0(1-\kappa_1)} \quad if\ \ \kappa_1 \end{cases} \quad [97]$$

Now consider the metal being extracted after time t_2 from all ore that had been stacked between time t_1 and t_2. Stacking stops at time $t = t_2$ while Production after Discontinued Stacking (PDS) continues. At any time $t \ge t_2$ (referred to as $t_{>2}$) the incremental amount of ore $\dot{W}'(t)\ \Delta t$, being stacked by the time an amount W'_b had been stacked, has an age of

$t_{>2} - t_b$

The cumulative amount of metal extracted from that element by time $t_{>2}$ is

$$\Delta PDS_{2,i}(t_{>2}) = C_i^0\ \dot{W}'\ X_i(t_{>2} - \ t_b)\ \Delta t$$

The cumulative amount of metal extracted by time $t_{>2}$ from all elements stacked between time t_1 and t_2 is

$$PDS_{2,i}(t_{>2}) = \sum_{t=\,t_1}^{t=\,t_2} C_i^0\ \ \dot{W}'\ X_i(t_{>2} - \ t)\ \ \Delta t$$

And in integral form:

$$PDS_{\,2,i}(t_{>2}) = \int_{t_1}^{t_2} C_i^0\ \ \dot{W}'\ X_i(t_{>2} - \ t)\ dt$$
$$\forall\ \ t_{>2}\ \geq\ t_2 \qquad\qquad if\ \ \kappa_1 > 1$$
$$\forall\ 0\ \leq\ (t_{>2} - t) \leq \frac{\kappa_x \kappa_w}{\kappa_0(1-\kappa_1)} \qquad if\ \ \kappa_1 < 1$$

and when substituting

$\theta_2 = (t_{>2} - t\,)$ so that $\mathrm{d}t = -\mathrm{d}\theta_2\ \ \forall\ \ t_1\ \leq t\ \leq\ t_2$

$$\begin{cases} PDS_{\,2,i}(t_{>2}) = \displaystyle\int_{t_{>2}-\,t_2}^{t_{>2}-\,t_1} C_i^0\ \ \dot{W}'\ X_i(\theta_2)\ d\theta_2 \ \ \forall\ \ t_{>2}\ \geq\ t_2 \quad if\ \ \kappa_1 > 1 \\ \qquad\qquad\qquad\qquad\qquad\qquad \leq\ \theta_2\ \leq \dfrac{\kappa_x \kappa_w}{\kappa_0(1-\kappa_1)}\ \ if\ \ \kappa_1 < 1 \end{cases} \qquad [98]$$

In summary three integration terms are provided for calculating the rate of extraction of species *i* from:

(a) a mass of ore stacked as a batch (denoted by integral *PIB*),

(b) ore being stacked while its irrigation is initiated during stacking continuously (denoted by integral *PCS*), and

(c) ore that continues to be irrigated after stacking has been discontinued (denoted by integral *PDS*).

During the various stages of the process illustrated in Figure 39, the total production of species *i* is therefore:

$$PIB_{0,i} \qquad \forall\ t_0 \leq t \leq t_1$$

$$PIB_{0,i} + PCS_{1,i} \qquad \forall\ t_1 \leq t \leq t_2$$

$$PIB_{0,i} + PDS_{2,i} \qquad \forall\ t_2 \leq t \leq t_3$$

$$PIB_{0,i} + PDS_{2,i} + PCS_{3,i} \qquad \forall\ t_3 \leq t \leq t_4$$

$$PIB_{0,i} + PDS_{2,i} + PDS_{4,i} \qquad \forall\ t_4 \leq t \leq t_5$$

From the time-boundaries it is evident that the "*PIB*" and "*PDS*" integrals survive for all times after their initiation (or until irrigation stops), while the "*PCS*" integrals exist only during the period of continuous stacking of that respective portion of ore. (The further time constraints in shown above for the case where $\kappa_1 < 1$ also apply in all cases but are not repeated each time).

6.5 Application to gangue lixiviant consumption

The only modification required to the derived expressions for calculating lixiviant consumption by gangue is the addition of a term W'_{cur} to equation [96] to represent the amount of curing reagent added to (and consumed by) the ore during time $t<t_0$. For an actual operation the amount of curing reagent added will be known, however since not all of it is necessarily consumed by the time irrigation starts at time $t=t_0$, this term W'_{cur} should be treated as an additional unknown parameter to be manipulated during optimisation of the data fit.

Taking the example of acid-leaching of oxide copper ore, the lixiviant is acid, and the consumption thereof by gangue is termed the gangue acid consumption (GAC). The expression used for calculating the GAC by the ore quantum W'_0 (i.e. equation [96] with *i*=GAC) is:

$$\begin{cases} PIB_{0,GAC}(t) = W'_{cur} + \ C^0_{GAC} W'_0 \, X_{GAC}(t) \ \ \forall \ \ 0 \leq t \leq \infty \quad if \ \ \kappa_1 > 1 \\ \qquad\qquad\qquad\qquad\qquad\qquad \forall \ \ 0 \leq t \leq \dfrac{\kappa_x \kappa_w}{\kappa_0 (1-\kappa_1)} \quad if \ \ \kappa_1 < 1 \end{cases} \qquad [99]$$

The GAC incurred during the time intervals after time t_1 is calculated by the same expressions for $PCS_{n,i}$ and $PDS_{n,i}$ used for any other species *i* as per equations [97] and [98].

6.6 QUALIFICATIONS AND LIMITATIONS

The summation and integration inherent in the method can smooth out differences between individual curves relating to individual cells, providing a potentially optimistic estimate of the goodness of fit between data sets.

The form chosen for $X_i(t)$ represents a monotonically rising function, and it is possible that there exist batch curves which are not amenable to fitting by such a function. An example would be where adsorptive clays or precipitation cause eventual loss of value metal from solution. Poor representation of the batch curve by $X_i(t)$ could also result where the leaching of a significant proportion of the valuable mineral is delayed by being occluded in gangue which needs to be consumed before access is gained to the mineral, or where the ore exhibits a bimodal particle size distribution, or where changes occur in the distribution of flow channels during the course of leaching, or where the rate of lixiviant consumption abruptly changes due to depletion of one gangue mineral followed by reaction of another. All these cases would lead to an irregularly shaped batch curve that would not fit well with the form selected for $X_i(t)$. It is assumed that such characteristics of complex ores would become known at the time of laboratory testing and hence it would in those cases be known in advance that this method cannot be applied to the commercial-scale data. In the Kipoi Case Study, where this technique was employed for the purpose of this study, the column leaching results were available as batch curves, only the commercial heap-scale data needed to be converted using this technique. There was no indication from the column leaching batch curves that any of the above complications applied, and the use of this technique is therefore considered to be applicable to the Kipoi ore.

In the manner in which the derivation is presented, it is implied that the instant when any ore is stacked coincides with the initiation of its irrigation and with the initiation of extracted metal reporting to the drainage solution. In reality it requires singular days to stack sufficient ore to provide surface area on top of the heap for the next assembly of drippers to be installed for irrigation to commence. It has been shown in van Staden et al. (2017b) that, considering the time scale of typically hundreds of days over which heap leaching occurs, the assumption of metal production coinciding with stacking is not a gross one for the case of a single lift of say 6m of ore.

Another limitation that may manifest itself when the method is applied to gangue lixiviant consumption is that the total consumption (by the combination of gangue and value-metal dissolution) is likely be dominated by dissolution of the valuable metal as in the case of acid leaching of oxide copper. (If the opposite applies, the process might well not be economical and would therefore be irrelevant). That means that the gangue lixiviant consumption, being the difference between total consumption and consumption by metal dissolution, could be a relatively small quantity that may be of the order of the statistical variance in the data of the two larger quantities, in which case the confidence ascribed to the optimised fit for gangue lixiviant consumption would be relatively low.

7 SCALE-UP CASE STUDY 1: RAND LEASES FREE-MILLING GOLD

7.1 EXPERIMENTAL METHOD

The experimental procedures are detailed in van Staden and Laxen (1988). Briefly, it involved column leaching experiments in three UPVC columns of 225mm diameter and 4m high on a gold-bearing sand dump material (92 percent <425µm) with a head grade value of 1.63 g/t gold. The three experiments involved leaching of sand dump material 'as is', after agglomeration and after desliming.

The sand was obtained as a representative sample of the material leached on a 10,000 t commercial heap of the same height. The sand destined for the heaps was truck-dumped onto on-off concrete pads. An amount of lime was tipped over each truck-load to neutralise acidity that had formed as a result of sulphide oxidation reactions occurring during the decades of exposure. The sand was then pushed up the advancing slope with loaders, which was the only action that provided any mixing of sand and lime.

Both heap and columns were irrigated at 12 L/(h.m^2). The large heap was irrigated by sprinklers, from which very even distribution of irrigation solution would be expected, so that the irrigation dripper spacing on the heap should approach zero. The column was irrigated by dripping onto a single point on a filter paper placed over the ore to provide solution distribution.

7.2 DATA RENDERING

The study by van Staden and Laxen (1988) was not originally undertaken for the purpose of serving as a case study here, hence the data collected was not as complete as would have been preferred for this pupose. Furthermore, while the data collected during column leaching was verified by the authors, the sand tonnage and cyanide consumption of the commercial heaps were quoted as provided by the owners/operators. As shown below, some assumptions needed to be made, since the opportunity no longer existed to re-validate or augment any of the data. While that is not ideal, the available data nevertheless permits some inferences to be drawn.

From the records provided in the paper, the bulk density to which the sand settled in the columns was 1,132 kg/m^3 (dry basis), which is a reliable number as it was simple to determine experimentally on a relatively small scale.

The amount of NaCN irrigated to the column over the 30 days of leaching can be calculated as:

$$(200) \quad (0.012) \quad \frac{1}{(1{,}132)(4)} \quad (24)(30) \quad = \; 0.38 \; \frac{\mathrm{g_{NaCN}}}{\mathrm{kg_{ore}}}$$

$$\equiv 0.38 \; \frac{\mathrm{kg_{NaCN}}}{\mathrm{t_{ore}}}$$

$$\left[\frac{\mathrm{g\_NaCN}}{\mathrm{m^3\_solution}}\right] \left[\frac{\mathrm{m^3\_solution}}{\mathrm{h.\,m^2\_heap}}\right] \left[\frac{\mathrm{m^2\_heap}}{\mathrm{kg\_ore}}\right] \left[\frac{\mathrm{h}}{\mathrm{leach\_campaign}}\right]$$

A reagent consumption of 0.2 kg/t NaCN (i.e. 200 g/t NaCN) was recorded. Practically 100 percent thereof can be attributed to competitive gangue reactions since 100 percent extraction of the gold content would account for less than 1 g/t of NaCN consumption. Unfortunately, no data of NaCN concentration in the drainage with time was provided against which model calculations could be compared.

Furthermore, the gangue species responsible for the consumption are not known either. For example, reaction with soluble iron where pockets of residual acidity might have prevailed in the heaps prior to neutralisation with the alkaline irrigation solution would yield the ferrous-ferric-cyanide known as Prussian blue which, by memory, was observed on occasion. That is an insoluble precipitate which represents a permanent loss of cyanide. Any thiocyanate (SCN^-) that might have formed would also have been recorded as a cyanide loss since it is not titrated by the $AgNO_3$ commonly used to titrate free cyanide CN^-. Yet SCN^- could still leach gold, hence any SCN^- formed would lead to an over-estimate of cyanide consumption and an under-estimate of the amount of cyanide effectively available for gold leaching.

Given this uncertainty, the best recourse is to consider the possible extremes, namely a) optimistically assume zero cyanide loss to gangue reactions, i.e. non-titratable cyanide was assumed to have converted to SCN^- which could still leach gold and b) conservatively

accept the recorded consumption as the true and irreversible cyanide loss to gangue reactions.

From the recorded cyanide consumption, it is calculated that (0.38-0.20)/0.38 = 47 percent of the NaCN irrigated was available for gold dissolution, the balance of 53 percent was consumed by gangue reactions. Of course, the optimistic extreme is that 100 percent of the NaCN irrigated was available for gold dissolution (albeit as a combination of CN^- and SCN^-) .

What is quoted as a 60m x 20m pad size for the 10,000 t commercial heap must in fact be referring to the upper surface of the heap. With a height of 4m and assuming a typical angle of repose of 35^o, the volume of sand below the 20 x 60 m^2 surface area is then calculated as 4,800 m^3 plus 2,083 m^3 contained in the sloping sides, yielding a total volume of 6,883 m^3 and hence a bulk density of 10,000/6,883 t/m^3 = 1.45 t/m^3. It is a higher bulk density than what was measured in the columns, which is not surprising given that the commercial heaps do not have side walls that assist in supporting part of the weight. On copper ore heaps bulk densities between 1.38 and 1.81 t/m^3 have been recorded (van Staden et al., 2017a), from which the calculated sand heap bulk density of 1.45 t/m^3 seems plausible.

If the said dimensions were taken as the pad footprint, the same calculation leads to a total sand volume of (1671 + 1564) m^3 = 3,236 m^3, resulting in a bulk density of 3,000 kg/m^3. This is impossible given that the density of solid quartzitic rock is around 2,700 kg/m^3.

Given the estimate of the heap bulk density, the amount of cyanide irrigated onto the heap over 36 days can be calculated, in terms of (g_NaCN)/(kg_ore), as:

$$(200) \quad (0.012) \quad \frac{1}{(1{,}450)(4)} \quad (24)(36) \quad = \quad 0.36 \ \frac{\mathrm{g_{NaCN}}}{\mathrm{kg_{ore}}}$$

$$\equiv 0.36 \ \frac{\mathrm{kg_{NaCN}}}{\mathrm{t_{ore}}}$$

$$\left[\frac{\mathrm{g\_NaCN}}{\mathrm{m^3\_solution}}\right] \left[\frac{\mathrm{m^3\_solution}}{\mathrm{h.\,m^2\_heap}}\right] \left[\frac{\mathrm{m^2\_heap}}{\mathrm{kg\_ore}}\right] \left[\frac{\mathrm{h}}{\mathrm{leach\_campaign}}\right]$$

This is very similar to the 0.38 kg/t calculated above for the column. The 0.8 to 1 kg/t NaCN reported as typical cyanide consumption for the heaps could therefore not have applied to the particular heap being studied. Hence even more uncertainty also exists regarding the cyanide consumption incurred on the heap. For the heap the same proportions of irrigated cyanide being available for gold extraction as those calculated above for the column were tested, namely 47 and 100 percent of irrigated NaCN. Furthermore, by trial modelling it was found that the recorded gold extraction could not have been achieved, had not at least 30 percent of the irrigated NaCN been available for gold leaching, no matter how short the Transfer Time. Therefore, for the heaps, the three scenarios of 30, 47 and 100 percent of irrigated NaCN being available for gold leaching were considered.

From the three columns, an average residue gold value of 0.56 g/t was reported after 30 days, achieving 66 percent gold extraction. From the commercial heap a residue value of 0.62 g/t was reported after 36 days of leaching, representing 62 percent extraction.

A rolling bottle dissolution test over 7 days on the same sand yielded a residue value of 0.51 g/t, assumed to represent the maximum extractable gold content of namely 69 percent. That means in the columns 66/69=96 percent of the maximum extractable gold was obtained, while the corresponding amount obtained from the heaps was 62/69=90 percent.

Bouffard and Dixon (2007) found that particles smaller than 1.7mm, flooded by leach solution, provided no intra-particle diffusional limitation of the effective rate of gold dissolution, being governed entirely by gold leaching kinetics. That still leaves open the possibilities for the leaching kinetics of this sand dump material under percolation leaching to have been limited by one or more of cyanide availability, gold leaching

kinetics and/or diffusional resistance between regions of flowing and stagnant solution in the sand (i.e. inter-particle diffusion).

7.3 STOICHIOMETRY

The cyanidation of gold proceeds according to equation [6], (copied here from page 14). It can be seen to require oxygen as reagent, but as discussed in the paragraph immediately after equation [6] on page 14, the oxygen requirement for gold leaching is so little that a sufficient quantity can be assumed to be present in the voidage and irrigated solution without the need for mechanical aeration of the heaps. It is therefore assumed that the reaction was never limited by oxygen supply.

$$Au + 2\ NaCN + {}^{1}/_{4}\ O_2 + ½\ H_2O = NaAu(CN)_2 + NaOH \qquad [6]$$

As discussed in the next section, the HeapSim model does not provide for gold species or for cyanide as reagent. Instead, the acid leaching of tenorite, CuO, was used in HeapSim, and the necessary stoichiometric conversions discussed in the next section were made between the NaCN requirement of reaction [6] and the acid requirement of reaction [2] (copied here from page 12). Due to the assumption that oxygen is not a limiting reagent, it is of no consequence that reaction [6] is a redox reaction while reaction [2] is a displacement reaction.

$$CuO_{(s)} + H_2SO_4 = CuSO_{4(aq)} + H_2O \qquad [2]$$

7.4 MODEL FITTING

The agglomerated and ‘as is’ materials tested in the columns yielded similar results, with the ‘as is’ material yielding a slightly higher ultimate extent of extraction. Only the results of the ‘as is’ material was used for model fitting, since on the commercial heap only sand ‘as is’ was being treated. Hence the opportunity for a direct comparison between leaching performance in a column and on a heap existed only for sand ‘as is’.

The HeapSim model available for this study did not provide for gold content in the solid phase or for NaCN content in the irrigation solution. Therefore, as a work-around, the

molar-equivalent copper content, as oxide-copper (represented hypothetically in HeapSim as tenorite, CuO), was specified as the solid-phase head value. That is namely:

$$\frac{1.63\ \text{g.Au/t}}{197\ \text{g.Au/mole}}\ \frac{63.5\ \text{g.Cu/mole}}{1} = 0.525\ \text{g. Cu/t} = 5.25\ \text{x}\ 10^{-5}\ \% \qquad [100]$$

Half of the molar cyanide concentration used for gold leaching was specified as the irrigation acid concentration, accounting for the fact that two moles of NaCN are required to leach one mole Au (as per reaction [6]) as opposed to one mole of H_2SO_4 being required to leach one mole of Cu (as per reaction [2]).

Instead of attempting to induce the equivalent proportion of lixiviant consumption by adjustment of the gangue rate constant (*k'*) in the model, *k'* was retained at zero and the lixiviant concentration in the irrigation solution was adjusted by a factor of 0.47 to represent the case where only 47 percent of the irrigated NaCN was available for gold leaching (the balance being consumed by gangue reactions). A similar approach was taken for representing 30 percent of the irrigated NaCN being available. The assumption in making that simplification is that all gangue cyanide reactions occur at the very top of the heap or column. This approach is justified since the gold dissolution reaction consumes so little cyanide relative to the amount irrigated (as shown above), that it does not alter the cyanide concentration in solution. Any change in cyanide concentration along the depth of the heap would be due only to gangue reactions, and that change is assumed to occur at the very top of the heap. That would not impact on the model calculation since the gold dissolution reaction would not become limited by cyanide supply, due to the over-supply of cyanide being available.

Illustrating the calculation for representing 47 percent of the NaCN being available for gold leaching, the acid concentration to be used in the model as irrigation solution was calculated as:

$$\frac{0.2\ \text{g.NaCN}}{\text{L}} . \frac{1\ \text{mole}\ H_2SO_4}{2\ \text{mole NaCN}} . \frac{98\ \text{g.}H_2SO_4/\text{mole}}{49\ \text{g.NaCN/mole}} . \frac{0.47\text{g.}H_2SO_4\ \text{available}}{\text{g.}H_2SO_4\ \text{irrigated}} \quad [101]$$

= 0.094g H_2SO_4 available/L

For the case where 100 percent of the irrigated cyanide was assumed to be available for gold extraction, the calculation would not include the factor of 0.47, to yield 0.2 g/L H_2SO_4 available/L. (Which equals the cyanide concentration in g/L terms, due to the 2:1 ratio of NaCN:H_2SO_4 required to leach a mole of metal, while incidentally NaCN possesses half the molar mass of H_2SO_4).

Upon completion of the model calculations, the copper and acid concentrations in the drainage solution were calculated back to equivalent gold and NaCN concentrations, using the same relations [100] and [101] above.

The extraction curve was found to be most sensitive to the Transfer Time (Θ), which was therefore the primary parameter selected for optimisation. However, it was also found that the optimisation could be improved by trial-and-error refinement of the CuO leach rate constant and exponent of unreacted fraction, each time followed by re-optimisation of Θ to within 1 percent of the minimum SSR. The values for the CuO leach rate constant k and Φ thus optimised on the column leaching data was also used for fitting of the heap leaching data, optimising by manipulation of only Θ. The reasoning being that k and Φ should be functions only of the properties of the sand, therefore the same values for these parameters should apply in both column and heap.

The maximum extractable fractions (i.e. the parameter grouping $\kappa_x\kappa_w$) were determined by fitting the logarithmically-shaped parts of the batch curves (i.e. from days 3 or 4 onwards) to equation [58] as shown in APPENDIX D, Figure 67 on page 281. Contrary to the results of the 7-day rolling bottle tests, extrapolation of the extraction curves suggested that the extraction in both column and heap could proceed to a maximum achievable of 100 percent.

7.5 RESULTS AND COMMENT ON KINETICS

The optimised parameters are shown in Table 7.

Table 7. Operating and fitted parameters for gold leaching from sand

Parameter	Column	Heap
Gold head value, ppm	1.63	1.63
Molar equivalent copper head value, ppm	0.53	0.53
NaCN content in irrigation solution, ppm	200	200
Half of molar equivalent irrigation acid concentration, g/L	0.2	0.2
Effective acid concentration, after deducting proportion consumed by gangue, g/L	0.094	0.094
Bulk density, kg/m^3	1,132	1,450
Immobile moisture content, kg/kg	0.23(1)	0.29(1)
CuO leaching reaction rate constant, h^{-1}	9 ± 0.5	9 ± 0.5
Exponent of the unreacted fraction (Φ)	4.1 ± 0.1	4.1 ± 0.1
GAC rate constant (k'), h^{-1}	0	0
Transfer time (Θ), days	0.071 to 0.225	8.28 to 75.9
Maximum extractable fraction, ($\kappa_x\kappa_w$)	1.0	1.0

(1)Assumptions for lack of recorded data.

The optimised model fits to the column leaching data are shown in Figure 40 below. The best fit was obtained to the column data assuming 100 percent of the NaCN was available for gold leaching, and using a Transfer Time of 0.225 days. This Transfer Time can, compared to observations on the other case studies presented in this document, be regarded as instantaneous, exhibiting no diffusional resistance to solid-liquid contanct. (If the other extreme, of 47 percent NaCN availability is assumed, the Transfer Time is even smaller at 0.016d).

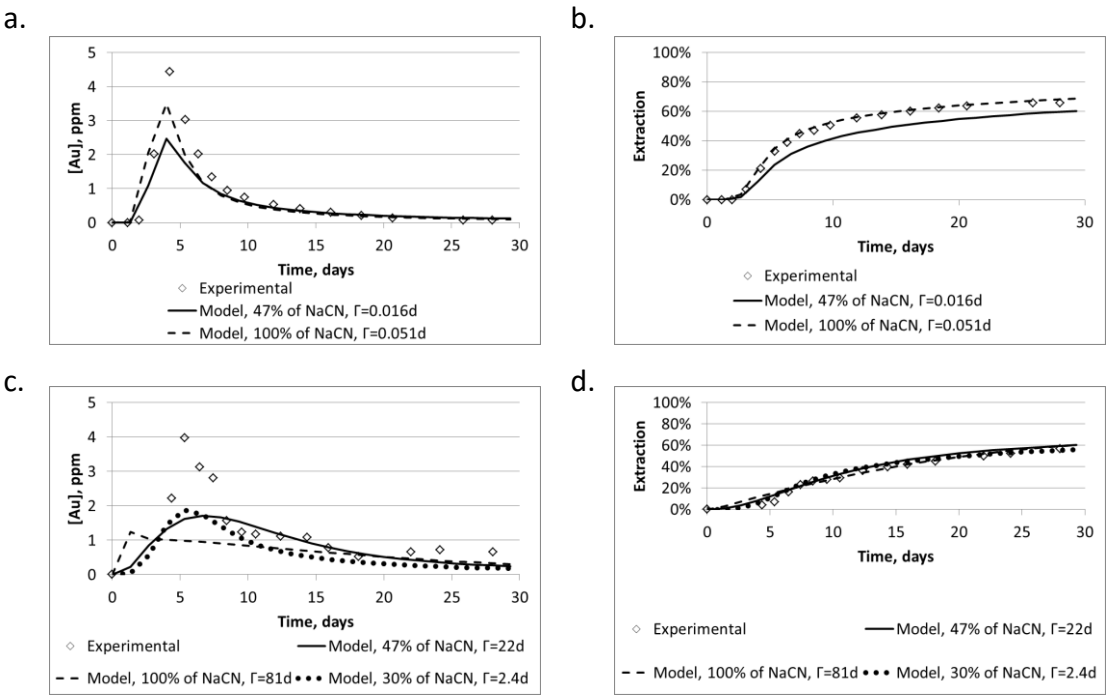

Figure 40. Model fits to gold heap leaching data.
(a) Column [Au] in drainage, (b) Column extraction, (c) Heap [Au] in drainage, (d) Heap extraction.

To the column data, equally good fits were obtained by modelling the leaching performance with either 30 percent of the NaCN being available for leaching (with 8.25 days Transfer Time), or 47 percent NaCN being available (with 75.9 days Transfer Time).

The uncertainties in the data therefore leave a wide range within which the Transfer Times could vary. Nevertheless, it is clear that the Transfer Time in the column was very short. That of the commercial heap was orders of magnitude larger, but, as will be shown later, it was still moderate to average, compared to Transfer Times determined for commercial heaps of copper ore. These very short Transfer Times (<15d) are problematic since the extraction curve becomes insensitive to the Transfer Time, as discussed in section 5.2.4.

The commercial heaps were irrigated by sprinklers, which should yield an effective dripper spacing close to zero.

The column was drip-irrigated onto a filter paper covering the column contents. It is not known whether that truly distributed the irrigated solution across the entire column cross section. It probably did little more than preventing the drip irrigation from impinging a hole into the sand mass, with dripping occurring from the filter paper into the sand mass from a single or singular points. To be conservative, the drip irrigation spacing in the column can therefore only be known to be between zero (in the case of perfect distribution across the cross section) and the column diameter of 225mm. That is to say the drip irrigation spacing in the column was at best as narrow as that of the sprinkler-irrigated heaps, at worst it was 225mm.

Despite that, the commercial heap exhibited the larger Transfer Time compared to that of the column by far, being two orders of magnitude longer than that observed in the column. Petersen and Dixon (2007b) suggested that the "side-branch length" (their terminology for the diffusional distance), is related to the dripper grid diagonal of a drip-irrigated heap, or to the diameter of a column. However, the data presented here indicates that the diffusional distance in a commercial heap is not necessarily kept very small by adopting a very narrow dripper spacing.

7.6 CONCLUSIONS, CASE STUDY 1

The drip irrigation spacing in the column was at best as narrow as that of the sprinkler-irrigated heaps, namely zero, since the heap was irrigated by sprinklers. At worst, and more likely, it was 225mm, which would have been a dripper spacing much wider than that of the heap. Yet the column exhibited the shorter Transfer Time, approximating zero, while that of the heap was much larger. This is contrary to the suggestion by Petersen and Dixon (2007b) that the Transfer Time should be related to the dripper spacing of a drip-irrigated heap, or to the diameter of a column.

Therefore, the results of Case study 1 indicates that the diffusional distance in a commercial heap is not necessarily kept small by adopting a very narrow dripper spacing.

Extrapolation of the extraction curves suggested that the extraction in both column and heap could proceed to a maximum achievable of 100 percent, given infinite time. Therefore the sprinkler irrigation might have helped ensure that none of the solid material on the heap is left unwetted, although it did not prevent the Transfer Time from being much longer than that observed in the column.

While the available data has been utilised as well as possible, several assumptions were required. The uncertainty about the fate of cyanide could be accounted for by modelling the extremes of the possibilities. However, since the recorded bulk density of the heap could not be reconciled with its recorded dimensions, it was necessary to assume that the stated dimensions referred to the upper surface area as opposed to the footprint, without any supporting evidence for doing so. There exists therefore considerable uncertainty about the actual bulk density of the heap.

Furthermore, at the very short Transfer Times (<15d), the extraction curve becomes insensitive to the Transfer Time, further detracting from the confidence of the Transfer Times fitted to the data.

8 SCALE-UP CASE STUDY 2: BARRICK FREE MILLING GOLD

8.1 INTRODUCTION

In 2009, a publication by Bouffard and West-Sells (2009) (produced and published with the support of Barrick Technology Centre and Barrick Gold Corporation) presented residence time distribution data collected from a 250mm diameter column, 2.4m x 2.4m crib and a 3,300 tonne heap of gold-bearing ore. The same ore sample was used in all three cases, and in all cases the ore had been crushed and agglomerated. (Data was also presented on cribs bearing run-of-mine ore and unagglomerated ore, but those are not considered here since they represent variations of multiple operating parameters, complicating comparisons).

Unfortunately the ore on the heap was not of exactly the same size distribution than that of the columns and cribs, namely 25 percent <74µm, as opposed to 17 percent <74µm in columns and cribs, which might have had some bearing on the hydraulic behaviour. The ore was loaded 6.1m high in the column and cribs and piled 3.4m high on the heap by a radial stacker.

Of all the case studies presented in this text, this one by Bouffard and West-Sells (2009) was the only one in which special means (in the form of a distribution plate) was provided to evenly distribute the irrigation solution over the column cross section. Therefore the effective dripper spacing used in the column can be regarded as zero.

At the end of the gold leaching stage, (using an unspecified lixiviant), the irrigation solution was replaced with clean water and the rate of lixiviant wash-out from the heap was monitored, representing a ‘step-down’ tracer test using lixiviant as tracer.

In their article, they fitted their results to the Levenspiel compartment model, (Levenspiel, 1972). It characterises the hydraulic behaviour in terms of the proportions of the solution content that is mixed, exhibiting plug-flow and being immobile (dead) volume, and the proportions of flow that passes through the ore and which by-passes.

8.2 ASSUMPTIONS

Amongst the parameters reported by these authors were the total moisture contents at the end of the 12-month leaching stage (i.e. prior to commencement of the rinsing phase which represented the step-down tracer test). For the purpose of this study, these values can be assumed to have remained constant throughout the step-down tracer test since the final ore heights, bulk densities and moisture contents had reportedly been reached within the first few weeks of the 12-month leaching period that preceded the tracer test. The moisture content varied from 12 percent in the column to 12.5 percent in the crib and 17 percent in the heap. However they did not report any experimental measurements of the stagnant moisture contents, which is required as an input parameter to the dual porosity models. The notion of immobile solution content to which dual porosity models have been calibrated is the solution content remaining in the ore after drainage under gravity, which can easily be determined experimentally. An example of that practice is provided by Bouffard and Dixon (2001), where they also mention that typically 7 to 13 percent of the total bed volume consists of immobile moisture. Furthermore they obtained reasonable agreement between immobile moisture content measured in that way, and immobile moisture content fitted to hydrodynamic models that they fitted to pulse test data.

Bouffard and West-Sells (2009) reported the mobile and immobile solution fractions that provided the best fits to their Levenspiel model. (Those model fits are shown in Figure 41 below on page 161). Of the solution prevailing in the column and the heap, their data fits indicated the immobile fraction being zero. However the Levenspiel compartment model concept of the immobile portion of a reactor differs from the immobile concept of the dual porosity model. The Levenspiel concept of the immobile fraction is volume that does not exchange any species with the mobile portion of the reactor. In contrast, although no advection passes through the immobile volume fraction of the dual porosity model, it does exchange species with surrounding mobile solution by diffusion. The immobile volume fractions reported by Bouffard and West-Sells (2009) does therefore not provide any guidance of the immobile fractions to be used in the dual porosity modelling of their results.

For the purpose of this analysis, it was assumed that 85 percent of the total moisture content was immobile during irrigation, in accordance with the typical experimental observations made by Bouffard and Dixon (2001).

The total moisture content, in terms of the immobile moisture content, is therefore $\varepsilon_{imm}/0.85$. The tracer concentrations observed in the drainage solutions by Bouffard and West-Sells (2009) were plotted against "fraction of total moisture content irrigated" (represented here by η). That scale can be converted to time (t, [h]) using:

$$\eta = \frac{q}{\rho\, H}\left(\frac{0.85}{\varepsilon_{imm}}\right) t \qquad [102]$$

with q being the irrigation flux [L/(h.m2)], ρ the bulk density [kg/m3] and H the height of the column of ore.

These authors reported the ore bulk densities both before and after leaching, with densification (hence an increase in bulk density), occurring during leaching. The final bulk density values (observed at the end of the leach period) were used for model fitting since the bulk density was reported to have stabilised within the first few weeks of leaching. This does not sacrifice rigour of modelling since, during densification, the density and height change are inversely proportional to one another. Hence the ore tonnage per square meter irrigated (calculated as $\rho.H$ [kg/m^2]), remains constant. As long as tonnage per square meter remains constant, the model results remain unaffected by densification.

8.3 MODEL FITTING

The tracer concentration data of Bouffard and West-Sells (2009) was fitted to the HeapSim dual porosity model by minimising the sum of squared residuals (SSR) between normalised drainage concentrations (normalised with respect to the initial irrigated-concentration, ranging therefore between 0 and 1). These authors did not mention the type of lixiviant used, only that they utilised the lixiviant concentration in the drainage as a tracer. However for modelling studies, the type of tracer does not need to be known, only the response of tracer concentration with time is required. Furthermore, the assumption is being made that the tracer is not being consumed during its passage

through the heap. Bouffard and West-Sells (2009) did not make any statement regarding this, however it is assumed that they would not have undertaken this test if they could not rely on preservation of the tracer.

The simulations were performed using irrigation solution, bearing 1g/L copper with no chemical reaction in the heap (as per the assumption discussed in the previous paragraph), until the copper in the drainage equalled the 1 g/L of the irrigation solution – in that way the simulated copper concentrations are already normalised to a scale between 0 and 1. (The reader is reminded that copper is being used as a proxy for the unknown lixiviant). This period was set at 60 days for the column, 100 days for the crib and 50 days for the heap, which yielded 1 g/L copper in the effluent thereby assuring that the entire simulated immobile solution inventory was bearing 1 g/L copper solution. The 'Event Manager' of HeapSim was set to change the irrigation solution at that point in time to clean water to mark time-zero of a 'step-down' tracer test, simulating the manner in which Bouffard and West-Sells (2009) performed their experiments.

Irrigation with clean water was set to continue for 25 days in the column, 50 days in the crib and 20 days on the heap which covered the period for which data was supplied for each respectrive case. The rate of reduction of dimensionless copper-concentration in the simulated drainage was fitted to the dimensionless lixiviant concentration data observed by Bouffard and West-Sells (2009).

Whether copper, the unknown lixiviant (if it can be assumed it is conserved) or any other species is used as tracer has no bearing on the validity of the simulation, the extent of wash-out with time defines the system hydrology uniquely regardless of the name assigned to the tracer species.

The optimised Transfer Time fitted to the data was recorded for each of the column, crib and heap.

8.4 RESULTS AND DISCUSSION

The conditions (relevant to this study) under which Bouffard and West-Sells (2009) performed the tests, as well as the Transfer Times fitted to each, are summarised in Table 8. The model fits to the experimental data appear in Figure 41, together with the best fits obtained by Bouffard and West-Sells (2009) using their Levenspiel model.

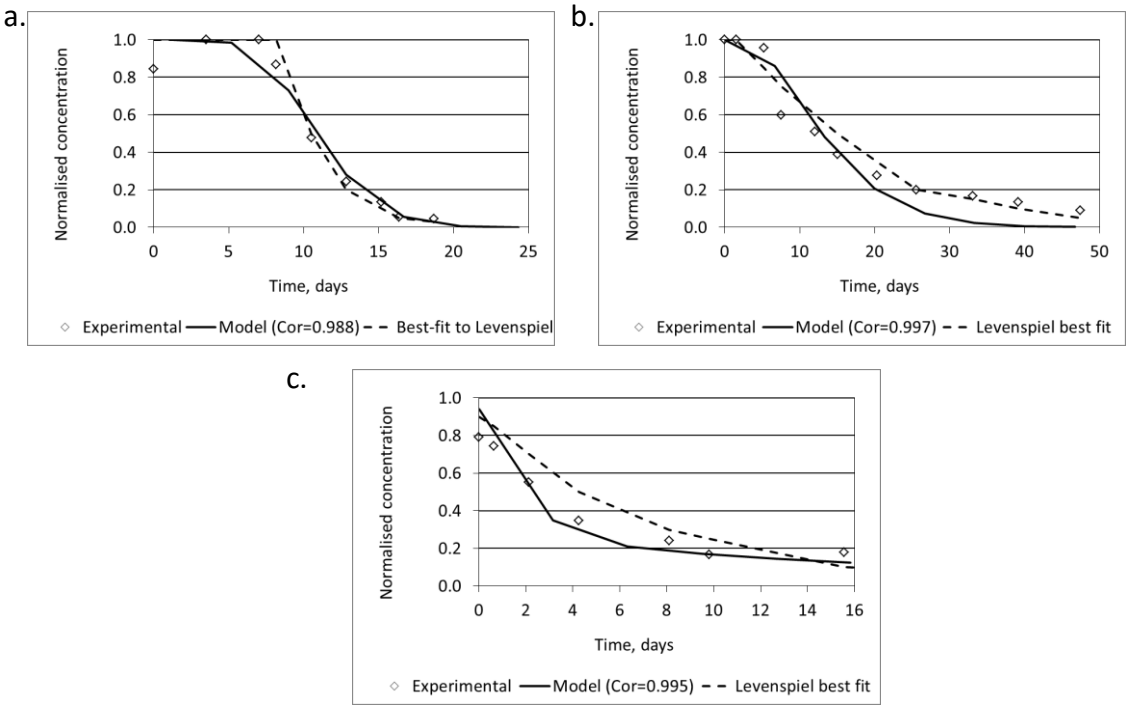

Figure 41. Fitting of Barric tracer results by Bouffard & West-Sells.
(a) Column, (b) Crib, (c) Heap

Table 8. Summary of the Barrick Gold Conditions and Fitted Parameters

Parameter	**Column**	**Crib**	**Heap**
Parameters reported by Bouffard and West-Sells (2009)			
Compacted[1] height, m	5.1	5.46	2.4[3]
Cross sectional dimension	250mm	2.4m x 2.4m	55m x 55m
Dripper spacing	0 mm[2]	460mm x 460mm	460mm x 460mm
Irrigation rate, L/(h.m^2)	3	3	3
Average total moisture content of compacted[1] ore, (kg/kg_dry)	0.14	0.13	0.20
Fraction of total moisture content regarded as immobile	0.85	0.85	0.85
Immobile moisture content of compacted[1] ore, ε_{imm} (kg/kg_dry)	0.116	0.110	0.174
Compacted bulk density[1], kg/m^3	1,370[3]	1,725[3]	2.014[3]
Results of HeapSim model fitting			
Transfer time Θ, days	8.77 (Γ_{ref})	109	862

[1] 'Compacted' being the state after 12 months of leaching, prior to commencement of the step-down tracer test being modelled here.

[2] A distributor plate was used in the 250 mm diameter column to ensure even distribution of irrigated solution over the column cross section, hence effective dripper spacing is taken as zero.

[3] The authors reported only 3 significant numbers for the bulk densities. The fourth decimals were manipulated to retain consistency between heights and bulk densities (a) after loading, i.e. before leaching, and (b) after leaching, i.e. before starting the step-down tracer test being modelled here. The consistency required is $\rho_1 H_1 = \rho_2 H_2$. They reported a final height of 2.3m for the heap, this had to be manipulated to 2.4m to retain this consistency, bearing in mind that the height they reported was the average observed over a cross sectional area of 55m x 55m.

It might be expected intuitively that the Transfer Time should increase with increasing dripper spacing, if it is assumed that the dripper spacing sets the distance whereby flow channels in the immediate vicinity of the irrigation points are separated. And it might be expected that such spacing between flow channels should more or less prevail throughout the height of the heap.

However, in this study the same dripper spacing was used in the crib as on the heap. Yet the Transfer Time can be seen to continue to increase from column to crib to heap. This provides another instance of the observation made during Case Study 1, namely that the Transfer Time is not purely determined by dripper spacing.

There was not in this case data available for estimating the extractable fraction, as was done for case study 1, since the data of this case study was derived from tracer tests, as opposed to leaching tests.

8.5 CONCLUSIONS, CASE STUDY 2.

Although the same dripper spacing was used in the crib than on the heap, the heap exhibited the longer Transfer Time. This is in accordance with the finding of case study 1, namely that the Transfer Time is not strictly related to the dripper spacing.

9 SCALE-UP CASE STUDY 3: KIPOI OXIDE COPPER

9.1 INTRODUCTION

Background and operational details of the Kipoi oxide copper operation in the DRC, southern Africa, is provided by van Staden et al. (2017a). In that publication the diagnostic technique for calculating the shape of the batch curve from a continuous stacking-and-leaching operation was required to compare the performance of the commercial heaps with the column leaching results obtained on the same ore.

Laboratory batch curves (LBC's, to retain the terminology used in the paper), were presented for the column leaching of the oxide-copper ore in two 6m-high laboratory columns, numbered C5 and C6.

The final result of the article cited above was the fitted batch curves (FBC's), derived from the production graphs for three commercial heaps, numbered 1-1, 2-1 and 3-1. Although that provided the shapes of the batch curves on the macro-scale of an entire heap/column, it did not provide insight into the micro-scale kinetics and transport phenomena at work at particle cluster scale within the heaps or columns. That is now further provided here.

9.2 STOICHIOMETRY

This instance involved essentially the acid leaching of malachite, according to equation [1] copied from page 12:

$$Cu_2(CO_3)(OH)_{2(s)} + 2\ H_2SO_4 = 2\ CuSO_{4(aq)} + CO_{2(g)} + 3H_2O \qquad [1]$$

It can be seen to require only the supply of sulphuric acid to proceed. Acid consumption by gangue reactions, discussed in sections 3.2.3 and 3.12.5, will be competing with reaction [1] for sulphuric acid.

9.3 MODEL FITTING

The batch curves obtained from the column leaching studies (i.e. the LBC's), as well as the batch curves derived from the continuous commercial production data (i.e. the

FBC's), were fitted to the PhreeqC dual-porosity heap leaching model. This allowed characterisation of both laboratory column and commercial heap leaching performance in terms of the dual-porosity model parameters. This was done for both copper extraction and GAC.

The HeapSim model is the preferred model due to its fast execution. However when it was attempted to fit the commercial data to the HeapSim model, it was found impossible to fit the GAC data with a single GAC rate constant. A poor fit of the GAC data also leads to a poor fit of the copper extraction data since the two reactions compete for acid.

The PhreeqC model was therefore used for fitting of both the LBC's of the columns and the FBC's of the commercial heaps, since it permits a change in GAC rate constant during the course of the simulation. Although the column leaching data could be fitted with a single value for the GAC rate constant, PhreeqC was used for the model fitting of both sets of data as an additional precaution to ensure direct comparisons can be made between the fitted model parameters of the columns and heaps. This is despite the calibration discussed in section 5.4, where good agreement between the HeapSim and PhreeqC models was demonstrated.

As optimisation criterion for fitting of the extents of extraction, it was aimed at minimising the SSR between individual data points. As optimisation criterion for fitting the GAC, it was aimed at minimising the differences in slopes of the linear parts of the experimental and modelled GAC curves.

9.4 RESULTS AND COMMENT ON KINETICS

The model input parameters appear in Table 9 below, together with a listing of those parameters that were manipulated to optimise the correspondence between the FBC's and the modelled batch curves (MBC's) of Heaps 1-1, 2-1 and 3-1.

The immobile moisture content prevailing in the columns was determined as 0.13 kg_moisture per kg_ore by drain-down tests on separate samples of the ore. For the two heaps 2-1 and 3-1, the same value was used for lack of directly measured data from the heaps. It was possible to model the leaching performance of the two laboratory columns

(C5 and C6) with a single GAC rate constant. This suggests that the majority of copper and GAC was solubilised during irrigation of the columns according to a single mechanism for the full duration of the leach. The complete set of model fits appear in Appendix F, Figure 68 and Figure 69 on page 282, showing copper concentration in drainage solution, copper extraction, acid concentration in drainage solution and acid consumption. For ease of reference, the model fitting of all copper extraction data is also shown in Figure 42 below.

a.

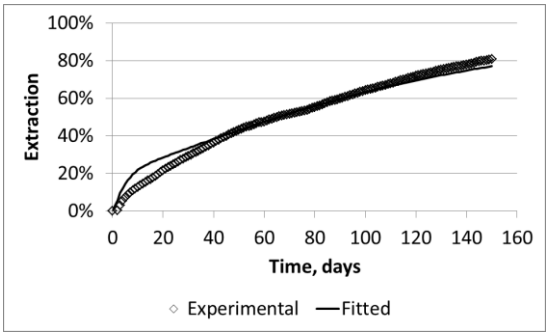

b.

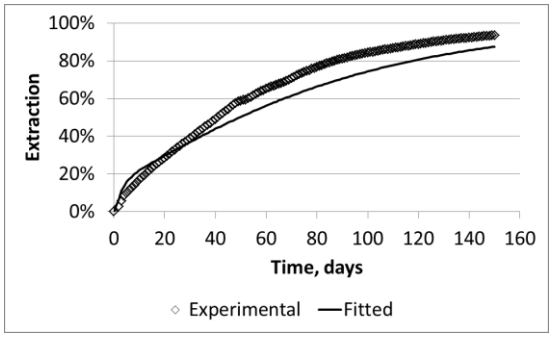

c.

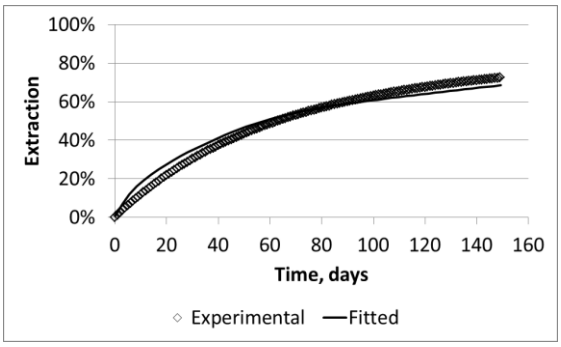

d.

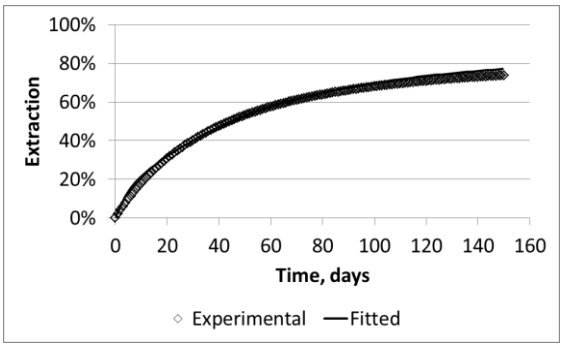

e.

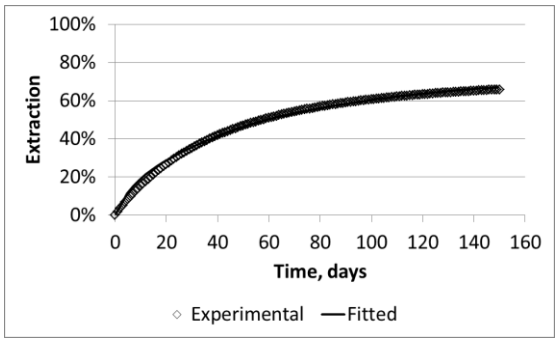

Figure 42. Fitting of Kipoi extraction data
(a) LBC for column C5; (b) LBC for column C6, (c) FBC for heap 1-1; (d) FBC for heap 2-1; (e) FBC for heap 3-1

As stated in the above-cited article the curing acid addition on the commercial heaps (12-13 kg/t) exceeded quite significantly the 5 kg/t used in the columns. The low curing acid dosage used for the columns seems to have been ineffective in changing the GAC behaviour of the columns. That is as opposed to the results of the commercial heaps that required two stages of modelling to fit the observed GAC behaviour which was namely extremely fast GAC consumption during a relatively short initial period (5-25 days), while for the rest of the duration of the leach the GAC rate constant was unusually low. The model fits are shown in Appendix F, Figure 70, Figure 71 and Figure 72 on page 284.

This is interpreted as representing the consumption of the curing acid by reactive gangue prior to initiation of irrigation, requiring the initial period of irrigation to re-establish the presence of acid throughout the heaps before acid once again starts breaking through to drainage. In the case of the commercial heaps the curing acid addition was successful in virtually eliminating all gangue reactivity prior to irrigation so that, after the initial period, the rate of GAC was very slow or, as in the case of heap 3-1, even zero.

In their analysis of the heap bioleaching of sulphidic ores, Dixon and Petersen (2003) found the leach performance to exhibit the highest level of sensitivity to the diffusional path length (as represented here in the Transfer Time). For the oxide heap leaching cases modelled here, the magnitude of the GAC rate constant is seen to be of no less importance than the Transfer Time, due to the competition for acid between the GAC and copper leaching reactions.

The dripper spacing of heaps 1-1 and 2-1 was narrowed from 1.0 to 0.5 m within the period under study, while that of heap 3-1 was 1.0 m for the full duration of time under study. However that did not lead to heap 3-1 exhibiting the longest Transfer Time, although it did lead to the lowest extractable fraction ($\alpha_x\alpha_w$) in heap 3-1. Heap 3-1 was also the tallest of the commercial heaps studied.

Table 9. Summary of Modelling Parameters to Construct MBC's

Parameter and Units	**Symbol**	**Value**				
PARAMETERS KNOWN, MEASURED or ASSUMED						
		C5	**C6**	**1-1**	**2-1**	**3-1**
Total Cu content, %	C^0_{Cu}	3.10	3.30	2.70	3.03	2.64
Extractable Cu content, %	$\kappa_x\kappa_w C^0_{Cu}$	2.95	3.17	2.30	2.42	1.88
Irrigation [H_2SO_4], g/L	C_{H2SO4}	10.2	11.0	11.9	12.4	10.1
Heap/Column Height, [m]	H	6	6	4	5	6
Irrigation rate, L/(h.m^2)	q	10	15	7.4	13.4	13.2
Dripper spacing, m				0.5x0.5	0.5x0.5	1.0x0.5
Column diameter, m		0.2	0.2			
Curing acid addition, kg/t	W_{cur}	5	5	13.7	13.1	11.9
Bulk density, [kg/m^3]	ρ	1,549	1,557	1,385	1,808	1,655
Immobile solution fraction, tonne water per tonne dry ore.	ε_{imm}			0.13		
PARAMETERS DETERMINED BY OPTIMISATION						
		C5	**C6**	**1-1**	**2-1**	**3-1**
Extractable Cu fraction	$\kappa_x\kappa_w$	0.95	0.96	0.85	0.80	0.711
GAC rate constant, h^{-1} Early period Later period	k'	 0.0228	 0.0313	 0-25d: 0.595 25d+ 0.0085	 0-20d: 0.50 20d+ 0.0021	 0-5d: 0.50 6d+ 0.0
Transfer time, days	Θ	43.5	32.4	569	196	280
MAGNITUDE OF PEARSON'S CORRELATION COEFFICIENT						
Cu Extraction Curve	Cor(Cu)	0.997	0.994	1.000	0.998	0.998
GAC Curve	Cor(GAC)	0.650	0.990	0.941	0.943	- (1)

(1) No correlation can be calculated for horizontal lines with zero gradient.

9.5 CONCLUSIONS, CASE STUDY 3

In this instance the extractable fraction $\kappa_x\kappa_w$ decreased with increasing dripper spacing. This suggests that portions of the ore was being left effectively out of contact with leach solution with the dripper spacing used on the Kipoi heaps.

It has further been observed during model fitting of the data that the GAC rate constant is as important to the performance of acid heap leaching as the Transfer Time, due to the competition for acid between the GAC and copper leaching reactions.

10 SCALE-UP CASE STUDY 4: NICICO SULPHIDE COPPER

10.1 INTRODUCTION

During this case study, sulphidic ore from the Darehzare mine, in the Kerman province of Iran, was heap bioleached. Chalcopyrite accounted for 66 percent of the copper content, with the balance contributed by chalcocite and covellite. Pyrite accounted for 78 to 86 percent of the sulphide content. The reasoning and justification was provided in the cited article for representing chalcocite as a combination of copper oxide (CuO) and covellite, since the version of HeapSim available to this study did not provide for chalcocite in the ore. More details about the ore, laboratory column, pilot plant and data analysis appear in van Staden et al. (2017c).

Samples of the ore were first bioleached in a 200mm diameter laboratory column (denoted Column 6.1), simulating the conditions anticipated to be encountered in the pilot heaps. This was followed by heap bioleaching the same ore on three truck-dumped pilot heaps, 6m high and each bearing about 20,000 t ore (dry basis). After stacking, a number of boreholes were drilled into the heaps which were fitted with temperature sensors and vacuum lysimeters for obtaining solution samples from various depths within the heaps.

Drip irrigation was used on a 1,000 mm x 400 mm grid. However ponding was reported to have occurred on both heaps, which renders the effective dripper spacing smaller than this grid, potentially as low as zero.

Of the three heaps, the data of only two was deemed suitable for detailed study. Upon completion of leaching, boreholes were once again drilled into various locations of each heap to collect residue samples as representatively as possible.

The engineering and operational features suggested by the theoretical energy balance study of Dixon (2000) were built into this pilot plant to preserve the heat of the exothermic sulphide oxidation reactions. The reasoning was that heat preservation would raise the heap temperature, thereby accelerating the leaching kinetics of slow-leaching minerals such as covellite and, of course, particularly chalcopyrite.

10.2 WHAT HAS ALREADY BEEN REPORTED

The available data was verified and reconciled to ensure consistency between the operational targets, the actual conditions prevailing and the inputs used for the modelling study. Firstly, the ore tonnage stacked on each heap could be verified to within 3 percent for Heap 1 and 10 percent for Heap 2, by comparison of weightometer data from the belt feeding the agglomerator, and the count and weigh-bridge information of the trucks that dumped the ore onto the heaps.

Next it was verified that the volume of drainage solution collected from each heap could be correlated to the rate of its irrigation. This was necessary since the heaps had been stacked with overlapping sides which gave rise to the possibility of solution irrigated on one heap migrating to the drainage of a neigbouring heap. Very good correlations between the rates of irrigation and drainage from both Heaps 1 and 2 was taken as assurance that this did not occur.

The next concern was the variability that might exist in the composition of solution emanating from different locations distributed over the heap footprint. This would be an indication of heterogeneous conditions existing across various points on the heap footprint, so that one unit cell of the heap selected around a given dripper is not behaving like another selected around another dripper. (Refer to section 3.7.4 for a discussion of a heap unit cell). Apart from the vacuum lysimiters installed in boreholes in the heaps, empty drums had also been installed in the drainage layer of each heap, in the centre of the footprint. A drainage pipe lead from each drum to the discharge end of the pad where the solution collected from the centre of the heap footprint could be sampled. It was found that the copper concentrations measured in the composite drainage from each heap correlated well with the drainage collected from the centre of each heap over the first 200 to 250 days. After that, the copper concentrations emanating from the centre of heap 1 were mostly lower, typically 50%, of that of the composite drainage. The correlation held better for heap 2, although after day 250 a number of data points existed where the drainage from the centre were up to double that of the composite drainage. It was not possible to correct for this discrepancy in any

way, other than to merely note the extent to which conditions and the rates at which processes occurred were heterogeneous with respect to location on the heap footprint.

The sides of the heaps were not irrigated due to their instability, but that left uncertainty about the true surface area (and ore tonnage) effectively being irrigated. The head and residue assays and copper recovered from the drainage were taken as accurate and the heights and bulk densities were known from the ore masses and land-surveys of the heap dimensions. From this, the effective areas under irrigation were back-calculated, although this back-calculation suggested that the amount of ore stacked was known within 6 to 13 percent (which is of similar magnitude to the 3 to 10 percent mentioned above with respect to the stacking reconciliation).

The last area of concern was the proportion of the air blown from the bottom that was indeed passing vertically through the heap, as opposed to escaping sideways through the drainage layer. The oxygen concentrations of the inlet and outlet gaseous phases were known, but the volumetric flow passing upward through the heaps could not be measured. The total oxygen consumption over the duration of the leach (OUR_{conv}, [kmol/m^2]) was calculated from a HeapSim simulation that best fitted the observed extent of extraction and temperature. The "best fit" comprised essentially of that combination of diffusional distance and oxygen inlet concentration that minimised the SSR between observed and calculated extraction profiles, following the logic described in more detail by van Staden et al. (2017c). The average rate of upward air flow could then be calculated as OUR_{conv} divided by the average difference between inlet and outlet oxygen concentrations. Of course the re-introduction of a new air flow leads HeapSim to calculate a slightly different extent of extraction and temperature profile. Hence a few iterations with different combinations of diffusional distance and inlet oxygen concentration were required before ultimately concluding that, in the column, 51 percent of the air supplied passed through the ore, in Heap 1 it was 12 percent and in Heap 2 it was 18 percent. These very low percentages of air actually passing through the heaps are consistent with the fact that van Staden et al. (2017c) reported that ponding was occurring on the heap surfaces. This indicates that at least the upper parts of the heap were saturated with solution which would have hindered the passage of air.

In the case of the heaps there was ample opportunity for air to escape sideways from under the heaps via the drainage layer in which the aeration pipes were installed. In the case of the column, air is suspected of having escaped past the solution drainage tube at the bottom the column, despite a gooseneck water trap being maintained in it. Alternatively, the air might have short-circuited along the wall where the packing of ore is not as random and not as dense as in the bulk of the ore, as discussed in 3.16.1.

HeapSim simulations were conducted of the column and the two heaps. In this case it was essential to use the HeapSim model for data fitting since the PhreeqC model does not provide for the counter-current flow of, or the mass and energy transfer between the solution and gaseous/vapour phases. The current version of the PhreeqC model does also not provide for adiabatic energy preservation, and adding it would no doubt slow it down even further. These are essential features for the modelling of the heap bioleaching encountered during this case study.

Moisture contents had been calculated as the cumulative difference between solution irrigated and solution drained. The drainage rate from the columns could be done accurately since all solution was collected. The drainage rates from the heaps were measured by a V-notch wear installed in the drainage trough, and readings were taken twice in 24 hours, with the two daily readings differing on average by slightly less than 5 percent. However, the moisture content of the heap calculated by mass balance between solution irrigated and solution drained suggested a continuously rising moisture content beyond practically possible values. Ponding was continuously evident on the surfaces of the heaps, indicating that at least the upper parts of the ore were indeed water-logged. The moisture content for the modelling of Heaps 1 and 2 was hence fixed at 0.2 t_water per t_ore as established by the calculations in section 3.7.5 for ore with a bulk density of 1,800 kg/m^3.

A single set of kinetic parameters was used for the column and both heaps, since the same ore was being treated in all cases. Mostly the default values suggested by the HeapSim authors were retained. By HeapSim modelling it was aimed to emulate all of the copper concentration in (composite) drainage, cumulative extent of copper extraction, net acid consumption (NAC) and extent of total-sulphide conversion. NAC

being the net result of acid consumption by all (sulphide) oxidation, precipitation and (copper) reduction reactions. (Refer to the Nomenclature for a distinction of the difference between GAC encountered in the acid leaching of oxide ores and the NAC encountered in the oxidative leaching of sulphidic ores).

The Transfer Time was the principal model parameter being manipulated to achieve the fit between experimental data and model outputs, but some manipulation of the ferric-iron-solubility constant ("Jarosite equilibrium constant" according to HeapSim terminology) and the GAC rate constants were also required.

10.3 WHAT REMAINS TO BE DONE ON THIS STUDY

The simulation reported in van Staden et al. (2017c) aimed to emulate the maximum temperatures measured. However, for the column as well as both heaps the extent of sulphide conversion thus modelled considerably exceeded the sulphide conversion indicated by the head and residue assays.

This is complicated by the fact that the ore below the 10x10m^2 core in the centre of the heap, being the best insulated, was expected to achieve the highest temperatures and reaction rates and to best represent a full-scale commercial heap. Instrumentation and sampling was therefore concentrated in this area of the heap, with fewer instrument readings and samples being obtained from other parts of the heap. The highest temperatures were measured in areas outside of the inner core, and it is possible that, in the heap as a whole, a higher average extent of sulphide oxidation was indeed achieved, but the only residual sulphide assays available were from the core which indicated a lower sulphide conversion.

As a solution, the simulations were recalculated with lower pyrite oxidation rate constants to match the average temperatures measured (as opposed to the maximum temperatures measured). This also required a re-estimate of the oxygen utilisation and hence of the proportion of supplied air that passed vertically through the ore.

This provided better modelling of the assayed sulphide conversions (an exact match for Heap 1, but still over-estimates for the column and for Heap 2), while still enabling fitting of the copper drainage concentration, extent of copper extraction and NAC. If the pyrite

rate constants are lowered much further, it becomes impossible to model the observed average heap temperature or copper extraction. This implies it has to be accepted that the residual sulphide analyses obtained from the heap cores were not representative of the heaps as a whole. However the sulphide conversion obtained for the column by assay was also lower than what could be reconciled with the observed average temperature and total copper extraction, while sampling of the column residue could be done fully representatively. Unfortunately, that leaves the sulphide reconciliation somewhat unresolved without another opportunity to verify that result. More reliance therefore needs to be placed on the average heap temperatures, being the results of multiple measurements over time at various locations, than in the singular residual sulphide analyses.

The best compromise available was to present the results of the recalculation (to fit the average temperatures) that follow below, as a second estimate of the model parameters fitting the experimental observations.

10.4 STOICHIOMETRY

The stoichiometry of the bioleaching of chalcopyrite, chalcocite, covellite and pyrite occur according to reactions [11] [7], [8] and [10] respectively, as discussed in section 3.2 and are repeated here for ease of reference:

$$CuFeS_2 + {}^{17}/_4\, O_2 + \tfrac{1}{2}\, H_2SO_4 = CuSO_4 + \tfrac{1}{2}\, Fe_2(SO_4)_3 + \tfrac{1}{2}\, H_2O \quad [11]$$

$$Cu_2S + {}^{1}/_2\, O_2 + H_2SO_4 = CuSO_4 + CuS + H_2O \quad [7]$$

$$CuS + 2O_2 = CuSO_4 \quad [8]$$

$$FeS_2 + {}^{7.5}/_2\, O_2 + \tfrac{1}{2}H_2O = \tfrac{1}{2}\, Fe_2(SO_4)_3 + \tfrac{1}{2}H_2SO_4 \quad [10]$$

10.5 RECALCULATED RESULTS

The updated reconciliation of air being supplied, and air calculated to have passed vertically through the ore, is provided in Table 10 below. It is shown together with the first set of results reported in van Staden et al. (2017c) (appearing as numbers in

brackets) as a comparison. Obviously, the effective aeration (i.e. proportion of air supplied that passed vertically through the ore) is now smaller for all cases, accounting for smaller extents of sulphide conversion.

Table 10. Reconciliation of oxygen consumption, air supplied and air utilised

Parameter	Column 6.1	Heap 1 (0-200d)	Heap 2 (0-340d)
a = *OUR_conv*, kmole O_2/m^2	(4.52)3.86	(2.11)0.81	(5.27)1.85
b = Aeration supplied, $Nm^3/(h.m^2)$	0.54	1.06	0.91
c = *OUR_supp*, kmole O_2/m^2	10.4	18.3	28.3
Aeration effective=*b*a/c*, $Nm^3/(h.m^2)$	(0.23)0.20	(0.12)0.05	(0.17)0.06
Aeration effective=*a/c*, % of supplied	(43%)37%	(12%)4%	(19%)7%

[1.] In van Staden et al. (2017c) these were incorrectly reported for respectively Column 6.1; Heap 1 and Heap 2 as 5.27; 5.43 and 7.50, which were not the results of the final iterations.

Modelling on that basis led to the parameters summarised in Table 11 below, which yielded the optimal fits between experimental and modelled results. For interest sake, the defaults suggested by the authors of HeapSim are also provided where applicable. As in the previous table, the numbers reported in van Staden et al. (2017c) are also shown in brackets. Only for the column was it necessary to adjust the Transfer Time from 72.5 days previously to 147 days during this recalculation. The pyrite oxidation rate constant was the only other parameter that needed adjustment, namely in all three cases (the column and the two heaps).

The quality of the model fits achieved are shown in APPENDIX F for the complete set of parameters. For ease of reference, the fits obtained of the extraction results are also shown in Figure 43 below.

10.6 COMMENT ON KINETICS

Between the figures originally reported in van Staden et al. (2017c) and this recalculation, the trend remains of Transfer Times in the two heaps being about an order of magnitude larger than that of the column. With these very large Transfer Times, it is clear that diffusional mass transfer was dominating the leaching kinetics, despite the sulphidic chalcopyrite and pyrite minerals being know to exhibit relatively slow chemical reaction kinetics as discussed in section 3.3.

Table 11. Summary of operational and modelled parameters

Parameter	HeapSim Default	Col 6.1	Heap 1	Heap 2
OPERATIONAL PARAMETERS				
Dripper spacing, mm		200(1)	1,000 x 400(2)	1,000 x 400(2)
(1)Stagnant moisture content, t_water/t_ore	0.06	0.2	0.3	0.3
Raffinate added for agglomeration, m^3/t_ore	0.0005	0.0526	0.0356	0.0316
Curing acid addition, kg/t	2.5	2.5	0.0	2.4
MODELLED PARAMETERS DETERMINED BY RECONSILIATION AND FITTING				
Extractable fraction		1.00	0.985	1.00
Tranfer time, days	Case-specific	(72.5)147	(873)873	(605)605
RATE CONSTANTS				
Oxide-Cu rate constant, h^{-1}			0.3	
Covellite rate constant, h^{-1}			10^{-4}	
Pyrite rate constant, h^{-1}	10^{-4}	$3.8x10^{-6}$	$8.0x10^{-6}$	$1.4x10^{-5}$
Chalcopyrite rate constant, h^{-1}			$1.5x10^{-4}$	
GAC rate constant, h^{-1}	0.001	$5x10^{-4}$	0.01	0.01
POWERS OF UNREACTED FRACTION				
Oxide-Cu power of unreacted fraction			1	
Covellite power of unreacted fraction			1	
Pyrite power of unreacted fraction			1	
Chalcopyrite power of unreacted fraction			1.5	
PARAMETERS RELATED TO ACID BALANCING				
Pyrite elemental S yield	0.5	0	0	0
Jarosite equilibrium constant K^{25degC}	2.0	0.25	0.51	0.51
(3)Gangue dissolution rate constant, $(mol/L)^{-1}$ h^{-1}	10^{-3}	$5x10^{-4}$	10^{-2}	10^{-2}

Notes:

(1) Column diameter

(2) Ponding was observed on both heaps, which leads to a smaller effective dripper spacing than this.

(3) Dixon and Petersen (2003) suggested values of 10^{-3} to 10^{-2} as the range for 'low' to 'high' gangue dissolution rate constants.

a.

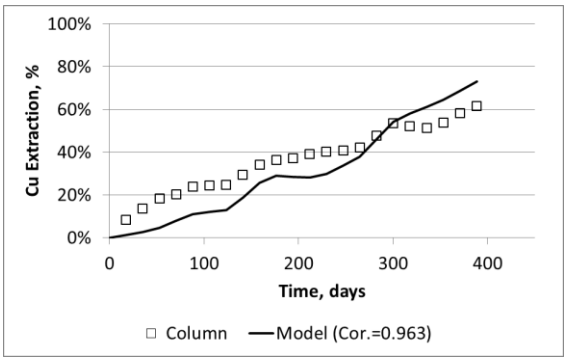

b.

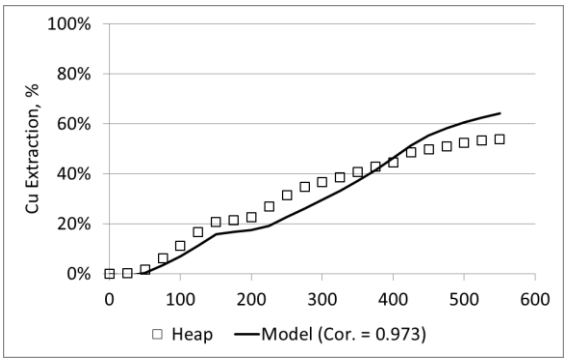

c.

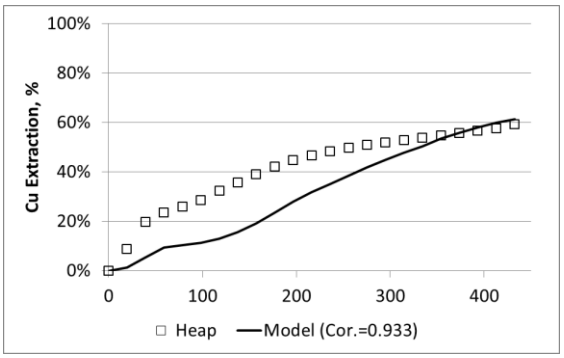

Figure 43. Fitting of NICICO results
(a) Column 6.1; (b) Heap 1; (c) Heap 2.

10.7 CONCLUSIONS, CASE STUDY 4

The several uncertainties mentioned with regard to the data of this case study were dealt with by analysing two extremes of extent of pyrite oxidation that could have occurred in the column and in the two heaps. Regardless of which extreme more closely represented reality, the trend remains of the Transfer Time in the heaps being about an order or magnitude longer than that of the column. That is despite ponding having occurred on the heaps which could have reduced the effective dripper spacing to as low as zero. That suggests that the condition illustrated in Figure 22(c) on page 97 applies

here, namely that the (effective) dripper spacing is narrower than the spacing of available flow channels in the ore.

The extractable fractions of the column as well as both heaps approximated unity, despite the longer Transfer Times observed on the heaps. At least the ponding on the heaps, resulting in an effectively narrow dripper spacing, ensured that none of the ore remained unwetted (although ponding is symptomatic of undesirably low permeability of the ore).

11 EFFECT OF SIMULATED SEGREGATION

11.1 INTRODUCTION

The preceding case studies seeked to verify independently whether indeed differences are consistently observed between the leaching performance achieved in laboratory columns versus large heaps (with unsupported sides). Case studies were considered of the cyanide leaching of free-milling gold ore, acid leaching of oxide-copper ore and bioleaching of sulphide copper ore. It was further endeavoured to determine the nature of the differences by fitting parameters such as the extractable fraction and Transfer Time (in the model with dual-porosity hydrology and diffusion with chemical reaction kinetics) to the experimental results. This also achieved quantification of the differences in terms of the magnitudes of the parameters that optimised the model fits to laboratory column leaching data, compared to the parameters that optimised the model fits to heap leaching data.

Segregation is absent from laboratory column leach tests, where it is strived to distribute the ore as homogenously as possible throughout the columns, from side to side and from top to bottom. However it is accepted as an unavoidable consequence of current stacking practices.

This section explores systematically the extent to which the observed differences between laboratory columns and large heaps can be attributed to segregation, to corroborate or dispel the supposition that segregation impacts on heap leaching performance.

11.2 SEGREGATION DEFINED

Segregation is defined in different ways in the published literature. Read in context, it appears that authors on heap leaching such as Gross and Gomer (1992), Guzman et al. (2006) and various others mentioned in Van Staden and Petersen (2018a) use it to imply any separation of particles by size during stacking, so that parts of a heap contain a greater than average proportion of fines, while the opposite applies in other parts. In more formally scientific studies such as those by Shimokawa and Ohta (2007) and Benito et al. (2013), the term segregation is reserved for a variation of size distribution in a

heap/pile vertically, while stratification refers to differently sized layers that form on the advancing slope during stacking. After stacking of a complete heap, the stratified layers extend from top to bottom in a heap, sloped at the internal angle of friction of the ore.

A more detailed discussion and illustration of segregation is provided in Van Staden and Petersen (2018a).

11.3 VERIFICATION OF THE EXISTENCE OF SEGREGATION IN ORE HEAPS

Segregation has long been known to occur when aggregate (not restricted to mineral ores) is stacked on a pile in the manner that heaps are stacked, be it by conveyors, trucks or loaders. The same should apply regardless of whether the stacking equipment approaches the advancing face from the pad or by passing over the upper heap surface. For example Tournier and Judd (1944) mention its effect on bin and hopper design.

With so many literature references mentioning the observation of segregation and attributing problematic heap leaching performance at least partly to segregation, it should hardly be necessary to confirm independently whether segregation does indeed occur in ore heaps. Nevertheless it is surprising that the only data to quantify the extent of segregation on an ore heap known to the author, is that by the author himself and co-workers in van Staden et al. (2017c), reporting on the NICICO ore treatment discussed as case study 4 in section 0. Immediately after agglomeration and stacking of a pilot scale heap, they drilled boreholes using a motorised auger drill into the heap for the placement of in-heap instruments. There is no air or water flow involved during auger drilling, and the drilling was performed while the ore was still moist, which was expected to prevent particle segregation during the extraction of the drilled material. The drillings were subjected to wet particle size distribution analysis, and the results are reproduced in Figure 44 below.

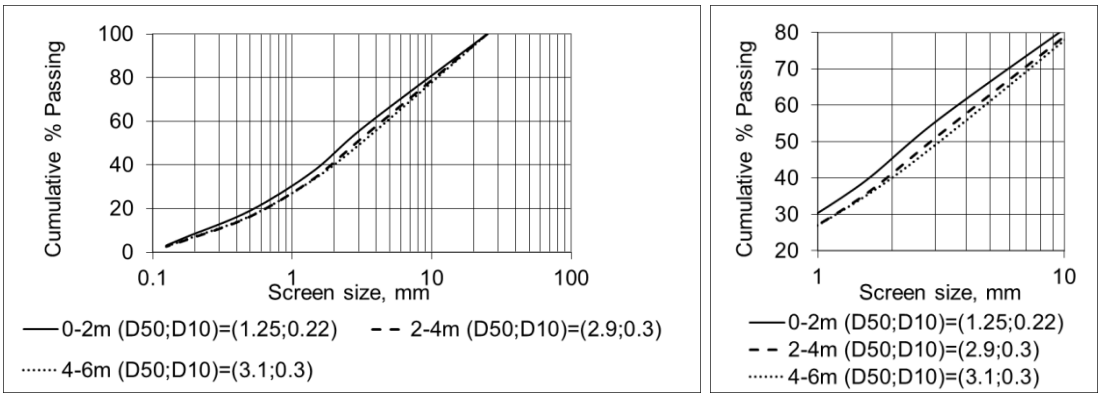

Figure 44. Segregation observed in a heap of copper sulphide ore.
Reproduced from: van Staden et al. (2017c)

The behaviour expected of segregation can be observed, of namely a greater proportion of finer particles being encountered in the upper 0-2m of the heap, and the largest proportion of coarser particles in the bottom 4-6m deep layer. The effect was most severe around the 3mm particle size, of which the upper 0-2m layer contained 6 percent more than the lower 4-6m layer. However, this can still be described as relatively modest, compared to the extent of segregation achieved during the laboratory simulations with deliberate segregation that are discussed below.

11.4 PROCEDURES

Details of the ore characterisation, experimental apparatus and procedures are provided in Van Staden and Petersen (2018a). In brief, a rectangular box shown in Figure 45 below on page 189, with the bottom sloped at 30^{o} (slightly less than the the internal angle of friction of the agglomerated ore), was constructed to simulate the advancing slope of a heap under construction. The ore was poured into the box from the end where the bottom was lifted and allowed to roll down the slope, to ensure that segregation would occur. It was found necessary to raise the entry-end of the box slightly to increase the angle of the slope to 39^{o} to ensure that the ore formed layers parallel to the sloping bottom, which hence represented the internal angle of friction of the agglomerates.

The photograph in Figure 45 (b) below shows the box after the first layer of agglomerates has been poured in, and the coarser particles prevailing towards the bottom end can be seen. Subsequent charges of agglomerates were poured in until the

box was filled to the top. Once the box was filled, it was unloaded to collect separately the ore from the upper side of the slope (Up), the middle (Mid) and the bottom (Bot). This procedure was repeated on 5 to 7 kg batches at a time until 108 kg ore (dry basis) had been segregated in this way.

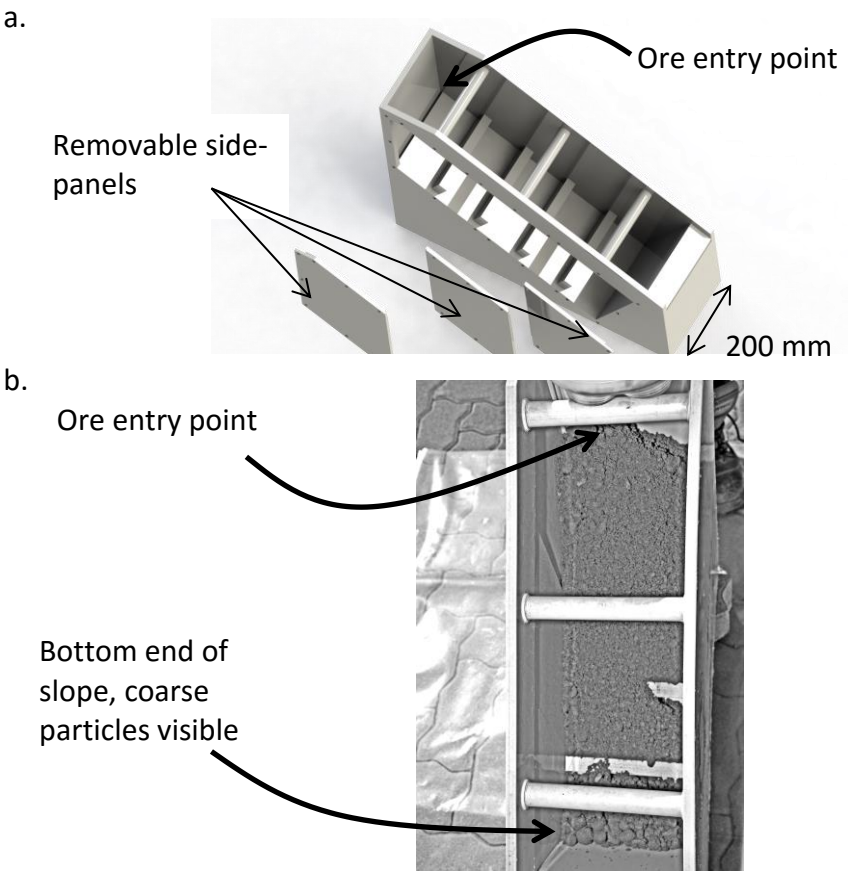

Figure 45. Illustration of segregation box.
(a) empty, (b) having just covered the bottom with ore

Each of the Up, Mid and Bot portions were then subjected to the range of tests listed in Figure 46 below, which provides a flow diagram of the test programme. The same tests were also conducted on unsegregated ore. Furthermore, those tests that were conducted in packed bed columns 770 mm in height and of 153 mm diameter, were also performed on a sample composed of the Up, Mid and Bot fractions layered to provide a simplistic simulation of a segregated heap.

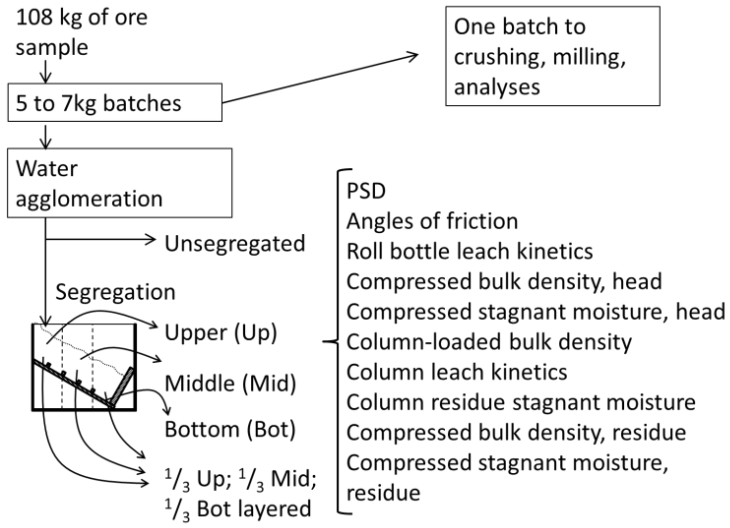

Figure 46. Illustration of tests conducted to determine the effect of segregation. Reproduced from Van Staden and Petersen (2018a)

11.5 STOICHIOMETRY

The ore contained copper essentrially as the oxide-mineral malachite. It leaching in sulphuric acid is represented by equation [1] copied from page 12:

$$Cu_2(CO_3)(OH)_{2(s)} + 2\ H_2SO_4 = 2\ CuSO_{4(aq)} + CO_{2(g)} + 3H_2O \qquad [1]$$

Acid consumption by gangue reactions, discussed in sections 3.2.3 and 3.12.5, will be competing with reaction [1] for sulphuric acid.

11.6 KINETICS

The leaching kinetics observed in rolling bottles of the unsegregated ore and segregated fractions provided rate constants for leaching at the particle scale for the given size distribution, in the absence of any mass transfer constraints in the solution phase. That eliminated the leaching rate constant as a parameter to be fitted during modelling of the column leaching results. The leaching rate constants thus determined (around 1 h^{-1} and greater) were of such magnitude that leaching kinetics did not limit the rate at which copper reported to the drainage solution during any stage of the experiments.

The intention was that determination of the GAC rate constant *k'* (discussed in section 3.12.5), during rolling bottle leaching could similarly eliminate that parameter as a

variable to be fitted to the model. (GAC is defined in 3.9.1 and the kinetic rate constant of GAC, *k'*, is defined in 3.12.5). However, during the subsequent model fitting it was found that the values of *k'* determined from rolling bottle results did not optimise the fit to the model predictions, even after having made the corrections for liquid-to-solid ratio discussed in the Nomenclature section with regard to parameter *k'*. That left *k'* and the Transfer Time Θ as the two parameters that required manipulation in order to optimise the fit between experimental data and model calculations. The techniques discussed in APPENDIX G were used for this multi-variable optimisation.

Even the optimised fits did not fit the GAC curves as faithfully as the copper extraction curves. As optimisation criterion, it was aimed at minimising the differences in slopes of the linear parts of the experimental and modelled GAC curves, as opposed to minimising the SSR between individual data points.

11.7 HYDRAULICS

Saturated hydraulic conductivity is measured as the solution flux (in such units as L/m^2) passing through a column of ore when flooded with solution. This was determined three times on each of the ore fractions generated. Firstly, a small sub-sample of the fresh ore was placed in a uni-axial compression apparatus, compressed to the pressure that the ore would experience at the bottom of a 6m high heap, and the saturated hydraulic conductivity was determined on the ore in this state. (That provided the "head comp." results in Table 12 below). A larger sample of the ore was then placed in the leaching column, the column leaching experiment was completed, following which the saturated hydraulic conductivity was conducted on the residue sample in the leaching column without disturbing the sample. (This provided the "residue in col." results in Table 12). Following that, the residue was excavated from the column, a sub-sample thereof was placed in the uni-axial compression apparatus again, compressed to the equivalent of 6m depth in a heap, and the hydraulic conductivity was measured again. (This yielded the "residue comp." results in Table 12).

11.8 CONSIDERATION OF WALL EFFECTS

Discussion is offered by both Van Staden and Petersen (2018a) and by Van Staden and Petersen (2019) on the wall effects that could be present. All available evidence

indicates that the solution was, during both segregation and stratification tests, essentially passing through the ore, with little if any by-passing between the ore and the vessel walls. Nevertheless, the support of part of the ore mass by the vessel walls is an inevitable compromise to be made during any laboratory tests. Even cribs, that are of much larger cross sectional area than the columns and boxes used here, have a measurable effect on the extent of ore densification, (Bouffard and West-Sells, 2009). Therefore, all of the observations made in columns and boxes need to carry the qualification that the ore contained in the vessels had not settled to the bulk density that is likely to be reached on a free-standing heap.

11.9 RESULTS AND DISCUSSION

11.9.1 Particle size distribution

The size distributions of the Up, Mid and Bot fractions are compared with that of the unsegregated ore in Figure 47 below. A much greater extent of segregation was achieved during the laboratory simulated segregation (as per Figure 47) than was observed on the sulphide heaps (as per Figure 44 on page 188).

Data is lacking to tell whether commercial heaps on average exhibit an extent of segregation more akin to that of the sulphide heaps illustrated in Figure 44, or to that of the laboratory simulated segregation illustrated in Figure 47. But it seems reasonable to suggest that any effects that segregation might have on heap leaching performance should be detectable on the laboratory segregated samples, due to the relatively severe extent of segregation that was achieved.

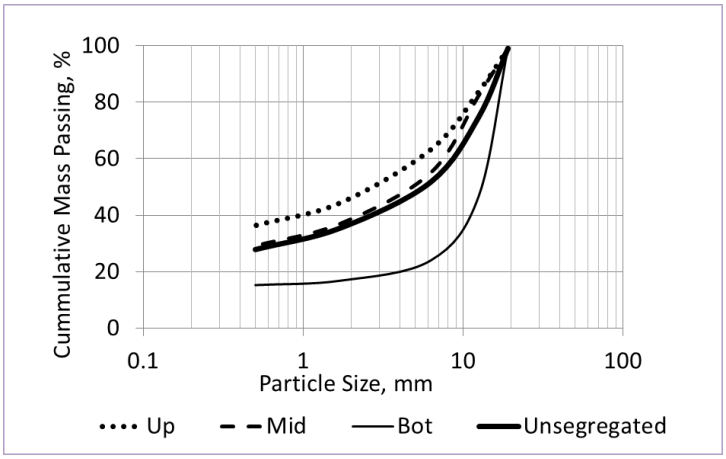

Figure 47. PSD of segregated and Unsegregated Fractions laboratory simulations

11.9.2 Angles of internal and wall friction

The unsegregated ore was repeatedly found to possess a larger internal angle of friction (by 2 to 4 degrees) than the Upper, Middle or Bottom fractions, as reported in Van Staden and Petersen (2018a). This is attributed to the fact that segregation narrows the size distributions of the ore, in this case towards the finer size range in the case of the Upper and Middle fractions, and towards the coarser size range of the Bottom fraction. This observation has previously been made by Carson and Pittenger (1998).

The angle of friction between leached ore samples and their columns were 10 to 20 degrees larger than the internal angles of friction, indicating the extent to which the leaching ore was being supported by friction and adhesion to the column walls. The only exception was the Bottom segregation fraction, with an angle of friction between ore and column wall of about the same magnitude (or even slightly less than) the internal angle of friction. The very narrow and relatively coarse size distribution of the Bottom fraction therefore led to that fraction being self-supported in a column.

11.9.3 Physical and hydraulic properties

A number of physical and hydraulic properties of the various fractions were determined by Van Staden and Petersen (2018a) under conditions of compression simulating the bottom of a 6m high heap. Most of the results were within the expected norms and are not repeated here.

A surprising result was that, comparing the “head comp.” and “residue comp.” results of the Bottom fraction in Table 12, it exhibited by far the highest hydraulic conductivity of the fresh ore fractions, but it became the least conductive fraction during leaching. In Table 12, the highest numbers in a row are double-underlined and the lowest are single-underlined. This behaviour is observed again from a comparison of the “residue in col.” results which reveals that the Layered residue sample in the column yielded virtually the identical hydraulic conductivity as the Bottom residue sample in the column (7,647 and 7,638 L/[h/m^2] respectively). This suggests that the hydraulic conductivity of the Layered residue sample was limited by that of the Bottom residue fraction which constituted the bottom layer of the Layered sample. Recall from the previous section that the Bottom fraction was found to have supported its own weight in the column, while the other fractions were partly supported by the column walls. This could have caused the Bottom fraction to settle more densely in the column than the other fractions. It can further be speculated that the removal of fines from the void spaces amongst the coarser particles during segregation left the coarse particles with less mechanical support and therefore render them more likely to deform into those voids, be it by the crumbling of hard but brittle particles under compression, or plastic deformation of particles that softened during leaching. This would leave the Bottom residue less conductive after leaching than the Bottom head sample was before leaching.

The Upper and Middle residue samples exhibited higher hydraulic conductivities under compression than did the fresh (head) samples, referring to the “residue comp.” and “head comp.” results respectively. For lack of microscopic analyses of these residues, it can only be speculated that leaching may have improved the hydraulic conductivities of these fractions by precipitates cementing the finer fractions into coarser agglomerates, or that the finest particles present in the fresh (head) samples might have been completely dissolved during leaching, preferentially to coarser particles.

Table 12. Saturated hydraulic conductivities of segregated ore fractions

Parameter	State	Units	Up	Mid	Bot	Un-segr.	Layered
Saturated hydraulic conductivity							
	head comp.	L/[h.m^2]	6,819	6,606	15,298	15,393	10,110
	residue comp.		9,941	11,378	9,170	14,798	10,276
	residue in col.		8,002	9,127	7,638	9,464	7,647

Notes: “comp.” = compressed by weight equivalent to 6m of ore;
“col.” = leaching column;

A comparison of the “residue com.” and “residue in col.” results shows that the natural densification occurring during column leaching yielded residues with lower hydraulic conductivities in the columns than the hydraulic conductivities measured on the same residues in a compression chamber. It should be borne in mind that the compression chamber brings about only the effects of vertical pressure upon the material. However, the re-precipitation of species from the percolating solution amongst the ore particles can also reduce the hydraulic conductivity, which is an effect that could be at work within a column during the course of leaching, but which is not emulated in a compression chamber. And upon excavation of the residue from a column, the bonds and seals created between particles by the precipitates are destroyed.

11.9.4 Metallurgical performance

The extraction curves of all segregated fractions are compared to that of the Unsegregated ore in Figure 48 below.

a. b.

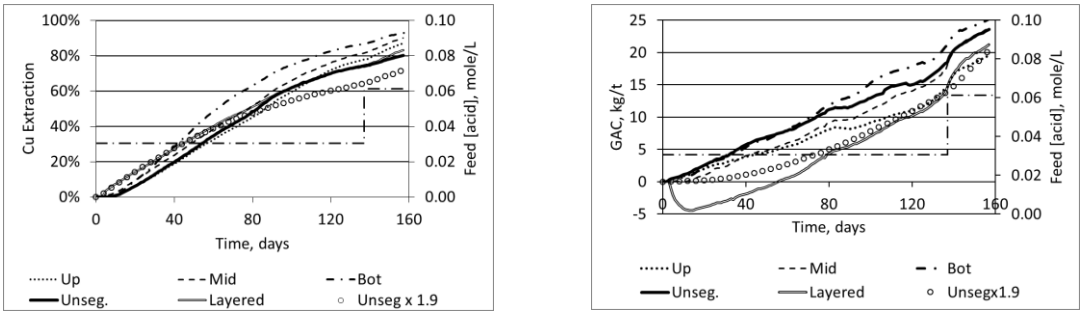

Figure 48. Column leaching performance data on segregated fractions.
(a) Copper leaching, (b) GAC
Reproduced from Van Staden and Petersen (2018a)
"Unseg x 1.9" indicates the leach curve with 90% larger Transfer Time than that of the Unsegregated sample, yielding 10 percent lower final extraction than the Unsegregated sample.

The divergence that did exist in the extraction curves resulted mostly from differences in the initial rates of extraction during the first 10 days. The slopes of the various extraction curves followed very similar trends. All segregated fractions yielded somewhat better final extents of extraction than the Unsegregated ore, as opposed to the inhibitory effect anticipated to be instigated by segregation. The final extents of extraction could not consistently be correlated to any of the physical or hydraulic parameters determined earlier, hence the observed variations in the extraction curves are assumed to be simply random variations exhibiting the repeatability of experimentation on coarse ore fractions.

Referring to section 1.3, it will be recalled that the experience of heap leaching design engineers such as Jansen and Taylor (2002) and John (2011) has been that heap leaching yields 10 to 20 percent lower extraction over a given time period. By trial and error manipulation of the Transfer Time of the model simulation of the Unsegregated column leaching result, it was found that the Transfer Time needs to be increased by a factor of 1.9 in order to reduce the final extraction by 10 percent. The extraction curve illustrating that simulation is labelled "Unseg. x 1.9 in Figure 48.

Of course, to reduce the final extraction by 20 percent would require an even greater increase in Transfer Time. However, the example of a 10 percent reduced extraction is sufficient to illustrate that segregation cannot account for the practically observed reduction in extraction during scale-up from columns to heaps. With the Unsegregated sample exhibiting a Transfer Time of 26.7 days, as shown in Table 13 below, a segregation fraction that yields a 10 percent lower final extraction due to increased diffusional restriction would exhibit a Transfer Time of (1.9)(26.7) = 50.7 days. The largest Transfer Time fitted was that of the Bottom fraction, being 32.8 days, which is well short of the required 50.7 days. Hence it is concluded that the difference in final extent of extraction reported to exist between columns and heaps cannot be attributed to segregation, since segregation could not be found to cause the requisite increase in Transfer Time.

The GAC rate constants, *k'*, fitted for the various fractions varied somewhat, with particularly that of the Upper fraction being considerably lower than that of the Unsegregated fraction. The slopes of the GAC curves over the period of roughly linear GAC with time (days 10 to 90) provides a more accurate indication of the true differences in rate of GAC.

In APPENDIX H, Figure 77 on page 295, the leaching results of unsegregated ore is compared to the ore that was layered with Upper, Middle and Bottom ore to provide an exaggerated simulation of segregation in a heap. Again very little difference is noted between the two.

Table 13. Model parameters fitted to column leaching performance of segregation fractions.
Reproduced from Van Staden and Petersen (2018a)

Parameter	Value, by ore fraction				
	Upper	**Middle**	**Bottom**	**Unsegregated**	**Layered**
Copper Extraction					
Extractable fraction, $\alpha_x\alpha_w$	1.00	1.00	0.951	1.00	Simulated per layer
Transfer time, Θ days	20.3	29.3	32.8	26.7 ($\Theta_{ref.}$)	28.1
Relative Transfer time, Θ/Θ_{ref}	0.76	1.10	1.23	1.0	1.05
GAC					
k', h^{-1}	0.0525	0.118	0.116	0.106	Per layer
GAC slope days 10-90, kg/(t.d)	0.091	0.12	0.16	0.15	0.12
Moisture and solids content					
(ε_{imm}), kg/kg	0.17	0.14	0.10	0.13	0.14
Bulk density, kg/m^3, dry basis	1,420	1,400	1,280	1,390	1,367 (o-all)
(θ_{imm}), m^3/m^3	0.24	0.20	0.13	0.18	0.19 (o-all)

11.10 IMPLICATIONS FOR LABORATORY COLUMN LEACH TESTWORK

It is concluded that artificially segregating the ore as part of its preparation would not yield laboratory column leaching results that emulate large scale heap leaching performance any more realistically than if segregation and stratification are absent.

However, it is recommended that hydraulic conductivity measurements should be determined on the Upper, Middle and Bottom segregation fractions of ore samples,

after having leached them. This will provide a more conservative estimate of the hydraulic conductivity to be encountered in a commercial heap. At least during the campaign discussed in this text, the Bottom fraction exhibited the lowest hydraulic conductivity. The reason for this can currently only be speculated to be related to the fact that the Bottom fraction was the only fraction that settled under its own weight in the column since it did not adhere to the column walls. It might also be related to expansion of the Bottom ore particles into voids left by the removal of the fine fractions from it. Furthermore, more conservative hydraulic conductivities were measured in the leaching columns on the leach residues, than in the un-axial compression apparatus on residues excavated from the columns. This suggests that the excavation of the residues from the columns disrupts the densified structure of the residues, possibly partly cemented together by precipitates during leaching, and compression in the un-axial apparatus does not compensate for this disruption.

12 EFFECT OF SIMULATED STRATIFICATION

12.1 INTRODUCTION

Similar to section 11 on the effect of segregation, this section explores the extent to which the differences observed between laboratory column and commercial heap leaching performance can be attributed to stratification.

12.2 STRATIFICATION DEFINED

A detailed discussion and illustration of stratification is provided in Van Staden and Petersen (2019). According to the formal terminology, segregation refers only to the separation of coarser and fine particles vertically. In contrast, stratification is the formation of successive layers of finer and coarser particles, with the layers orientated at the angle of internal friction. This reflects the fact that the layering occurs as the particles come to rest on the advancing face of the heap being stacked, which slopes at the internal angle of friction of the ore.

The combination of simultaneous segregation and stratification in a heap is illustrated in Figure 49, with Φ being the angle of friction.

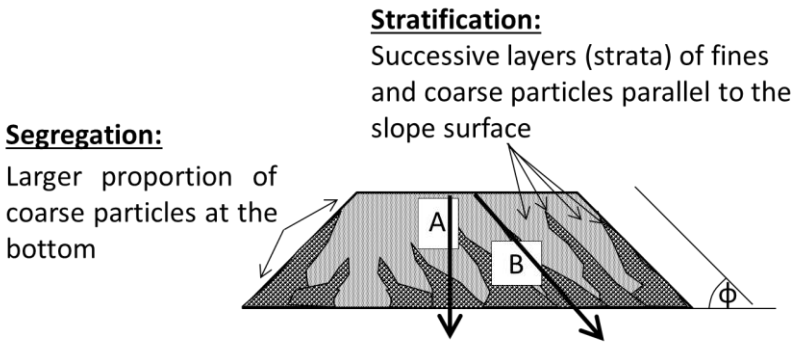

Figure 49. Combination of segregation and stratification in a heap of aggregate
Reproduced from Van Staden and Petersen (2019)

Formal studies on segregation and stratification have to date been limited to binary systems only, addressing mixtures of only two types of particles. The two types of particles would always differ in size, and may at the same time differ with regard to other properties such as density, smoothness or shape.

From the work of authors such as Benito et al. (2014) it is clear that segregation (dealt with in the previous section) always occurs whenever an aggregate is stacked on a pile. However, according to Benito et al. (2013), simultaneous stratification only occurs under certain conditions. Although not stated explicitly as such by any of these authors, in summary of their observations it seems to require the inclusion of particles that bear conflicting properties for continued movement. For example, it requires that the larger particles (with their higher momentum allowing them to roll further before coming to rest) should also be the more faceted (with the flat facets tending to halt their movement sooner). Or similarly, the larger particles should possess the rougher surfaces. Its existence is visually characterised by the bordering between successive layers, orientated at the angle of internal friction, of particles of different properties (which could be size, density, shape or any other property according to which stratification occurs).

12.3 APPARATUS

The methodology is detailed in Van Staden and Petersen (2019). The approach consisted in principle of simulating the stacking of ore on a heap, by stacking ore in two rectangular boxes (the “Stratified boxes”), illustrated in Figure 50 on page 203 below.

The boxes were built 900 mm long (from left to right), 600 mm high (i.e. top to bottom) and with the width of the cross section being 85 mm. The width of 85 mm was chosen to restrict the direction of flow development of the plume of moisture essentially to only 2 dimensions, i.e. downward and from left to right. Yet, the width of 85 mm was just sufficient to satisfy the requirement prescribed by Potter (1981) for avoiding ”undue wall-effects” (referring to the possibility of solution short-circuiting between the ore and the container wall, instead of passing via the ore). The height of 600 mm was chosen based on the simulation results of Dixon and Afewu (2011) which indicated that the shape of the plume of moisture traversing a column of ore is fully developed after

progressing about 500 mm down into the ore. Therefore, the nature of interactions between solid and solution would not be expected to have been different had deeper boxes been chosen. Deeper boxes would have prolonged the duration of the experiments required to reach the same extent of leaching, while it is believed it would not have affected the conclusions drawn from this testwork. Each box was fitted with six outlet points distributed along the bottom.

12.4 LOADING PROCEDURE

The procedure for filling the boxes is illustrated in Figure 51 and Figure 52 below on page 204. The first batch of ore was poured into the box from the one end until the ore reached the top of the box, with ore resting at the angle of internal friction. This could be assumed to be 39^{o} with respect to the horizontal, as discussed in section 11.4, while the boxes were maintained level. The feed chute was then moved by about 100 mm and another charge of ore was loaded, with that ore coming to rest as another layer over the angled side of the first charge of ore. A total of 7 such layers were stacked over one another in order to completely fill the box.

A control was created by loading a second, identical rectangular box (the “Unstratified box”), as homogenously as possible in horizontal layers.

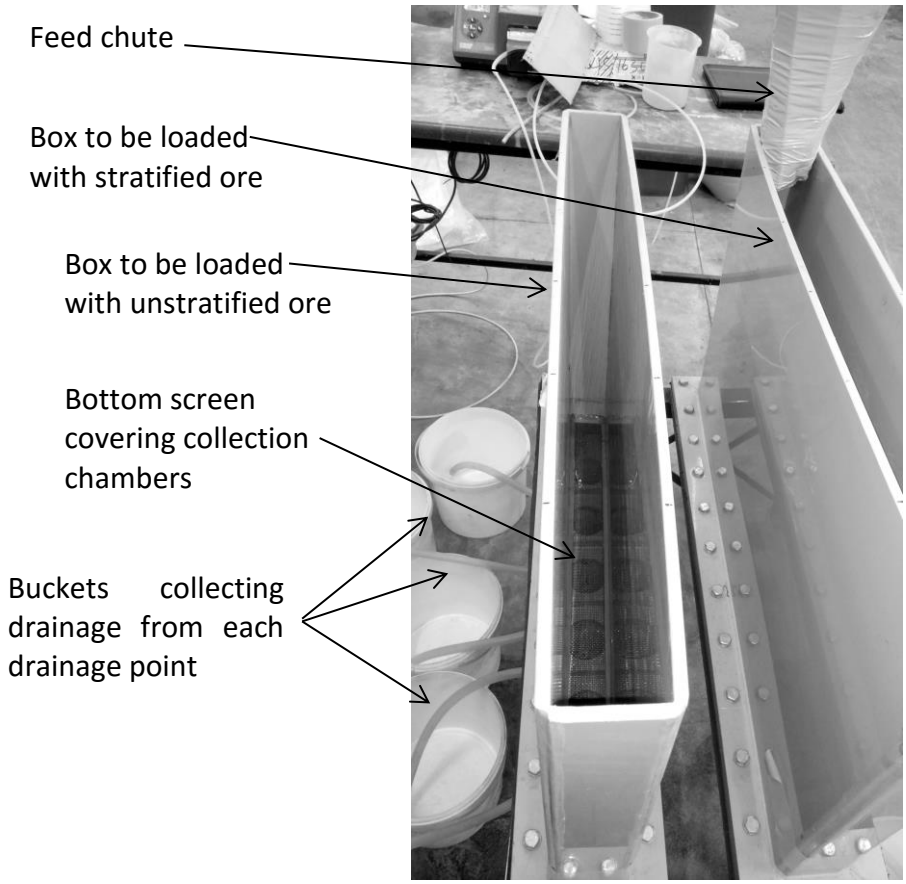

Figure 50. Image of stratification boxes

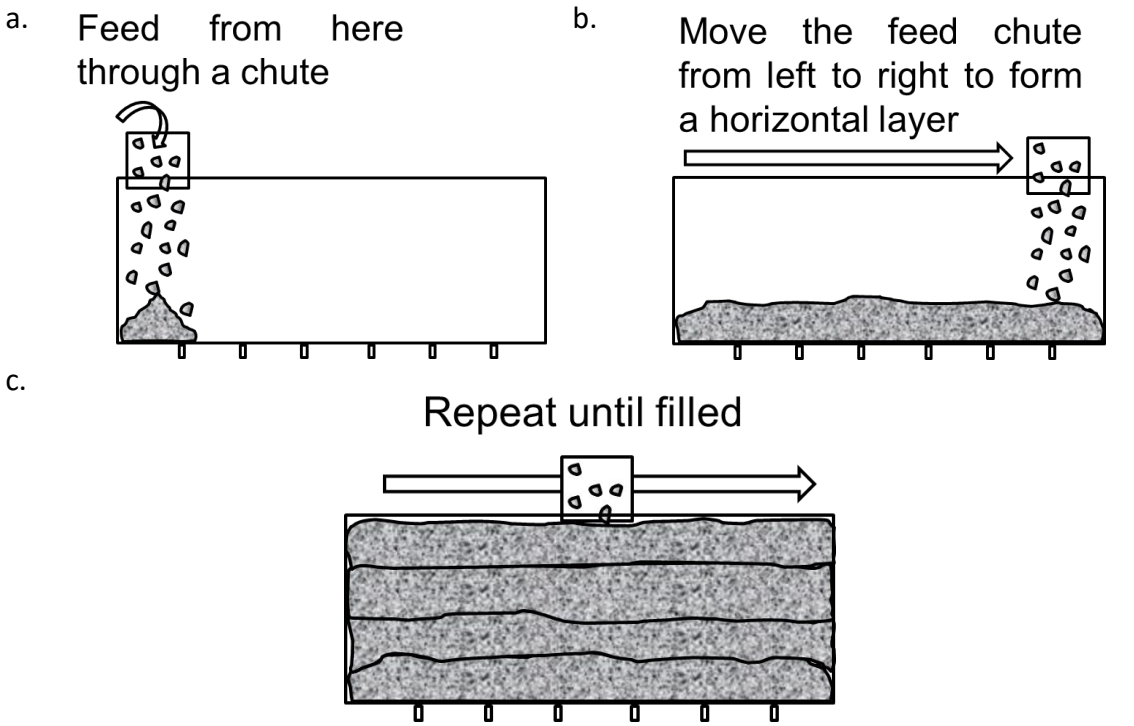

Figure 51. Progression of ore being loaded homogenously into the unstratified box.

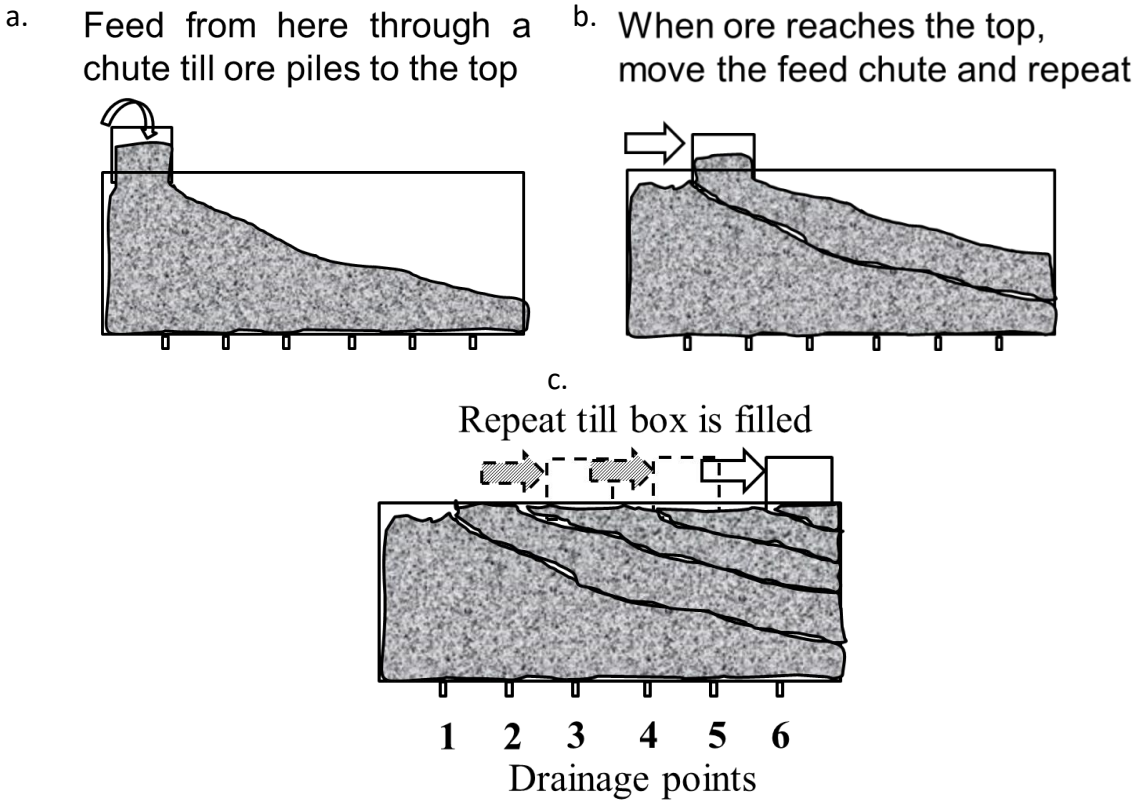

Figure 52. Progression of stacking of ore in stratified box

In the Stratified box, stratification would occur in combination with segregation. Therefore, any effect observed in the Stratified box should be ascribed to the combination of segregation and stratification. The contribution to the effect by stratification alone would be the extent to which the same effect exceeds that which has been observed during the segregation tests, described in the previous section. For example suppose that, during the segregation tests, it is found that segregation increases the Transfer Time by 10 percent, compared to that of unsegregated ore. And further suppose that the wide box test with stratification increases the Transfer Time by 15 percent, compared to the stratification time of the unstratified box. It would then be concluded that stratification alone increases the Transfer Time by 5 percent, in addition to the 10 percent increase caused by segregation.

12.5 WATER IRRIGATION PROCEDURE

The boxes were first irrigated with water only to observe the distribution patterns according to which the drainage solution exited each of the boxes. Irrigation was applied continuously, but drainage solutions were accumulated, weighed and assayed in batches collected over 24 h periods.

To determine the reproducibility of the test results, the entire procedure was conducted twice consecutively, each time on a fresh sample of the same oxide-copper ore type as that used for the Segregation testwork. Hence reference will be made to Oxide-1 and Oxide-2 to indicate respectively the first and second trials of the test.

Water-irrigation of the Oxide-1 boxes was initiated at 5 L/(h.m^2) in the middle of the upper surface, corresponding to a lateral position between drainage points 3 and 4. After 16 days of irrigation, the irrigation rate was changed to 15 L/(h.m^2), and after another 13 days (i.e. 29 days since the start of irrigation) back to 5 L/(h.m^2). On day 38, the irrigation point was positioned laterally between drainage points 2 and 3 and back to between drainage points 3 and 4 on day 63, where it was left until the end of 84 days of water irrigation. The water was then acidified to initiate the leaching test described in the next sub-section below on the Oxide-1 ore.

Water-irrigation of the Oxide-2 boxes was performed over 27 days at 5 L/(h.m^2) applied only in the centre of the box, namely at the lateral position between drainage points 3 and 4. The water was then once again acidified to initiate the leaching test described in the next sub-section below on the Oxide-2 ore.

12.6 LEACHING TEST PROCEDURE

Irrigation with acid solution was applied in the centre of the cross section of the box, i.e. corresponding to a lateral position between outlets 3 and 4. The irrigation rates used during the various experiments appear in Table 14 below, on page 216.

The resulting leach curves representing the total copper extraction from all drainage points summed together were fitted to the PhreeqC version of the dual porosity heap leaching model to observe the differences between the model parameters that fit the leaching performance of the stratified and unstratified boxes of ore respectively.

The most important difference between the two rounds of leaching testwork performed on the Oxide-1 and Oxide-2 samples was that the (stratified and unstratified) residues of the Oxide-1 test were assayed in their entirety, to obtain a single average residue assay for each box. On the other hand, the residues resulting from the stratified and unstratified Oxide-2 set of tests were excavated from the boxes in three vertical layers (top, middle and bottom, each layer being slightly less than 200 mm deep since the ore that was initially loaded 600 mm deep sagged somewhat during irrigation). Each layer was divided horizontally into three sections (drainage-1-side, middle and drainage-6 side, each section being 300 mm wide). This yielded nine residue fractions that were assayed individually to provide a residual profile of each box.

The manner in which the three sections of ore relate to the positions of the drainage points and their catchments is illustrated in Figure 53 below. The drainage points were spaced 129 mm from each end and from one another. The compartment dividers were spaced 129 mm from one another, but those on the two ends were spaced 192 mm from the ends. The solution draining from any drainage point will have been collected between the two compartment dividers, (or a compartment divider and an end wall in the case of drainage points 1 and 6), on either side of it.

The three sections in which the Oxide-2 ore was excavated extended horizontally over 300 mm each. From Figure 53, the left-most 300 mm wide section can be seen to almost coincide with the catchment area between the wall on the drainage-1 side and the wall formed by the two left-most compartment dividers, the middle 300 mm wide section corresponds essentially with the catchment areas of drainage points 3 and 4, and the right-hand 300 mm wide section corresponds essentially with the catchments of drainage points 5 and 6. To be exact, the catchment areas of drainage points 1 and 2 correspond to the entire left-most ore section plus the proportion (192+129-300)/300=7% of the middle 300 mm wide ore section. Similarly, the cathment areas of drainage points 5 and 6 correspond to the entire right-most ore section plus 7% of the middle 300 mm wide ore section. The catchment areas of drainage points 3 and 4 correspond to (100-7-7)=86% of the width of the middle ore fraction.

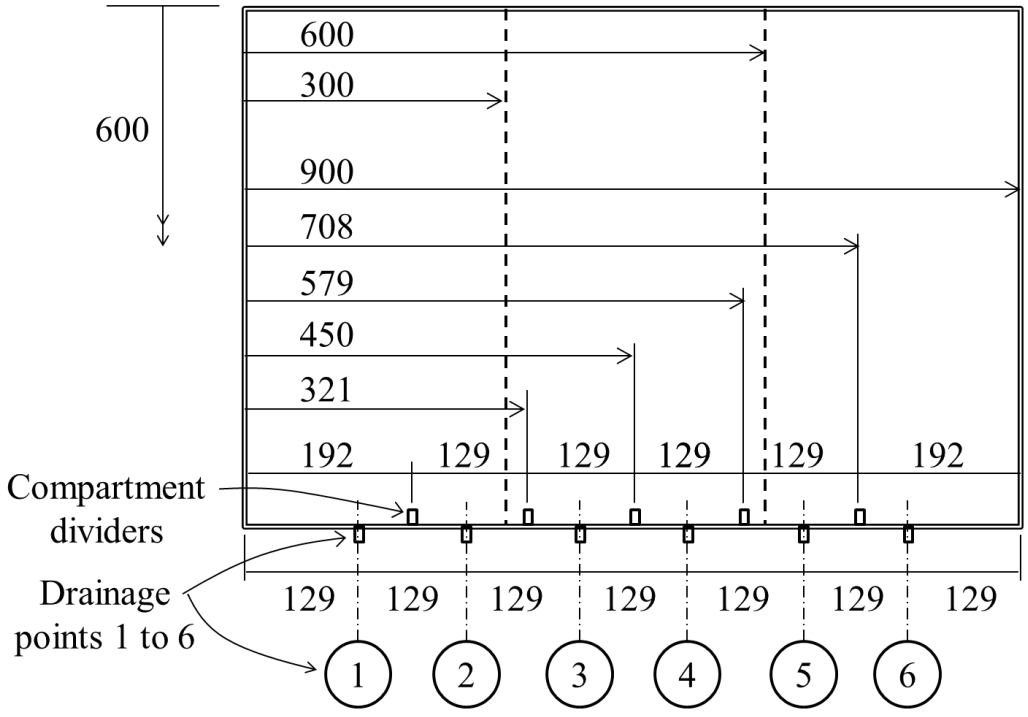

Figure 53. Stratification box dimensions and catchments.
(All dimensions in mm).

Apart from chemical analyses, selected samples were also subjected to X-ray diffraction and scanning electron microscopy for general observations and specifically to search for reprecipitated forms of copper.

12.7 STAINING TEST PROCEDURE

To provide a visual impression of the solution flow paths through the ore masses, a residue sample of a heap of copper-sulphide ore (denoted “sulphide-res”) was used to construct stratified and unstratified boxes for irrigation with colour-staining solution. These boxes were first irrigated with water only for 35 days, followed by irrigation with water to which colour-stain (120 mL of blue Penguin oil-free stamp pad ink in 100 L water) had been added for another 45 days. Upon completion, the boxes were excavated in layers and photographs were taken of the stain marks left on the ore, with the intensity of staining assumed to be proportional to the average flux density that had occurred at each point over the time course of the entire experiment. (Note that it could not be expected to correlate the observed staining with the flux occurring at any particular point in time, since the stain was only observed upon completion of the test).

12.8 STOICHIOMETRY AND KINETICS

The ore sample used for the stratified/unstratified water irrigation and leaching testwork was the same oxide-copper ore as that used for the segregation testwork, discussed in the previous section. Hence the comments on stoichiometry and kinetics of the segregation testwork described in section 11 will also apply here.

12.9 CONFIRMING THAT STRATIFICATION OCCURRED IN THE BOXES

Kinard and Schweizer (1987) provided photographic evidence of alternating strata of coarser and finer particles in large heaps obtained from a large number of heaps. Guzman et al. (2006) also observed that areas of similar residual copper contents in intensively instrumented and sampled heaps exhibited strata orientated at the angle of internal friction. They interpreted this as the result of more and less conductive flow channels that alternate one another in accordance with the hydraulic conductivities of alternating segregation and stratification layers. That evidence suggests that stratification occurs quite readily, provided commercial stacking practise is adequately emulated.

Benito et al. (2013), remarked that stratification in binary particle mixtures occurs when the particles in the aggregate meet at least one of the following conditions: (a) they differ in both shape and size, or (b) the larger particles are more faceted than the smaller

particles, or (c) the rougher particles are at least 1.5 times larger than the smoother particles. At least condition (a) has been met by the conditions employed here. The fact that many of the finer particles agglomerate into roughly spherical shapes, as opposed to the angular shapes of the coarser particles, should also satisfy condition (b). Therefore the likelihood that stratification occurred during the loading of the wide boxes was very high.

The wide boxes used for stratification were not transparent, so that stratification could not be visually observed in them. And making excavations for sampling from the boxes to verify the existence of stratification would have disturbed the ore samples. As an indirect measure for obtaining visual evidence that stratification (would have) occurred in the wide boxes, the segregation box shown in Figure 45 on page 189 was used instead. One agglomerated ore sample was dedicated to being loaded into the segregation box purely for the purpose of obtaining this evidence. In the segregation box, ore is also allowed to fill by coming to rest at the angle of internal friction. One difference is that the bottom of the segregation is sloped at the angle of internal friction, which should have no bearing on the result. Furthermore the segregation box, when loaded, will represent only a single layer of ore, while the wide “stratification” box was loaded with seven layers of ore stacking over one another.

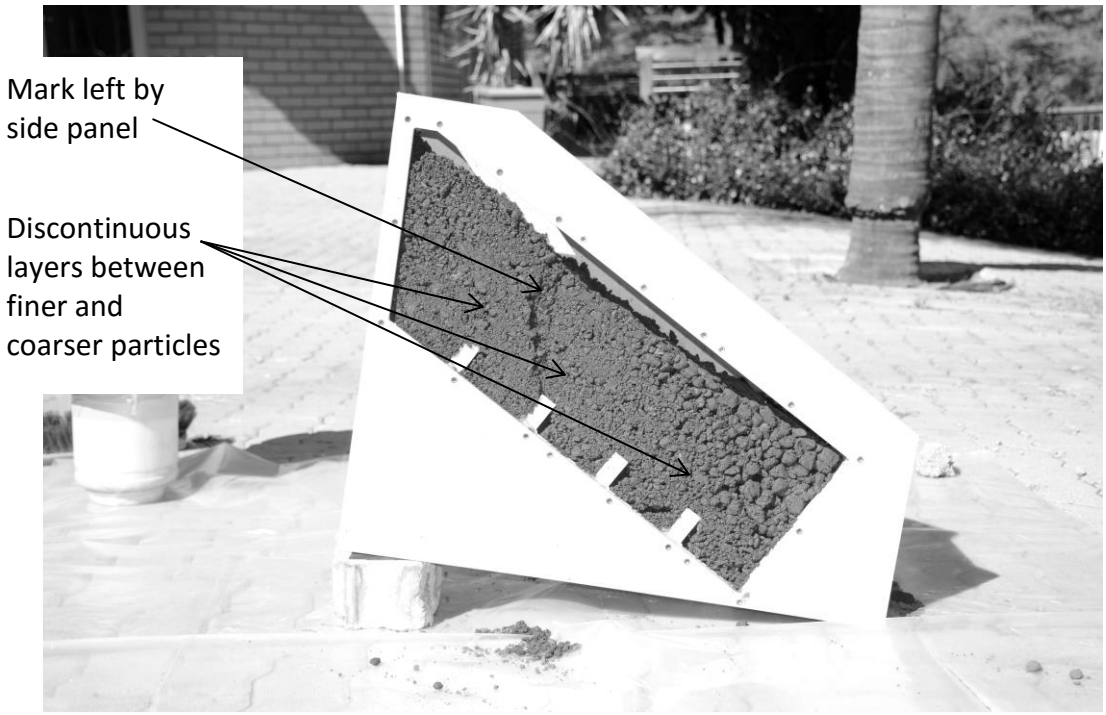

Figure 54. Evidence of stratification as seen in exposed segregation box

After filling the segregation box up to the top of the box, the ore was pressed down using a flat piece of wood, just sufficiently that the side panels could be removed for observation from the side without the ore falling out. A photograph of the exposed ore appears in Figure 54. The seam between two of the side panels left a mark on the ore which is pointed out and can be ignored. However at least two layers, orientated at the angle of repose (i.e. parallel to the sloping bottom), of particles coarser than those above and below them are observed and are pointed out in Figure 54. A third layer layer is formed around the predominantly coarse particles at the bottom end of the box that protrudes upward.

This provided visual evidence, albeit somewhat indirectly, that stratification by particle size would have been present in the stratification boxes.

12.10 RESULTS

12.10.1 Drainage flow distributions

Intuitively it was expected to observe the maximum rate of drainage passing from the unstratified box via the drainage point(s) connected by the shortest straight line(s) from the irrigation point. The flows were expected to become progressively smaller via points further away from the irrigation point. At times a pattern approximating this type of distribution was indeed observed, for example around day 28 of irrigation of the Oxide-1 sample with water only, as shown in Figure 55(a) below. (Note the indication of the positions of the irrigation points at the top of the boxes, namely laterally between drainage points 3 and 4 in Figure 55(a) and between drainage points 2 and 3 in Figure 55(b)).

a. b.

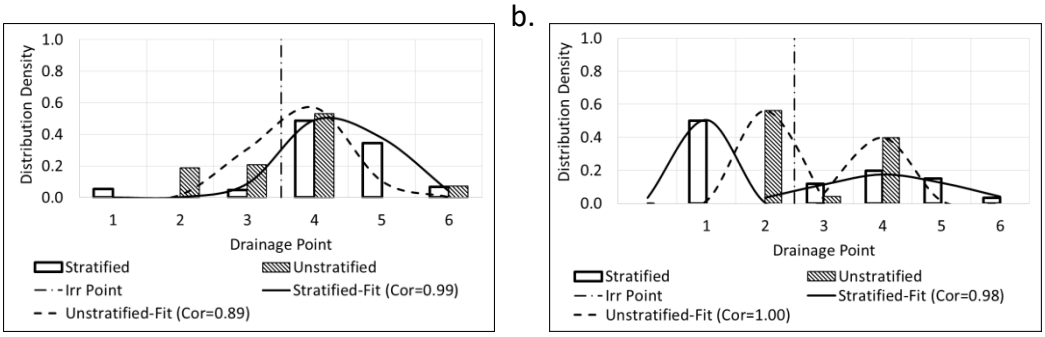

Figure 55. Drainage flow distributions observed using Oxide-1 sample.
(a) day 28 and (b) day 63 of irrigation with water only.
Reproduced from Van Staden and Petersen (2019)

It was further expected that, from the stratified box, the flow distribution should be shifted in the direction in which ore was sloping from top to bottom, that is (referring to Figure 52(c) on page 204) towards the direction of outlet point number 6. This would follow solution on its downward path, encountering strata that are more conducive to flow than the average mass of the ore. This would direct the flow in the direction of the angle of friction of the ore, away from an average vertically downward path. By fitting normal statistical distribution curves to the drainage flow distributions of day 28, this trend can also be observed, with the mean drainage location of the stratified ore being located at point 4.4 (i.e. about half-way between drainage points 4 and 5) and that of the unstratified ore at point 3.8 (i.e. close to drainage point 4 but on the drainage-3 side of it).

However, these distributions did not hold for the full duration of the test. By day 63 of irrigation of the Oxide-1 sample, both the stratified and unstratified boxes had developed bi-modal drainage distributions, with flow peaks observed on either side of the irrigation point for both the stratified and unstratified boxes. This is shown in Figure 55(b) above. More similar examples were observed on both the Oxide-1 and Oxide-2 samples, in general the drainage distributions of the stratified boxes were not shifted in any direction relative to that of the unstratified boxes.

One trend that was observed consistently was that solutions from the stratified boxes were, with very few exceptions, draining from more drainage points than the unstratified boxes. This was observed during both the Oxide-1 and Oxide-2 tests as well as the staining test on the sulphide leach residue. Very often, the Stratified boxes were draining from all 6 drainage points and very seldom from fewer than 5, while the unstratified boxes were more typically draining from 4 to 5 drainage points. The points that were not draining were found, with more or less equal probability, on the drainage-point-1 or drainage-point-6 extremes of the boxes. This rules out systematic bias in either construction, loading or levelling of the boxes as the cause for the differences in drainage distribution.

12.10.2 Ore staining

Analysis of the staining test images that appear in Figure 56 below showed that the solution seemed to find randomly distributed preferred solution channels in both the stratified and unstratified ores. The width of the stained areas could be seen to increase with depth down to 100 to 200mm below the surface, where-after it seemed to remain at a fixed width of about 250mm, compared to the 600mm distance between the catchments of drainage points 1 and 6. It is therefore clear that staining had not become visible in all areas reached by the irrigation solution by the time the ore was excavated. The only conclusion to be drawn from it is that no visible difference could be found between the staining patterns of the Stratified and Unstratified ores.

a.

b.

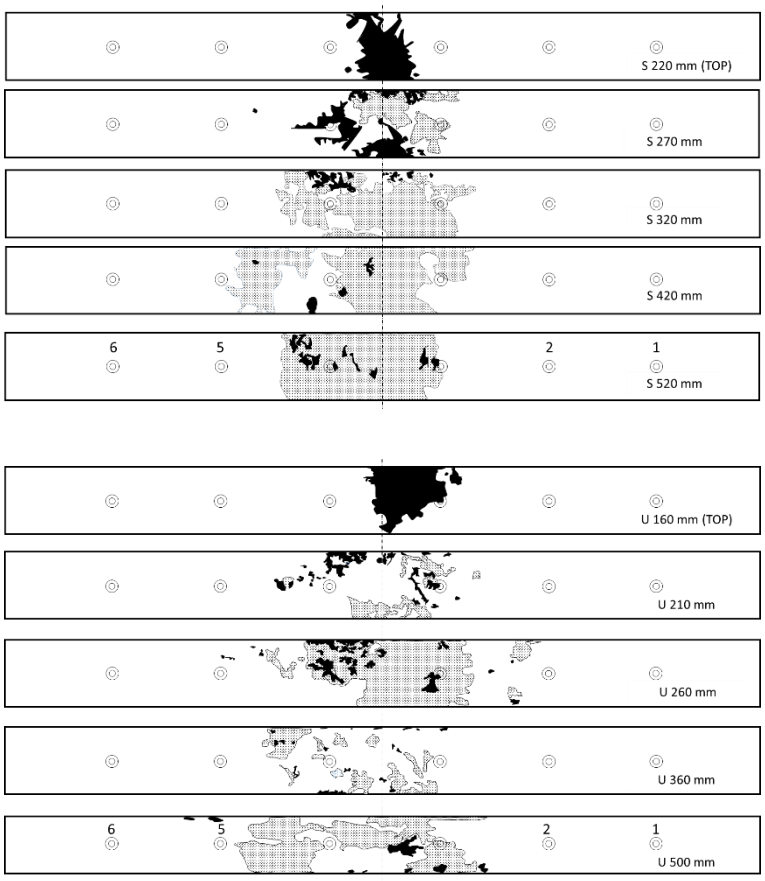

Figure 56. Staining images obtained from wide boxes
(a) Stratified ore, (b) unstratified ore.

12.10.3 Hydrology and extraction performance

The experimental conditions employed, and the model parameters fitted to the leaching performance, appear in Table 14. The extrapolation of the batch leach curves to estimate the extractable fractions are shown in APPENDIX J, Figure 78 and Figure 81 on page 298. The model fits achieved in order to optimise the model parameters are shown in APPENDIX J, Figure 79, Figure 80, Figure 82 and Figure 83 on page 299.

Note that during the water irrigation and staining tests, no leaching was performed, hence no leaching- or consumption-related parameters were recorded for those tests.

On the Oxide-1 sample, the stratified ore exhibited a significantly (25 percent) higher extractable fraction than the unstratified ore, yet on the Oxide-2 sample the difference was much smaller (12 percent higher). On the Oxide-1 sample, the stratified sample

exhibited the higher Transfer Time, yet on the Oxide-2 sample the unstratified sample exhibited the higher Transfer Time. Hence there exists no reproducible difference in Transfer Time between the straficied and unstratified ores.

The values for *k'* would have been expected to be invariable, being related to ore mineralogy, which was common to all Oxide-1 and Oxide-2 tests. Hence the variation observed represents statistical uncertainty with regard to the value of *k'*.

The distribution of the total drainage volumes and total grams of copper collected over the course of all four wide-box leaching tests are shown in Figure 57 below. In the case of the stratified ore, the drainage points from where the largest drainage volume and copper mass were obtained are all shifted towards drainage point 6, which is the direction in which the ore strata sloped in the boxes. Such a general trend exists also for the Unstratified boxes, but the copper deportment from the Oxide-1 box (Figure 57(b)) is an exception. However, the effect is more pronounced in the case of the Stratified boxes, where the highest peaks prevail at drainage point 5. For the Unstratified boxes, the highest peak is observed at drainage point 4 in 3 of the 4 cases and at drainage point 2 in the case of Figure 57(b).

This suggests that the strata in the stratified boxes did cause some shift of the solution flow in the direction in which the strata sloped. Further discussion on the shift in copper deportment follows later in this section with respect to the the data presented in Figure 58 below on page 219.

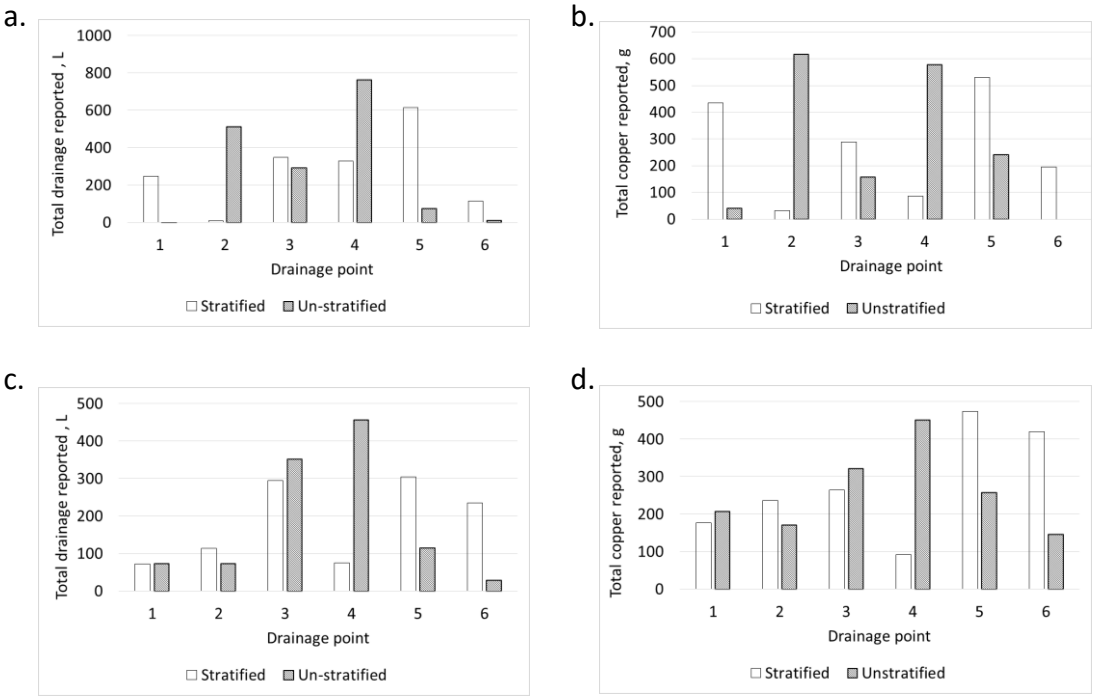

Figure 57. Cumulative flow and copper mass per drainage point.
(a) Drainage volume, Oxide-1, (b) mass of copper, Oxide-1, (c) Drainage volume, Oxide-2, (d) mass of copper, Oxide-2

The residual copper values and extents of extraction appear in Table 15 below. For the Oxide 1 samples a single extraction result appears per test since only the entire residue was assayed for residual copper value. For the oxide-2 samples, the same results are shown for each of the nine sections of ore excavated from the boxes.

In Table 14, values for the GAC rate constant, *k'*, are shown both as determined from rolling bottle experiments, and as fitted to the model. As can be seen, there is very poor correlation between the two, with rolling bottle experiments providing a very poor prediction of the value of *k'* that would prevail during percolation leaching.

Table 14. Parameters observed during repeated stratification box tests
Reproduced from Van Staden and Petersen (2019)

Parameter	Oxide-1 Stratified	Oxide-1 Un-stratified	Oxide-2 Stratified	Oxide-2 Un-stratified	Sulphide-res Stratified (Staining)	Sulphide-res Un-stratified (Staining)
Experimentally determined or assumed parameters						
Total area, m^2	0.072	0.072	0.072	0.072	0.072	0.072
Ore mass, kg dry basis	56.2	58.2	57.3	60.0	52.2	61.5
Effective feed acid concentration, g/L	10	10	10	10	0	0
Recalculated head value, % Cu	5.2	4.9	5.6	5.3	N.A.	N.A.
Loaded bulk density, kg/m^3	1,348	1,327	1,341	1,464	1,151	1,337
Over-all irrigation rate, L/(h.m2)	4.79	4.71	4.20	4.24	4.58	4.52
Irrigation acid concentration, g/L	10	10	10	10	0	0
Moisture content, kg moisture/kg dry solids	0.162	0.20	0.14	0.22	N.D.	N.D.
k, from rolling bottles, h^{-1}	0.032	0.032	0.032	0.032	N.D.	N.D.
Optimised fitting parameters						
Extractable fraction, $K_x.K_w$	0.69	0.55	0.58	0.52	N.D.	N.D.
Transfer time, Θ, days	120	56.5	115	121	N.D.	N.D.
k' fitted, h^{-1}	0.010	0.0068	0.0048	0.0118	N.D.	N.D.

N.D.: Not determined

Table 15. Residue analyses and extents of extraction
Reproduced from Van Staden and Petersen (2019)

Sample	Drainage-1 side	Centre	Drainage-6 side
OXIDE-1 SAMPLES			
Stratified		2.4% (53%) [W=0.140; ε=0.163; θ=0.219]	
Unstratified		2.1% (56%) [W=0.170; ε=0.205; θ=0.272]	
OXIDE-2 SAMPLES			
Stratified Upper layer	6.1%(-29%) [W=0.116; ε=0.131; θ=0.176]	0.70%(85%) [W=0.141; ε=0.164; θ=0.220]	5.0%(-7.0%) [W=0.104; ε=0.116; θ=0.156]
Stratified Middle layer	5.1%(-8.0%) [W=0.131; ε=0.151; θ=0.202]	0.30%(94%) [W=0.145; ε=0.170; θ=0.227]	3.7%(22%) [W=0.108; ε=0.121; θ=0.162]
Stratified Bottom layer	3.9%(17%) [W=0.129; ε=0.148; θ=0.199]	0.10%(98%) [W=0.134; ε=0.155; θ=0.208]	1.7%(63%) [W=0.110; ε=0.124; θ=0.166]
Stratified Over-all		2.89%(38%) [W=0.120; ε=0.136; θ=0.183]	
Unstratified Upper layer	5.3%(-14%) [W=0.103; ε=0.115; θ=0.168]	0.80%(84%) [W=0.129; ε=0.148; θ=0.217]	4.5%(3.0%) [W=0.101; ε=0.112; θ=0.165]
Unstratified Middle layer	4.3%(8.0%) [W=0.118; ε=0.134; θ=0.196]	0.20%(95%) [W=0.141; ε=0.164; θ=0.240]	4.3%(7.0%) [W=0.119; ε=0.135; θ=0.198]
Unstratified Bottom layer	3.4%(27%) [W=0.127; ε=0.146; θ=0.213]	0.10%(98%) [W=0.155; ε=0.183; θ=0.269]	3.7%(21%) [W=0.130; ε=0.149; θ=0.219]
Unstratified Overall		2.81%(40%) [W=0.130; ε=0.149; θ=0.219]	

Note: residue values are shown, followed by extraction as a percentage of recalculated head in round brackets (), followed by final moisture content in square brackets [] in three sets of units, W_{imm} [mass-fraction]; ε_{imm} [g moist/g dry solids]; θ_{imm} [vol-fraction].

On the Oxide-1 sample, the unstratified ore yielded a slightly superior extent of extraction (56% compared to 53% from the Stratified sample). On the Oxide-2 sample, the Stratified sample yielded slightly superior performance (43% versus 40% from the Unstratified sample). Hence it is concluded that stratification has no reproducibly significant effect on the extent of extraction.

It can be seen that virtually complete extraction had been achieved in the Centre of the Oxide-2 box, from the Upper to the Bottom layer. However there was also consistently an increase in extent of extraction from the top to the bottom. This is counter-intuitive since the highest acid concentration prevails in the immediate vicinity of the irrigation point, on top of the Upper layer. This suggests that the contact between leach solution and ore was improving from top to bottom, which in turn can be interpreted as a splitting of flow streams leaving shorter diffusion paths as solution travels from the Upper to the Lower layer.

On the far extremities (Drainage-1 side and Drainage-6 side) in the upper layer, the residue values were reported higher than the recalculated head values, indicating a negative extent of extraction. This suggests that solution laden with dissolved copper must have moved sideways from the irrigation point (at the centre) and evaporated out the top to leave re-precipitated copper in the ore.

Three sets of residue analyses were obtained to confirm the result, two sets were performed in the Mintek laboratories and a third at another independent laboratory. Of the 54 analyses performed, only 6 differed from the average for a given position by more than 10 percent. However, the analyses for the positions at the extremities where copper precipitation apparently occurred were all within 10 percent of the average, lending credibility to those analyses. Relatively large deviations (40 percent) from the average were reported only for the sample at the centre in the bottom layer of the unstratified box, where the copper content was approaching zero. This is reasonable and does not materially affect the recalculated head value or the other conclusions drawn from this work.

The mineralogical analysis did indicate the presence of copper-bearing iron hydroxide in the residue sample obtained from the upper layer (Drainage-1 side) of the stratified sample, where -22 percent copper “extraction” had been observed. This suggests that copper was co-precipitated with iron in this location. This lends circumstancial support to the evidence by the chemical analyses for some copper precipitation to have occurred in that location. However, the mineralogical data was not sufficient to quantitatively confirm the amount of copper precipitation that had taken place there.

The masses of copper extracted from each 300 mm wide horizontal section excavated from the Oxide-2 boxes were compared to the amounts of copper reporting to the respective drainage points representing the catchment areas below each section of ore. In doing so, the amount of copper leached from the ore was corrected for the extent to which each ore section corresponded with the catchments of the various drainage points, as according to the discussion around Figure 53 on page 207. Namely, assuming solution was draining perfectly vertically from top to bottom, 100% of the copper leached from the left-most section plus 7% of the copper from the middle section could be expected to report to drainage points 1 and 2, 100% of the copper from the right-most section plus 7% of the copper from the middle section should report to drainage points 5 and 6, while 86% of the copper from the middle section should report to drainage points 3 and 4. The comparison is shown in Figure 58 below.

In the case of the stratified ore, there was no correlation between the dissolved copper collected from the drainage points, and the amount of copper that was leached from the corresponding catchments. The largest amount of copper was leached from the central catchment area above drainage points 3 and 4 in both cases. But in the case of the stratified ore, the largest amount of copper drained through drainage points 5 and 6, i.e. once again shifted in the direction in which the ore layers sloped in the stratified box. In contrast, in the case of the unstratified ore, there was a correlation of 1.00 between the amount of copper reporting via the drainage points, and the amount of copper leached from the corresponding catchments.

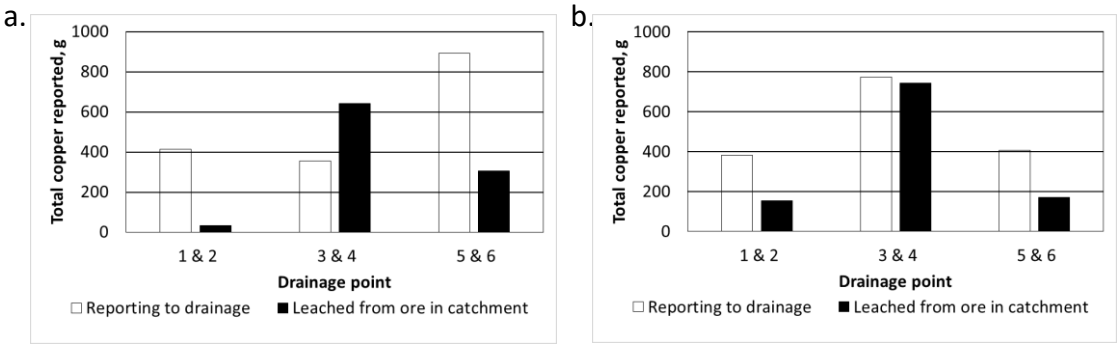

Figure 58. Copper collected from drainage points versus catchments.
(a) Oxide-2 stratified (no correlation) and (b) Oxide-2 unstratified (Corr.=1.00)

12.11 IMPLICATIONS FOR LABORATORY COLUMN LEACH TESTWORK

It has been found that the stratification of ore assists in spreading the leach solution over a slightly wider area throughout the ore, than is the case with unstratified ore. In the stratified ore, both the volumetric solution flow and the flow of dissolved copper were shifted in the direction in which the ore sloped in the boxes. However, no significant or reproducible difference could be observed in either the leaching kinetics (as quantified by the Transfer Time) or the final extent of extraction of stratified and unstratified ores.

It is concluded that artificially stratifying the ore as part of its preparation would not yield laboratory column leaching results that emulate large scale heap leaching performance any more realistically than if segregation and stratification are absent.

It is further apparent that a laboratory method for estimating the GAC rate constant, *k'*, would be essential for predictive modelling of heap leaching. However a simple agitated laboratory experiment does not provide such an estimate.

13 COMPARISON BETWEEN RESULTS FROM SEGREGATION AND RESULTS FROM STRATIFICATION EXPERIMENTS

13.1 INTRODUCTION

The column leaching of the segregated-versus-unsegregated ore described in van Staden et al. (2017a) was performed in 153mm diameter columns, while that of the stratified-versus-unstratified ore discussed in van Staden et al. (2017c) was performed in 80x900 mm^2 boxes. With a single drip irrigation point being used in the centre of the box, it represents a dripper spacing of 900 mm. Therefore, a comparison of the results of the segration study with that of the stratification study can also provide insight into the effect of dripper spacing.

13.2 DATA ANALYSIS

In Figure 59 below on page 224, the leaching performance of the Unsegregated ore and the Segregated ore fractions stacked in narrow columns, (discussed in section 11), is compared to the data obtained on the wide Stratified and Unstratified boxes on the Oxide-1 sample discussed in section 12.

The Oxide-1 and Oxide-2 samples yielded sufficiently similar performance results to lead to the same conclusions from this discussion. Graphical representations of the results obtained during the stratification study on both Oxide-1 and Oxide-2 samples can be seen in APPENDIX J.

The operating conditions used in the columns (H=0.77m high, irrigation acid concentration of initially C_{acid} = 3 and later 6 g/L and irrigation rate of around q=8.5 L/(h/m^2), differed somewhat from those used in the wide boxes (0.6m high, irrigation acid concentration of 10 g/L and irrigation rate of around 5 L/(h/m^2). Therefore presenting the data against time as independent variable as in Figure 59(a) is not very useful, a more meaningful comparison is obtained from Figure 59(b) where extraction is presented as a function of "kg/t acid irrigated", the latter being calculated from:

$$\text{Acid irrigated } \left[\frac{kg}{t}\right] = \frac{1}{\rho\, H} \int_0^t q\, C_{acid}\, dt \qquad [103]$$

Figure 59 illustrates the extraction kinetics deteriorating with increasing effective dripper spacing.

The difference in leaching performance shown in Figure 59 between Unsegregated and segregated (Layered) ore is relatively small, and so is the difference in performance between the unstratified and stratified ore samples. The much bigger difference exists between the performance obtained in the narrow-diameter columns (on the segregated and unsegregated samples) versus that obtained in the wide boxes (on the stratified and unstratified samples).

Referring to Figure 59(b), the first 35 kg/t acid irrigated was utilised equally well in both the columns and the Stratification boxes. From that point onwards, better copper extraction was achieved from the columns than from the Stratification boxes for a given amount of acid irrigated. The extraction curves of the boxes tend towards about 60 percent extraction after irrigation of 150 kg/t of acid. That is 2.6 times more acid irrigated than the 58 kg/t acid irrigated to achieve the same extent of extraction in the columns. If the Stratification boxes and columns were of equal height, irrigation rate and irrigation acid strength, that would require the same multiple of irrigation time longer in the boxes than in the columns. This seems of the order of the leaching time difference suggested by the design rules of thumb cited in section 1.3, although the multiple depends on the extent of extraction chosen for the comparison.

The ultimate extent of extraction, indicated by the parameter $\kappa_x.\kappa_w$, was 100% for the Unsegregated column and varied from 50 to 70 percent for the Stratification boxes. This is a larger difference than the 10 to 20 percent difference suggested by the rules of thumb. However the Stratification boxes used here represent a relatively wide dripper spacing and the $\kappa x.\kappa w$ values calculated for the Stratification boxes are reminiscent of the value of 0.71 determined for the Kipoi heap 3-1 reported by van Staden et al. (2017a) for the period when that heap operated temporarily with a 1 m dripper spacing, compared to values around unity obtained on the same ore in 200mm laboratory columns.

The relatively early breakthrough of acid to the drainage solutions from the boxes, relative to the much delayed breakthroughs observed from the columns, is a characteristic of the long Transfer Time encountered in the boxes compared to that of the columns. (Apart from the differences with regards to irrigation rate, column/box height and irrigation acid strength). With a longer Transfer Time, the flow channel(s) are in direct contact with a smaller proportion of the total ore mass being irrigated, the acid demand of which is satisfied very quickly. Breakthrough then occurs since the diffusion of acid from the flow channel(s) to the relatively larger region of stagnant solution occurs more slowly than acid is being irrigated. In the narrow-diameter columns, a closer approach to plug flow is attained which leads to better utilisation of the acid being irrigated, with a longer delay before acid breaks through to drainage, and a longer leach time before the rate of copper extraction changes from linear to logarithmic.

13.3 IMPLICATIONS FOR HEAP LEACHING DESIGN

In summary, of the parameters that were varied during the segregation and stratification studies, the effect of dripper spacing is much more significant than that of either segregation or stratification. And the magnitudes of the effect on final extent of extraction and the effect on extraction kinetics seem similar to the reported differences between narrow-diameter laboratory column leaching and commercial scale heap leaching.

It should therefore be further investigated whether a rectangular box, with the cross section having only one long side (of length equal to the intended dripper spacing) and one short side, (but of course of the intended stacking height), might yield similar results to a crib with the two sides of the cross section equal. If so it would save on sample requirement for achieving a given scale-up effect.

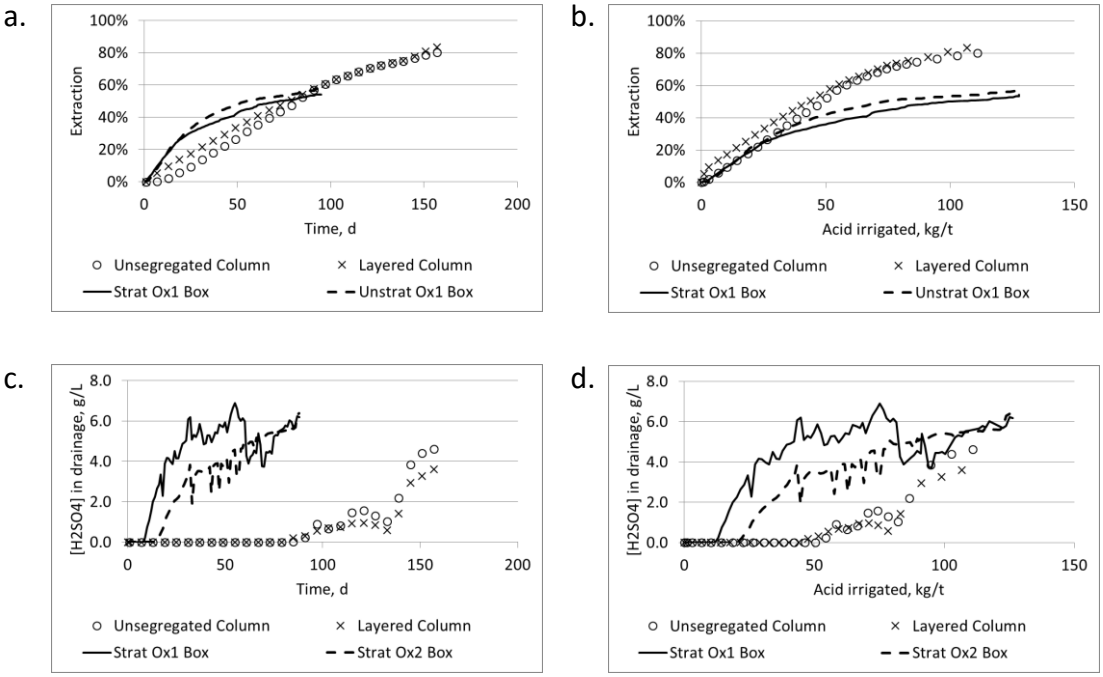

Figure 59. Leaching performance in column versus boxes.
(a) Extraction vs. time (b) Extraction vs. acid irrigated,(c) Drainage acidity vs. time, (d) Drainage acidity vs. acid irrigated.
(For the box leaching performance, the time scale indicates time since acid addition was started on day 84 of irrigation).

The results presented here represent another case study where the dripper spacing was scaled up. The effects on leaching performance are quantified in terms of the parameters appearing in Table 13 on page 198 and Table 14 on page 216. The parameters of highest importance are the extractable fraction ($\kappa_x.\kappa_w$) which approached unity in the narrow columns and varied around 0.5-0.7 in the wide boxes, and the Transfer Time Θ which was around 30 days in the narrow columns and 56-121 days in the wide boxes. This very large increase in Transfer Time is highly significant, considering the criterion established in section 3.15, namely that an increase in Transfer Time by a factor of 2 would be statistically significant.

14 MODEL PARAMETER TRENDS WITH SCALE-UP

14.1 REVIEW

All modelling discussed in this document so far consisted of retrospective model-fitting to observed heap/column leaching performance. However, the ideal being strived for is being able to perform predictive modelling of anticipated heap leaching performance, for the purpose of preparing heap leaching design specifications. That in turn, would require accurate predictions of the model input parameters to use for such predictive modelling, at least of the parameters that heap leaching performance is most sensitive to.

It has been hypothesised that heap leaching kinetics would be rendered slower than that of column leaching by three mechanisms, namely

a. Densification, leading to a reduction in the number of flow channels, and therefore in an increase in the distance between flow channels, and hence in an increase in the distance over which solution and reagents need to diffuse to reach mineral surfaces. This slows down the heap leaching kinetics.
b. Dripper spacing, in the case that dripper spacing were to be made wider than the natural spacing of flow channels occurring in a heap, which also slows down leaching kinetics. In extreme cases, this may leave parts of the heap effectively out of contact with leach solution, thereby also reducing the achievable ultimate extent of extraction.
c. Segregation and stratification, by increasing the distance between flow channels as illustrated in the Hypothesis in section 4.2. However these two mechanisms have been discounted above as contributors to heap leaching kinetics and therefore need not be considered further.

In section 5.2.2, the Transfer Time Θ, was defined as:

$$\Theta = \frac{R^2}{D_e} = \frac{R^2 \tau_\delta^2}{D \theta_{imm}} \text{ with units of time} \qquad [67]$$

where R is the maximum distance over which diffusion needs to occur, D_e is the effective diffusivity defined by equation [42] in section 3.11.5, τ_δ^2 is the constrictivity-tortuosity'

defined in section 3.11.5, D is the free diffusivity and θ_{imm} is the volumetric content of immobile solution.

The Transfer Time characterises the rate of leaching in a dual-porosity system such as heap or column leaching, which occurs by diffusion with chemical reaction as reagents are transported via the immobile solution. The governing equation first shown in section 5.2.2 is:

$$\frac{\partial C}{\partial t} = \frac{D_e}{R^2}\left[\frac{\partial^2 C}{\partial \xi^2} + \frac{2}{\xi}\frac{\partial C}{\partial \xi}\right] + \sum s_i \qquad [66]$$

where C is the concentration of the diffusing species, t is time, ξ is the distance away from the supply of flowing solution as a fraction of the maximum distance R, as per equation [65] in section 5.2.2, and s_i are the source terms producing or consuming the respective diffusing species.

The dimensionless ratio for quantifying densification was defined by equation [88] in section 5.5.4, while the dimensionless ratio for quantifying dripper-spread was defined by equation [91] in section 5.5.5 namely:

$$\text{Densification} = \left[\frac{(\rho^* - \rho_{ref})}{(\rho^* - \rho)}\right] \qquad [88]$$

$$\text{Dripper spread} = \frac{Dia}{Dia_{ref}} \qquad [91]$$

where ρ_{ref} is the bulk density of the ore during column leaching, ρ is the bulk density of the ore in a heap and ρ^* is the true density of the solid phase, all on a dry basis. Dia is the equivalent column diameter of a unit cell on a heap, as illustrated in section 3.7.4, with $Dia = (4.W.L/\pi)^{0.5}$, and Dia_{ref} is the diameter of the column in which the column leaching results were generated, from which the scale-up is to be done.

The concept of Dimensionless Transfer Radius (DTR) was developed in section 5.5.3, in terms of which the Transfer Time of a heap Θ, is expressed as a multiple of the Transfer Time exhibited by the column leaching of the same ore, Θ_{ref}, as follows:

$$\text{experimental} - DTR = \sqrt{\frac{\Theta}{\Theta_{ref}}} = \sqrt{\frac{\tau_\delta^2\ \theta_{imm,ref}}{\tau_{\delta,ref}^2\ \theta_{imm}}}\ \frac{R}{R_{ref}} \quad [81]$$

To be able to relate the observed ratio Θ/Θ_{ref} to either increased densification or wider dripper spacing on the heap, relative to the column, correlations were derived according to which the DTR is expected to vary as a result of either:

a. Densification, being a power function of heap and column bulk densities and immobile moisture contents, as per equation [87]:

$$\text{densification} - DTR = \sqrt{\frac{\Theta}{\Theta_{ref}}} = \sqrt{\frac{\theta_{imm,ref}}{\theta_{imm}}}\ \left[\frac{(\rho^* - \rho_{ref}\ )}{(\rho^* - \ \rho)}\right]^p \quad [87]$$

or

b. Dripper spread, being a power-function of heap and column bulk densities, immobile moisture content and equivalent column diameter represented by the dripper grid, as per equation [90]:

$$\text{dripper} - \text{spread} - DTR = \sqrt{\frac{\Theta}{\Theta_{ref}}} \quad [90]$$

$$= \left[\frac{(\rho^* - \rho_{ref}\ )}{(\rho^* - \ \rho)}\right]^{p-\frac{1}{2}} \sqrt{\frac{\theta_{imm,ref}}{\theta_{imm}}}\frac{Dia}{Dia_{ref}}$$

Both equations [87] and [90] contain an assumed power-law relationship between tortuosity and densification, as per equation [86] namely:

$$\sqrt{\frac{\tau_\delta^2}{\tau_{\delta,ref}^2}} = \left[\frac{(\rho^* - \rho_{ref}\ )}{(\rho^* - \ \rho)}\right]^{p-\frac{1}{2}} \quad [86]$$

The parameter "*p*" was manipulated to optimise the fits between the square roots of the Transfer Time ratios (appearing on the left-hand side of equations [87] and [90]), and the expressions on the right-hand sides of equations [87] and [90]).

It was further hypothesised that instances could occur where parts of the heap are, within the time scale of heap leaching, never contacted by leach solution and hence effective left dry. That would lead to the extractable fraction, $\kappa_x\kappa_w$ becoming less than

unity, which places an upper limit on the extent of extraction that could be achieved,in accordance with equation [75].

14.2 DATA RENDERING

The relevant parameters required to verify whether the trends predicted by the hypotheses could be observed are collated in Table 16 below on page 232. The data is grouped according to each of the case studies discussed above, and the case studies are further grouped into the Copper and Gold applications.

Note that the "Dripper spread" values share a column with the "Equivalent column diameter" values, and the "Densification" values share a column with the "Bulk density" values.

The calculation of DTR, densification and dripper spread relied on 'reference' (ref.) values. For each case, the column-leaching data generated on the corresponding ore was used as reference. In cases where more than one column result was available, the reference values were taken as the average of the two column tests.

The GAC rate constants (*k'*) which optimally fitted the data (while using the recorded value for θ_{imm} as moisture content during modelling) denoted $k'(\theta_{imm})$, are summarised in Table 17 below on page 235. That is followed by another value for the GAC rate constant denoted $k'(0.15)$, which was calculated for a common moisture content of ε_{imm}=0.15 kg/kg, as per equation [62] in section 3.12.5. (The reference moisture content is preferably expressed in units of solution mass per dry-solids mass ε_{imm} since its meaning is independent of bulk density, which the volume-fraction moisture content θ_{imm} is not). That provides a better basis for comparing the GAC rate constants amongst different sets of data, since the rate of GAC is affected by the moisture content as discussed in section 3.12.5.

As shown in Table 16, in some cases the moisture content had to be estimated, or limited to within physical limitations. However this does not affect the Transfer Time Θ or the GAC rate constant *k'* (as expressed on the basis of a common moisture content) that together uniquely define the leaching performance. (Refer to section 5.2.3 for a

discussion on the combinations of diffusional distance *R*, diffusivity *D*, moisture content ε_{imm} and GAC rate constant *k'* that uniquely characterise the leaching performance).

In the case of the NICICO sulphide copper, the drippers were arranged on a 400 mm x 1,000 mm grid, however severe ponding had been reported, which therefore spread the irrigated solution evenly over much of the upper surface. On the Rand Leases gold heap, sprinklers were used as opposed to drippers, with sprinklers providing very even distribution of droplets over the entire heap surface as opposed to the fixed-point irrigation provided by drippers. For both these cases the equivalent column diameter applicable to the heap was therefore taken as zero.

The Kipoi 3-1 data shown only applied during a temporary widening of dripper spacing to 1,000 mm between dripper lines and 500 mm in-line.

During the column leach of the Barrick gold application, the solution was evenly spread over the cross sectional area of the column, so that an effective column diameter of $Dia,_{ref}$=0 should be attributed to it. However, so as not to divide by zero in the calculation of the Dripper-Spread-DTR of equation [90], a value of $Dia,_{ref}$=50 mm was allocated to it to facilitate the division but set the reference value to an order of magnitude smaller than the effective column diameters of the crib and heap dripper spacings.

From equations [87] and [90] it is expected that the relative kinetics of heap leaching versus column leaching, expressed in terms of the DTR, be characterised by the parameter *p* (a power). The DTR's were first calculated using the Transfer Times (Θ) that optimised the model fits to the experimental data of each case study. Using the Transfer Time fitted to the column leaching experiment(s) of each case as reference, the 'experimental' DTR was calculated as $(\Theta/\Theta_{ref})^{0.5}$. Then followed calculation of a 'densification' DTR using equation [87] and then a 'dripper spread' DTR using equation [90].

The value of *p* was then sought that optimised the correlation between the 'experimental' and 'densification' DTR's, and then between the 'experimental' and 'dripper spread' DTR's.

In most cases it was obvious that the 'experimental' DTR could be correlated to only one of either the 'densification' or the 'dripper spread' DTR's. For example, since densification in the stratification boxes remained within 0.95-1.0, the 'experimental' DTR's between 1.46 and 2.13 could only have resulted from the significant increase in dripper spread (from 1.0 to 1.98). Those results could therefore only be correlated to the 'dripper spread' DTR. It was similarly found that the trend in 'experimental' DTR of the Kipoi results could only be correlated to the 'dripper spread' DTR. Using the Solver function of Excel, the sum of squared residuals (SSR) between the 'experimental' DTR's and the 'dripper spread' DTR's was then minimised by manipulating the value of p.

The DTR's of the NICICO copper and Rand Leases gold case studies could only be correlated to the 'densification' DTR's since the even distribution of solution over the heaps implied that the dripper spread was zero.

In the case of the Barrick gold case study it was not immediately obvious whether only one, or possibly both of the 'densification' and 'dripper spread' DTR's could be correlated to the 'experimental' DTR. Both correlations were therefore done, using different values for p to optimise the correlations. However the correlation obtained versus the 'densification'-DTR of 0.999 using p=4.08 was much better than the best correlation versus the 'dripper spread'-DTR of 0.446 using p=0.35. It was therefore concluded that scale-up during the Barrick Gold case study was governed by densification, not by dripper-spread.

The data of the Rand Leases (gold) case study with 47% of NaCN being available for leaching was excluded from this SSR calculation, since it generated errors that dominated the SSR. The assumption that 30 percent of the cyanide irrigated to the heap was available for gold leaching, discussed as part of Case Study 1, corresponds very well with the expected response in DTR. Unfortunately that remains an inference for which no better verification can be obtained. Another weakness of the data of the Rand Leases case study is the large uncertainty regarding the density that prevailed on the heap and the very low Transfer Times, as discussed in section 7.5. This led to commensurate uncertainty in the calculation of the densification calculated from equation [88] and the

model-fitting of the Transfer Times and hence of the DTR-correlations obtained for this case study.

Table 16. Summary of scale-up data

Case Study	Height (H), m	Equivalent column diameter, mm and (Dripper Spread)	Bulk density[2] (ρ), kg/m^3 and (Densification)	Moisture content (θ_{imm}), cum/cu m	Moisture measured, estimated, fitted or limited[1]	Transfer time (Θ), days	Experimental Dimensionless transfer radius (DTR), $\sqrt{(\Theta/\Theta_{ref})}$	Extractable fraction, ($K_x K_w$)	DTR calculated from densification	DTR calculated from dripper spread
COPPER										
Kipoi Oxide Cu (p=0.0)										
Kipoi C5 (ref)	6	200 (1.0)	1,549 (1.0)	0.20	meas.	43.5	1.07	0.946	1.00	1.00
Kipoi C6 (ref)	6	200 (1.0)	1,557 (1.0)	0.20	meas.	32.4	0.924	0.957	1.00	1.00
Kipoi 1-1	4	564 (2.82)	1,385 (0.87)	0.18	model fit	569	3.87	0.85	1.06	3.20
Kipoi 2-1	5	564 (2.82)	1,808 (1.29)	0.24	est.	196	2.27	0.804	0.93	2.31
Kipoi 3-1	6	798 (3.99)	1,655 (1.10)	0.22	est.	280	2.72	0.711	0.97	3.69
Seg/Strat Oxide Cu (p=1.47)										
Unsegr Col (ref)	0.668	153 (1.0)	1,390 (1.0)	0.18	meas.	26.7	1.00	1.00	1.00	1.00
Strat box 1	0.590	303 (1.98)	1,348 (0.97)	0.22	meas.	120	2.12	0.69	0.87	1.75
Unstrat box 1	0.610	303 (1.98)	1,327 (0.95)	0.27	meas.	56.5	1.46	0.55	0.77	1.56
Strat box 2	0.600	303 (1.98)	1,341 (0.96)	0.18	meas.	115	2.07	0.58	0.94	1.90
Unstrat box 2	0.580	303 (1.98)	1,464 (1.06)	0.22	meas.	121	2.13	0.52	0.99	1.90

Case Study	Height (H), m	Equivalent column diameter, mm and (Dripper Spread)	Bulk density[2] (ρ), kg/m^3 and (Densification)	Moisture content (θ_{imm}), cum/cum	Moisture measured, estimated, fitted or limited[1]	Transfer time (Θ), days	Experimental Dimensionless transfer radius (DTR), $\sqrt{(\Theta/\Theta_{ref})}$	Extractable fraction, ($\kappa_x\kappa_w$)	DTR calculated from densification	DTR calculated from dripper spread
SULPHIDE COPPER (NICICO heap dripper grid was 400 x 1,000 mm^2) (p=4.84)										
NICICO Col 6.1 (fit temp) (ref)	6.0	200 (1)	1,566 (1.0)	0.31	meas.	72.5	0.813	1.00	1.00	1.00
NICICO Col 6.1 (fit S ox) (ref)	6.0	200 (1)	1,566 (1.0)	0.31	meas.	147	1.16	1.00	1.00	1.00
NICICO Heap 1 (fit temp)	6.56	- (0)	1,809 (1.27)	0.36	limited	873	2.82	0.985	3.00	-
NICICO Heap 2 (fit temp)	6.42	- (0)	1,718 (1.15)	0.36	limited	605	2.35	1.00	1.87	-
NICICO Heap 1 (fit S ox)	6.56	- (0)	1,809 (1.27)	0.36	limited	873	2.82	0.99	3.00	-
NICICO Heap 2 (fit S ox)	6.42	- (0)	1,718 (1.15)	0.36	limited	605	2.35	1.00	1.87	-
GOLD										
Gold, Rand Leases (p=9.42)										
Gold (Rand Leases Col 47% of NaCN) (ref)	4	225 (1.0)	1,132 (1.0)	0.23	estimate	0.071	0.691	1.00	1.00	1.00
Gold (Rand Leases Col 100% of NaCN) (ref)	4	225 (1.0)	1,132 (1.0)	0.23	estimate	0.225	1.23	1.00	1.00	1.00
Gold (Rand Leases Heap, 30% of NaCN)	4	- (0)	1,450 (1.25)	0.29	estimate	8.28	7.48	1.00	7.48	-

Case Study	Height (H), m	Equivalent column diameter, mm and (Dripper Spread)	Bulk density[2] (ρ), kg/m^3 and (Densification)	Moisture content (θ_{imm}), cum/cum	Moisture measured, estimated, fitted or limited[1]	Transfer time (Θ), days	Experimental Dimensionless transfer radius (DTR), $\sqrt{(\Theta/\Theta_{ref})}$	Extractable fraction, ($\kappa_x\kappa_w$)	DTR calculated from densification	DTR calculated from dripper spread
Gold (Rand Leases Heap, 47% of NaCN)	4	- (0)	1,450 (1.25)	0.29	estimate	75.9	22.6	1.00	7.48	-
Gold, Barrick									p=4.08	p=0.35
Gold (Barrick, Bouff.) Col. (ref)	5.1	50[3] (1.0)	1,370 (1.0)	0.159	meas.	10.1	1.00	ND	1.00	1.00
Gold (Barrick, Bouff.,) Crib	5.46	519 (10.4)	1,725 (1.36)	0.191	meas.	127	3.55	ND	3.24	9.04
Gold (Barrick, Bouff.) Heap	2.4	519 (10.4)	2,014 (1.94)	0.351	meas.	1,011	10.0	ND	10.1	6.32

Notes to Table 16:

1. The moisture content data was either measured (m), estimated (est) or constrained within physical limits (lim).
2. True density ρ^* = 2,700 kg/m^3.
3. The column diameter was 250 mm, but with irrigation spread evenly over it, as opposed to being irrigated on the column axis. Hence the effective column diameter should be zero. However to avoid division by zero in the dripper-spread calculation, the column diameter was set at 50 mm to render it an order of magnitude smaller than that of the crib and column.

ND: Not determined.

Table 17. Summary of GAC constants

Case Study	Moisture content (θ_{imm}), cum/cum	Moisture measured, estimated, fitted or limited	$k'(\theta_{imm})$, h^{-1}	$k'(\varepsilon_{imm}=0.15)$, h^{-1}
Kipoi Oxide Cu				
Kipoi C5 (ref)	0.20	measured	0.0228	0.0198
Kipoi C6 (ref)	0.20	measured	0.0313	0.0271
Kipoi 1-1	0.36	model fit	0.00850	0.0147
Kipoi 2-1	0.24	estimate	0.00210	0.00182
Kipoi 3-1	0.22	estimate	0	-
Seg/Strat Oxide Cu				
Unsegr Col (ref)	0.25	measured	0.106	0.127
Strat box 1	0.22	measured	0.0100	0.0120
Unstrat box 1	0.27	measured	0.00680	0.00816
Strat box 2	0.18	measured	0.00480	0.00576
Unstrat box 2	0.22	measured	0.0120	0.0144
SULPHIDE COPPER (NICICO heap dripper grid was 400 x 1,000 mm^2)				
NICICO Col 6.1 (fit temp) (ref)	0.31	measured	5.00E-04	0.0007
NICICO Col 6.1 (fit S ox) (ref)	0.31	measured	5.00E-04	0.0007
NICICO Heap 1 (fit temp)	0.54	limited	0.015	0.020
NICICO Heap 2 (fit temp)	0.52	limited	0.015	0.020
NICICO Heap 1 (fit S ox)	0.54	limited	0.015	0.020
NICICO Heap 2 (fit S ox)	0.52	limited	0.015	0.020

As discussed in the sections that follow, the DTR data of each ore type could in each case be correlated either to the Densification-DTR or to the Dripper-Spread-DTR. The value of *p* was fitted individually for each ore type, a summary of which appears in Table 18 below.

Table 18. Summary of governing scale-up phenomena and values of p

Ore type	**Governing scale-up phenomenon**	**Optimised value of *p***
Kipoi	Dripper spread	0.0
Oxide Cu (segregation/stratification boxes)	Dripper spread	1.47
Average of *p* where dripper-spread dominates scale-up		0.73 (*p*-0.5) = 0.24
NICICO copper sulphide	Densification	4.84
Barrick gold	Densification	4.08
Average of *p* where densification dominates scale-up (excluding Rand Leases due to uncertainty re. heap density)		4.46
Rand Leases gold	Densification	9.42

Notes:

1. In the case where Dripper spread governs the scale-up of mass transfer kinetics, the power of the term bearing the bulk densities is *p*-0.5, as per equation [90]. For the two case studies listed in this table where that applies (Kipoi and segregation/stratification boxes), *p*-0.5 yields values around zero, namely (0-0.5 = -0.5) and (1.47-0.5 = 0.97). That suggests that the term bearing the bulk densities might be dropped from equation [90] (i.e. setting *p*-0.5 = 0), which makes intuitive sense since mass transfer governed by dripper spacing is not expected to be affected by density variations.
2. For the cases where densification governs the scale-up in mass transfer kinetics, the data of the Rand Leases case study is disregarded since the very small Transfer Times observed for that case suggested that diffusional mass transfer had little effect on the effective leaching kinetics as discussed in section 7.6. That renders determination of the Transfer Times (and therefore of the DTR's) very uncertain, to which the large deviation is ascribed that is seen between the fitted values of *p* for the NICICO and Barrick cases versus the Rand Leases case.
3. For the two remaining cases where the scale-up in diffusional mass transfer was governed by densification, i.e. NICICO and Barrick gold, the two values fitted for *p* were quite close (4.84 and 4.08), so that where densification applies the power appearing in the Densification-DTR of equation [87] can be stated as 4.46 ± 0.38 or, to two significant numbers, as the average of 4.5.

14.3 EFFECT OF DENSIFICATION ON DIMENSIONLESS TRANSPORT RADIUS (DTR)

If the change in DTR from column scale to heap scale is governed by increased densification, the "Experimental-DTR" (as per equation [81]) can theoretically be set equal to the "Densification-DTR" (as per equation [87]). Therefore, a plot of these two

formulations of DTR against one another should yield a straight line passing through the origin, as per the line labelled “expectation” in Figure 60 below on page 238.

From Figure 60(a) and (b) it is seen that the DTR’s calculated from densification of the sulphide copper (from the NICICO case study) as well as the two gold case studies could be correlated to the ‘experimental’ DTR’s. This is to be expected since the NICICO heaps were known to have compacted to high densities. From the data in Table 16 on page 232 it is seen that densification of 1.27 was observed in the NICICO heap 1. Also in the case of the Barrick gold case study were densifications of 1.36 and 1.94 observed. Sprinkler irrigation was used on the Rand Leases gold heap and hence any increase in DTR could only have resulted from the densification of 1.25.

The DTR’s of the Kipoi heaps were apparently not related to densification, since it exhibited no trend versus densification in Figure 60(a). This is also not surprising as only heap 2-1 exhibited significant densification of 1.29 while densification on heap 3-1 was only 1.1 and on heap 1-1 it was even less than unity, being 0.87.

Where densification was the governing phenomenon, the value of *p* was found to be 4.84 and 4.08 for the NICICO and Barrick case studies respectively, i.e. varying around a value close to 4.5, as shown in Table 18 on page 236. The Rand Leases data yielded *p*=9.42, but very little confidence can be attached to that value, due to the uncertainty regarding the Rand Leases heap density and the loss of model sensitivity at the very low Transfer Times fitted to this data, as discussed in section 7.5. It is therefore proposed that, for densification, a value of *p*=4.5 should be adopted, albeit only on the basis of two case studies. It can therefore be proposed that the expression for the Densification-DTR of equation [87] could be simplified to:

$$\text{densification} - DTR(mod) = \sqrt{\frac{\Theta}{\Theta_{ref}}} = \sqrt{\frac{\theta_{imm,ref}}{\theta_{imm}}} \left[\frac{(\rho^* - \rho_{ref})}{(\rho^* - \rho)}\right]^{4.5} \qquad [104]$$

The reader may refer to the derivation of the Densification-DTR in section 5.5.4, where it can be seen that the densification term defined by equation [88], insofar as it accounts for the effect of the reduction in number of conductive flow channels with densification, appears in equation [88] only to the power of 0.5. However, in the power-function

proposed between densification and tortuosity, as per equation [86], the effect of change in tortuosity appears in the 'densification'-DTR to the power of (p-0.5). Together they add up to the power p that appears in equation [87]. Accepting the value of p=4.5 during densification, it follows that the contribution of the tortuosity change to the power p (namely (p-0.5) = (4.5-0.5) = 4.0) is much stronger than the contribution (of p=0.5) made by the reduction in the number of conductive flow channels.

a.

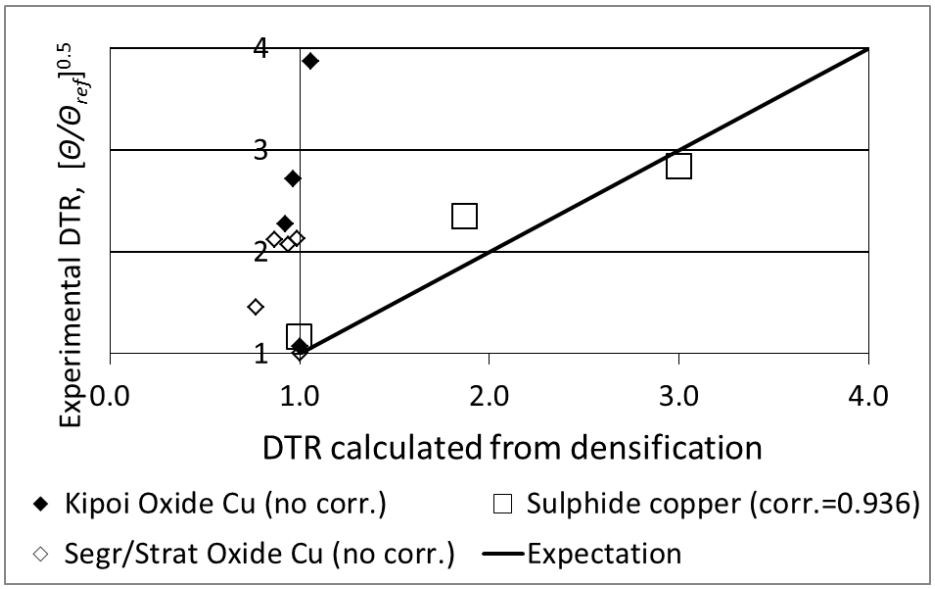

b.

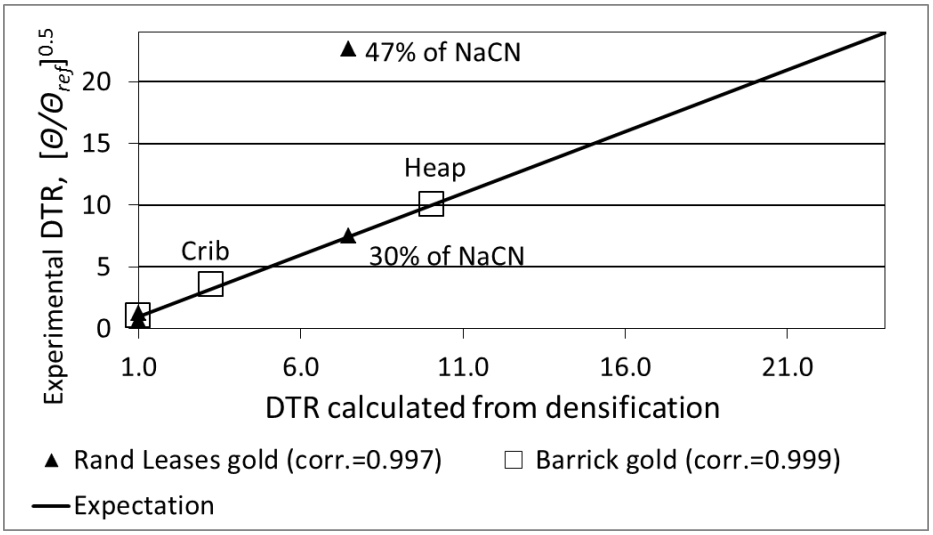

Figure 60. Effect of densification on relative diffusional distance.
(a) Copper ores and (b) Gold ores.
(This plots all "Experimental DTR" versus all "DTR calculated from densification" data from Table 16 [page 232]. The correlation coefficient shown for "Rand Leases gold" in (b) excludes the "47% of NaCN" data point. Note the two "Rand Leases gold" data points that are very close to one another in the vicinity of (1.0;0) in graph (b)).

14.4 EFFECT OF Ddensification ON EXTRACTABLE FRACTION

In Figure 61 below, the data from columns ("Narrow spread") are shown distinct from data for cribs, heaps and wide boxes ("Wide spread"), to ease interpretation. The extractable fraction does not seem to be correlated to densification. Values of unity for $\kappa_x\kappa_w$ are observed up to a densification of 1.29, while values for $\kappa_x\kappa_w$ as low as 0.55 are observed at densification of unity (representing the bulk density of the reference case, this particular data point belonging to the un-stratified box number 1). (Densification being a dimensionless number).

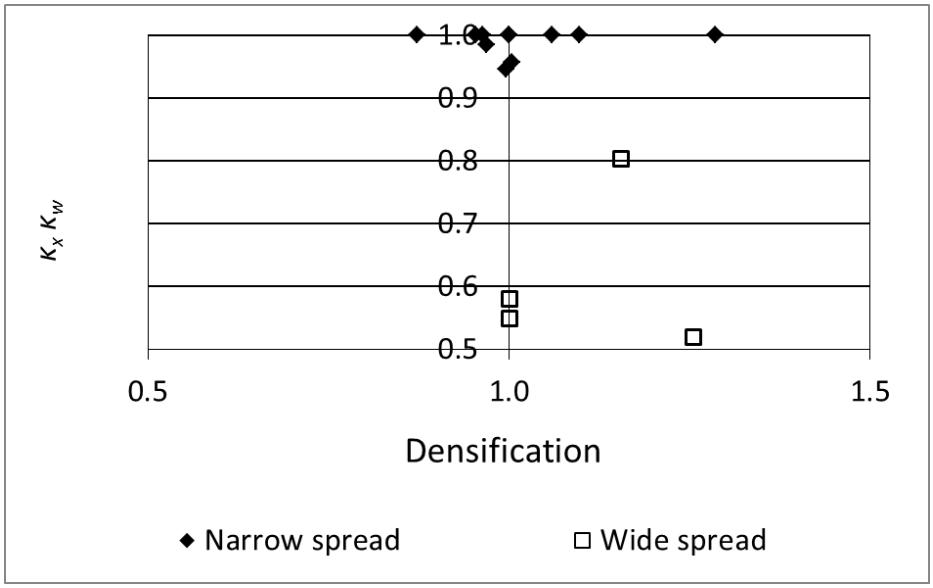

Figure 61. Effect of densification on extractable fraction
("Narrow spread" represents all column leaching data from Table 16 [page 232], while "Wide spread" represents all heap and crib leaching data as well as the data obtained from the stratification boxes, i.e. case studies named "Strat box" and "Unstrat box").

14.5 EFFECT OF DRIPPER SPREAD ON DIMENSIONLESS TRANSPORT RADIUS (DTR)

If the change in DTR from column scale to heap scale is governed by increased dripper spread, the "Experimental-DTR" (as per equation [81]) can theoretically be set equal to the "Dripper-Spread-DTR" (as per equation [90]). Therefore, a plot of these two formulations of DTR against one another should yield a straight line passing through the origin, as per the line labelled "expectation" in Figure 62 below on page 242.

From Figure 62(a) it can be seen that the kinetics of the Kipoi case study and the segregation/stratification boxes (which showed no correlation to densification) do exhibit correlations with dripper spread. The DTR of the NICICO case study exhibits the non-sensical trend of decreasing DTR with increasing dripper spread, which can be taken as being unrelated to dripper spread. This is to be expected since the NICICO case study did not involve much variation in dripper spread, varying only between 0 and 1, compared to the dripper spreads of Kipoi (1.0-3.99) and of the segregation/stratification boxes (1.0-1.98), (dripper spread being a dimensionless number).

Similarly to the NICICO case study, the Rand Leases (gold) case study shown in Figure 62(b), exhibits no trend between DTR and dripper spread, and its dripper spread also varied only between 0 and 1. However, it did exhibit a trend between DTR and densification.

The Barrick (gold) case exhibits a trend between DTR and dripper spread, and its dripper spread in the crib and heap was 10.4.

Where dripper spread was the governing phenomenon as summarised in Table 18 on page 236, the value of p remained relatively small, between 0 and 1.47. Referring equation [90] defining the 'dripper-spread'-DTR, the densification term (defined by equation [88]) appears to the power of (p-0.5), hence in the cases of the Kipoi and oxide segregation/stratification boxes, to a power of -0.5 to 0.97. From the derivation of equation [90] in section 5.5.5, the densification term can be seen to appear in it for the sake of accounting for any possible changes in tortuosity that might accompany the increase in dripper spread, if the DTR were to be affected by a combination of dripper spread and densification.

However, at least during the case studies investigated here, it seems rather that the DTR is affected either by densification, or by dripper spread, but not a combination of the two. It was argued in section 5.5.5 that the densification term (incorporated to account for a change in tortuosity, in accordance with equation [86]), may not need to appear in the Dripper-Spread-DTR expression of equation [90]. It was included in order to remain fully generic. However, since the Dripper-Spread-DTR is now found to be dependent on

densification to a power close to zero, it suggests that the Dripper-Spread-DTR could be modified to yield (more simply):

$$\text{dripper} - \text{spread} - DTR(mod) = \sqrt{\frac{\Theta}{\Theta_{ref}}} = \sqrt{\frac{\theta_{imm,ref}}{\theta_{imm}}}\frac{Dia}{Dia_{ref}} \quad [105]$$

If both densification and dripper spread are affecting the DTR's observed during the case studies, it must be concluded that in each of the case studies either one of the phenomena dominated over the effect of the other. From Figure 64 below on page 248 that follows below, it will become clear that a regime exists where densification will determine the DTR, but above a certain width of dripper spacing the DTR will be governed by the dripper-spread. Therefore, over the wide range of possible dripper spacing arrangements that could be chosen, densification and dripper spread will equally determine the DTR only in a single point, while either the one or the other will prevail over the rest of the range of possible dripper spacing.

a.

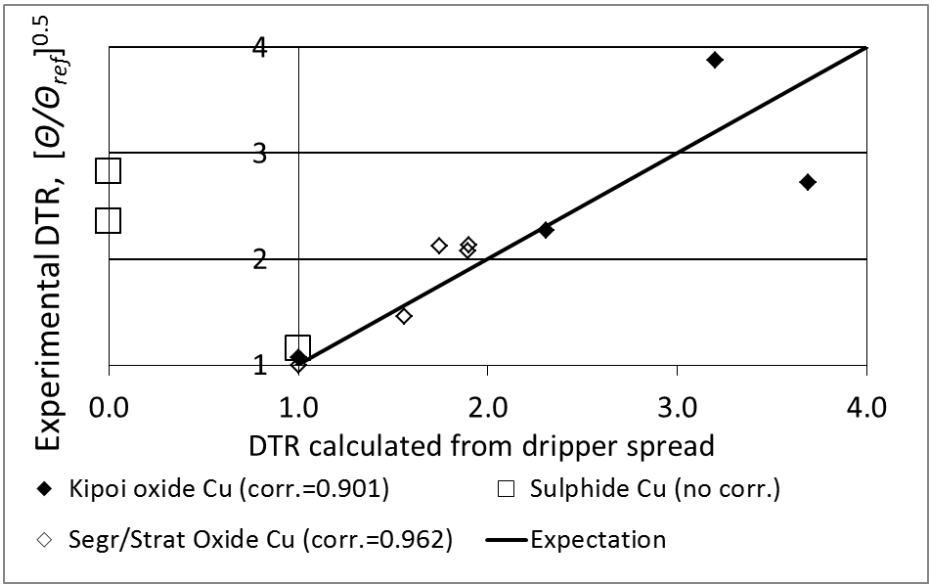

b.

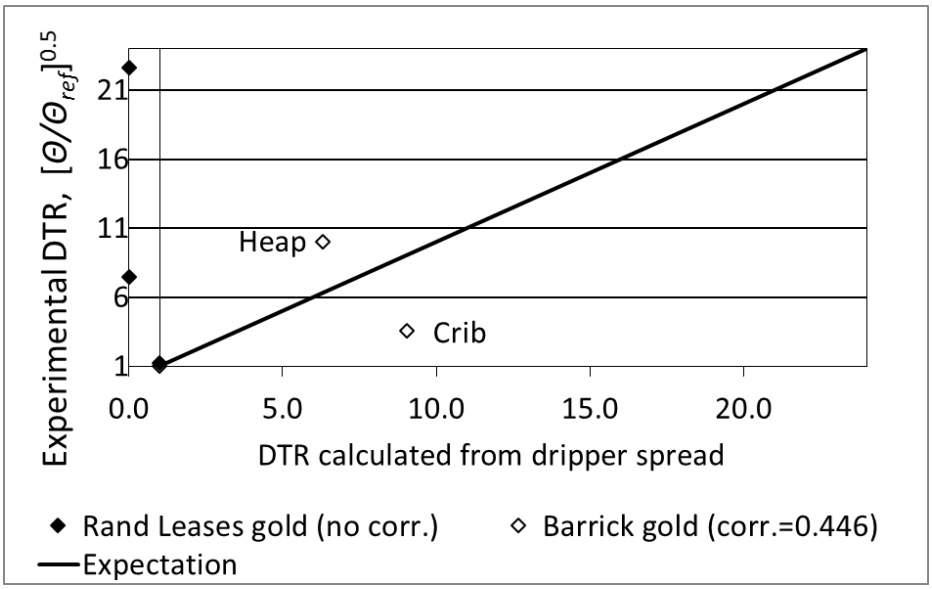

Figure 62. Effect of dripper spread on relative diffusional distance
(a) Copper applications, (b) Gold applications
(This plots all "Experimental DTR" versus all "DTR calculated from dripper spread" data from Table 16 [page 232]).

14.6 EFFECT OF DRIPPER SPREAD ON EXTRACTABLE FRACTION

No explicit function was hypothesised whereby the extractable fraction $\kappa_x\kappa_w$ would vary, except to expect that it would decrease below unity for excessively wide dripper spacings.

From Figure 63(a) there appears a clear trend of decreasing extractable fraction with increasing dripper spread. The correlation drawn between the data points, extrapolated to the y-axis, passes through (0;1) suggesting that $\kappa_x\kappa_w$ starts reducing with any increase in dripper spread.

Figure 63(b) permits an alternative view of the data albeit an empirical one, being plotted with simply equivalent column diameter on the *x*-axis. This is admittedly a less fundamental parameter than the dripper spread, but is included to show that extrapolation of the correlation drawn through the data represented in this way passes through (111;1.0) suggesting that $\kappa_x\kappa_w$ starts reducing at dripper diagnoals larger than 111 mm. And simply considering the individual data points, it shows that $\kappa_x\kappa_w$ values of unity were still observed at dripper diagonals up to 225 mm. This places the range of dripper diagonals that can yield extractable fractions equal to that achieved in columns between 111 and 225 mm.

a.

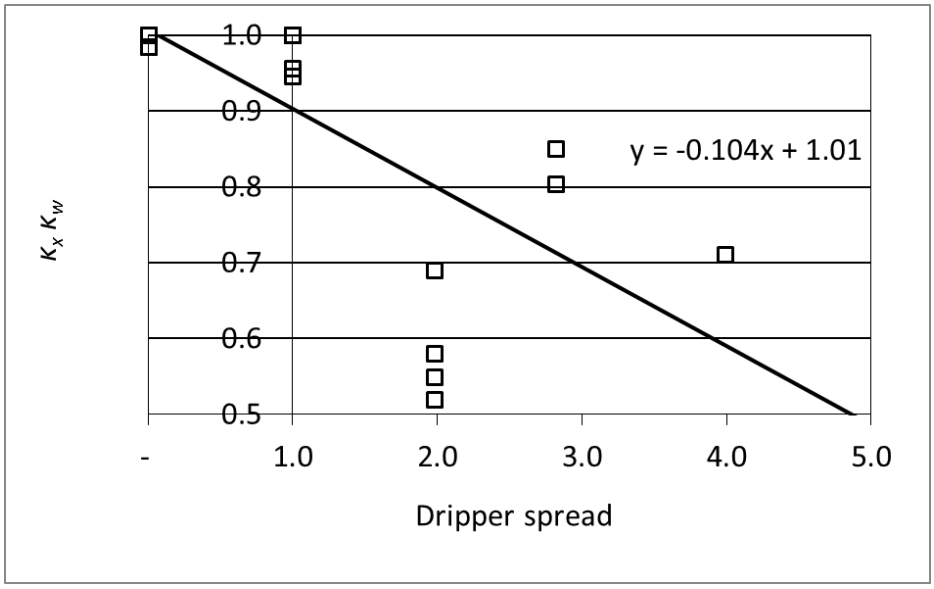

b.

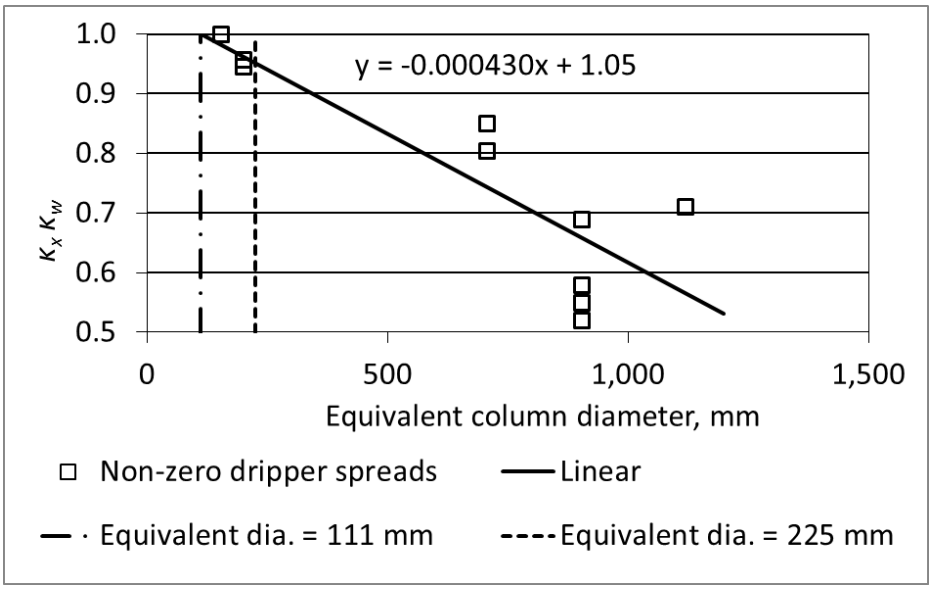

Figure 63. Effect of dripper spacing on extractable fraction
(a) Versus Dripper spread, and (b) versus Equivalent column diameter (mm)

14.7 RESPONSE OF GAC RATE CONSTANT

During the segregation and stratification testwork discussed above, it was observed that attempts to experimentally determine values for the GAC rate constant *k'* were not very successful at finding values for *k'* that yielded the optimal model fits. Furthermore, GAC rate constants fitted to the various cases varied quite significantly. This poses a remaining challenge to the predictive modelling of acid heap leaching. The rate of

copper extraction is very sensitive to GAC rate constant, particularly for oxide-copper ore. In combination with the Transfer Time, the GAC rate constant determines the rate of acid supply to the copper surfaces.

The GAC rate constant *k'* was not expected to exhibit any trend against any of the other parameters in Table 16 on page 232. The value of *k'* is expected to be a function of the gangue mineralogy of the ore, and is therefore expected to remain constant for a given ore type. However, as explained in section 3.12.5, the numerical value of *k'* needs to be stated within context of the moisture content used. In accordance with the procedure shown there, the values of *k'* are also restated in Table 17 on page 235 in terms of a common moisture content of ε_{imm}=0.15 kg moisture per kg dry solids.

Methods for correlating the GAC rate constant, *k'*, to ore mineralogy towards better predictions of the values for *k'* that emulate the experimentally observed rate of GAC during column or heap leaching is suggested as a topic for future research.

14.8 EXAMPLE OF APPLICATION OF THE METHOD

The application of the scale-up method thus far developed will be demonstrated using the Kipoi Heap 3-1 case study as an example. Being an oxide heap application, it lends itself to acid leaching, thereby avoiding the added complication of parameters such as aeration, bacterial kinetics and sulphide oxidation kinetics associated with a sulphide leaching case such as the NICICO case study. The gold applications are complicated by the large uncertainty regarding the bulk density and very low Transfer Time of the Rand Leases heap and the fact that the Barrick heap did not produce leaching kinetic data.

This illustration is meant to show how the data from laboratory column C6 would be used in this method, how the dripper spacing for Kipoi Heap 3-1 would be selected, how the model-input parameters would be specified for modelling the heap-scale behaviour, and the resulting modelling results whereby the anticipated performance of Heap 3-1 would be predicted.

During the Kipoi case study discussed in section 9, the total copper content, irrigation rate, acid concentration in the irrigation solution and curing acid additions used on Heap 3-1 differed somewhat from those used in the laboratory colums. For the illustration used here, those parameters will be kept to that used for column C6, to eliminate any effect that those parameters have on the modelled leaching performance. That requires that some of the Heap 3-1 parameter values used for this illustration be modified from the actual recorded numbers (which appear in Table 9, page 175). Due to higher curing acid dosages being used on the Kipoi heaps than on the columns, the GAC rate constants *k'* also varied between the columns and heaps, as discussed in section 9.4. Similarly, for the illustration, the values of *k'* found to apply to column C6 will be specified here for both column and heap. That is to assume that *k'* would remain constant, provided the same curing dosage and irrigation acid concentration are used in both the column and the heap. For those parameters that were changed from those reported in Table 9 on page 175, the original values appear in Table 19 (page 250) in round brackets ().

Firstly, an estimate is required of the final bulk density that Heap 3-1 would densify towards. For this illustration, it is assumed that Heap 3-1 would reach a bulk density of 1,732 kg/m^3, being the average of the two higher bulk densities observed on the Kipoi

heaps namely the 1,808 kg/m^3 of Heap 2-1 and the 1,655 kg/m^3 observed on Heap 3-1). In the case of a green-fields project for which there would not be any such experience-based data available, this parameter can be estimated based on compression tests such as those described by Guzman (2011). And the compression tests could be conducted on ore samples subjected to different combinations of crushing, agglomeration and curing conditions in order to select the optimal combination of ore preparation parameters and final anticipated bulk density.

Using as the rock density ρ^* = 2,700 kg/m^3, the reference (i.e. column) density ρ_{ref} = 1,557 kg/m^3, and the predicted heap density ρ = 1,732 kg/m^3, all information is available to calculate the densification from equation [88], being 1.18 (dimensionless). For simplicity sake, Heap 3-1 is assumed to retain the same immobile moisture content θ_{imm} than that of the 0.23 m^3/m^3 observed in column C6, leaving the term θ_{ref}/θ at unity. In a more complete analysis, the analysis illustrated here could be repeated for a range of conceivable ratios of θ_{ref}/θ.

The next step is selection of the dripper spacing for Heap 3-1. The approach is to select the widest dripper spacing that is possible without rending the Transfer Time of the heap governed by the width of the dripper spacing. To state this in terms of (a) the equivalent column diameter represented by the dripper spacing and (b) the DTR: the equivalent column diameter represented by the dripper spacing, (*Dia* in equation [90]), is selected in such a way that the Dripper-Spread-DTR does not govern the scale-up in the Transfer Time of the heap, (Θ). That is to say, the Dripper-spread-DTR is kept smaller than the Densification-DTR. The dripper spread is a simple parameter to control by correct selection of the dripper spacing, compared to the extent of heap densification over which the plant operator holds less control. The use of a dripper spacing that yields a Transfer Time larger than that caused by densification would be allowing the heap Transfer Time to be unnecessarily large.

For any dripper spacing that is assumed, the equivalent column diameter operational on the heap, *Dia*, can be calculated, as well as the multiple Dia/Dia_{ref} where Dia_{ref} is the column diameter of 0.2 m. All information is now available for calculating the Densification-DTR from equation [87] and the Dripper-Spread-DTR from equation [90].

This is done for a range of equivalent column diameters, yielding the graph shown in Figure 64.

From Figure 64, it can be seen that, as long as the equivalent column diameter is <400 mm, the Dripper-Spread-DTR's are smaller than the Densification-DTR's and the Dripper-Spread-DTR's would therefore not be determining the heap Transfer Time. Equivalent column diameters larger than that would render the heap Transfer Time larger than the Transfer Time that would be calculated from the Densification-DTR. From equation [28] in section 3.7.4, an equivalent column diameter of 400 mm can be calculated to be equivalent to a dripper spacing of 0.35 x 0.35 m, which becomes the dripper spacing specification for Heap 3-1.

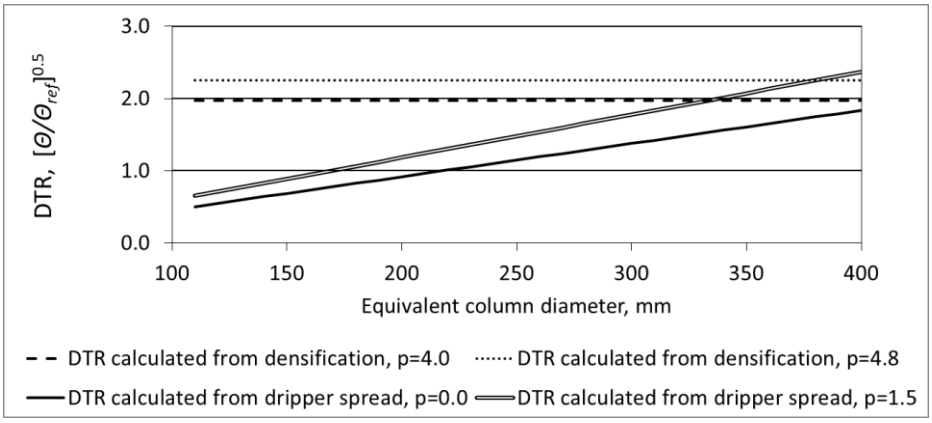

Figure 64. Ranges where either densification or dripper-spread determine the DTR

Although the simpler modified equations [104] and [105] have been proposed which use constant values for the power *p*, this illustrative calculation was still done using values for *p* of both 4.0 and 4.8 for calculating the Densification-DTR from equation [87], and values of *p* of both 0 and 1.5 were used to calculate the Dripper-Spread-DTR from equation [90]. This is according to the ranges of values of *p* listed in Table 18 on page 236 and it illustrates the sensitivities of the DTR's to the values of *p*. It can be seen that the sensitivities are not excessive. The two Densification-DTR values remain constant, being independent of equivalent column diameter, (*Dia*) since parameter *Dia* appears only in the Dripper-Spread-DTR as per equation [90], as opposed to the Dripper-Spread-DTR which is a rising function of *Dia*.

From Figure 63(b) on page 244 it can be seen that an equivalent column diameter of 0.4 m is expected to yield an extractable fraction $\kappa_x\kappa_w$ of 0.9. Alternatively, with the column diameters Dia_{ref} having been 0.2m, an equivalent column diameter on the heaps Dia of 0.4m represents a dripper spread, calculated from equation [91], of 0.4/0.2 = 2.0. Using this dripper spread, it could more conservatively be derived from Figure 63(a) that the extractable fraction would be 0.8. For the illustration, the value of 0.9 will be used, for a more complete analysis the effect of both extremes for values of $\kappa_x\kappa_w$ could be explored.

To ensure that the column C6 and Heap 3-1 simulations contain the same amount of ore per square meter irrigated, the height of Heap 3-1 was calculated from the height and bulk density of column C6 (H_{C6} and ρ_{C6} respectively), and from the predicted bulk density of Heap 3-1 ($\rho_{3\text{-}1}$), as follows:

$$\rho_{C6}\, H_{C6} \;=\; \rho_{3-1}\, H_{3-1} \qquad \text{OR} \qquad H_{3-1} \;=\; \frac{\rho_{C6}\, H_{C6}}{\rho_{3-1}} \qquad [106]$$

This is equivalent to assuming that column C6 and heap 3-1 get initially stacked to the same height and same bulk density, but that they then settle to their respective bulk densities shown in Table 19 on page 250, with heap 3-1 possessing the higher bulk density and, therefore, the commensurate lower height.

Table 19. Parameter values used for illustration of scale-up methodology

Parameter	**Symbol**	**Kipoi Column C6**	**Kipoi Heap 3-1 illustrative**
Total Cu content, %	C^0_{Cu}	3.30	3.30 (2.64)
Extractable fraction	$\kappa_x\kappa_w$	0.96	0.90 (0.711)
Extractable Cu content	$\kappa_x\kappa_w\ C^0_{Cu}$	3.17	2.97 (1.88)
Bulk density, kg/m^3	ρ	1,557	1,732 (1,655)
Irrigation flux, L/(h.m^2)	q	15	15(13.2)
Irrigation [H_2SO_4], g/L	C_{H2SO4}	11	11 (10.1)
Curing acid addition, kg/t	W_{cur}	5	5 (11.9)
Height, m	H	6	5.2 (6)
Column diameter, m	Dia	0.2	N.A.
Dripper spacing, m	W, L	N.A.	0.35 x 0.35 (1.0 x 0.5)
Effective heap irrigation diameter, m	Dia_{ref}	0.2	0.40 (0.80)
Immobile solution fraction, m^3 water per m^3 heap	Θ_{imm}	0.22	0.22
GAC rate constant, h^{-1}	k'		
Early period:		0.0313	0.0313 (0.5)
Late period:		0.0313	0.0313 (0.0)
Column Transfer Time, days	Θ_{ref}	32.4	
Heap Transfer Time, days	Θ		164 (280)

Note: The numbers in brackets indicate the actual observations reported in Table 9 (page 175), before changing the numbers to the illustrative values appearing in this table to render the "Heap 3-1 illustrative" case a more direct extrapolation of the "Column C6 illustrative" case. Where the value from Table 9 is used, only a single numer appears.
N.A.: Not Applicable.

From the fitting of the leaching kinetics of column C6, as discussed in section 9.2, the Transfer Time of column C6 was found to be 32.4 days, which is specified in Table 19 as the reference Transfer Time, $\Theta_{ref.}$

(If a Transfer Time of one or more orders of magnitude smaller than 15 days had been found for the column leaching kinetics, it would have suggested that the column leaching kinetics were not strongly affected by diffusional mass transfer. As illustrated in Figure 28 on page 115, the model result then becomes insensitive to the Transfer Time, lending uncertainty to the true magnitude of the Transfer Time that optimises the model fit. It might be possible that both column and heap leaching kinetics of that ore might not be governed by diffusional mass transfer in which case the column and heap

would exhibit exactly the same kinetics, but that cannot be known in advance. It would then be conservative to rather assign a Transfer Time of 15 days to the column leaching kinetics as if the column were border-line diffusional mass transfer-limited, from which to scale up towards the heap leaching kinetics. In this example, with the Transfer Time of 32.4 days, that does not apply).

From Figure 64 on page 248, following the horizontal line calculated for *p*=4.8 (being the larger and hence more conservative value of the two Densification-DTR's), the DTR governing the scale-up behaviour is read as DTR = 2.25. Knowing that the Transfer Time for the column was 32.4 days, the Transfer Time for the heap *Θ* can be calculated from:

$$\Theta = \Theta_{ref}.(\mathrm{DTR})^2 = 32.4\ (2.25)^2 = 164\ \text{days} \qquad [107]$$

(This is a smaller Transfer Time than the 280 days reported for Heap 3-1 in section 9.4, reflecting the fact that a narrowed dripper spacing has now been selected for Heap 3-1 to prevent the DTR from being governed by dripper-spread).

The predicted performance of heap 3-1 can now be modelled by using the parameters appearing in Table 19 on page 250. The Cu extraction, drainage acid concentration and GAC predicted by the model for Heap 3-1 appear in Figure 65 below, together with the experimentally observed and model-fitted data for column C6.

For this illustrative example, the extent of extraction from heap 3-1 is predicted to be 60 percent in 158 days and 72 percent in 250 days, compared to the experimentally observed values during column leaching of 60 percent in 51 days and 72 percent in 70 days. These yield multiples of 3.0 to 3.5 times the time required for a given extent of extraction from the heap, compared to the time required from the column. This is larger than the experience-based empirical multiple of 2.0 that is often suggested by design engineers, as illustrated in Figure 2 on page 5 and discussed in section 1.3. But of course this multiple would change depending on the anticipated densification and the dripper spacing selected.

The larger Transfer Time (i.e. long diffusional distance) predicted for Heap 3-1 leads to virtually immediate break-through of acid to the drainage solution as shown in Figure

65(b), compared to column C6 where acid became detectable in the drainage solution only after about 100 days. This is due to the acid being washed from the heap via the flow channels faster than the acid can migrate from the flow channels to distribute throughout the immobile solution to contact the ore. This leads to poorer utilisation of the acid, which in turn leads to both slower copper extraction and slower GAC.

a.

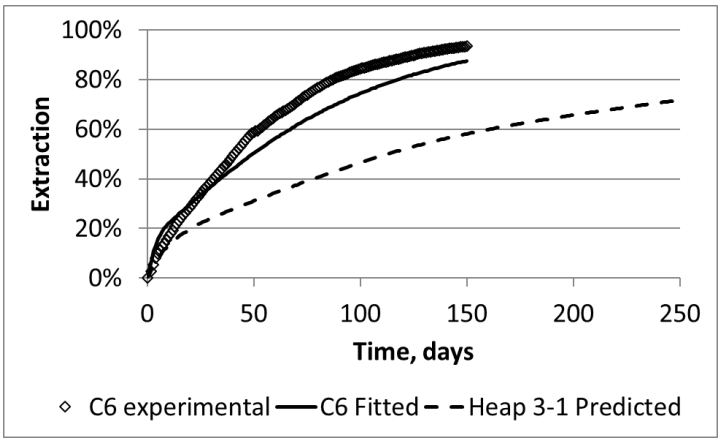

b.

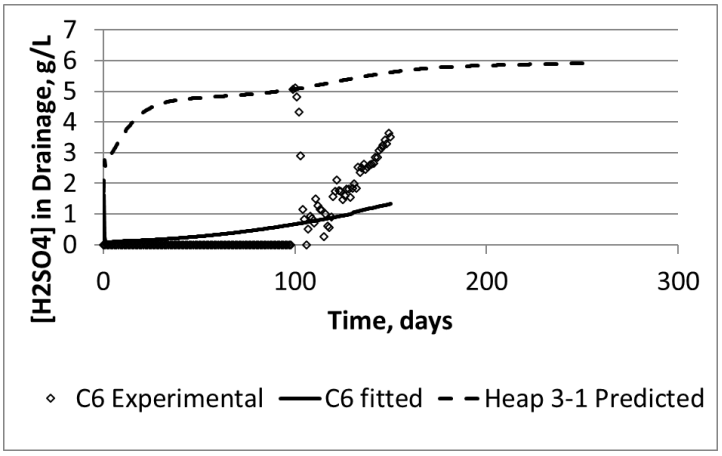

c.

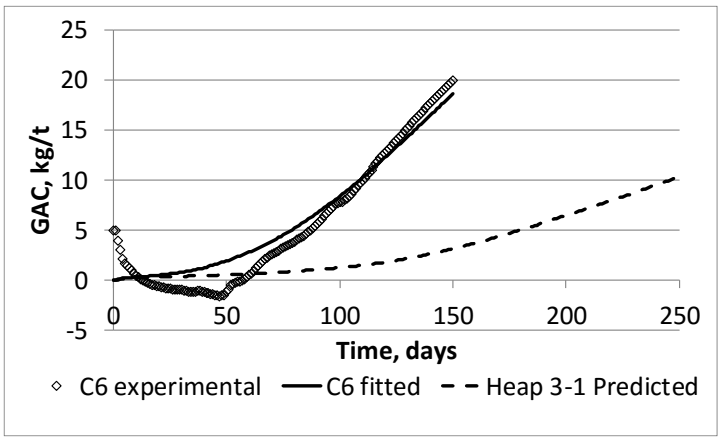

Figure 65. Heap 3-1 performance predicted by scale-up from column C6 data
(a) Rate of Cu extraction; (b) Acid concentration in drainage, (c) Rate of GAC.

This example made it evident that this scale-up procedure requires predictions about the bulk density that the heap will densify to, and the immobile moisture content that will prevail. However, that is a vast improvement over the current practice of assuming an empirical scale-up factor. Test methods exist and could probably still be futher refined for measuring the bulk density and immobile moisture content to be anticipated under the anticipated heap conditions. Furthermore, bulk density and moisture content are parameters with physical meaning and for which the possible physical bounds are known. Therefore, even if bulk density and moisture content cannot be predicted accurately, it would still be possible to predict at least the range of Transfer Times that could be possible.

15 CONCLUSIONS AND RECOMMENDATIONS

15.1 FACILITATION

This study has provided additional means for analysing heap leaching data towards more confident scale-up calculations. Firstly, a batch-from-continous technique has been developed for converting the data of simultaneous stacking and leaching operations into batch curves so that it can be modelled. Furthermore, the PhreeqC codification has been provided to make (at least chemical) heap leach modelling more accessible to those who do not have access to means for coding a model or purchasing the software. This model further facilitates the modelling of heaps in which the physical parameters vary spatially in a heap.

15.2 DIFFERENCES BETWEEN HEAP AND COLUMN LEACHING KINETICS

The model fitting of leaching kinetics obtained from the case studies, and its quantification in terms of Transfer Times, demonstrated that heap leaching kinetics is indeed consistently slower than column leaching kinetics. The longer Transfer Times consistently observed in heaps than in columns indicate that heap leaching is subject to effectively longer diffusional distances between flow channels and the mineral surfaces than in the case of column leaching. The metric used for quantifying the difference between heap leaching performance and column leaching performance is the Dimensionless Transfer Radius (DTR). A DTR>1 signifies that the effective diffusional distance of the heap is longer than that of the corresponding column and the effective leaching kinetics of the heap will be slower than that of the column accordingly.

The effectively longer diffusional distances in heaps can be ascribed to two contributing factors, namely (a) higher densification and (b) increased dripper spread in heaps, compared to columns. In the case studies investigated here, it was found that either densification or dripper spread could be governing the change in performance during scale-up, but a combination of both is not very likely. In a graph of the DTR due to densification and the DTR due to dripper spacing as a function of dripper spacing, the two graphs cross at only one single point. At dripper spacings smaller than this ‘cross-over’ value, the Densification-DTR is larger (and hence governs the diffusional distance),

and with larger dripper spacings the DTR due to dripper spacing is larger (and hence governs the diffusional distance in that regime). Densification results because the sides of heaps are not supported, hence the full weight of the ore in a heap is carried by the ore below it, as opposed to ore contained in a column where the column walls support part of the weight. Furthermore, column walls limit the possible packing arrangement of particles in the vicinity of the walls, thereby limiting the maximum density that ore can achieve in a column. This causes heaps to achieve higher bulk densities than are achieved in columns. A higher bulk density implies a reduced voidage, which in turn implies a smaller probability for the existence of connected channels via which leach solution can flow without being retained by capillary forces. Fewer flow channels means that those flow channels that do exist are spaced further apart, thereby increasing the diffusional path lengths in heaps.

Furthermore, densification causes the diffusional paths to become more tortuous which further increases the effective length of the diffusional flow paths. From the magnitude of the power p appearing in equation [87] for the Densification-DTR, it is inferred that increased tortuosity plays a far bigger role than the reduction in number of flow paths. The 'densification' parameter, defined by equation [88], appears in the expression for the Densification-DTR in equation [87] by the power of p. From the derivation of equation [87] in section 5.5.4, it can be seen that p equals the sum of 0.5 and (p-0.5). The proportion of 0.5 accounts for the reduction in number of flow paths with densification, while the balance of (p-0.5) accounts for the increase in tortuosity with densification. Where densification governed the scaled-up performance, the minimum value found for p was 4.0, meaning that the DTR increased with an increase in tortuosity by a power of at least 3.5, compared to the power of only 0.5 assigned to the effect of increased flow channel spacing.

Densification has been found to govern the heap leaching kinetics of the NICICO sulphide copper, the Rand Leases gold case study and the Barrick Gold case study. This is supported by the good correlations obtained between the DTR's found experimentally, and the DTR's calculated as a function of the densification parameter.

In the cases where the 'experimental'-DTR's could be correlated to dripper spread, the value of *p* was relatively small, suggesting that the "densification" term might be eliminated from the expression for "dripper-spacing"-DTR.

The data of the Kipoi copper case studies and of the copper segregation and stratification leaching experiments did not correlate to the DTR's calculated as a function of densification. However they did correlate to the DTR's calculated as a function of the dripper spread, as defined in Equation [90], indicating that the dripper spread was in those instances the mechanism determining the DTR's. The Rand Leases gold data did not correlate with the dripper spread function, indicating that its kinetics was governed solely by densification on the heaps. The Barrick gold application exhibited a very poor correlation to the dripper spread DTR's, suggesting that its kinetics was governed by increased densification as opposed to increase in dripper spread.

That elevated density and wide dripper spacing can retard heap leaching kinetics have been suggested by previous authors. However, the theoretical basis for this retardation has now been established by demonstrating the correlation of the heap leaching performance upon scale-up with either of the two DTR correlations developed, namely the Densification-DTR in equation [87] and the Dripper-Spread-DTR in equation [90].

In two out of the three cases governed by densification, the power *p* varied closely around 4.5, and in the two cases governed by dripper-spread, the power *p* varied closerly around 0.5, so that (p – 0.5) varied closely around zero. Therefore, it currently seems likely that the variable power *p* can be replaced by constant values of p=4.5 in cases governed by densification and (p-0.5)=0 in cases governed by dripper-spread. That stands to be verified by further case studies in future, but if found to hold more generally, equations [87] and [90]. can be simplied to respectively equations [104] and [105], from which *p* as a variable has been eliminated.

Furthermore, it has been shown that a relatively narrow dripper spacing (between 111 and 225 mm) is required to ensure that no part of the ore remains effectively out of contact with leaching solution. However, a denser distribution of drippers on the heap implies a smaller flow per dripper for a given irrigation rate. The practicality of

implementing such a narrow dripper spacing would therefore be determined by the minimum flow that can reliably be passed per dripper before the distribution of flow across all drippers on the heap surface becomes non-uniform.

Segregation and strafication have been eliminated as factors contributing to differences between column leaching and heap leaching kinetics. The experimental comparisons of the leaching kinetics of ore samples that had been carefully packed versus samples that were deliberately segregated or stratified failed to detect significant or reproducible differences in leaching kinetics. This supports the finding by Ilankoon and Neethling (2016) that even microscopic deviations from homogenous packing of ore leads to an uneven and variable distribution of flow channels in a bed of ore under percolation. That is to say, the presence or absence of segregation and/or stratification in an ore pile makes hardly any difference to the efficiency with which solution will become distributed throughout the ore mass.

Segregation has been found to negatively affect the hydraulic conductivity of an ore. It is hence recommended that hydraulic conductivity tests be performed on segregated ore fractions in order to be conservative.

Stratification has apparently assisted in somewhat wider dispersion of solution from the irrigation point, as was made evident by a larger number of drainage points on the Stratified box yielding drainage solution than on the Unstratified box. In this respect, stratification actually provided a surprisingly positive effect, whereas it was expected to have a detrimental effect on solution distribution. However, this did not lead to any significant difference in the pattern of flow channels (as observed by the staining tests), the rate or extent of extraction or reagent consumption.

Therefore the differences observed between laboratory column and commercial heap performance cannot be ascribed to either segregation or stratification to any extent. It further leads to the conclusion that laboratory testwork cannot be made more representative of the expected commercial scale heap leaching performance by either segregating or stratifying the ore in the columns prior to leaching. It also signifies that

no effort needs to be expended in devising alternative heap stacking methods in an attempt to avoid segregation and/or stratification.

15.3 HEAP LEACH SCALE-UP

This work has established means for quantifying, on a fundamental basis, the extent to which heap leaching performance would be inferior to column leaching performance. The data from a column leaching experiment on an ore can be modelled to find the Transfer Time Θ_{ref}, that characterises the column leaching kinetics. With estimates of the power p that characterises the response of tortuosity to densification, the ultimate bulk density to which the ore is likely to compact on a heap, and the intended dripper grid to be used, equations [87] and [90]. can be used to plot the anticipated Dimensional Transfer Radius (DTR = $(\Theta/\Theta_{ref})^{0.5}$) that will prevail as a result of respectively (a) the densification and (b) the increase in dripper spacing that will occur upon scale-up. An example of such a plot is shown in Figure 64 on page 248. The Transfer Time that will characterise the heap leach kinetics is then calculated as $\Theta = \Theta_{ref} \times (\text{DTR})^2$. The heap leaching kinetics can then be modelled by entering a set of input parameters that represent the Transfer Time Θ thus calculated. (Refer to section 14.8 for an example of the application of the method, and how to deal with the case where the column leaching kinetics is governed only slightly or not at all by diffusional mass transfer).

Of course the first priority should be to limit the extent to which heap leaching performance becomes inferior to column leaching performance. The specification of the conditions for agglomeration, such as type and dosage of binder, should be aimed at minimising densification and its effects during heap leaching. The ideal dripper spacing should be sufficiently small to prevent dripper spread from governing heap leaching performance, with the further constraint that is should not exceed 225 mm to ensure complete wetting of all ore with leach solution.

15.4 FUTURE RESEARCH

Challenges that remain are (a) predicting the bulk density to which ore will compact on a heap and (b) verifying the value of the parameter p that describes the response of the tortuosity of the ore to densification. The constant values for p reflected in the simplified and modified versions of the DTR's, namely equations [104] and [105], are based on only

two cases studies each, and still need to be verified by more case studies in future before adopting it with confidence. Laboratory apparatus does exist for determining (a) at laboratory scale. The method suggested by Saripalli et al. (2002) might provide a means of estimating the response of tortuosity to densification in the laboratory, if that technique can be executed on ore samples compressed to different extents.

Another topic for future research would be devising a more fundamentally-based means of predicting the gangue acid consumption rate constant, *k'*, and possibly a more realistic approach could be recommended for formulating the GAC source term in the dual porosity model. During the acid leaching of oxide ore, gangue acid consumption has a strong effect on the effective rate of value-metal extraction, due to competition for the active reagent. During the tests described in this work, *k'* always had to be obtained by fitting the model to the experimental data. In order to perform predictive modelling of anticipated heap leaching performance, being able to predict reasonably accurately a value for *k'* would be just as important as predicting values for Θ and $\alpha_x\alpha_w$.

15.5 QUALIFICATIONS

The case studies analysed here are obviously limited in number and do not include all ore types that are currently being heap leached. This is a consequence of the difficulty in making all the necessary reliable measurements at large scale to provide the data required for analysis. The considerable data rendering required in the case of the NICICO case study, which ultimately still left some uncertainties, illustrates this point. However, this study has now provided clear guidance on which information is required and how to analyse it, in order to grow the database of case studies and improve confidence in the application of the methods proposed here.

The method effectively assigns all differences between column and heap leaching kinetics to differences in the diffusional mass transfer resistance at the two scales which in turn is correlated to differences in densification and effective dripper spacing. This is not to say that the method breaks down completely if either the column, or both column and heap leaching kinetics are completely limited by slow reaction kinetics as opposed to diffusional mass transfer. The method is still valid, provided the parameters are substituted into a generic model such as HeapSim, which accounts for both kinetic and

mass transfer phenomena. All that would happen in a case where both column and heap are purely reaction-kinetics-limited due to very slow reaction-kinetics is that variation of the Transfer Time would leave the leach curve unchanged, i.e. it would predict that the heap would leach at the same (slow) rate as the column. And this would be the correct result, provided the reaction kinetic expressions are correct. But in practice a problem does arise if a Transfer Time of one or more orders of magnitude smaller than 15 days is found in the column, because (as follows from Figure 28 on page 115) any small Transfer Time would fit the data more or less equally well. While this would indicate that there is no mass transfer limitation in the column, it would not be known whether the column might be border-line mass transfer limited and that hence mass transfer might arise in the heap. Therefore, if a very small Transfer Time is recorded for the column, it would be conservative to assume a Transfer Time of 15 days for the column, upon which to base the scale up calculation for the heap.

16 REFERENCES

Afewu, K.I., 2009, Development and testing of a 2D axisymmetric water flow and solute transport model for heap leaching, PhD Thesis, University of British Columbia.

Agrawal, R.D., Kapoor, M.L., 1982. Theoretical considerations of the cementation of copper with iron. Journal of the South African Institute of Mining and Metallurgy April pp. 106-111.

Andrew, G., 2006. Overview of Quasi-Newton optimization methods, in: Nocedal, J., Wright, S.J. (Eds.), Numerical Optimization Springer Verlag.

Atkins, P.W., 1978. Physical chemistry Oxford University Press.

Bahamondez, C., Castro, R., Vargas, T., Arancibia, E., 2016. In situ mining through leaching: experimental methodology for evaluating its implementation and economic considerations. Journal of the Southern African Institute of Mining and Metallurgy vol. 116, pp. 689-698.

Bartlett, R.W., 1995. Solution Mining, Leaching and Fluid Recovery of Materials Gordon and Breach Publishers.

Bartlett, R.W., Prisbrey, K.A., 1995. Diffusion limited aeration during biooxidation of shallow ore heaps, TMS Extraction and Processing Division Symposium, 365-372.

Batchelor, 2000. Introduction to fluid dynamics.

Benito, J.G., Ippolito, I., Vidales, A.M., 2013. Novel aspects on the segregation in quasi 2D piles. Powder Technology 2134, 123-131.

Benito, J.G., Uñac, R.O., Vidales, A.M., Ippolito, I., 2014. Influence of geometry on stratification and segregation phenomena in bidimentional piles. Physica A 396, 19-28.

Bennett, C.R., McBride, D., Cross, M., Gebhardt, J.E., 2012. A comprehensive model for copper sulphide heap leaching, Part 1 Basic formulation and validation through column test simulation. Hydrometallurgy October, 127-128, 150-161.

Bikerman, D., Bikerman, M., McGrail, T., Deming, D.A., 2007. Johnson Camp mine project feasibility study. Technical Report., 234 pp.

Bingol, D., Canbazoglu, M., 2004. Dissolution kinetics of malachite in sulphuric acid. Hydrometallurgy vol. 72, pp. 159-165.

BioMinE, 2018. Reaction controlled leaching, Developed in the FP6 BioMInE project, funded by the European Union. http://wiki.biomine.skelleftea.se/biomine/leaching/letheo_03.htm.

Bouffard, S.C., 2003a, Understanding the Heap Biooxidation of Sulfidic Refractory Gold Ores, PhD Thesis, University of British Columbia.

Bouffard, S.C., 2003b, Understanding the Heap Biooxidation of Sulfidic Refractory Gold Ores, PhD Thesis Thesis, University of British Columbia.

Bouffard, S.C., 2005. Review of agglomeration practice and fundamentals in heap leaching. Mineral processing & extractive metallurgy review vol. 26, pp. 233-294.

Bouffard, S.C., 2008. Application of the HeapSim model to the heap bioleaching of the Peublo Viejo ore deposit. Hydrometallurgy 93, 116-128.

Bouffard, S.C., Dixon, D.G., 2001. Investigative Study into the Hydrodynamics of Heap Leaching Processes, Metallurgical and Material Transactions B., pp. 763 – 776.

Bouffard, S.C., Dixon, D.G., 2007. Evaluation of kinetic and diffusion phenomena in cyanide leaching of crushed and run-of-mine gold ores. Hydrometallurgy vol. 86, pp. 63-71.

Bouffard, S.C., West-Sells, P.G., 2009. Hydrodynamic behaviour of heap leach piles: Influence of testing scale and material properties. Hydrometallurgy 98, 136 – 142.

Brierley, C.L., 2001. Bacterial succession in bioheap leaching. Hydrometallurgy vol. 59, pp. 249-255.

Brooks, R.H., Corey, A.T., 1964. Hydraulic properties of porous media, Hydrology Papers Colorado state university, 37 pp.

Bryan, C.G., Davis-Belmar, C.S., Van Wyk, N., Fraser, M.K., Dew, D., Rautenbach, G.F., Harrison, S.T.L., 2012. The effect of CO2 availability on the growth, iron oxidation and CO2-fixation rates of pure cultures of *Leptospirillum Ferriphilum* and *Aciditiobacillus ferrooxidans*. Biotechnology and Bioengineering No. 7, vol. 109, pp. 1693-.

Carson, J.W., Pittenger, B.H., 1998. Bulk Properties of Powders, in: Lee, P.W., Trudel, Y., Iacocca, R., German, R.M., Ferguson, B.L., Eisen, W.B., Moyer, K., Madad, D., Sanderow, H.E. (Eds.), Powder Metal Technologies and Applications, pp. 287-301.

Chen, H., Li, Z., Wang, F., Wang, Z., Zhihan, G., 2017. Extrapolation of surface tensions of electrolyte and associating mixtures solutions. Chemical Engineering Science vol. 162, pp. 10-20.

Chetty, D., 2018. Acid-gangue interactions in heap leach operations: a review of the role of mineralogy for predicting ore behaviour. Minerals 47, 8(2), 11 pp. https://doi.org/10.3390/min8020047

Clennell, M.B., 1997. Tortuosity: a guide through the maze. Geological society special publication 122, pp. 299-344.

Corrans, I.J., Harris, B., Ralph, B.J., 1972. Bacterial leaching: an introduction to its application and theory and a study on its mechanism of operation. Journal of the Southern African Institute of Mining and Metallurgy, pp. 221-229.

Crundwell, F.K., 2014. The mechanism of dissolution of minerals in acidic and alkaline solution: Part II Application of a new theory to silicates, aluminosilicates and quartz. Hydrometallurgy Vol. 149, pp. 265-275. http://www.cm-solutions.co.za/resources/thought-leadership/dissolution/109-crundwell-the-mechanism-of-dissolution-of-minerals-in-acidic-and-alkaline-solutions-part-ii-silicates-aluminosilcates-and-quartz-hydrometallurgy/file

Crundwell, F.K., Holmes, P.R., Fowler, T.A., 2000. How do bacteria interact with minerals? Journal of the Southern African Institute of Mining and Metallurgy, pp. 399-402.

Dhawan, N., Safarzadeh, M.S., Miller, J.D., Rajamani, R.K., Moats, M.S., 2012. Insights into heap leach technology, SME Annual Meeting SME, Seattle, WA.

Dixon, D.G., 2000. Analysis of heat conservation during copper suphide heap leaching. Hydrometallurgy 58, 27-41.

Dixon, D.G., 2003. Heap leach modelling - The current state of the art, in: Young, C.A., Alfantazi, A.M., Anderson, C.G., Dreisinger, D.B., Harris, B., James, A. (Eds.), Hydrometallurgy 2003 - Fifth International Conference TMS, Vancouver, pp. 289 - 314.

Dixon, D.G., Afewu, K.I., 2011. Mathematical modelling of heap leaching under drip irrigation, Percolation Leaching: The Status Globally and in Southern Africa SAIMM, Misty Hills, Muldersdrift South Africa, 255 – 284.

Dixon, D.G., Hendrix, J.L., 1993. A mathematical model for heap leaching of one or more solid reactants from porous ore pellets. Metallurgical transactions B December, 24B, 1087 - 1102.

Dixon, D.G., Petersen, J., 2003. Comprehensive modeling study of chalcocite column and heap bioleaching, in: Riveros, P.A., Dixon, D.G., Dreisinger, D.B., Menacho, J. (Eds.), Copper 2003 - Cobre 2003, Santiago, Chile, pp. 493 - 515.

Dobek, S., 2012. Fluid dynamics and the Navier-Stokes equation, Coordinate Metrology Society Conference https://www.cs.umd.edu/~mount/Indep/Steven_Dobek/dobek-stable-fluid-final-2012.pdf.

Dreier, J., 1999. The chemistry of copper heap leaching. http://jedreiergeo.com/copper/article1/Chemistry_of_Copper_Leaching.html

Dutrizac, J.E., 1984. Plenary address: Recent advances in the leaching of sulphides and the precipitation of iron, in: Haughton, L.F. (Ed.), Proceedings of Mintek 50: International conference on minerals science and technology, Sandton, South Africa, pp. 39-62.

Dutrizac, J.E., MacDonald, R.J.C., 1974. Ferric ion as a leaching medium. Minerals Science Engineering 2, 6, 59-100.

Ethington, E.F., 1990. Interfacial contact angle measurements of water, mercury, and 20 organic liquids on quartz, calcite, biotite, and Ca-montmorillonite substrates, United States Geolocial Survey, Golden, Colorado, USA.

Fagan-Endres, M.A., Harrison, S.T.L., Johns, M.L., Sederman, A.J., 2015. Magnetic resonance imaging characterisation of the influence of flowrate on liquid distribution in drip irrigated heap leaching. Hydrometallurgy vol. 158, pp. 157-164.

Ferrier, R.J., Cai, L., Lin, Q., Gorman, G.J., Neethling, S.J., 2016. Models for apparent reaction kinetics in heap leaching: a new semi-empirical approach and its comparison to shrinking core and other particle-scale models. Hydrometallurgy vol. 166, pp. 22-33.

Geldenhuys, S.J.J., 1988. Regulatory aspects of heap leaching, in: Van Zyl, D.J.A., Hutchison, I.P.G. (Eds.), Evaluation, design and operation of heap leaching projects, Mintek, Randburg, Transvaal, South Africa, 10 pp.

Gericke, M., 2012. Review of the role of microbiology in the design and operation of heap bioleaching processes. Journal of the Southern African Institute of Mining and Metallurgy vol. 112, pp. 1005-1112.

Gericke, M., Neale, J.W., van Staden, P.J., 2009. A Mintek perspective of the past 25 years in minerals bioleaching. Journal of the South African Institute of Mining and Metallurgy vol. 109, pp. 567-585.

Gerke, H.H., Van Genuchten, M.T., 1993. A dual-porosity model for simulating the preferential movement of water and solutes in structured porous media. Water resources research no. 2, vol. 29, pp. 305-319. https://www.researchgate.net/publication/234217311_A_dual-porosity_model_for_simulating_the_preferential_movement_of_water_and_solutes_in_structured_porous_media

German, R.M., 2009. Handbook of mathematical relations in particulate materials processing.

Ghorbani, Y., Franzidis, J.P., Petersen, J., 2016. Heap leaching technology – current state, innovations and future directions: A review. Minerals Processing and Extractive Metallurgy Review vol. 37 no 2, pp. 73-119.

Ghorbani, Y., Petersen, J., Becker, M., Mainza, A.N., Franzidis, J.P., 2013. Investigation and modelling of the progression of zinc leaching from large sphalerite ore particles. Hydrometallurgy 8–23, 131–132.

Giaveno, M.A., Urbieta, M.S., Donati, E., 2011. Chapter 2: Mechanisms of bioleaching: basic understanding and possible industrial applications., in: Santos Sobral, L.G., Monteiro de Oliveira, D., Gomes de Souza, C.E. (Eds.), Biohydrometallurgical processes: A practical approach, Rio de Janeiro.

Gommes, C.J., Bons, A.J., Blacher, S., Dansmuir, J.H., Tsou, A.H., 2009a. Practical methods for measuring the tortuosity of porour materials from binary or gray-tone tomographic reconstructions. AIChE Journal 8, 55, 2000-2012.

Gommes, C.J., Bons, A.J., Blacher, S., Dansmuir, J.H., Tsou, A.H., 2009b. Practical methods for measuring the tortuosity of porous materials from binary or gray-tone tomographic reconstructions. AIChE Journal 8, 55, 2000-2012.

Gorbatenko, O., 2018. In-situ leaching method in uranium production in Kazakhstan. https://www.iaea.org/OurWork/ST/NE/NEFW/documents/RawMaterials/CD_TM_IBPinUM&P%20200810/37In-situ%20leaching%20method%20in%20uranium%20prodaction%20in%20Kazakhstan.pdf.

Gross, A.E., Gomer, J.S., 1992. Bacterial-assisted heap leaching of ores, in: USPTO (Ed.) Nalco Chemical Company, United States.

Guzman, A., 2011. Advances on Ore Characterization, Percolation Leaching: The Status Globally and in Southern Africa SAIMM, Misty Hills, Muldersdrift, Johannesburg, South Africa, 15 - 23.

Guzman, A., Scheffel, R.E., Flaherty, S.M., 2006. Geochemical Profiling Of A Sulfide Leaching Operation: A Case Study, SME Annual Meeting 2006 SME, St. Louis, 1-16.

Hackl, R.P., Dreisinger, D.B., Peters, E., King, J.A., 1995. Passivation of chalcopyrite during oxidative leachingb in sulfate media. Hydrometallurgy vol. 39, pp. 25-48.

Hohls, G., 2009. The role of enzymes, VEA Pty Ltd, 9 pp. http://www.zengermedia.com/pdf/VEA187DVG.pdf.

Holmes, P.R., Crundwell, F.K., 2000. The kinetics of the oxidation of pyrite by ferric ions and dissolved oxygen: An electrochemical study. Geochimica et cosmochimica acta 2, vol. 64, pp. 263-274.

Ilankoon, I.M.S.K., Neethling, S.J., 2016. Liquid spread mechanisms in packed beds and heaps. The separation of length and time scales due to particle porosity. Minerals Engineering vol. 86, pp. 130-139.

Jansen, M., Taylor, A., 2002. A new approach to heap leach modelling and scale-up, ALTA 2002, Perth, Australia, 18 pp.

Jansen, M., Taylor, A., 2003. Overview of Gangue Mineralogy Issues in Oxide Copper Heap Leaching, ALTA 2003 Copper - 8 Alta Metallurgical Services., Rendevous Observation City Hotel Perth, Western Australia.

John, L.W., 2011. The art of heap leaching - The fundamentals, International Conference on Percolation Leaching: The status globally and in southern Africa. Southern African Institute of Mining and Metallurgy., Misty Hills, Muldersdrift, South Africa., 17-42.

Johnson, G.K., Steele, W.V., 1981. The standard enthalpy of formation of chalcopyrite (CuFeS2) by fluorine bomb calorimitry. The Journal of Chemical Thermodynamics (10), Vol. 13, pp. 991-997. https://doi.org/10.1016/0021-9614(81)90076-8

Johnson, P.H., 1975. Thin layer leaching method, Homes & Narver Inc., Anaheim, California, USA, 24 pp. https://patentimages.storage.googleapis.com/11/f5/d8/8609fbaa338c30/US4017309.pdf.

Kappes, D.W., 2002. Precious metals heap leach design and practice, in: Mular, A.L., Halbe, D.N., Barratt, D.J. (Eds.), Mineral Processing Plant Design, Practice and Control SME, 1606 - 1630.

Kerr, E.M., 1997. Polymeric combinations used as copper and precious metal heap leaching agglomeration aids, in: WIPO (Ed.) Nalco Chemical Company.

Kinard, D.T., Schweizer, A.A., 1987. Engineering properties of agglomerated ore in a heap leach pile, in: Brawner, C.O.e. (Ed.), First international conference on gold mining Society of Mining Engineers, Littleton, Colorado (publishers), Vancouver, British Columbia, Canada, pp. 318 - 335.

Klauber, C., 2008. A critical review of the surface chemistry of acidic ferric sulphate dissolution of chalcopyrite with regards to hindered dissolution. International Journal of Mineral Processing vol. 86, pp. 1-17.

Kordosky, G.A., 2002. Copper recovery using leach/solvent extraction/electrowinning technology: Forty years of innovation, 2.2 million tonnes of copper annually. Journal of the South African Institute of Mining and Metallurgy, pp. 445-450.

Leahy, M.J., Davidson, M.R., Schwartz, M.P., 2004. A column bioleaching model for chalcocite: An investigation of oxygen limitation and bacterial inoculation on leaching., Bac-Min 2004 Conference, Bendigo, Victoria, Australia, 19 pp.

Leahy, M.J., Davidson, M.R., Schwartz, M.P., 2005. A two-dimensional CFD model for heap bioleaching of chalcocite. ANZIAM Journal vol. 46(E), pp. C439-C457.

Leahy, M.J., Davidson, M.R., Schwarz, M.P., 2007. A model for heap bioleaching of chalcocite with heat balance: Mesophiles and moderate thermophiles. Hydrometallurgy 1, January, 85, 24 - 41.

Lee, D.I., Kaguei, S., Wakao, N., 1981. Relation between adsorption equilibrium constant, fluid dispersion coefficient and intraparticle effective diffusivity in time-domain analysis of adsorption chromatophraphy curves. Journal of chemical Engineering of Japan, pp. 161-163.

Leelamanie, D.A.L., Karube, J., 2013. Soil-water contact angle as affected by the aqueous electrolyte concentration. Soil science and plant nutrition vol. 59, pp. 501-508.

Levenspiel, O., 1972. Chemical Reaction Engineering, Second Edition ed John Wiley & Sons, New York.

Lin, C.L., Miller, J.D., Garcia, C., 2005. Saturated flow characteristics in column leaching as described by LB simulation. Minerals Engineering vol. 18, pp. 1045-1051.

Lizama, H.M., Harlamovs, J.R., McKay, D.J., Dai, Z., 2004. Heap leaching kinetics are proportional to the irrigation rate divided by heap height. Minerals Engineering 18, 623-630.

Lundstrom, M., Liipo, J., Karonen, J., Aromaa, J., 2009. Dissolution of six sulfide concentrates in the Hydrocopper(R) environment., Fifth base metals conference 2009 Southern African Institute of Mining and Metallurgy, Kasane, Botswana, pp. 127-138.

Maerten, H., 2013. In-situ recovery of uranium - From environmental management and optimisation of operation to mine closure, Hotel Skalský Dvůr, Dolní Rožínka, Czech Republic. https://www.iaea.org/OurWork/ST/NE/NEFW/Technical-Areas/NFC/documents/uranium/tm-UMREG-2013/13_Maerten_ISR_enviro_mgmt_&_closure(Aust).pdf.

Mahanta, D.J., Borah, M., Saikia, P., 2014. A study on kinetic models for analysing the bacterial growth rate. American international journal of research in science, technology, engineering & mathematics 4-724, pp. 68-72. https://pdfs.semanticscholar.org/e9d3/581badc97cd3dc7b4c1866a1154567aed760.pdf

Mantra Resources Ltd, 2010. Building a mid-tier uranium producer in southern Tanzania. http://hotcopper.com.au/documentdownload?id=tuE7JrfFgm%2FOGe3lZXGZBW%2BlTE4PsV2%2BnA302YMKkqsnH7nSEIxACwpmNEmkk1NO2T8sMN9McJqnod%2FOBY4yyeEjZA%3D%3D

Marsden, J.O., Jouse, C.I., 2006. The chemistry of gold extraction.

McBride, D., Ilankoon, I.M.S.K., Neethling, S.J., Gebhardt, J.E., Cross, M., 2017. Preferential flow behaviour in unsaturated packed beds and heaps: Incorporating into a CFD model. Hydrometallurgy vol. 171, pp. 402-411.

McCarthy, D.F., 2014. Essentials of soil mechanics and foundations: Basic geotechnics, 7th ed., 847 pp.

McClelland, G.E., Van Zyl, D.J.A., 1988. Ore preparation: crushing and agglomeration, in: Van Zyl, D.J.A., Hutchison, I.P.G. (Eds.), School: Evaluation, design and operation of heap leaching projects. South African Institute of Mining and Metallurgy, Mintek, Randburg, Transvaal, South Africa, 23 pp.

Merritt, R.C., 1971. The extractive metallurgy of uranium Colorado School of Mines Research Institute.

Messerklinger, S., Bleiker, E., Zweidler, A., Springman, S.M., 2004. Displacement measurement with laser scanning in triaxial testing apparatuses. Geotechnical testing journal vol. 27(1), pp. 1-10.

Mezedur, M.M., Kaviany, M., Moore, W., 2002. Effect of pore structure, randomness and size on effective mass diffusivity. Journal of the American Institute of Chemical Engineering 1, 48, 15-24.

Miller, G., 1998. Factors controlling heap leach performance with fine and clayey ores, ALTA 1998, Perth, Australia, 24 pp.

Miller, G., 2003a. Ore Geotechnical Effects on Copper Heap Leach Kinetics, Hydrometallurgy 2003, Proceedings of the 5th International Symposium Honoring Professor Ian M. Ritchie The Minerals, Metals and Materials Society (TMS), Vancouver BC Canada, 329–342.

Miller, G.M., 2003b. Analysis of commerical heap leaching data, in: Riveros, P.A., Dixon, D., Dreisinger, D.B., Menacho, J. (Eds.), Copper 2003 - Cobre 2003, Santiago, Chile, pp. 531-545.

Muhtadi, O.A., 1988. Chapter 7: Metal extraction (recovery systems), in: Van Zyl, D.J.A., I.P.G., H. (Eds.), Evaluation, design and operation of heap leaching projects South African institute of mining and metallurgy, Mintek, Randburg, Transvaal, South Africa, 17 pp.

Muller, B., Newton, T., 2008. Look before you leach: Dynamic simulation of heap leach flowsheets, ALTA 2008, Perth, Australia.

Nimmo, J.R., Akstin, K.C., Mello, K.A., 1992. Improved apparatus for measuring hydraulic conductivity at low water content. Soil Science Society of America Journal November-December, vol. 56, pp. 1758-1761.

Nisbett, A., Baxter, K., Marte, K., Urbani, M., 2009. Flowsheet considerations for copper-cobalt projects, Base Metals Conference 2009, Kasane, Botswana.

Norgaard, H., Nygaard, L., 2014, Measurement and calculation of surface tension of oil, gas and glycol, Master of energy and environmental engineering Thesis, Norwegian university of science and technology.

Nunez, J., Zarate, G., 2011. Optimisation of vat leaching operation at Mantos Blancos division of Anglo Americal Copper, International conference on percolation leaching: the status globally and in southern Africa Southern African Institute of Mining and Metallurgy, Misty Hills, Muldersdrift, South Africa, pp. 43-52.

O'Kane, M., Barbour, S.L., Haug, M.D., 1999. A framework for improving the ability to understand and predict the performance of heap leach piles, in: Young, S.K., Dreisinger, D.B., Hackl, R.P., Dixon, D.G. (Eds.), Copper 99-Cobre 99 International Conference, pp. 409-419.

Ojumu, T.V., Petersen, J., Searby, G.E., Hansford, G.S., 2006. A review of rate equations proposed for microbial ferrous-iron oxidation with a view to application to heap bioleaching. Hydrometallurgy vol. 83, pp. 21-28.

Parkhurst, D.L., 2015. PhreeqC Interactive, Version 3.1.7.9213 ed USGS.

Parkhurst, D.L., Appelo, C.A.J., 1999. User's guide to Phreeqc (Version 2) - A computer program for speciation, batch-reaction, one-dimensional transport, and inverse geochemical calculations., U.S. Department of the Interior, U.S. Geological Survey, Denver, Colorado, 1-312.

Paynter, J.C., 1973. A review of copper hydrometallurgy. Journal of the South African Institute of Mining and Metallurgy, pp. 158-170.

Perry, R.H., Chilton, C.H., 1973. Chemical Engineers' Handbook, Fifth edition ed McGraw-Hill Kogakusha Ltd.

Petersen, J., 2010a. Determination of oxygen gas-liquid mass transfer rates in heap bioleach reactors. Minerals Engineering 23, 504-510.

Petersen, J., 2010b. Modelling of bioleach processes: Connection between science and engineering. Hydrometallurgy vol. 104, pp. 404-409.

Petersen, J., 2011. 'Speed Limits' in Heap Leaching and how to overcome them., Percolation Leaching: The Status Globally and in southern Africa SAIMM, Misty Hills, Muldersdrift, South Africa, 47 - 61.

Petersen, J., 2016. Heap Leaching as a Key Technology for Recovery of Values from Low-grade Ores – A Brief Overview. Hydrometallurgy vol. 165, pp. 206-212.

Petersen, J., Dixon, D.G., 2002. Thermophilic heap leaching of a chalcopyrite concentrate. Minerals Engineering vol. 15, pp. 777-785.

Petersen, J., Dixon, D.G., 2003a. The dynamics of chalcocite heap bioleaching, in: Young, C.A., Alfantazi, A.M., Anderson, C.G., Dreisinger, D.B., Harris, B., James, A. (Eds.), Hydrometallurgy 2003 - Fifth International Conference in Honor of Professor Ian Ritchie The Minerals, Metals & Materials Society, pp. 351-364.

Petersen, J., Dixon, D.G., 2003b. HeapSim Heap Bioleach Simulation Package Version 2.01, User Reference Manual.

Petersen, J., Dixon, D.G., 2006. Competitive bioleaching of pyrite and chalcopyrite. Hydrometallurgy vol. 83, pp. 40-49.

Petersen, J., Dixon, D.G., 2007a. Modeling and optimisation of heap bioleach processes., in: Rawlings, D.E., Johnson, D.B. (Eds.), Biomining Springer-Verlag Berlin Heidelberg, pp. 153-176.

Petersen, J., Dixon, D.G., 2007b. Modelling zinc heap bioleaching. Hydrometallurgy 85, pp. 127-143.

Potter, G.M., 1981. Design factors for heap leaching operations. Mining Engineering vol. 33, pp. 277-281.

Rademan, L., Groot, D.R., 2012. Cyanidation of reef and surface gold ores. Journal of the South African Institute of Mining and Metallurgy vol. 112, pp. 295-300.

Rawlings, D.E., Dew, D., Du Plessis, C., 2003. Biomineralization of metal-containing ores and concentrates. TRENDS in Biotechnology No. 1, vol. 21, pp. 38-44.

Readett, D., Townson, B., 1997. Practical aspects of copper solvent extraction from acidic leach liquors, ALTA Copper hydrometallurgy forum, Sheraton hotel, Brisbane, Australia, 38 pp.

Richards, L.A., 1931. Capillary conduction of liquids through porous mediums. Physics November, vol. 1, 16 pp.

Rivadenaira, J., 2011. Chapter 1: Challenges in practicing the bioleaching process, in: Santos Sobral, L.G., Monteiro de Oliveira, D., Gomes de Souza, C.E. (Eds.), Biohydrometallurgical processes: A practical approach, Rio de Janeiro.

Robertson, S.W., 2017. Development of an integrated heap leach solution flow and mineral leaching model. Hydrometallurgy vol. 169, pp. 79-88.

Roman, R.J., Benner, B.R., Becker, G.W., 1974. Diffusion model for heap leaching and its application to scale-up, Society of Mining Engineers, AIME, 247 – 252.

Roodt, J., Sandenbergh, R.F., 2003. Characterization of the leaching properties of a uranium leaching pulp. Journal of the South African Institute of Mining and Metallurgy March, pp. 111-112.

Sand, W., Gehrke, T., Jozsa, P.G., Schippers, A., 2001. (Bio)chemistry of bacterial leaching - direct vs. indirect bioleaching. Hydrometallurgy vol. 59, pp. 159-175.

Sarangi, A.K., Beri, K.K., 2000. Uranium mining by in-situ leaching, International conference on technology management for mining, processing and environment., Kharagpur, India, 8 pp.

Saripalli, K.P., Serne, R.J., P.D., M., B.P., M., 2002. Prediction of diffusion coefficients in porous media using tortuosity factors based on interfacial areas. Goundwater July-August, Vol. 40 No. 4, 346 - 352.

Scheffel, R.E., 2002. Copper heap leach design and practice, in: Mular, A.L., Halbe, D.N., Barratt, D.J. (Eds.), Mineral processing plant design, practice and control Society for mining, metallurgy and exploration Inc. (SME), Fairmont hotel, Vancouver, Canada., pp. 1571-1605.

Scheffel, R.E., Guzmán, A., Dreier, J.E., 2016. Development metallurgy guidelines for copper heap leach. Minerals & Metallurgical Processing: Special issue on process development testing No. 4, vol. 33, pp. 187-199.

Seyedbagheri, A., van Staden, P.J., McLaren, C., 2009. A study of acid-gangue reactions in heap-leach operations, HydroCopper, V International Copper Hydrometallurgy Workshop Gecamin, Antofagasta, Chile.

Shimokawa, M., Ohta, S., 2007. Dual stratification of a sand pile formed by trapped kink. Physics Letters A 366, 591-595.

Smith, E.M., 2002. Potential Problems in Copper Dump Leaching. Mining Magazine July, pp. 1-10. http://www.ausenco.com/uploads/papers/64065_Potential_Problems_in_Copper_Dump_Leaching.pdf

Stange, W., 1999. The process design of gold leaching and carbon-in-pulp circuits. Journal of the South African Institute of Mining and Metallurgy, pp. 13-26.

Stibinger, J., 2014. Examples of determining the hydraulic conductivity of soils: Theory and applications of selected basic methods, Jan Evangelista Purkyne university, faculty of the environment, 72 pp. http://envimod.fzp.ujep.cz/sites/default/files/skripta/16e_final_tisk.pdf.

Szekely, J., Themelis, N.J., 1971. Rate phenomena in process metallurgy Wiley-Interscience, New York.

Taggart, A.F., 1954. Gravity concentration, Handbook of mineral dressing John Wiley & Sons, Inc.

Tournier, E.J., Judd, E.K., 1944. Storage and Mill Transport, in: Taggart, A.F. (Ed.), Handbook of Mineral Dressing John Wiley & Sons Inc, 18-01 to 18-107.

Tournier, E.J., Judd, E.K., 1954. Storage and Mill Transport, in: Taggart, A.F. (Ed.), Handbook of Mineral Dressing John Wiley & Sons Inc, 18-01 to 18-107.

Ulrich, B., Andrade, H., Gardner, T., 2003. Lessons learnt from heap leaching operations in South America-An update. Journal of the South African Institute of Mining and Metallurgy, pp. 23-28.

Van Genuchten, M.T., 1980. A closed-form equation for predicting the hydraulic conductivity of unsaturated soils. Soil Science Society of America Journal no. 5, vol. 44, pp. 892-898.

van Genuchten, M.T., 1985. A general approach for modeling solute transport in structured soils, The 17th International Congress "Hydrogeology of Rocks of Low Permeability" International Association of Hydrogeologists, Tucson, Arizona, USA, pp. 513 - 526.

Van Genuchten, M.T., Wierenga, P.J., 1976. Mass transfer studies in sorbing porous media I. Analytical solutions. Soil Science Society of America Journal No. 4, vol. 40, pp. 473-480.

van Staden, P.J., 2011. Opening Address: Percolation leaching in southern Africa, Internation Conference on Percolation Leaching: The status globally and in southern Africa SAIMM, Misty Hills, Muldersdrift, South Africa, i - x.

van Staden, P.J., Huynh, T.D., Kiel, M.K., Clark, R.I., Petersen, J., 2017a. Comparative Assessment of Heap Leach Production Data – 2. Heap Leaching Kinetics of Kipoi HMS Floats Material , Laboratory vs. Commercial Scale. Minerals Engineering Volume 101C, Pages 58-70.

van Staden, P.J., Kolesnikov, A.V., Petersen, J., 2017b. Comparative Assessment of Heap Leach Production Data – 1. A Procedure for Deriving the Batch Leach Curve. Minerals Engineering Volume 101C, pp. 47-57.

van Staden, P.J., Laxen, P.A., 1988. Process Options for the Retreatment of Gold-Bearing Sand Sumps. Journal of the Southern African Institute of Mining and Metallurgy No. 8., vol. 88, pp. 257-264.

van Staden, P.J., Naseri, A., Petersen, J., 2017c. HeapSim modelling of high temperature heap bioleaching data, ALTA 2017 Conference and Exhibition, Pan Pacific Hotel, Perth, Western Australia, pp. 210-246.

Van Staden, P.J., Petersen, J., 2018a. The Effects of Simulated Stacking Phenomena on the Percolation Leaching of Crushed Ore, Part 1: Segregation. Minerals Engineering vol. 128, pp. 202-214.

van Staden, P.J., Petersen, J., 2018b. First order exchange and spherical diffusion models of heap leaching in PhreeqC. Journal of the Southern African Institute of Mining and Metallurgy In Press.

Van Staden, P.J., Petersen, J., 2019. The Effects of Simulated Stacking Phenomena on the Percolation Leaching of Crushed Ore, Part 2: Stratification. Minerals Engineering vol. 131, pp. 216-229.

Van Tonder, D., Edwards, C., 2012. Strong acid versus ammonia strip in uranium SX circuits, ALTA 2012 uranium conference, Burswood convention centre, Perth, Australia, pp. 38-53.

Wagner, A.J., 2008. A practical introduction to the Lattice Botzmann method, Department of physics, North Dakota State University.

Walsh, D., Lancaster, T., James, B., 1997. Recent developments at the Girilambone heap leach-SX/EW operation, Alta 1997, Sheraton Hotel, Brisbane, Australia, 17 pp.

Watling, H.R., 2006. The bioleaching of sulphide minerals with emphasis on copper sulphides. Hydrometallurgy pp. 81-108, vol. 84.

Weast, R.C., Astle, M.J., 1980. CRC Handbook of Chemistry and Physics, 61st ed CRC Press, Inc.

Weissenborn, P.K., Pugh, R.J., 1996. Surface tension of aqueous solutions of electrolytes: Relationship with ion hydration, oxygen solubility, and bubble coalescence. Journal of colloid and interface science vol. 184, pp. 550-563.

West, 2018. Elementary soil mechanics, School of Engineering, University of Connecticut, 21 pp. http://www.engr.uconn.edu/~lanbo/G229Lect06052SoilMech3.pdf.

Williams, T., Gunn, M.J., Jaffer, A., Harvey, P., Tittes, P., 2018 (accessed). The application of Geobiotics, LLC's Geocoat(R) technology to the bacterial oxidation of a refractory arsenopyrite gold concentrate, 10 pp. https://www.911metallurgist.com/blog/wp-content/uploads/2015/10/BACTERIAL-OXIDATION-OF-A-REFRACTORY-ARSENOPYRITE-GOLD-CONCENTRATE.pdf.

Wu, A., Liu, J., Yin, S., Wang, H., 2010. Analysis of coupled flow-reaction with heat transfer in heap bioleaching processes. Applied mathematics and mechanics (English Edition) 12, vol. 31, pp. 1473-1480.

Wu, A., Yin, S., Yang, B., Wang, J., Qui, G., 2007. Study on preferential flow in dump leaching of low-grade ores. Hydrometallurgy 87, pp. 124-132.

Wyethe, J.P., Vegter, N.M., Rordriques, J.M.S., 2008. Recent recovery improvement initiatives at Zincor: the use of zinc oxide fume and low-ferrite calcine for iron removal to reduce un-dissolved zinc losses, International symposium on lead and zinc processing Southern African Institute of Mining and Metallurgy, Cruiseliner symposium, 'The Melody', Durban Harbour, 12 pp.

Yang, B., Kang, Y., You, L., Li, X., Chen, Q., 2016. Measurement of the surface diffusion coefficient for adsorbed gas in the fine mesopores and micropores of shale organic matter. Fuel vol. 181, pp. 793-804.

Zalc, J.M., Reyes, S.C., Iglesia, E., 2004. The effects of diffusion mechanism and void structure on transport rates and tortuosity factors in complex porous structures. Chemical Engineering Science vol. 59, pp. 2974-2960.

APPENDIX A. SIMPLIFIED EXAMPLE OF HEAP SPECIFICATION

Authors such as Kappes (2002) and John (2011) provide generic information from which the following scenario can be sketched. A key design criterion for any metal production plant is the steady-state metal production rate, $\dot{W}_{metal}$ [t/d]. Assuming a constant rate of mining, stacking and leaching and constant ore grade, this can be calculated as:

$$\dot{W}_{metal} = \dot{W}_{ore}\, C^0_{metal}\, X_i(t_{final}) \qquad [108]$$

where $\dot{W}_{ore}$ [$^{t\_ore}/_{d}$] is the rate at which ore is stacked, C^0_{metal} [$^{t\_metal}/_{t\_ore}$] is the metal grade in the unreacted ore, $X_i(t_{final})$ [$^{t\_extracted}/_{t\_metal}$] is the final extent of extraction to be obtained from the heap over its life cycle of duration t_{final}.

Laboratory column leaching test results provide the design engineer with the data from which to derive (after applying empirical scale-up factors) the expected batch curve for the commercial scale heaps, as a function $X_i(t)$ with t being time [d] for the period $0 \le t \le t_{final}$. Authors such as Jansen and Taylor (2002) and John (2011) suggest that the ultimate extent of extraction obtained in the laboratory could be multiplied by 0.8 to 0.9, and/or the time required for achieving the ultimate extraction under commercial conditions is taken as 50 to 200 percent more than the time required in the laboratory columns.

The pad capacity [tonne ore] is the product of the stacking rate and the required leach residence time t_{final}, namely:

$$\text{pad capacity [tonne ore]} = A \cdot H \cdot \rho = t_{final} \cdot \dot{W}_{ore} \qquad [109]$$

where A is the pad footprint area [m^2], H is the average stacking height and ρ is the ore bulk density on a dry basis [t/m^3]. In the formulation of [109], it is assumed that all ore spends exactly a duration of t_{final} under irrigation, after which it is either removed from the pad or over-lain with a new lift. In practice the first ore to be stacked on a heap could continue to be irrigated until the last ore on the heap has been exhausted, in which case the various cells would be subjected to different leach times. Furthermore, for simplicity only the leach duration is considered in t_{final} in [109]; in practice additional residence

time t_{prep} should be added to it to account for the additional non-productive residence time required for stacking, irrigation installation, rinsing, etc.

Given $\dot{W}_{metal}$, C^0_{metal} and $X_i(t_{final})$, the design engineer can calculate $\dot{W}_{ore}$ from [108] and with knowledge of ρ (from geomechanical tests) and t_{final} the combination of $A.H$ can be calculated from [109]. Both the $X_i(t_{final})$ and t_{final} are obtained from the design batch curve.

From [109] it can be seen that increasing t_{final} leads to an increase in the combination of $A.H$ required (and therefore in the capex for pad construction), although according to [108] it yields a larger metal production rate (by increasing $X_i(t_{final})$) for a given stacking rate. The optimal choice for t_{final} and $X_i(t_{final})$ therefore requires economic consideration.

APPENDIX B. SUMMARY OF THE DATA PUBLISHED BY MILLER (2003)

Data per individual heap or column

	Operation	Scale	Top-size	W_{imm}	θ_{imm}	Bulk density	R_{eff}
			mm	m-frac	vol-frac	t/cum	mm
	B	Heap	8	0.140	0.269	1.65	121
	B	Heap	8	0.140	0.275	1.69	94
	B	Heap	8	0.140	0.290	1.78	137
	B	Heap	8	0.140	0.285	1.75	101
	B	Heap	8	0.140	0.275	1.69	115
	B	Heap	8	0.140	0.238	1.46	151
	B	Heap	8	0.140	0.241	1.48	115
	B	Heap	8	0.140	0.249	1.53	84
	B	Heap	8	0.140	0.269	1.65	115
	B	Heap	8	0.140	0.301	1.85	111
Avg	B	Heap	8	0.140	0.269	1.65	114
Min	B	Heap	8	0.140	0.238	1.46	84
Max	B	Heap	8	0.140	0.301	1.85	151
	C	Heap	25	0.120	0.218	1.60	95
	C	Heap	25	0.120	0.218	1.60	121
	C	Heap	25	0.120	0.205	1.50	60
Avg	C	Heap	25	0.120	0.214	1.57	92
Min	C	Heap	25	0.120	0.205	1.50	60
Max	C	Heap	25	0.120	0.218	1.60	121
	F	Heap	19	0.062	0.100	1.51	80
	F	Heap	19	0.099	0.167	1.52	74
	F	Heap	19	0.080	0.138	1.59	64
	F	Heap	19	0.080	0.140	1.61	57
	F	Heap	19	0.080	0.129	1.49	59
	F	Heap	19	0.080	0.139	1.60	52
	F	Heap	19	0.080	0.132	1.52	58
	F	Heap	19	0.080	0.131	1.51	41
	F	Heap	19	0.080	0.130	1.50	54
	F	Heap	19	0.080	0.132	1.52	46
	F	Heap	19	0.080	0.124	1.43	44
	F	Heap	19	0.080	0.132	1.52	61
	F	Heap	19	0.080	0.131	1.51	41
	F	Heap	19	0.080	0.125	1.43	71
	F	Heap	19	0.080	0.120	1.38	55
	F	Heap	19	0.080	0.116	1.33	59
	F	Heap	19	0.080	0.120	1.38	57
	F	Heap	19	0.080	0.119	1.37	54
	F	Heap	19	0.080	0.117	1.34	40

	Operation	Scale	Top-size	W_{imm}	θ_{imm}	Bulk density	R_{eff}
			mm	m-frac	vol-frac	t/cum	mm
	F	Heap	19	0.080	0.119	1.37	41
	F	Heap	19	0.080	0.122	1.41	44
	F	Heap	19	0.080	0.119	1.37	72
	F	Heap	19	0.080	0.120	1.38	47
	F	Heap	19	0.080	0.119	1.37	62
Avg	F	Heap	19	0.080	0.127	1.46	56
Min	F	Heap	19	0.062	0.100	1.33	40
Max	F	Heap	19	0.099	0.167	1.61	80
variance	F						12
95% confidence interval	F						31.4 - 79.6
	G	Heap	25	0.140	0.219	1.35	115
	G	Heap	25	0.140	0.302	1.86	152
	G	Heap	25	0.140	0.174	1.07	60
	G	Heap	25	0.140	0.293	1.80	127
	G	Heap	25	0.140	0.223	1.37	49
	G	Heap	25	0.140	0.233	1.43	44
	G	Heap	25	0.140	0.282	1.73	75
	G	Heap	25	0.140	0.267	1.64	77
	G	Heap	25	0.140	0.197	1.21	158
Avg	G	Heap	25	0.140	0.243	1.49	95
Min	G	Heap	25	0.140	0.174	1.07	44
Max	G	Heap	25	0.140	0.302	1.86	158
	H	Heap	25	0.080	0.163	1.87	135
	H	Heap	25	0.080	0.152	1.75	157
	H	Heap	25	0.080	0.147	1.69	218
Avg	H	Heap	25	0.080	0.154	1.77	170
Min	H	Heap	25	0.080	0.154	1.77	170
Max	H	Heap	25	0.080	0.154	1.77	170
	D	Column	25	0.160	0.253	1.33	51
	D	Column	25	0.182	0.272	1.22	43
	D	Column	25	0.224	0.300	1.04	60
	D	Column	25	0.224	0.300	1.04	94
Avg	D	Column	25	0.198	0.281	1.16	62
Min	D	Column	25	0.160	0.253	1.04	43
Max	D	Column	25	0.224	0.300	1.33	94
	E	Column	25	0.100	0.191	1.72	51
	E	Column	25	0.132	0.290	1.91	30
Avg	E	Column	25	0.116	0.241	1.82	41
Min	E	Column	25	0.100	0.191	1.72	30
Max	E	Column	25	0.132	0.290	1.91	51

Summary of averages per operation

Operation	Scale	Average bulk density t/cum	Average R_{eff} mm
B	Heap	1.65	114
C	Heap	1.57	92.0
F	Heap	1.46	55.5
G	Heap	1.49	95.2
H	Heap	1.77	170
D	Column	1.16	62.0
E	Column	1.82	40.5

APPENDIX C. DERIVATION OF CONTINUITY EQUATIONS FOR DIFFUSION WITH CHEMICAL REACTION

To illustrate how seemingly different formulations can come about from analyses of the same system, two examples of different (yet equally valid) derivations are offered here. Particular attention needs to be paid to the sets of units employed during the different derivations. Therefore, to always distinguish between length or volume of the entire spherical bed versus that of the solution, the unit measures are allocated footnotes that refer to the relevant phase, (be it immobile solution or bed).

First approach: Considering the entire porous spherical volume shown in Figure 66 below on page 277 with radius *R*. The solid, solution and gaseous phases are considered together as a single continuum bed (denoted *bed*), possessing an effective diffusivity D_e (with units of m^2_{bed}/s) and holding a concentration *C'* in units of [mole-i /m^3 bed], of a dissolved species.

The volume fraction of immobilised solution is θ_{imm} and the initial concentration of species *i* in the solid phase is C_i^0.

At a given time *t* in a spherical element of thickness Δr at radial position *r* within the space, species *i* is being converted from the solid to the solution phase at rate $\dot{X}$ $\left[\frac{\text{mole } i \text{ into solution phase}}{\text{mole } i \text{ in solids at } t=0}\right]\left[\frac{1}{\text{s}}\right]$, which is used to calculate the 'source term' (*s*):

$$s = 1000 \dot{X} C_i^0 \qquad [110]$$

$$\left[\frac{\text{mole}}{\text{m}^3_{\text{imm}}.\, s}\right] \equiv \left[\frac{\text{L}_{\text{imm}}}{\text{m}^3_{\text{imm}}}\right]\left[\frac{\text{mole}}{\text{mole}|_{\text{t=0}}\ \text{s}}\right]\left[\frac{\text{mole}|_{\text{t=0}}}{\text{L}_{\text{imm}}}\right]$$

A mass balance over the incremental time period *Δt* yields:

$$(4\pi r^2)(C'|_{t+\Delta t} - C'|_t)\Delta r = D_e(4\pi r^2)\left(\left.\frac{\partial C'}{\partial r}\right|_{r+\Delta r} - \left.\frac{\partial C'}{\partial r}\right|_r\right)\Delta t + 1000\dot{X}\, C_i^0 \theta_{imm}(4\pi r^2 \Delta r \Delta t) \qquad [111]$$

$$\left[\frac{\text{m}^3_{\text{bed}}}{1}\right]\left[\frac{\text{mole}}{\text{m}^3_{\text{bed}}}\right] \equiv \left[\frac{\text{m}^2_{\text{bed}}}{\text{s}}\right]\left[\frac{\text{m}^2_{\text{bed}}}{1}\right]\left[\frac{\text{mole}}{\text{m}^4_{\text{bed}}}\right]\left[\frac{\text{s}}{1}\right] \qquad \left[\frac{\text{L}_{\text{imm}}}{\text{m}^3_{\text{imm}}}\right]\left[\frac{\text{mole}}{\text{mole}|_{\text{t=0}}\ \text{s}}\right]\left[\frac{\text{mole}|_{\text{t=0}}}{\text{L}_{\text{imm}}}\right]\left[\frac{\text{m}^3_{\text{imm}}}{\text{m}^3_{\text{bed}}}\right]\left[\frac{\text{m}^3_{\text{bed}}}{1}\right]\left[\frac{\text{s}}{1}\right]$$

with effectively units of [mole].

Re-arrangement and differentiation yields:

$$\frac{\partial C'}{\partial t} = D_e\left[\frac{\partial^2 C'}{\partial r^2} + \frac{2}{r}\frac{\partial C'}{\partial r}\right] + 1000 \;.\; \dot{X} \;.\; C_i^0 \;.\; \theta_{imm} \qquad [112]$$

$$\left[\frac{\text{mole}}{\text{m}_{\text{bed}}^3}\right]\left[\frac{1}{s}\right] \equiv \left[\frac{\text{m}_{\text{bed}}^2}{\text{s}}\right]\left[\frac{\text{mole}}{\text{m}_{\text{bed}}^5}\right] \qquad \left[\frac{\text{L}_{\text{imm}}}{\text{m}_{\text{imm}}^3}\right]\left[\frac{\text{mole}}{\text{mole}|_{\text{t=0}}\ \text{s}}\right]\left[\frac{\text{mole}|_{\text{t=0}}}{\text{L}_{\text{imm}}}\right]\left[\frac{\text{m}_{\text{imm}}^3}{\text{m}_{\text{bed}}^3}\right]$$

with effectively units of $\left[\frac{\text{mole}}{\text{m}_{\text{bed}}^3\ s}\right]$

Equation [112] can be re-written in terms of concentration in the immobile solution *C* [mole-i /m^3_{imm}] by substitution of:

$$C' = \theta_{imm} C$$

to yield after division throughout by θ_{imm} the form used by Parkhurst (2015) in Example 13c (except that his formulation did not contain the source term since he did not consider chemical reaction):

$$\frac{\partial C}{\partial t} = D_e\left[\frac{\partial^2 C}{\partial r^2} + \frac{2}{r}\frac{\partial C}{\partial r}\right] + 1000\dot{X}\, C_i^0 \qquad [113]$$

with effectively units of $\left[\frac{\text{mole}}{\text{m}_{\text{imm}}^3\ s}\right]$.

It is also the form used in equation 8-8 of Petersen and Dixon (2007a), albeit with a somewhat different source term due to a different set of units being employed.

The equation is second-order with respect to radial position *r* and first-order with respect to time *t*, hence requires two boundary conditions for radial position and one boundary condition for time. These are namely (a) the concentration in the soluble species is zero at all radial positions at time *t*=0; (b) the concentration gradient is zero at the origin of the sphere and (c) at the outer boundary, where *r*=*R*, the concentration of the dissolved species equals that of the mobile solution at the given vertical location and time, (Petersen and Dixon, 2007b).

$$C_{i,imm}(r,0) = 0; \quad \left.\frac{\partial C_{i,imm}}{\partial r}\right|_{r=0} = 0; \quad \text{and} \quad C_{i,imm}(R,t) = C_{i,mob} \qquad [114]$$

For the solution of the continuity equation for the mobile solution flowing vertically (i.e. the solution at the outer surface of the immobile spheres where *r=R*), consider the space shown in Figure 66, situated at vertical position z below the upper surface of the heap, of incremental height *Δz,* over time step *Δt*,

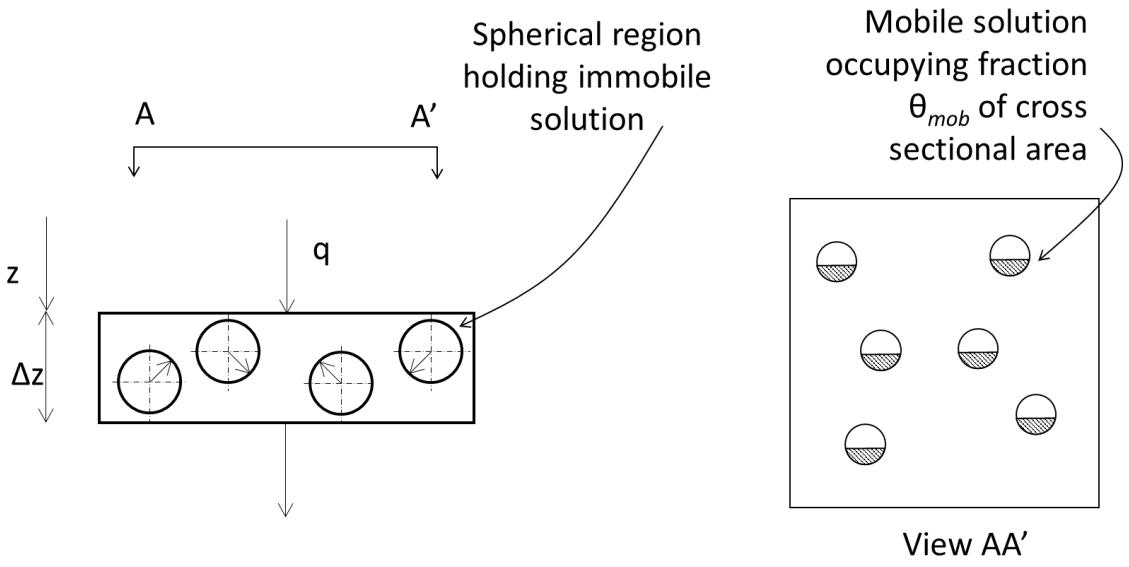

Figure 66. Visualisation of mobile solution flow

Mobile solution (denoted *mob*) arrives at position *z*, and departs at position *z+Δz*, at a volumetric flux equalling the irrigated flux of *q* [$m^3_{mob}/(s.m^2_{bed})$]. The volume fraction of the bed that is occupied by mobile solution is θ_{mob}, which equals the fraction of the cross sectional area of mobile porosity via which the mobile solution passes. (Hence the smaller θ_{mob}, the higher the velocity with which the mobile solution passes vertically down the bed).

If the heap bulk density is *ρ* and its height is *H*, then the mass of ore equals *ρ.H* kg per m^2 cross sectional area of bed. The mass of ore in a single spherical immobile zone of radius *R* is $4\rho\pi R^3/3$ kg. Over the height of the heap, the number of immobile spheres (N_H) existing per m^2 of bed must be such that their total mass also equals *ρ.H*, therefore:

$$N_H.\frac{4}{3}\,\rho\,\pi R^{\,3} = \rho\,H$$

From which follows that the number of immobile spheres $N_{\Delta z}$ with which the mobile solution in the vertical element Δz is exchanging soluble species is, per m^2 of bed, is:

$$N_{\Delta z} = \frac{3\,H}{4\pi R^{3}}\,\Delta z$$

Hence the rate at which soluble species diffuse into the mobile zone Δz from the immobile spherical zones, per m^2 of bed, is:

(number of spheres per length Δz) x (outer surfpace area per sphere)

x (effective diffusivity) x (negative of concentration gradient at $r=R$)

$$= -\left(\frac{3\,H}{4\pi R^{3}}\right)(4\pi R^{2})(D_e)\left.\frac{\partial C}{\partial r}\right|_{r=R}\Delta z = -3\frac{D_e}{R}\left.\frac{\partial C}{\partial r}\right|_{r=R}\Delta z$$

For a cross sectional area of 1m^2 of bed, the mass balance is:

[moles in element Δz at time $t+\Delta t$]= [moles in element Δz at time t]
+ [moles flowing in at position z over time increment Δt]
- [moles flowing out at position $z+\Delta z$ over time increment Δt]
[diffusing from the immobile spheres over time increment Δt]

$$\theta_{mob}(1)\Delta z C_{t+\Delta t} = \theta_{mob}(1)\Delta z C_t + q(1)(C_z - C_{z+\Delta z})\Delta t - 3\frac{D_e}{R}(1)\theta_{imm}\left.\frac{\partial C}{\partial r}\right|_{r=R}\Delta z\Delta t$$

$$\left[\frac{m^3_{mob}}{m^3_{bed}}\frac{m^2_{bed}}{1}\frac{m_{bed}}{1}\frac{mole}{m^3_{mob}}\right] \equiv \left[\frac{m^3_{mob}}{m^2_{bed}.s}\right]\left[\frac{m^2_{bed}}{1}\right]\left[\frac{mole}{m^3_{mob}}\right]\left[\frac{s}{1}\right]$$

$$\equiv \left[\frac{m^2_{bed}}{s.m_{bed}}\right]\left[\frac{m^2_{bed}}{1}\right]\left[\frac{m^3_{imm}}{m^3_{bed}}\right]\left[\frac{mole}{m^3_{imm}m_{bed}}\right]\left[\frac{m_{bed}}{1}\right]\left[\frac{s}{1}\right]$$

with effectively units of [moles] for each term.

Division throughout by $\Delta z.\Delta t.\theta_{mob}$ and noting that the mobile solution concentration represents the solution concentration at the outer surface of the immobile spheres, where $r=R$, yields:

$$\left.\frac{\partial C}{\partial t}\right|_{r=R} + \frac{q}{\theta_{mob}}\left.\frac{\partial C}{\partial z}\right|_{r=R} = -3\frac{D_e}{R}\frac{\theta_{imm}}{\theta_{mob}}\left.\frac{\partial C}{\partial r}\right|_{r=R} \quad [115]$$

This form was used by Petersen and Dixon (2007b) with some slight modifications. Their mobile solution fraction was expressed as a mass percentage, as opposed to the volume-percentage used here. Therefore, their second term also contains the heap bulk density to include the required relation between mass and volume. Further, what appears here as D_e appears in their equation as free diffusivity divided by effective tortuosity, $^{D}/\tau$.

Second approach: Considering only the immobile solution phase (as opposed to the porous zone as a whole) in a pore of length R^*, possessing free diffusivity D and concentration C in the solution phase of species i. The effective length of the pore in which the immobile solution is held is $R^*=\tau^2 R$ and the concentration of dissolved species i in it being C. The volume of immobile solution is smaller than the volume of the entire spherical space within which it is contained by a factor of θ_{imm}, and the same applies to the pore-area in the plane perpendicular to the direction of diffusion across which diffusion occurs. The concentration gradient acting as driving force for diffusion is smaller than in the first case considered above by the factor whereby the length R^* of the diffusional path is longer than the radius R, which is τ^2. The mass balance becomes:

$$\begin{aligned}(\theta_{imm}4\pi r^2)(C|_{t+\Delta t} - C|_t)\Delta r \\ = \frac{D}{\tau^2} \quad (\theta_{imm}\ 4\pi r^2) \quad \left(\left.\frac{\partial C}{\partial r}\right|_{r+\Delta r} - \left.\frac{\partial C}{\partial r}\right|_r\right)\Delta t \\ + 1000\dot{X}\, C_i^0\theta_{imm}(4\pi r^2\Delta r)\Delta t\end{aligned} \quad [116]$$

$$\left[\frac{\mathrm{m}^3_{imm}}{1}\right]\left[\frac{\mathrm{mole}}{\mathrm{m}^3_{\mathrm{imm}}}\right] \equiv \left[\frac{\mathrm{m}^2_{imm}}{\mathrm{s.[units\ of}\ \tau^2]}\right]\left[\frac{\mathrm{m}^3_{imm}}{m^3_{bed}}\right]\left[\frac{m^2_{bed}}{1}\right]\left[\frac{\mathrm{mole}}{\mathrm{m}^3_{imm}m_{bed}}\right]\left[\frac{\mathrm{s}}{1}\right]$$

$$[\mathrm{mole}] \equiv \left[\frac{\mathrm{mole}}{[\mathrm{units\ of}\ \tau^2]}\right]\left[\frac{\mathrm{m}^2_{imm}}{m^2_{bed}}\right]$$

In the formulation above, specification of the units of τ^2 (referred to in the discussion above on effective diffusivity), is reserved until the dimensions of the final terms left and right of the equal sign can be compared. From the comparison of the resulting sets of units, it follows that the units of τ^2 must be:

$$\left[\frac{\mathrm{m}^2_{imm}}{m^2_{bed}}\right]$$

The dimensions of the source term remain the same as in [111] and are not repeated here.

Re-arrangement prior to the elimination of θ_{imm}, leads to:

$$\theta_{imm}\frac{\partial C}{\partial t} = \frac{\theta_{imm}D}{\tau^2}\left(\frac{1}{r^2}\frac{\partial}{\partial r}\left(r^2\frac{\partial C}{\partial r}\right)\right) + 1000\dot{X}\,\theta_{imm}C_i^0 \quad [117]$$

which is the form encountered in Bouffard (2003a), page 67, equation 3-10, for diffusion in a spherical space.

This can be further differentiated and θ_{imm} can be eliminated throughout to yield:

$$\frac{\partial C}{\partial t} = \frac{D}{\tau^2}\left[\frac{\partial^2 C}{\partial r^2} + \frac{2}{r}\frac{\partial C}{\partial r}\right] + 1000\dot{X}\,C_i^0 \quad [118]$$

This is the form used by Petersen and Dixon (2007b), it facilitates the use of free diffusivity *D* which is known for many species in aqueous solution, yet it still requires the tortuosity factor τ^2 to account for the tortuous diffusional path being longer than the radius of the sphere. It will yield exactly the same result as [113] as long as the respective model parameters are calibrated such that

$$D_e = \frac{D}{\tau^2} \quad [119]$$

The continuity equation for the mobile solution flowing vertically will be the same as [115], except that the above substitution should be made for D_e.

APPENDIX D. FITTING OF RAND LEASES FREE MILLING GOLD EXTRACTION PERFORMANCE

a. b.

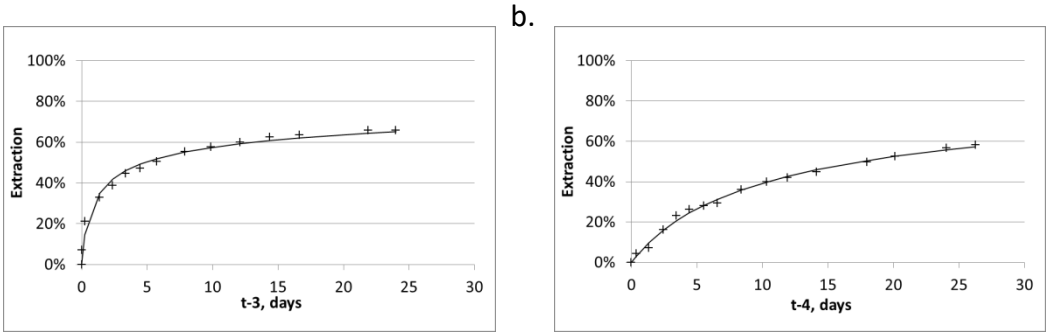

Figure 67. Batch curve fits to extrapolate maximum extent of extraction.
(a) Column, (b) Heap

Notes: For the column and heap there were 3 and 5-day delays between the onset of irrigation and appearance of first gold in drainage solution, hence for (a) time (t-3) is taken as time-zero, and for (b) (t-4) is taken as time-zero.

APPENDIX E. FITTING OF KIPOI OXIDE COPPER LEACHING

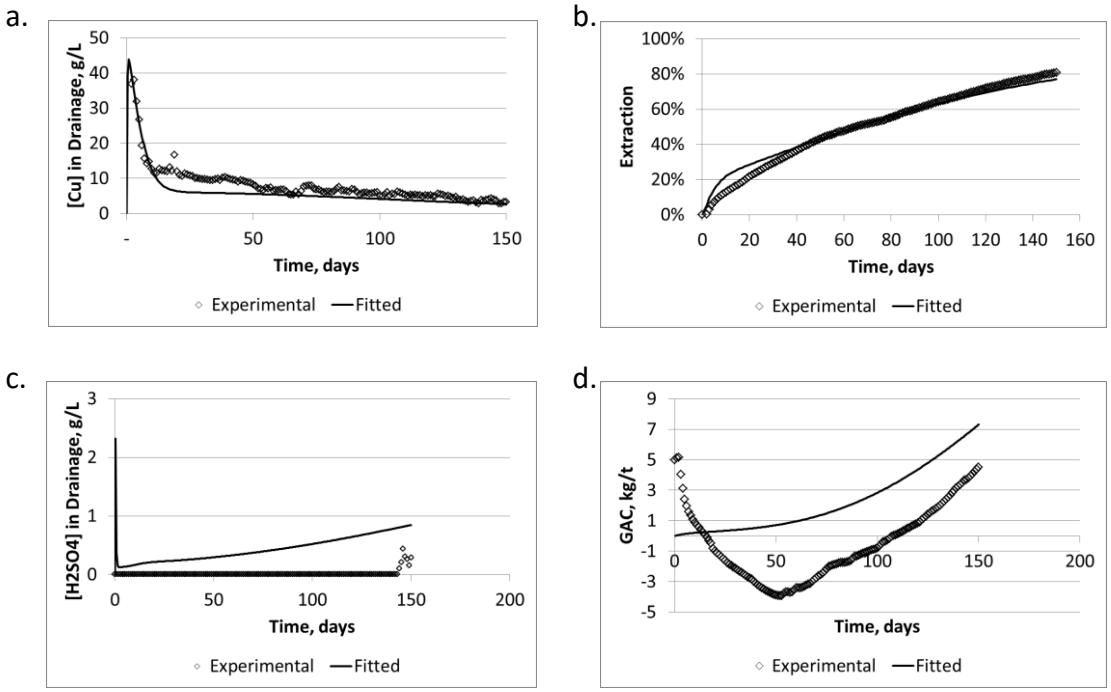

Figure 68. Fitting of LBC for Column C5

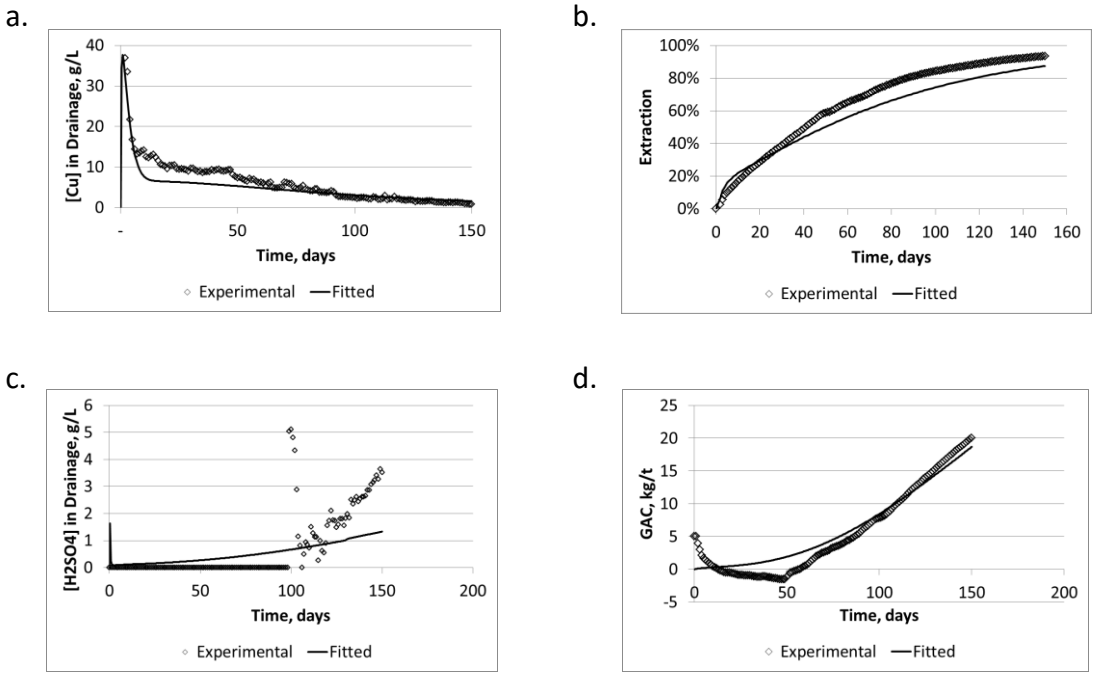

Figure 69. Fitting of LBC for Column C6

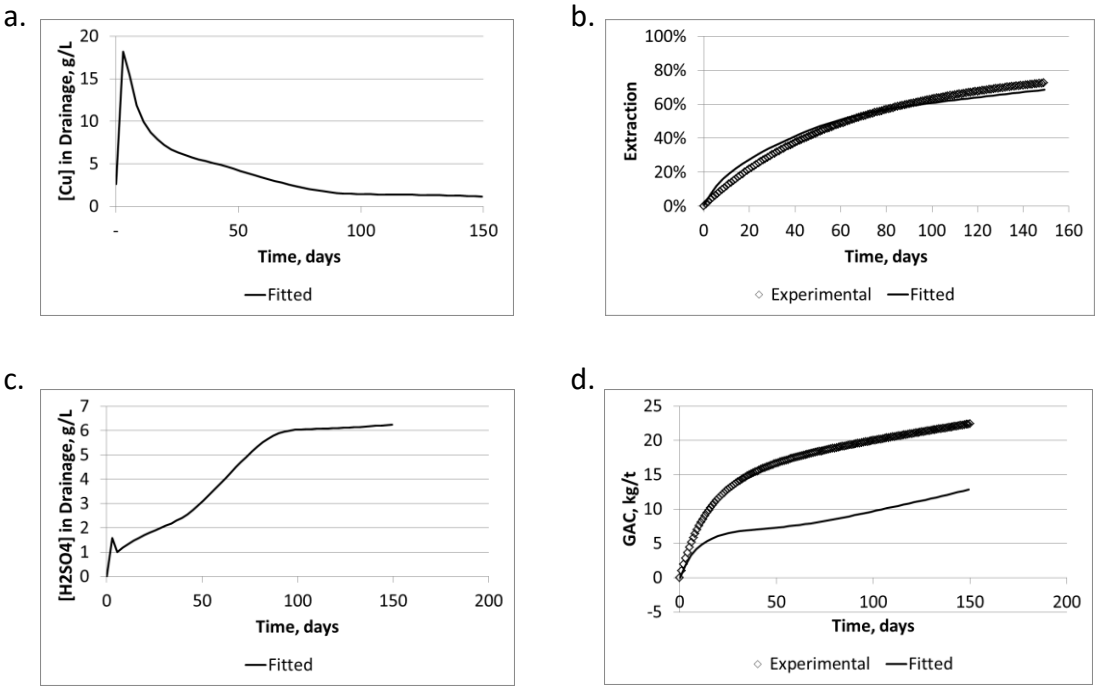

Figure 70. Fitting of FBC for Kipoi heap 1-1

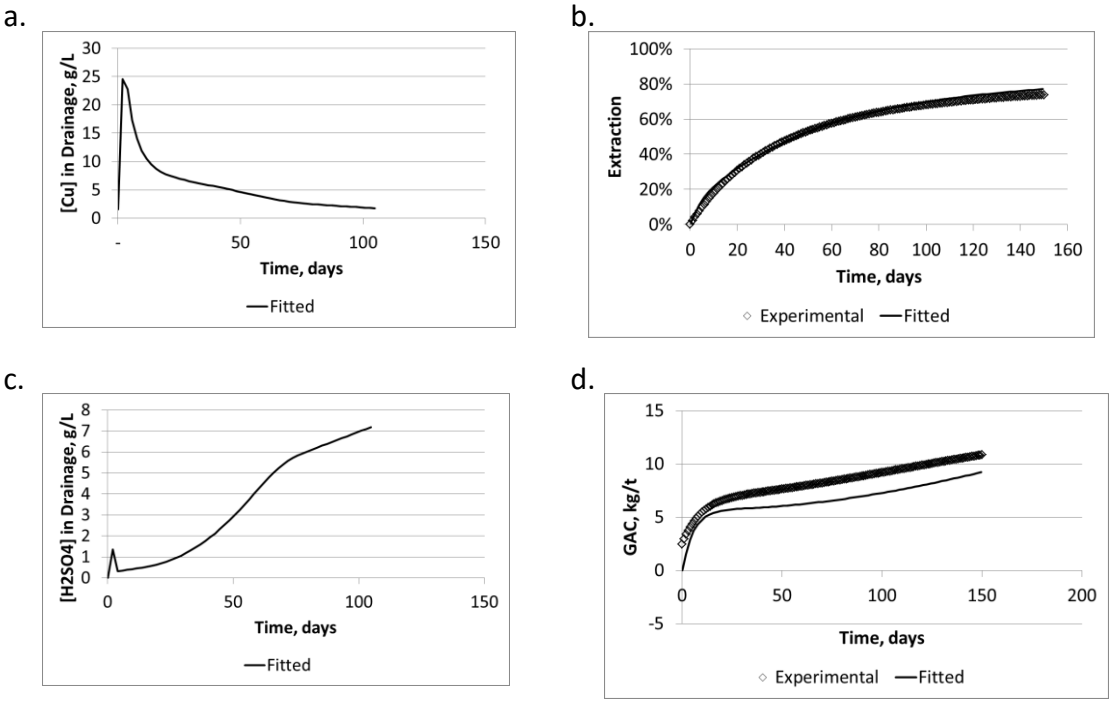

Figure 71. Fitting of FBC for Kipoi heap 2-1

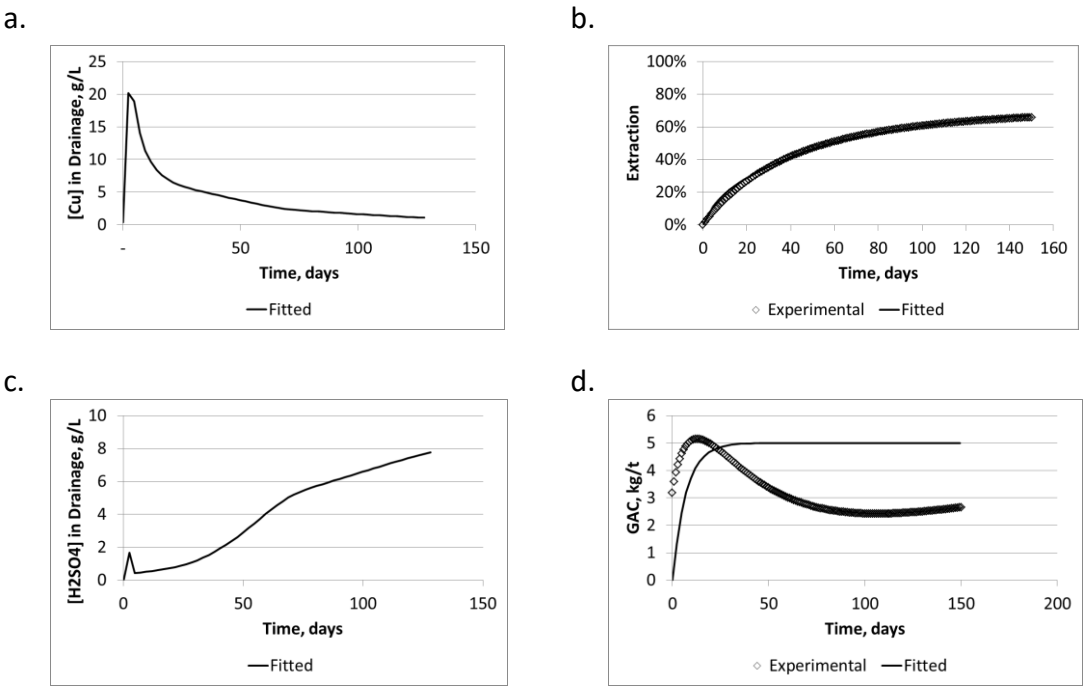

Figure 72. Fitting of FBC for Kipoi heap 3-1

APPENDIX F. FITTING OF NICICO SULPHIDE COPPER LEACHING

a.

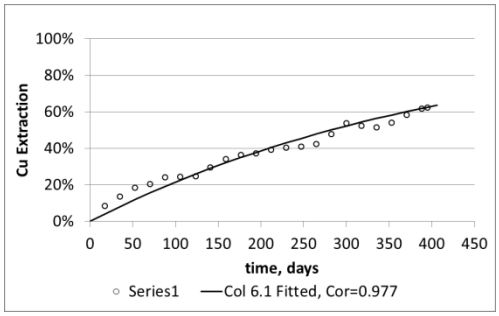

b.

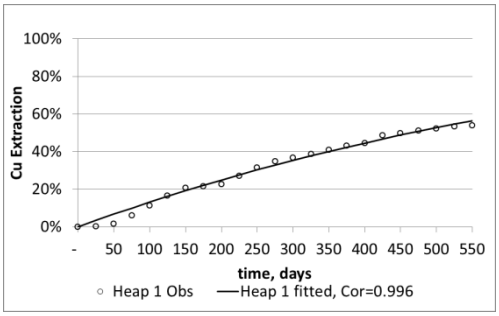

c.

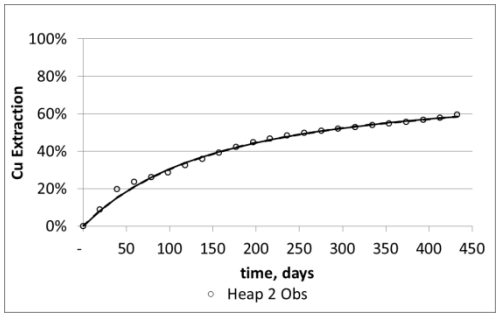

Figure 73. Fitting of batch curve to determine extractable fraction.
(a) Column 6.1, (b) Heap 1, (c) Heap 2

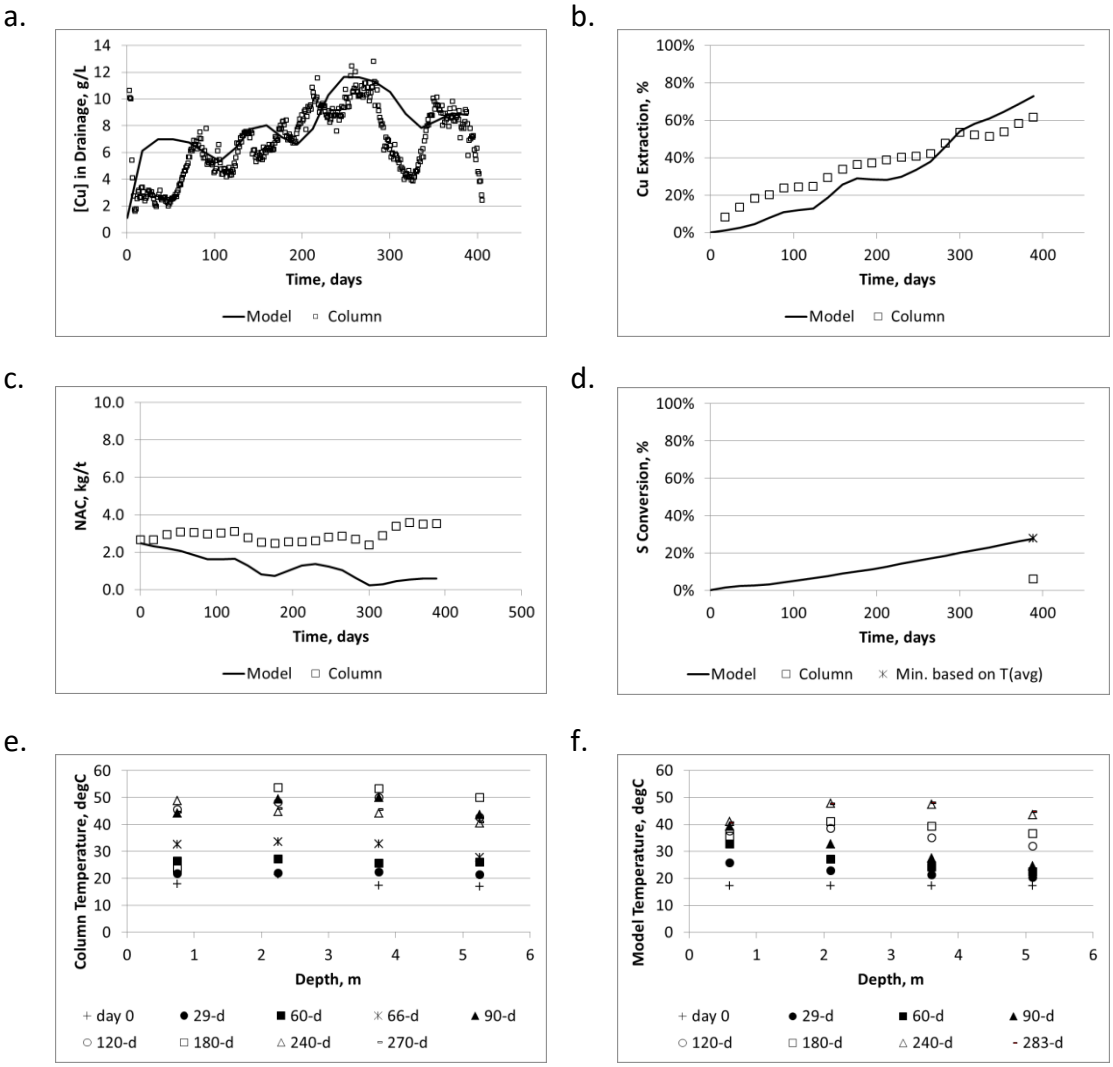

Figure 74. Column 6.1 leaching performance.
(a) [Cu] in drainage, (b) Cumulative Cu extraction, (c) NAC, (d) S conversion, (e) Column temperatures, (f) Model temperatures

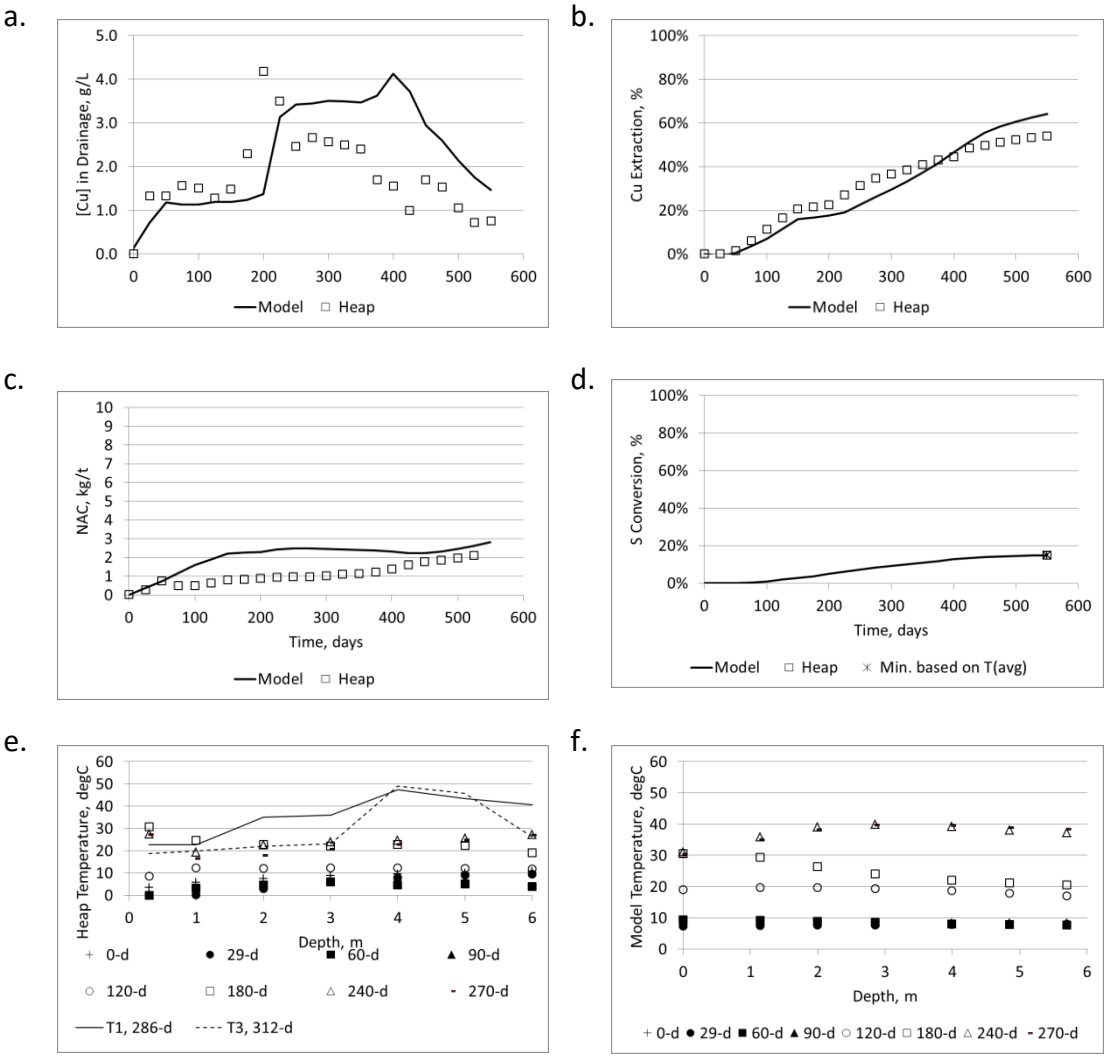

Figure 75. Heap 1 leaching performance.

(a) [Cu] in drainage, (b) Cumulative Cu extraction, (c) NAC, (d) S conversion, (e) Average heap temperatures, (f) Model temperatures

Note: The heap temperature profiles measured in borehole T1 on day 286, and in borehole T3 on day 312, included the highest temperatures measured in Heap 1.

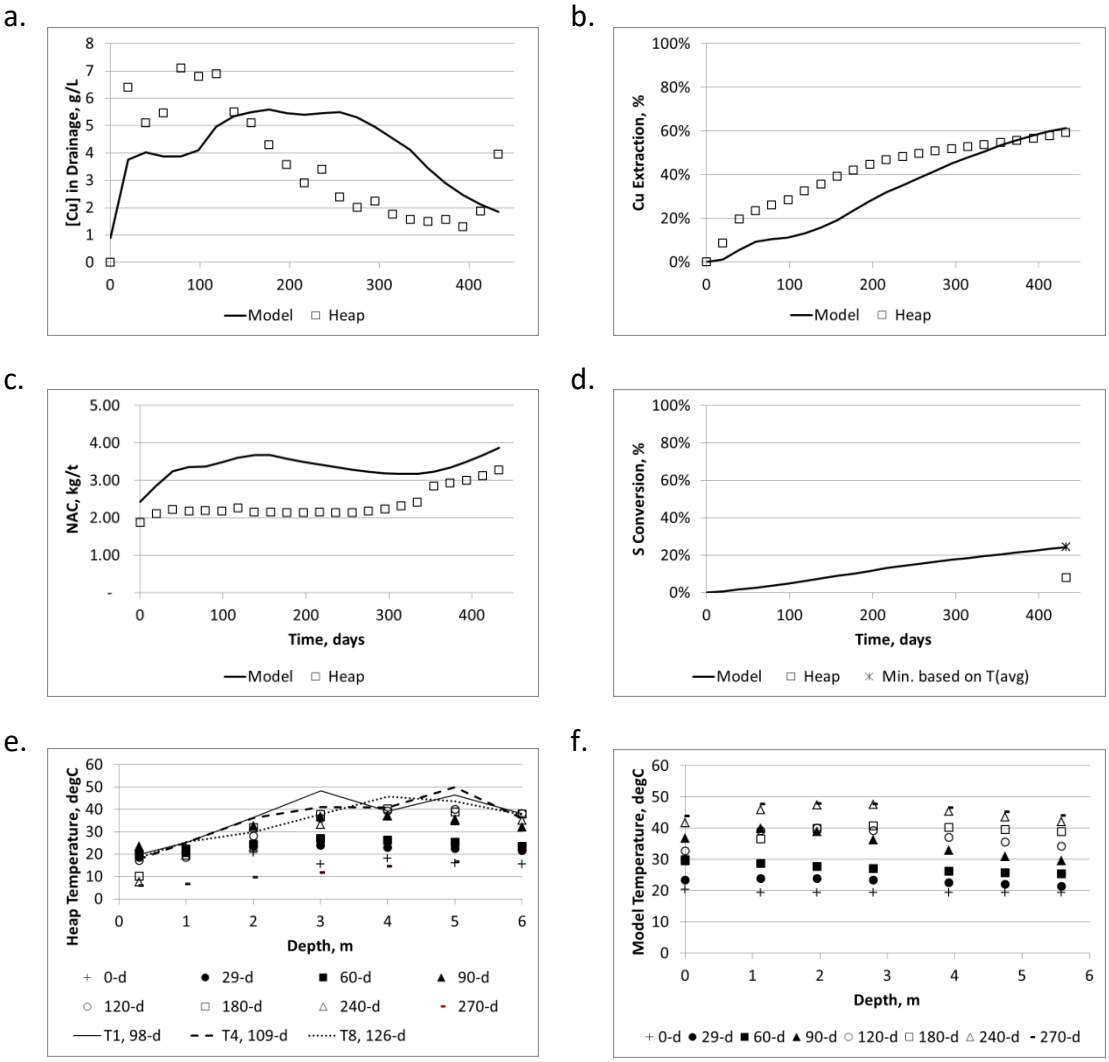

Figure 76. Heap 2 leaching performance.

(a) [Cu] in drainage, (b) Cumulative Cu extraction, (c) NAC, (d) S conversion, (e) Average heap temperatures, (f) Model temperatures

Note: The heap temperature profiles measured in borehole T1 on day 98, in borehole T4 on day 109, and in borehole T8 on day 126, included the highest temperatures measured in Heap 2.

APPENDIX G. SINGLE AND MULTI-VARIABLE FITTING OF MODEL PARAMETERS

The objective function

The objective function $f_k(\boldsymbol{x_k})$ to be optimised is selected according to the specific requirement of each case. Typically for the work described here it required minimisation of the SSR between one or more sets of experimental data and corresponding sets of model outputs. It could also be composed of the weighted sum of the SSR of any number of model-experimental data pairs.

Single variable optimisation

In the case of single variable optimisation, $f_k(\boldsymbol{x_k})$ is a function of only a single independent variable which gets manipulated to optimise (minimise) $f_k(\boldsymbol{x_k})$. The procedure followed has been to firstly determine $f_k(\boldsymbol{x_k})$ for three values of the independent variable, selected in the vicinity of the expected optimum value. As an example, consider the Transfer Time Θ, as the independent variable that is manipulated to minimise the sum of squared residuals (SSR) between observed and modelled data points.

A parabola of the form

$$SSR = a\Theta^2 + b\Theta + c$$

is fitted to the three resulting data points (Θ_i ; SSR_i) for i = 1 to 3, and the optimal value for Θ(yielding the minimum SSR) is estimated as $\Theta_{opt} = {}^{-b}/_{2a}$. The model calculation is repeated using Θ_{opt} thus calculated to add an additional data point (Θ_4 ; SSR_4), the parabola fit and calculation of a new Θ_{opt} is repeated to confirm the location of the optimum for Θ.

Convergence is indicated by the difference in successive values of Θ_{opt} being less than 1 percent.

The line search that concludes a multi-variable optimisation iteration, which is discussed next, is another example of single-variable optimisation.

Multi-variable optimisation in two dimensions

Newton's method was used for two-variable optimisation as discussed by (Andrew, 2006), which is based on a second-order Taylor expansion around the supposed optimum point $\boldsymbol{x}$ (which in this study was typically the combination of Transfer Time Θ and GAC rate constant k').

What follows below is the application of the published generic method to the specific case of two independent variables. The author of this text suggests a procedure for selecting the points on the two-dimensional independent variable surface at which to determine the values of the multi-variable objective function, from which follow the relevant gradients to be calculated. The algebra is written out fully for ease of coding.

The conventional nomenclature is adopted of using bold symbols for vectors (ex. $\boldsymbol{x}_k$) and bold capitol symbols for matrices (ex. $\boldsymbol{B}_k$). The current estimate of the optimum is $\boldsymbol{x}_k$, and therefore the difference between the optimum point and current estimate is $\boldsymbol{p}_k = \boldsymbol{x} - \boldsymbol{x}_k$.

Setting the gradient of the Taylor expansion for this expression to zero yields the following expression to be solved for calculating the optimum:

$$\boldsymbol{p}_k = -\boldsymbol{B}_k^{-1} \nabla \boldsymbol{f}_k \qquad or \qquad \boldsymbol{B}_k \boldsymbol{p}_k = -\nabla \boldsymbol{f}_k \tag{120}$$

where

$\boldsymbol{B}$ is the *Hessian* (i.e. matrix of second partial derivatives). The calculated vector $\boldsymbol{p}_k$ is used to indicate the direction in which to search for the optimum (or at least the new solution $\boldsymbol{x}_{k+1}$ which is closer to the optimum) to be found by means of a line search by manipulating the scalar α_s in:

$$\boldsymbol{x}_{k+1} = \boldsymbol{x}_k + \alpha_s . \boldsymbol{p}, \text{ where } \alpha_s \in (0; \infty) \tag{121}$$

For only two dimensions it is still practical to fully write out [120] as follows:

$$\begin{bmatrix} f_{xx} & f_{xy} \\ f_{xy} & f_{yy} \end{bmatrix} \begin{bmatrix} p_x \\ p_y \end{bmatrix} = -\begin{bmatrix} f_x \\ f_y \end{bmatrix}$$

Multiplying it out, followed by elimination and substitution yields:

$$p_x = x_{k+1} - x_k = -\left[\frac{f_x}{f_{xx}} + \frac{f_{xy}}{f_{xx}} \frac{(f_{xx}f_y - f_{xy}f_x)}{(f_{xy}f_{xy} - f_{xx}f_{yy})}\right] \; or \; -\left[\frac{f_x}{f_{xx}} + \frac{f_{xy}}{f_{xx}} p_y\right] \; \forall f_{xx} \neq 0 \qquad [122]$$

$$p_y = y_{k+1} - y_k = \frac{(f_{xx}f_y - f_{xy}f_x)}{(f_{xy}f_{xy} - f_{xx}f_{yy})} \quad \forall \; (f_{xy}f_{xy} - f_{xx}f_{yy}) \neq 0 \qquad [123]$$

The optimisation now proceeds as follows:

The boundaries of constraints for the independent variables are defined as:

$x \in [x_{min};\, x_{max}]$

$y \in [y_{min};\, y_{max}]$

The initial solution $\boldsymbol{x}_k$ is chosen as the mid-point in the constraint boundaries:

$$\boldsymbol{x}_k = \begin{bmatrix} x_k \\ y_k \end{bmatrix} = \begin{bmatrix} (x_{max} + x_{min})/2 \\ (y_{max} + y_{min})/2 \end{bmatrix}$$

A good combination of efficiency and economy of calculation is found by approximating first derivatives f_x and f_y by middle-differences and the higher-order derivatives f_{xx}, f_{yy} and f_{xy} by forward-differences (higher-order derivatives become weaker functions of the independent variables thereby reducing the magnitude of any errors introduced). If the function to be optimised is analytically a second-order function the second derivatives are constants in which case forward-, backward- and middle-difference calculations will yield the second derivative exactly, and the exact optimum will be found upon the first iteration.

Calculating the first derivatives requires determination of the function *f* at the following points, which are evenly distributed around $\boldsymbol{x}_k$:

$$\begin{bmatrix} x \\ y_k \end{bmatrix} = \begin{bmatrix} \frac{(x_k + x_{min})}{2} \\ y_k \end{bmatrix} \text{ and } \begin{bmatrix} x \\ y_k \end{bmatrix} = \begin{bmatrix} \frac{(x_k + x_{max})}{2} \\ y_k \end{bmatrix}$$

$$\begin{bmatrix} x_k \\ y \end{bmatrix} = \begin{bmatrix} x_k \\ \frac{(y_k + y_{min})}{2} \end{bmatrix} \text{ and } \begin{bmatrix} x_k \\ y \end{bmatrix} = \begin{bmatrix} x_k \\ \frac{(y_k + y_{max})}{2} \end{bmatrix}$$

Upon which the first derivatives at $\boldsymbol{x}_k$ can be calculated from:

$$\begin{bmatrix} f_x(x_k; y_k) \\ f_y(x_k; y_k \end{bmatrix} = \begin{bmatrix} \frac{f\left[\frac{(x_k + x_{max})}{2};\ y_k\right] - f\left[\frac{(x_k + x_{min})}{2};\ y_k\right]}{(x_{max} - x_{min})/2} \\ \frac{f\left[x_k;\ \frac{(y_k + y_{max})}{2}\right] - f\left[x_k;\ \frac{(y_k + y_{min})}{2}\right]}{(y_{max} - y_{min})/2} \end{bmatrix} \quad [124]$$

Before the second-order derivatives can be calculated, it is necessary to determine the first-order derivatives at another 'forward' position of $\boldsymbol{x}_k$, denoted $\boldsymbol{x}_{k+}$, which is chosen on that side of $\boldsymbol{x}_k$ that is suggested by the sign of the first derivatives to be closer to the optimum point, namely:

$$\boldsymbol{x}_{k+} = \begin{bmatrix} x_{k+} \\ y_{k+} \end{bmatrix} = \begin{bmatrix} \begin{cases} \frac{(x_k + x_{min})}{2} & \forall\ f_x > 0 \\ \frac{(x_k + x_{max})}{2} & \forall\ f_x \leq 0 \end{cases} \\ \begin{cases} \frac{(y_k + y_{min})}{2} & \forall\ f_y > 0 \\ \frac{(y_k + y_{max})}{2} & \forall\ f_y \leq 0 \end{cases} \end{bmatrix}$$

The terms required for the first derivative $f_x(\boldsymbol{x}_{k+})$ are obtained by firstly calculating f at the following points, which are evenly distributed around $\boldsymbol{x}_{k+}$:

$$\begin{bmatrix} x \\ y_k \end{bmatrix} = \begin{bmatrix} \begin{cases} x_{min} \ \forall\ f_x > 0 \\ x_k \ \forall\ f_x \leq 0 \end{cases} \\ y_k \end{bmatrix} \text{ and } \begin{bmatrix} x \\ y_k \end{bmatrix} = \begin{bmatrix} \begin{cases} x_k \ \forall\ f_x > 0 \\ x_{max} \ \forall\ f_x \leq 0 \end{cases} \\ y_k \end{bmatrix}$$

The calculation of $f_x(\boldsymbol{x}_{k+})$ then follows as per [124] above except that it is performed around point $\boldsymbol{x}_{k+}$ using the function values calculated at the above two points.

The terms required for the first derivative $f_y(\boldsymbol{x}_{k+})$ are obtained by calculating the function $f(\boldsymbol{x}_{k+})$ at the following points, which are also evenly distributed around $\boldsymbol{x}_{k+}$:

$$\begin{bmatrix} x_k \\ y \end{bmatrix} = \begin{bmatrix} x_k \\ \begin{cases} y_{min} \; \forall \; f_y > 0 \\ y_k \; \forall \; f_y \leq 0 \end{cases} \end{bmatrix} \text{ and } \begin{bmatrix} x_k \\ y \end{bmatrix} = \begin{bmatrix} x_k \\ \begin{cases} y_k \; \forall \; f_y > 0 \\ y_{max} \; \forall \; f_y \leq 0 \end{cases} \end{bmatrix}$$

The calculation of $f_y(\boldsymbol{x}_{k+})$ then follows by the same calculation as in [124] above except that it is performed around point $\boldsymbol{x}_{k+}$ using the function values calculated at the above two points.

The second-order derivatives f_{xx} and f_{yy} are then calculated from:

$$\begin{bmatrix} f_{xx} \\ f_{yy} \end{bmatrix} = \begin{bmatrix} \dfrac{f_x(x_{k+};\, y_k) - f_x(x_k;\, y_k)}{(x_{k+} - x_k)} \\ \dfrac{f_y(x_k;\, y_{k+}) - f_y(x_k;\, y_k)}{(y_{k+} - y_k)} \end{bmatrix}$$

Calculation of the derivative f_{xy} further requires the function value at the point $\boldsymbol{x}_k$ (which will already have been calculated as one of the terms required for the calculation of $f_x(\boldsymbol{x}_{k+})$ and $f_y(\boldsymbol{x}_{k+})$ above, as well as at the point $\boldsymbol{x}_{k+}$ defined above. Then follows:

$$f_{xy} = \frac{f(x_{k+};\, y_{k+}) - f(x_{k+}; y_k) - f(x_k;\, y_{k+}) + f(x_k; y_k)}{(y_{k+} - y_k)(x_{k+} - x_k)} \qquad [125]$$

All terms required for calculating $\boldsymbol{p}_x$ in [122] and [123] and from that the next iteration of the optimum $\boldsymbol{x}_{k+1}$ from [121], are then available. Each iteration requires the function value to be determined at eight points, although the combination of which possible points of $\boldsymbol{x}_{k+}$ are required depends on the signs of f_x and f_y as discussed.

After having calculated the direction vector, perform a line search by varying α_s in [121] in the direction of the most recently determined vector $\boldsymbol{p}_x$ according to the single variable optimisation routine discussed above.

As a next iteration, a new set of constraint boundaries can be defined symmetrically around $\boldsymbol{x}_{k+1}$, which then becomes the new mid-point $\boldsymbol{x}_k$ and the entire routine is

repeated. A condition that can be set for convergence is to select a suitably small value for ε in:

$$\frac{|\boldsymbol{p_k}|}{|\boldsymbol{x_k}|} \leq \varepsilon \qquad [126]$$

However in the work described here the objective function was frequently found to become a much weaker function of one of the two independent variables than of the other, once the solution is near the global optimum. This leads to slow convergence of the weaker variable upon further multi-variable iterations, while the objective function remains weakly responsive. However this implies that the objective function is then responding to the weaker variable on a smaller scale than to the stronger variable. This allows further single-variable optimisation of the weaker variable while keeping the stronger variable constant, without significantly changing the two-variable objective function. It only requires final verification that the two-variable objective function has not responded significantly after the weaker variable has been finally optimised, i.e. that the optimum point for the weaker variable has not moved beyond the region where the two-variable objective function is insensitive to the weaker variable.

APPENDIX H. FITTING OF COPPER EXTRACTION DATA FROM SEGREGATION TESTWORK

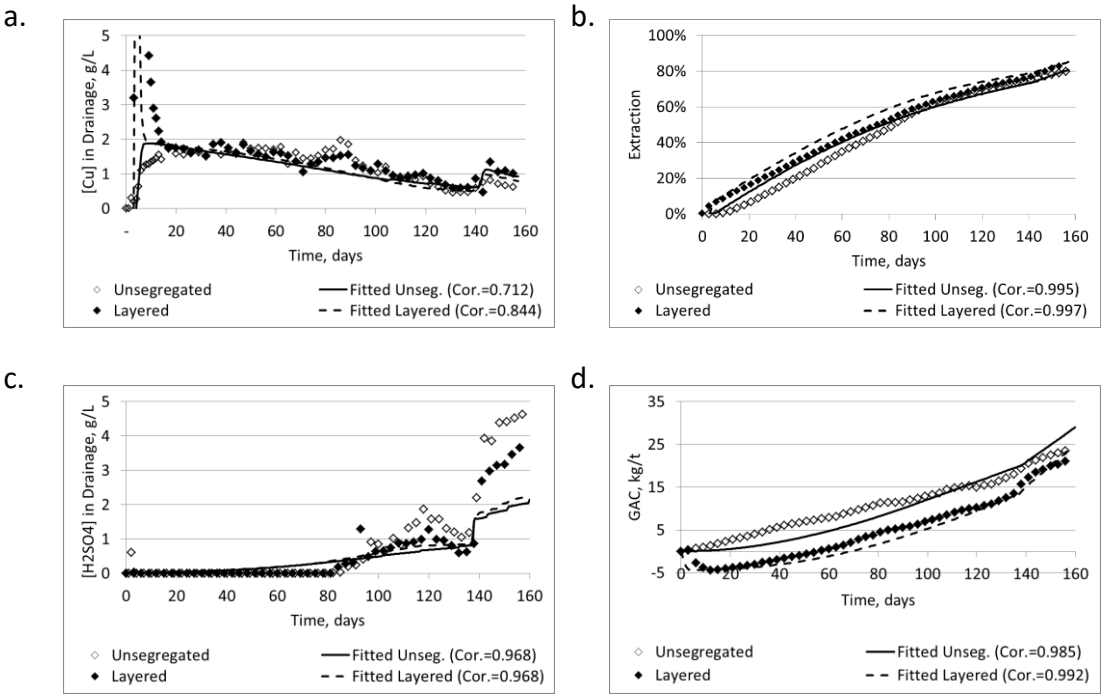

Figure 77. Fitting of leaching performance: unsegregated ore vs ore segregated in layers.

(a) Cu in drainage, (b) Cu extraction, (c) Acid in drainage, (d) GAC

Reproduced from Van Staden and Petersen (2018a)

APPENDIX J. FITTING OF COPPER EXTRACTION DATA FROM STRATIFICATION TESTWORK

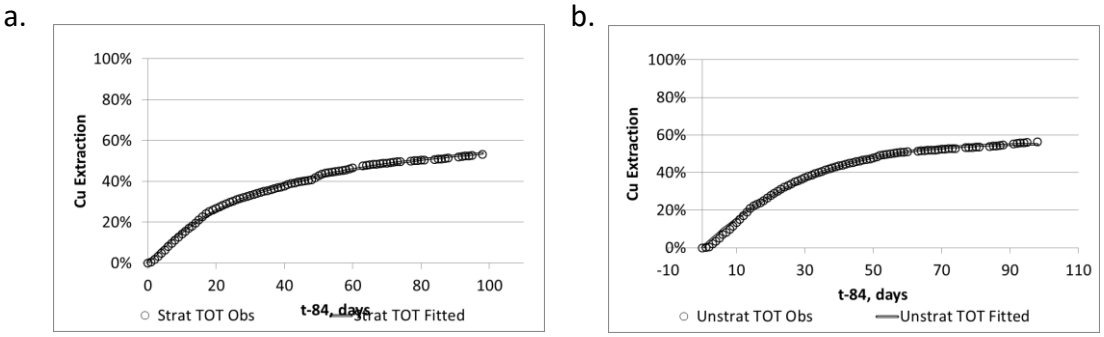

Figure 78 Fitting of Oxide-1 batch curves to determine extractable fraction.
a) Stratified ore, b) Unstratified ore

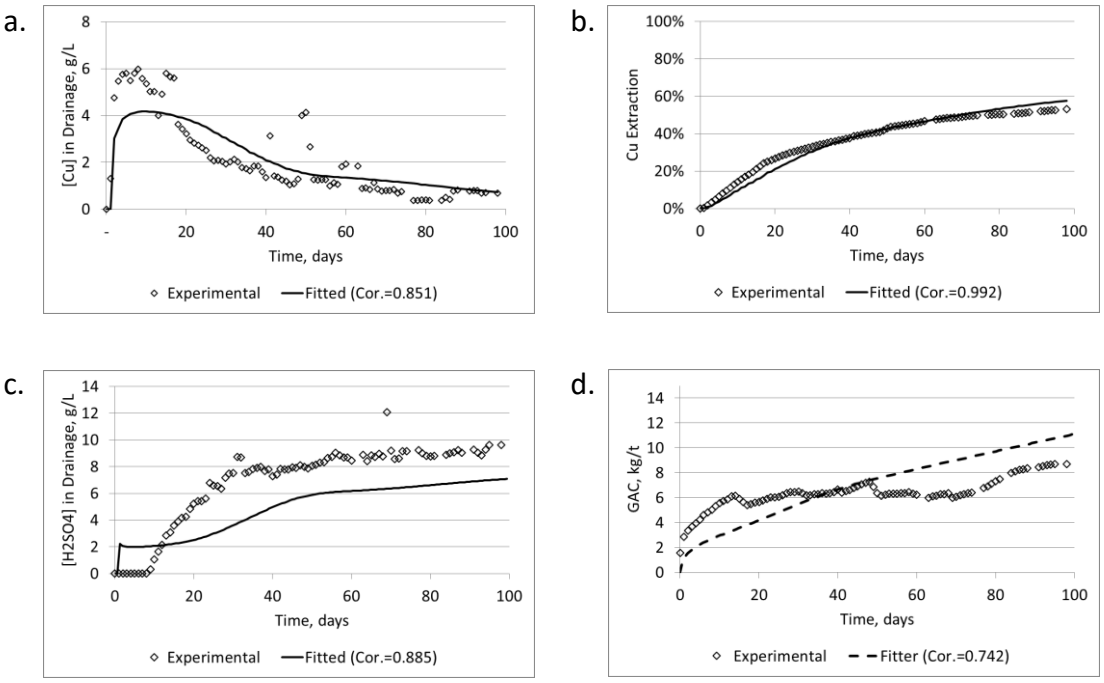

Figure 79. Model fitting of leaching data of Oxide-1 stratified ore.
(a) Cu in drainage, (b) Cu extraction to drainage, (c) drainage acid concentration, (d) GAC.
(The time scale indicates time since acid addition was started on day 84 of irrigation).
Reproduced from Van Staden and Petersen (2019)

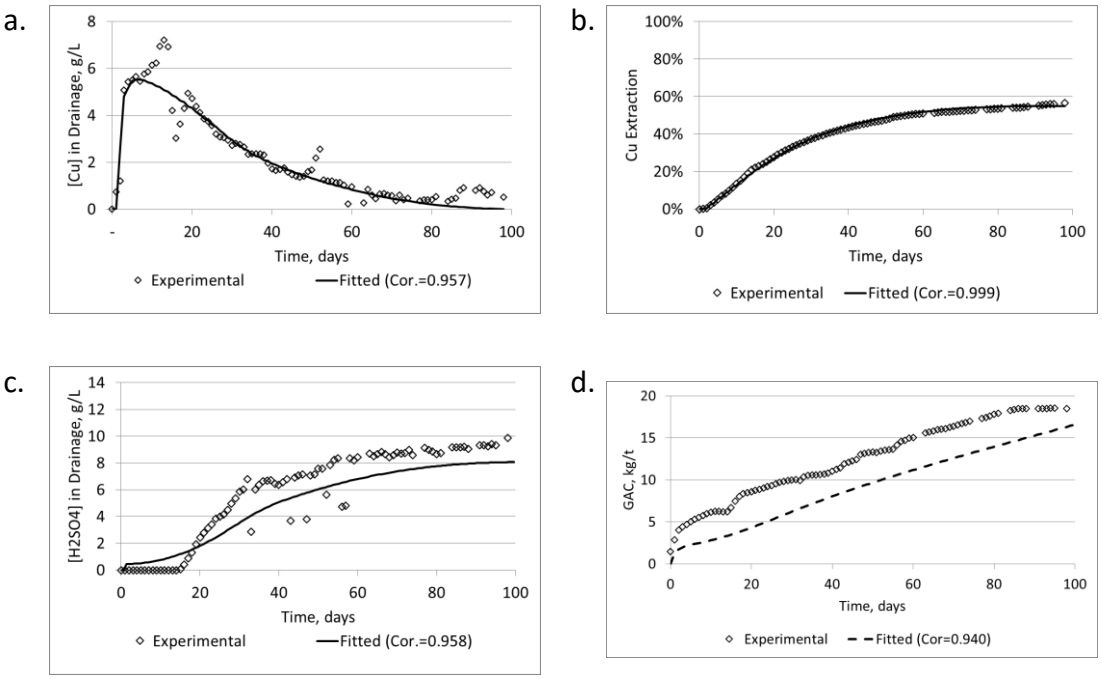

Figure 80. Model fitting of leaching data of Oxide-1 unstratified ore.
(a) Cu in drainage, (b) copper extraction to drainage, (c) drainage acid concentration, (d) GAC.
(The time scale indicates time since acid addition was started on day 84 of irrigation).
Reproduced from Van Staden and Petersen (2019)

a.

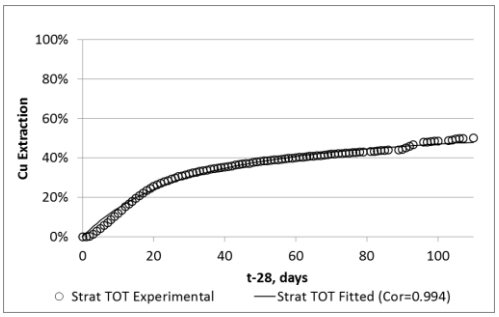

b.

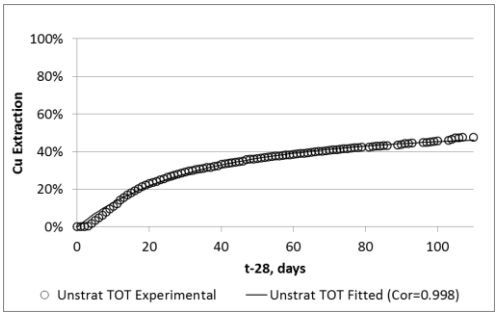

Figure 81 Fitting of Oxide-II batch curves to determine extractable fraction.
a) Stratified ore, b) Unstratified ore

a.

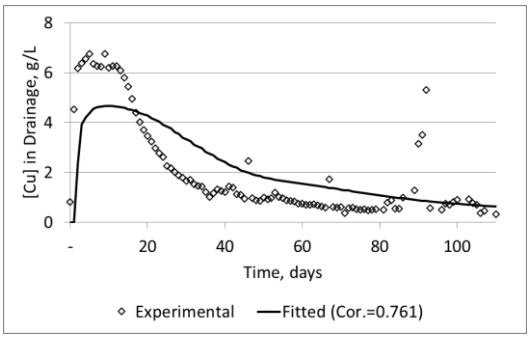

b.

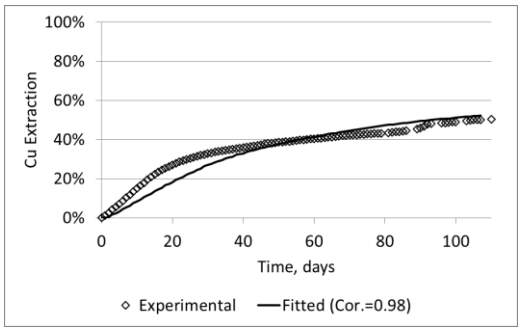

c.

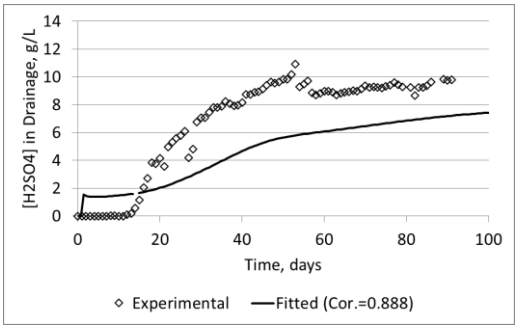

d.

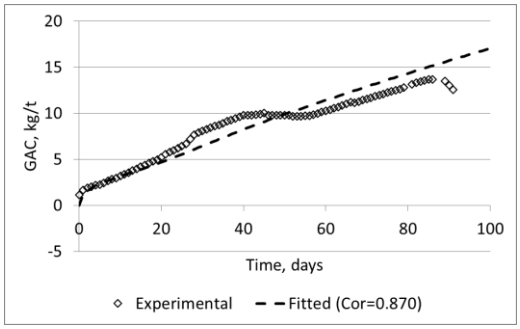

Figure 82. Model fitting of leaching data of Oxide-2 stratified ore.
(a) Cu in drainage, (b) Cu extraction to drainage, (c) drainage acid concentration, (d) GAC.
(The time scale indicates time since acid addition was started on day 28 of irrigation).

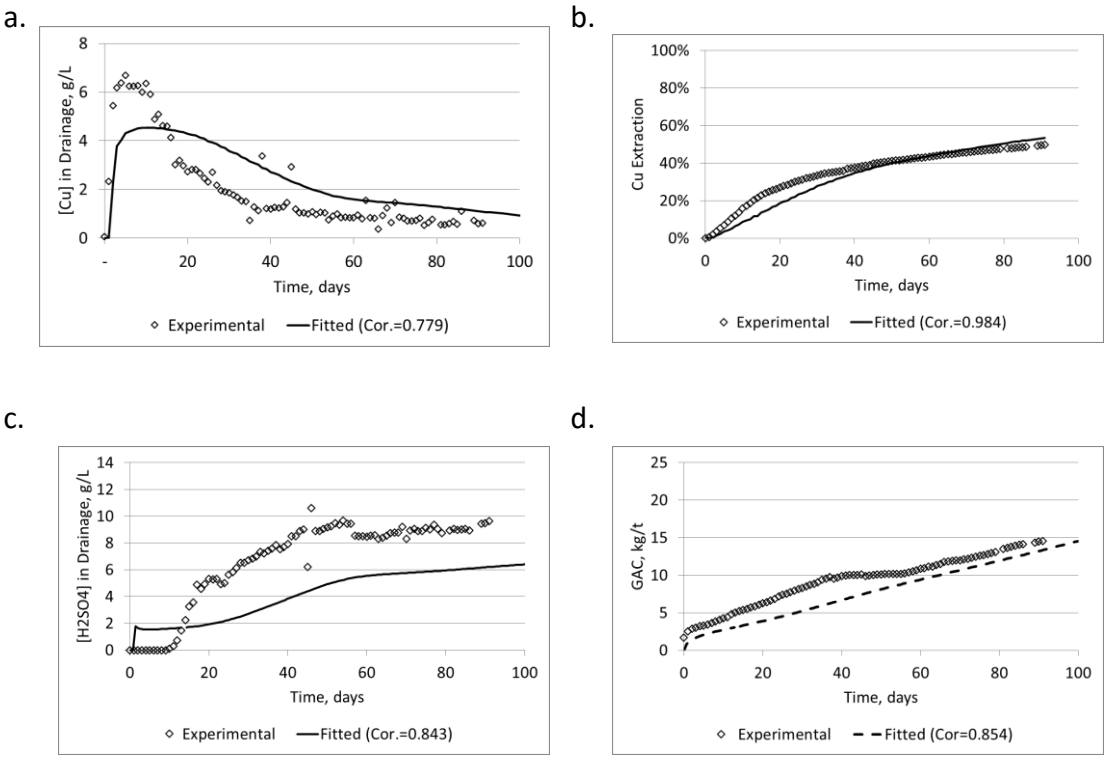

Figure 83. Model fitting of leaching data of Oxide-2 unstratified ore.
(a) Cu in drainage, (b) copper extraction to drainage, (c) drainage acid concentration, (d) GAC.
(The time scale indicates time since acid addition was started on day 28 of irrigation).